AD-A055 892 PRINCETON UNIV N J DEPT OF AEROSPACE AND MECHANICAL--ETC F/G 1/2
THE INFLUENCE OF THROTTLE AUGMENTED STABILITY (APCS) AND SHORT --ETC(U)
MAR 78 G E MILLER, S SEMBONGI, E SECKEL N00019-75-C-0528

UNCLASSIFIED AMS-1325 NL

1 OF 2
AD
A055 892

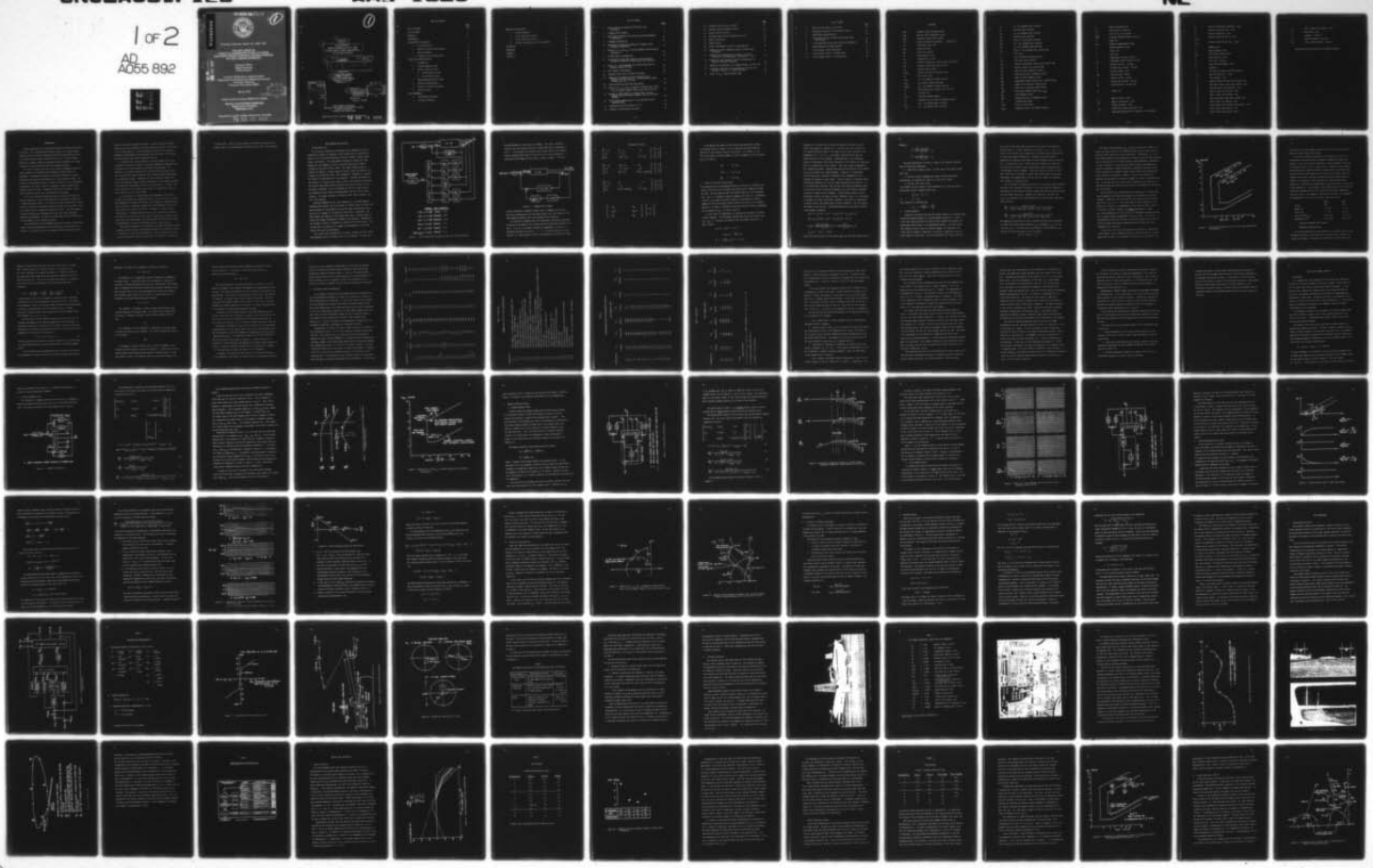

Princeton University Report No. AMS 1325

THE INFLUENCE OF THROTTLE AUGMENTED STABILITY (APCS) AND SHORT PERIOD CONTROL CHARACTERISTICS ON THE LANDING APPROACH

George E. Miller
Shigeo Sembongi
Edward Seckel

FLIGHT RESEARCH LABORATORY
Department of Aerospace and Mechanical Sciences
Princeton University
Princeton, New Jersey 08540

March 1978

Under Contract Number N00019-75-C-0528

NAVAL AIR SYSTEMS COMMAND
Department of the Navy
Washington, D.C.

(1)

(14) AMS-1325

(6)

THE INFLUENCE OF THROTTLE AUGMENTED STABILITY (APCS) AND SHORT PERIOD CONTROL CHARACTERISTICS ON THE LANDING APPROACH.

(11) Mar[illegible]78 (12) 181 p.

(9) Final technical rept. Jul 75 - Jun 76,

Prepared for:

Under Contract Number

(15) N00019-75-C-0528

NAVAL AIR SYSTEMS COMMAND
Department of the Navy
Washington, D. C.

(10) Prepared by:

George E. Miller
Shigeo Sembongi
Edward Seckel

Approved by:

Robert F. Stengel

FLIGHT RESEARCH LABORATORY
Department of Aerospace and Mechanical Sciences
Princeton University
Princeton, New Jersey 08540

TABLE OF CONTENTS

LIST OF FIGURES

LIST OF TABLES

NOTATIONS

ACLS	Automatic Carrier Landing System
APCS	Approach Power Compensator System
AFCS	Automatic Flight Control System
CAP	Control Anticipation Parameter (deg/sec^2/g)
C.F.	centrifugal force (lbs)
CRT	Cathode-Ray Tube
DLC	Direct Lift Control
D_v	drag damping (1/sec)
D_α	induced drag (ft/sec^2)
$D_{\delta e}$	elevator (stabilator) control drag (ft/sec^2/rad)
$D_{\delta t}$	throttle control drag (ft/sec^2/rad)
D_θ	attitude drag (ft/sec^2)
FLOLS	Fresnel Lens Optical Landing System
F_s	stick force (lbs)
$G_{\delta e\theta}$	$\Delta\theta \rightarrow \Delta\delta_e$ feedback transfer function
$G_{\delta e\theta_c}$	pitch angle command input gain
$G_{\delta t\delta e}$	$\Delta\delta_e \rightarrow \Delta\delta_t$ feedback transfer function
g	acceleration due to gravity (32.2 ft/sec^2)
h	altitude (ft)
IAS	indicated airspeed (knots)
$j\omega$	imaginary part of Laplace transform operator
K_{n_x}	$\Delta n_x \rightarrow \Delta\delta_t$ feedback gain (rad/fps^2)
K_{n_z}	$\Delta n_z \rightarrow \Delta\delta_t$ feedback gain (rad/fps^2)

K_v	$\Delta V \rightarrow \Delta\delta_t$ feedback gain (rad/fps)
K_v^*	pseudo K_v gain (rad/fps)
K_α	$\Delta\alpha \rightarrow \Delta\delta_t$ feedback gain (rad/rad)
K_α^*	pseudo K_α gain (rad/rad)
K'_α	sum of K_α and K_α^* gains (rad/rad)
$K_{\delta e}$	$\Delta\delta_e \rightarrow \Delta\delta_t$ feedback gain (rad/rad)
K_θ	$\Delta\theta \rightarrow \Delta\delta_t$ feedback gain (rad/rad)
$K_{\int\alpha}$	$\int_0^t \Delta\alpha\, dt \rightarrow \Delta\delta_t$ feedback gain (rad/sec-rad)
L	lift (lbs)
L_v	lift variation with speed (1/sec)
L_α	lift curve slope (ft/sec^2)
$L_{\delta e}$	elevator (stabilator) control lift ($ft/sec^2/rad$)
$L_{\delta t}$	throttle control lift ($ft/sec^2/rad$)
M_α	angle of attack stability ($1/sec^2$)
M_α^*	equivalent M_α due to feedback ($1/sec^2$)
$M_\alpha^\bullet$	angle of attack damping (1/sec)
$M_{\delta e}$	longitudinal control sensitivity ($rad/sec^2/rad$)
$M_{\delta t}$	moment due to throttle ($rad/sec^2/rad$)
M_θ	moment due to attitude ($rad/sec^2/rad$)
$\lvert M_\theta \rvert$	pitch angle command input gain, $G_{\delta e\theta_c}$
$M_\theta^\bullet$	pitch damping (1/sec)
$M_\theta^{\bullet *}$	equivalent M_θ due to feedback (1/sec)
m	airplane mass (slug)
NATC	Naval Air Test Center
$N_{\delta sV}$	numerator of $\Delta\delta_s \rightarrow \Delta V$ transfer function

n_z	normal acceleration (g)
n_{zt}	load factor in a turn (g)
n_{z_α}	ratio of Δn_z to $\Delta\alpha$ (g/rad)
PVSN	Princeton Variable Stability Navion
R	range (ft)
SAS	Stability Augmentation System
s	Laplace operator (1/sec)
T	thrust (lb)
t	time (sec)
u	longitudinal velocity (ft/sec)
u_g	longitudinal gust velocity (ft/sec)
V	aircraft velocity (ft/sec)
V_o	aircraft trim velocity (ft/sec)
W	aircraft weight (lbs)
WOD	wind over deck (knots)
w	lateral velocity (ft/sec)
w_g	lateral gust velocity (ft/sec)
Y_β	crosswind force ($ft/sec^2/rad$)
$\mathfrak{E}$	center line
α	angle of attack (rad)
α_g	angle of attack gust (rad)
γ	flight path angle (rad)
γ_{ss}	steady state flight path angle (rad)
Δ	longitudinal characteristic equation, or incremental

δ_e	elevator (stabilator) deflection (rad)
δ_s	control stick deflection (rad)
δ_t	throttle deflection (rad)
$\delta_{t_{u_g}}$	throttle deflection due u_g (rad)
$\delta_{t_{u_g}}$	throttle deflection due to α_g (rad)
ζ	damping ratio
ζ_p	phugoid damping ratio
ζ_{sp}	short period damping ratio
θ	pitch attitude (rad)
$\dot{\theta}$	pitch rate (rad/sec)
θ_c	pitch attitude command (rad)
Σ	summation
σ	real part of Laplace transform operator
σ_{δ_t}	throttle thrash rms (rad)
τ	time constant (sec)
τ'	Washout Prefilter System time constant (sec)
τ_d	APCS down elevator input time constant (sec)
τ_E	effective engine time constant (sec)
τ_{nx}	APCS n_x input time constant (sec)
τ_{nz}	APCS n_z input time constant (sec)
τ_u	APCS up elevator input time constant (sec)
τ_v	APCS V input time constant (sec)
τ_{wo}	APCS elevator input washout time constant (sec)
τ_α	APCS α input time constant (sec)
τ_θ	APCS θ input time constant (sec)

$\tau_{\int\alpha}$	APCS $\int\alpha$ input time constant (sec)
ϕ	bank angle (rad)
ω	frequency (rad/sec)
ω_p	phugoid frequency (rad/sec)
ω_{sp}	short period frequency (rad/sec)

Lateral-Directional Notations may be found on page 66.

INTRODUCTION

Carrier operation of jet aircraft dates back to the Korean War period of the 50's. The increased approach speed coupled with sluggish engine response, and the relatively unforgiving handling characteristics of the jet aircraft placed a greater workload on the pilot. Angle of attack, rather than airspeed, became the approach reference because of the large variations in gross weight from fuel and expendable payload.

As an aid to relieve the pilot of the throttle management during the carrier approach, the Approach Power Compensator System (APCS) was developed. As orginally conceived, the system was designed to control airspeed on the approach with reference to a fixed angle of attack. Two "reliable" potentiometer sensors, an angle of attack vane and a mechanical accelerometer, were used to provide a computed airspeed indexed to the reference angle of attack. Although not used on all aircraft, a third input, elevator position, was also provided in the design.

In its early form the system served only to replace the "backside" throttle required vs velocity characteristics of the basic aircraft with a strong "frontside" effect. In essence this latter characteristic allows the pilot to control the approach flight path angle with the control stick only without worry of airspeed divergences or errors. With the computed or pseudo airspeed type of mechanization the short time flight path response was unchanged. The APCS of aircraft such as the A-4, RA-5, and A-6 are examples of this design philosophy.

The system gains were restructured within the constraint of the three sensors to provide augmentation of the flight path response for the F-4 aircraft. The success on the F-4 encouraged further application of the

concept to some later generation aircraft. However, despite increased sophistication the performance on current generation aircraft is deficient in one or more respects. Such shortcomings and the desire to develop a fundamental understanding of the potential and limitations of the system have motivated the APCS research presented herein.

In conducting this study attention is directed towards the A-7E as a reference aircraft both because it has objectionable APCS characteristics and because it has been extensively evaluated and documented. The capability to accurately simulate this aircraft and its production APCS with the Princeton Variable Stability Navion (PVSN) had been demonstrated in a preliminary program (Reference 1). The validation included time history and frequency domain response comparisons of the simulator aircraft with flight test measurements of the A-7E with and without its APCS. The final evaluation of the simulation was made by an experienced A-7E pilot from the Naval Air Test Center (NATC).

An initial matrix of configurations was programmed on the PVSN to attempt to understand the tradeoffs inherent in pseudo velocity vs flight path augmentation oriented APCS designs, the influence of additional feedbacks on burble or turbulence response and turn performance, and the use of auxiliary pilot inputs to the APCS. An analysis of some of these configurations is presented herein; however, pilot availability problems precluded data collection with NATC pilots. Inasmuch as preliminary tests showed small APCS improvements, the research effort was redirected towards the fundamentals of controlling flight path with a single control.

The report presentation is in essentially the same chronological order. A general review of factors influencing APCS design is discussed, followed by an analysis of some APCS configurations. The next sections deal with a study of flight path control systems and their evaluation in ground and

in flight tests. Finally, certain aspects not formally addressed in the program, such as turn performance and engine control limits, are discussed.

APCS CONCEPTS AND ANALYSIS

1. System Definition

For the sake of definition the Approach Power Compensator System is considered to consist of feedbacks of the aircraft motion variables and control stick (or elevator/stabilator) position through a single control output, the throttle. This description includes all current Navy APCS designs with the exception of the S-3 aircraft APCS which includes a crossfeed to the pitch control system. The current design concept is limited with regard to inputs (angle of attack, normal acceleration, and elevator) by the APCS Mil. Spec. MIL-C-23866A(WP), (Reference 2); however, the effects of other inputs will be considered. Although constrained in this report to a single control output, thrust line inclination and offset and in some cases engine derived boundary layer control results in lift and moment crossfeeds. The A-7E airframe with the TF-41 engine used as the reference for this report has approximately 19% lift due to thrust coupling. The moment crossfeed is relatively small and is assumed to be zero in the analysis.

Rewording somewhat the Mil. Spec (Reference 2), the APCS computer determines the throttle position necessary to control angle of attack, and hence airspeed, by using angle of attack and normal acceleration inputs. The use of an integral of the angle of attack error is specified. The APCS concept thus implies, in the steady state case, a constant angle of attack stall margin throughout all phases of the approach. Consequently, the airspeed in turns is increased as a function of the load factor. For the most part, the analysis will ignore the compromises in the system required for good turn performance.

The overall block diagram shown in Figure 1 contains the four current APCS feedbacks as well as others which will be examined. An inner loop

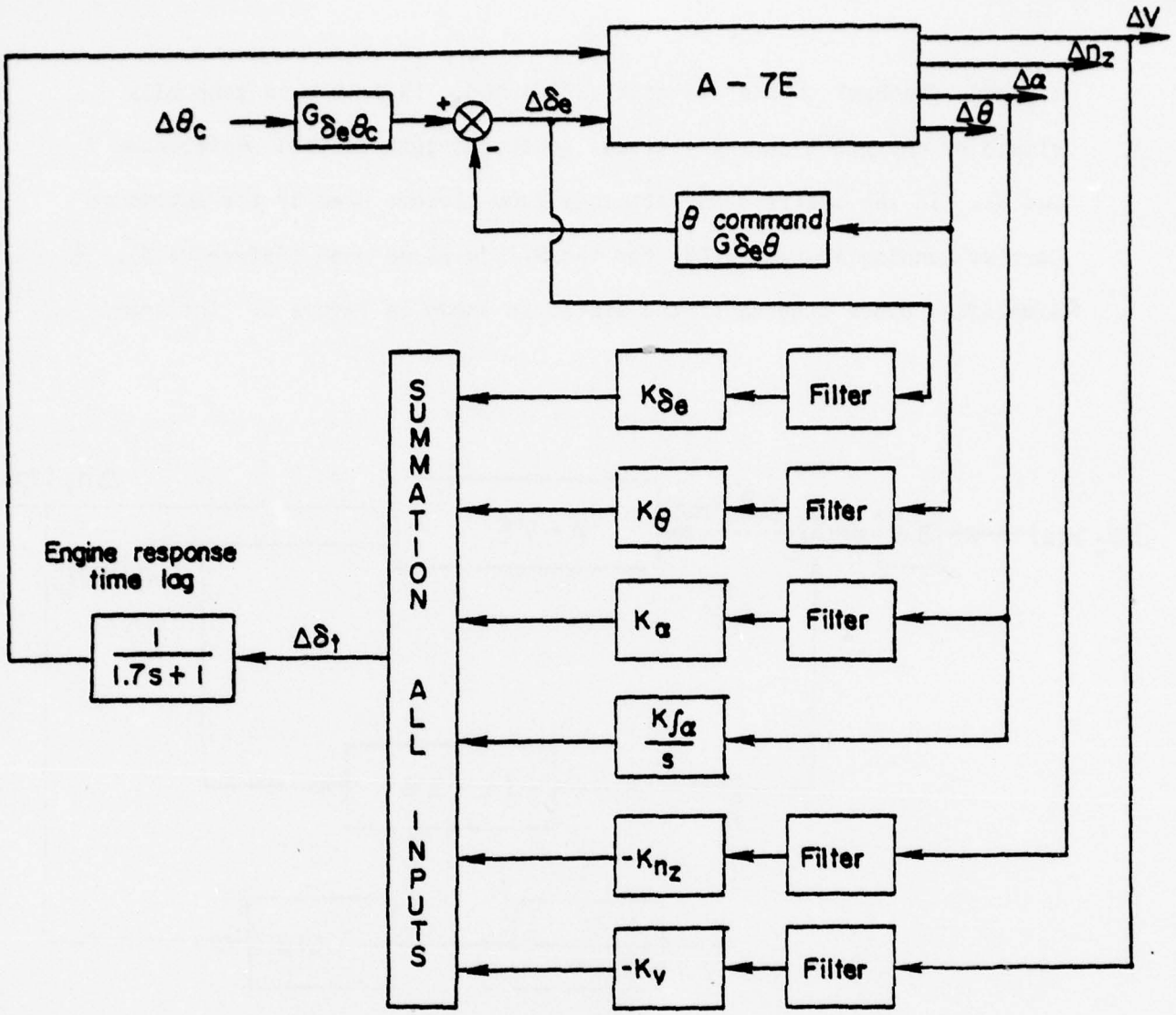

Feedback Sign Conventions

$+\Delta\theta \longrightarrow \Delta\delta_e$ (Down) (+)

$+\Delta\theta \longrightarrow \Delta\delta_t$ (Advance) (+)

$+\Delta\alpha \longrightarrow \Delta\delta_t$ (Advance) (+)

$+\Delta n_z \longrightarrow \Delta\delta_t$ (Retard) (−)

$+\Delta V \longrightarrow \Delta\delta_t$ (Retard) (−)

$+\Delta\delta_e$ (down) $\longrightarrow \Delta\delta_t$ (Retard) (−)

Figure 1. Total System Block Diagram and APCS Gain Sign Conventions

attitude feedback to the elevator is assumed. This loop is generally closed by the pilot during altitude or flight path control (References 3 and 4). In the analysis the attitude loop closure used by the Automatic Carrier Landing System (ACLS) for the A-7E will be used (Reference 5). A simplified block diagram of the system is shown in Figure 2. The very

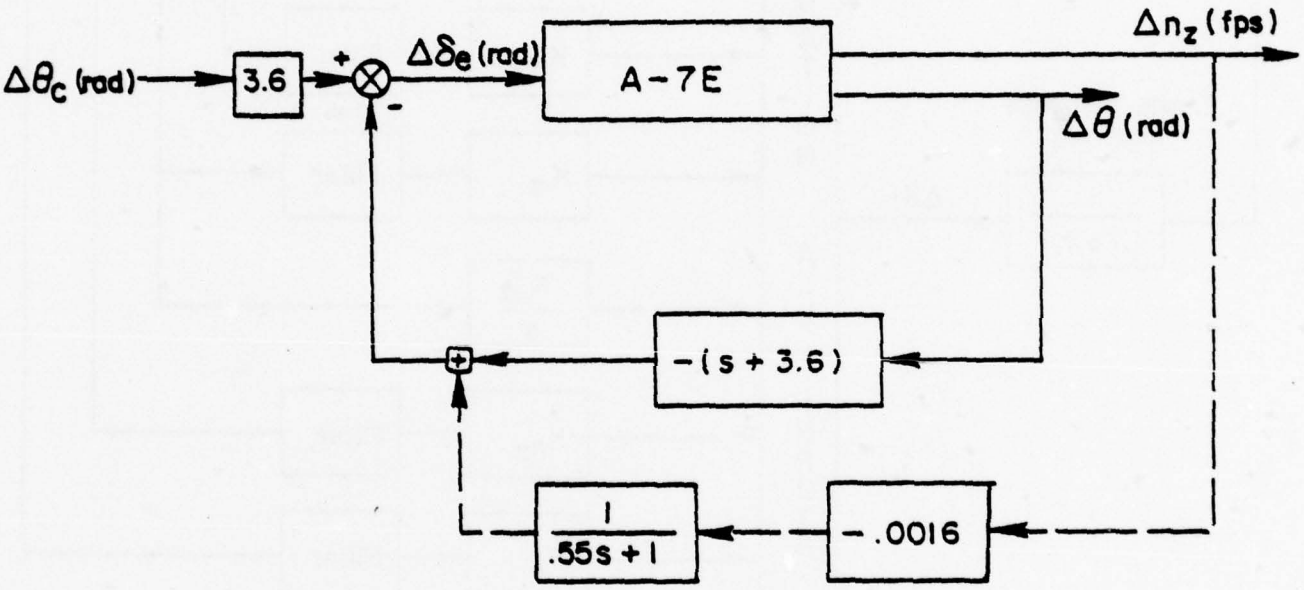

Figure 2. θ Command Block Diagram

low gain acceleration feedback (dashed line), a remenant of the stick force per g mechanization for high speed flight, has little effect in the power approach condition and will be neglected for simplicity.

The analytical framework uses the longitudinal perturbation equations of motion in the stability axis system with the flight path variables, V, γ, α and θ. Only two of the angle variables are independent; the third is determined through the relation $\gamma = \theta - \alpha$. For the convenience of later analysis, all three possible forms of the perturbation equations are shown.

Equations of Motion

$$\begin{bmatrix} s + D_V & D_\alpha - g & g \\ L_V/V & s + L_\alpha/V & -s \\ -M_V & -(M_{\dot{\alpha}}s + M_\alpha) & s(s - M_{\dot{\theta}}) \end{bmatrix} \begin{bmatrix} \Delta V \\ \Delta\alpha \\ \Delta\theta \end{bmatrix} =$$

$$\begin{bmatrix} s + D_V & -(D_\alpha - g) & D_\alpha \\ L_V/V & -(s + L_\alpha/V) & L_\alpha/V \\ -M_V & M_{\dot{\alpha}}s + M_\alpha & s^2 - (M_{\dot{\alpha}} + M_{\dot{\theta}})s - M_\alpha \end{bmatrix} \begin{bmatrix} \Delta V \\ \Delta\gamma \\ \Delta\theta \end{bmatrix} =$$

$$\begin{bmatrix} s + D_V & D_\alpha & g \\ L_V/V & L_\alpha/V & -s \\ -M_V & s^2 - (M_{\dot{\alpha}} + M_{\dot{\theta}})s - M_\alpha & s(s - M_{\dot{\theta}}) \end{bmatrix} \begin{bmatrix} \Delta V \\ \Delta\alpha \\ \Delta\gamma \end{bmatrix} =$$

$$\begin{bmatrix} D_{\delta t} & D_{\delta e} \\ L_{\delta t}/V & L_{\delta e}/V \\ M_{\delta t} & M_{\delta e} \end{bmatrix} \begin{bmatrix} \Delta\delta_t \\ \Delta\delta_e \end{bmatrix}$$

If we neglect the effects of the filters and engine time constant the feedbacks shown in Figure 1 can be interpreted as modifications or additions to the aircraft stability derivatives. For example, in the case of the angle of attack feedback, K_α may be thought of as an equivalent ΔD_α, $\Delta L_\alpha/V$ and M_α

$$\Delta D_\alpha = K_\alpha \times D_{\delta t}$$

$$\Delta L_\alpha/V = K_\alpha \times L_{\delta t}/V$$

$$\Delta M_\alpha = K_\alpha \times M_{\delta t}$$

2. Stability Derivative Equivalence

The existence of the crosscoupling terms $L_{\delta t}/V$ and $M_{\delta t}$ will determine the extent to which the lift and moment derivatives can be augmented through the APCS. For the analysis herein the moment effect $M_{\delta t}$ will be assumed zero. This is a reasonably accurate assumption for the A-7E. Furthermore, a control is available to minimize throttle crosscoupling or directly augment the pitch derivatives whereas direct lift control is not normally available. As noted, a crossfeed to the pitch control system to compensate for the effects of $M_{\delta t}$ is in use on the S-3.

At this time it is appropriate to introduce the concept of a pseudo velocity feedback. For the moment consider the case of zero control lift, $L_{\delta t} = L_{\delta e} = 0$. From the lift equation with the flight variables V, α, and γ we have:

$$L_V/V\ \Delta V + L_\alpha/V\ \Delta\alpha - s\ \Delta\gamma = 0$$

$$\text{since } s\Delta\gamma = \frac{\Delta n_z}{V}, \text{ then}$$

$$\Delta V = -\frac{1}{L_V/V}\left(L_\alpha/V\ \Delta\alpha - 1/V\ \Delta n_z\right)$$

Therefore, it is possible in principle to measure the $\Delta\alpha$ and Δn_z, and combine the signals to compute a ΔV. It may be noted that the ratio of the normal acceleration gain to the angle of attack gain required in the computation is $V \times L_\alpha/V$ or n_{z_α}, the normal acceleration per angle of attack derivative of the airplane. Neglecting small scale turbulence effects on the sensors, the velocity measured in this fashion will duplicate that of a conventional velocity sensor. There are several advantages to this computation scheme. Adequate resolution and reliability of the sensors are easily attained with simple hardware. Inasmuch as a perturbation velocity from trim is desired for feedback, bias compensation is not required for changes in gross weight (both the angle of attack and normal acceleration feedbacks will have the same operating point as before). It is not surprising, therefore, that the Navy APCS design incorporates angle of attack and normal acceleration feedbacks with early designs configured to provide a pseudo velocity feedback. Since aircraft dynamics involve aerodynamic velocity and angle of attack "feedback" terms, it is convenient to consider any normal acceleration feedback in the APCS as a combination of pseudo velocity and pseudo angle of attack feedbacks. For this purpose the effect of the throttle crosscoupling term can be included to provide a more general expression:

$$L_v/V\ \Delta V + L_\alpha/V\ \Delta\alpha - s\ \Delta\gamma = K_\alpha\ L_{\delta t}/V\ \Delta\alpha + K_{n_z}\ L_{\delta t}/V\ \Delta n_z$$

$$(\frac{1}{V} + K_{n_z}\ L_{\delta t}/V)\Delta n_z = (L_\alpha/V - K_\alpha\ L_{\delta t}/V)\Delta\alpha + L_v/V\ \Delta V$$

$$K_{n_z}\Delta n_z = \frac{L_\alpha/V - K_\alpha\ L_{\delta t}/V}{1/V + K_{n_z}\ L_{\delta t}/V}\ K_{n_z}\ \Delta\alpha + \frac{L_v/V}{1/V + K_{n_z}\ L_{\delta t}/V}\ K_{n_z}\ \Delta V$$

$$K_{n_z}\ \Delta n_z = K^*_\alpha\ \Delta\alpha + K^*_v\ \Delta V$$

where the terms K^*_α and K^*_v are the pseudo angle of attack and pseudo velocity

feedbacks.

$$K_\alpha^* = \frac{L_\alpha/V - K_\alpha L_{\delta t}/V}{1/V + K_{n_z} L_{\delta t}/V} \quad K_{n_z}$$

$$K_v^* = \frac{L_v/V}{1/V + K_{n_z} L_{\delta t}/V} \quad K_{n_z}$$

The above expressions are exact in terms of the transfer functions under the following conditions:

1. There are no engine, sensor, or other lags in the throttle feedback loop.

2. The only throttle feedbacks are angle of attack and normal acceleration, or alternatively there is no lift due to thrust.

3. The tail lift term is zero.

If we define the total angle of attack feedback as K'_α, then the case of a pure pseudo velocity feedback occurs when

$$K'_\alpha = K_\alpha + K^*_\alpha = 0$$

or $$K^*_\alpha = -K_\alpha$$

This condition is satisfied when

$$K_{n_z} = -\frac{K_\alpha}{V L_\alpha/V} = -\frac{K_\alpha}{n_{z_\alpha}}$$

3. System Parameters

Assume for the moment that the APCS design concept is to minimize speed excursions through feedbacks of the perturbation variables V, α, and θ. If the time lags associated with engine thrust response are ignored, the design goal could be met in a straightforward manner. In order to maintain constant velocity when the airplane changes its flight path, the thrust must be changed in magnitude by the gravity component of the airplane along its flight path. An attitude feedback with a gain such that

the g term of the upper right hand corner of the matrix (perturbation equations with V, α, and θ variables) is cancelled ($K_\theta = -g/D_{\delta t}$) will result in this steady state "decoupling" of airspeed from attitude as well as flight path angle perturbations. Transient decoupling could be obtained by the addition of an angle of attack feedback chosen to make the $(D_\alpha - g)$ term equal to zero. While these two feedbacks are sufficient, a similar relative effect could be obtained by greatly increasing the D_V term through a velocity feedback. This would reduce the effect of non-exact cancelling of the angle of attack and attitude terms of the matrix. Furthermore, the augmentation of the D_V term will improve the response time constant to airspeed errors.

Let us continue to assume that our goal is to minimize speed excursions and that we are reasonably successful. We can now focus our thoughts on the problem of controlling altitude or flight path angle and pitch attitude with the moment controller. Assuming, for simplicity, the tail lift $(L_{\delta e}/V)$ is negligible, the transfer functions of attitude and flight path angle reduce to:

$$\frac{\Delta\theta}{\Delta\delta_e} = \frac{M_{\delta e}\,(s + L_\alpha/V)}{s\left[s^2 + (-M_{\dot\alpha} - M_{\dot\theta} + L_\alpha/V)s + (-M_\alpha - M_{\dot\theta}\,L_\alpha/V)\right]}$$

$$\frac{\Delta\gamma}{\Delta\delta_e} = \frac{M_{\delta e}\,(L_\alpha/V)}{s\left[s^2 + (-M_{\dot\alpha} - M_{\dot\theta} + L_\alpha/V)s + (-M_\alpha - M_{\dot\theta}\,L_\alpha/V)\right]}$$

The important characteristics of the transfer functions can be expressed in terms of the short period frequency, ω_{sp}, and damping, ζ_{sp}, and the lift term, L_α/V. The latter may be considered as establishing the time constant of flight path angle to pitch attitude.

$$\Delta\gamma/\Delta\theta = (L_\alpha/V)/(s + L_\alpha/V) \qquad (1)$$

The range of the parameters ω_{sp}, ζ_{sp} and L_α/V which are conducive to precise and rapid control of attitude and flight path (altitude) has been treated in many studies and is well established (References 6, 7, & 8). The allowable range of these parameters as required by the Military Specification, Flying Qualities of Piloted Airplanes (MIL-F-8685B(ASG), Reference 9) is shown in Figure 3. Since the short period frequency and damping are primarily determined by moment derivatives, reasonably desireable values can be provided by an Automatic Flight Control System (AFCS) through the pitch controller if necessary. However, a direct lift controller is generally not available on aircraft to augment low values of the derivative L_α/V. Given the case of an aircraft with a relatively low value of L_α/V, desireable flight path control may not be realized although the APCS design goal was achieved.

Such situations have redirected the APCS design goal in recent years toward augmenting the flight path response at the expense of the speed response. Assume that some inclination of the thrust line to the flight path exists ($L_{\delta t}/V \neq 0$). In this case angle of attack feedback to the throttle will result in an augmentation of the values of both D_α and L_α/V of the basic aircraft. However, the typical inclination is small and large augmentation of the D_α term, with consequent airspeed coupling, will accompany moderate augmentation of the L_α/V term. As a result, a straightforward design for the APCS is not always evident due to the conflicting concepts and dynamic responses arising from the lack of an independent lift controller.

Historically, the early APCS designs were essentially configured to provide pseudo velocity feedback and minimize speed excursions. Current operational aircraft in this category are the A-4, A-6, and RA-5C. The

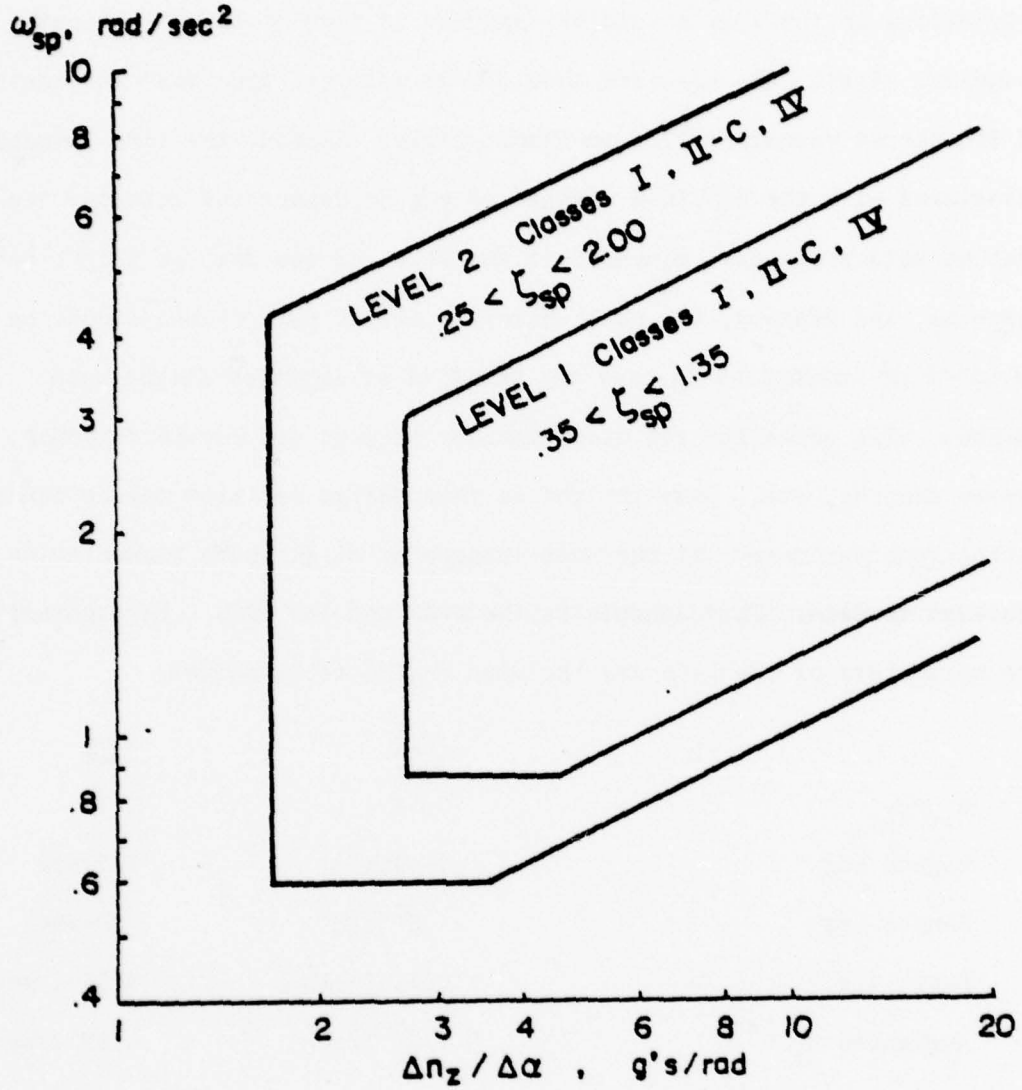

Figure 3. Short Period Frequency and Lift Curve Slope Requirements of Reference 9.

F-4B/J and the A-7E are examples where the objective was to provide augmentation of the flight path response.

As an initial design consideration, three factors are crucial in determining if the APCS should be designed to augment the flight path response. First, the aircraft should have a large "apparent" inclination of the thrust vector or lift to thrust ratio. Second, the time response associated with the combined effects of engine, sensor and actuator lags must be relatively fast compared to the level of the desired flight path response, and finally, the basic aircraft flight path response must be marginal or inadequate so that the benefits of improved flight path response will outweigh the disadvantages of gust and burble response, poor system damping, etc. Some insight in this design decision may be found by noting some parameters of the most successful flight path augmentation achieved to date. This example is the F-4B and its APCS. For comparison the parameters of the A-7E are included in the table below:

	F-4J	A-7E
$L_{\delta t}/D_{\delta t}$	0.34	0.19
Engine Lag	0.14 sec	1.7 sec
Sensor Lag	.5* sec	1.0 sec
Basic Aircraft L_α/V	0.31 1/sec	0.53 1/sec
Augmented L_α/V▲	$\sim$ 1.3* 1/sec	0.62 1/sec

*Nonlinear feedback and filtering

▲Ignoring system time lags

We have discussed thus far the capability of the APCS to minimize the airspeed excursions during flight path corrections, and to improve the flight path response. Elaborating on the former, the APCS improves the

apparent aircraft flight path stability from a "back side" to a "front side" throttle required vs airspeed situation. As defined in the Mil. Spec. (Reference 9), flight path stability is measured in terms of the flight path angle change where the airspeed is changed by the use of elevator control only. This level of flight path stability is related to the aircraft stability derivatives by the following steady state expression:

$$\Delta\gamma/\Delta V = -\frac{1}{D_\theta + g}\left[D_V - D_\alpha \frac{L_V/V}{L_\alpha/V} + \frac{D_{\delta e}}{M_{\delta e}} M_\alpha \frac{L_V/V}{L_\alpha/V}\right] \qquad (2)$$

A large negative value of this parameter is desired so that flight path corrections will not cause significant airspeed deviations. The current APCS feedbacks of angle of attack and normal acceleration provide the means to adjust D_V (through pseudo velocity feedback) and D_α. As noted previously, complete steady state decoupling is possible through an attitude feedback ($K_\theta \times D_{\delta t} = D_\theta = -g$).

The time history of any airspeed excursions will be related to the frequency and damping of the long term phugoid mode of the aircraft. An approximate characteristic equation for this mode is useful to provide an indication of the effect on the dynamic response of the aircraft from APCS augmentation of the stability derivatives:

$$s^2 + D_V s + (D_\theta + g) L_V/V = 0 \qquad (3)$$

It may be noted that this mode is relatively insensitive to an APCS angle of attack feedback whereas velocity feedback offers a favorable damping effect.

In the following brief paragraphs the effect of each of the current APCS feedbacks is discussed, based on the simplified equations previously

developed. The sense of the feedback is that shown in Figure 1.

$$K_\alpha \rightarrow D_\alpha, L_\alpha/V$$

The feedback will not appreciably alter the frequency or damping of the phugoid mode. A relatively small level of feedback is required for the purpose of decoupling speed from flight path maneuvering. Much larger levels of feedback are required to achieve any appreciable increase in the basic aircraft level of L_α/V and hence improve the flight path response. The attendent large levels of D_α will result in strong sensitivity to turbulence, and strong flight path/speed coupling.

$$K_V \rightarrow D_V, L_V/V$$

This feedback is favorable in terms of flight path stability, and increased damping of the phugoid mode. The control cross coupling tends to reduce L_V/V somewhat indicating a lower frequency phugoid oscillation.

$$K_{n_z}$$

This feedback may be interpreted as a combination of a pseudo angle of attack and pseudo velocity feedback. The level of flight path stability is not altered.

$$K_{\int\alpha}$$

An integral of angle of attack error is used for feedback in the current Navy APCS system as required by Reference 2 to remove static errors, provide steady state decoupling, and maintain a constant angle of attack stall margin in turns. The feedback tends to increase the frequency and

lower the damping of the phugoid mode, somewhat as suggested by the D_θ term of equation 3. A discussion of the equivalence between $K_{f\alpha}$ and K_θ may be found on page 41.

$$K_{\delta e} \rightarrow D_{\delta e},\ L_{\delta e}/V$$

This term represents a crossfeed of elevator to throttle. As such, there is no change in the frequency and damping of the phugoid mode of the aircraft. The flight path stability will be increased as indicated by the approximation. The possibility of obtaining a form of direct lift control is appealing but again, large levels of gain are required. The effective $L_{\delta e}/V$ with somewhat higher levels of gain is still small, typically changing the inherent adverse tail lift term to a slightly favorable value at the expense of strong flight path/speed coupling.

The effect on the airframe dynamics of the APCS feedbacks may also be seen in the root loci of Figure 14 on page 50 of the next section. The root loci are for an A-7E airframe with the simplifying conditions of zero control lift ($L_{\delta e}/V = L_{\delta t}/V = 0$) and zero engine and sensor time lags.

Reviewing the discussion thus far, an indication of the performance characteristics of an APCS can be made using several simple equations and the interpretation of the APCS feedbacks as augmentation of the aircraft stability derivatives. The equations suggest the APCS characteristics in the areas of flight path response (equation 1), flight path stability (equation 2) and the frequency and damping of the phugoid mode (equation 3). Finally, a normal acceleration feedback can be interpreted as a combination of pseudo angle of attack and pseudo velocity feedbacks.

In general, the simplified expressions will indicate the potential of the feedbacks in the absence of engine time lags and feedback filtering.

The analysis of the complete airframe/APCS with time lags and coupling terms will be made using analog computer generated time histories and through Bode frequency response analysis. Finally, although the parameters identified thus far, and others dealing with turn performance and burble response, may be calculated or known, the acceptability of an APCS and the relative tradeoffs must be assessed through pilot evaluation.

4. Preliminary Test Configurations

As an attempt to understand the tradeoffs and relative importance of the APCS performance parameters, a flight test evaluation of a matrix of APCS configurations was formulated. At this early stage of the investigation the configuration variations were based on orderly changes in the basic APCS feedback gains with variations which were felt to be significant to the pilot, particularly compared to the fine tuning changes which were made during the APCS development program for the A-7E shown in Table 1. The comments on the configurations of Table 1 were condensed from Reference 10. A partial listing of the configurations selected for this preliminary flight test investigation is presented in Table 2.

Configuration 0' of Table 2 is the A-7E APCS (Config. 6.12 of Table 1). The configuration series 7', 0', 6', 2' has essentially constant flight path stability. The variation of K_{n_z} in this series may be considered as changing the angle of attack feedback to a (pseudo) velocity feedback with consequent changes in the flight path response and the long period damping. The configuration series 1', 2', 3' and 1A', 2', 3A' were selected to vary the flight path stability at a fixed level of flight path response. Configuration 27A' is a true velocity feedback equivalent to the pseudo velocity configuration 2'. The variations in the integral of angle of attack feedback were made to evaluate both damping and turn performance. For the most

TABLE 1

HISTORY OF APCS GAINS ON A-7E/TF-41

Configuration	K_α	$K_{f\alpha}$	K_{n_z}	$K_{\delta e}$	τ_α	$\tau_{u/d}$	$\tau_{wo-u/d}$
	rad/rad	rad-sec/rad	rad/fps^2	rad/rad	sec	sec	sec
-3	5.7	2.0	.030	2.9	.35	0	2.3
-4	3.0	.72	.020	1.4	.35	0	2.3
5.1	4.9	1.1	.016	2.7	.30	0	2.3
5.2	3.7	.79	.016	2.6	.30	0	2.3
5.3	5.2	.79	.016	2.7	.30	0	2.3
5.4	5.2	.79	.016	1.9	.55	0	2.3
5.5	5.2	1.2	.016	1.9	.55	0	2.3
5.6	5.2	1.2	.022	1.9	.55	0	2.3
5.7	5.2	1.2	.022	2.3	.55	0	2.3
5.8	4.7	1.0	.019	2.3	.55	0	2.3
5.9(-5)	4.7	1.0	.016	2.3	.35	0	2.3
6.1	3.7/5.6	.79	.016	2.6	.85	.1/1.0	2.7/5.0
6.2	3.7/5.6	.81	.016	2.6	.55	.1/1.0	2.7/5.0
6.3	5.2	.78	.017	2.6	.55	.1/1.0	2.7/5.0
6.4	4.7	1.0	.016	2.9	.55	.1/1.0	7.0
6.5	4.7	1.0	.016	3.3	.55	.1/1.0	7.0
6.6	4.7	1.0	.016	3.7	.55	.1/1.0	7.0
6.7	4.7	1.0	.016	4.8	.55	.1/1.0	7.0
6.8	4.7	1.0	.016	4.1	.55	.1/1.0	7.0/7.5
6.9	4.7	.91	.016	4.1	.95	.1/ .98	7.0/7.5
6.10	4.7	.91	.016	4.1	.58	.1/ .95	7.0/6.5
6.11	4.6	.82	.016	4.1	.98	.1/ .90	7.0
6.12(-6)	5.5	.87	.015	4.4	.95	.1/ .90	7.0
6.13	5.5	.87	.047	4.4	.95	.1/ .90	7.0

TABLE 1 (Continued)

COMMENTS ON A-7E/TF-41 APCS CONFIGURATIONS

Configuration	
-3	TF-30 computer - acceptable manual, but unacceptable ACLS
-4	production model - unacceptable manual
5.1	not flown - incorrect values
5.2	corrections too slow, turn corrections slow
5.3	excessive throttle in turbulence - due to either α or δ_e
5.4	still excessive throttle, therefore problem is the α gain
5.5	better on turn but the AOA overshoots
5.6	turn degraded but acceptable - otherwise about the same (damping?)
5.7	still excessive throttle in turbulence
5.8	overall reduction of gains - poor glide slope performance
5.9	improved glide slope performance, excessive turbulence response, marginally acceptable manual
6.1	better than all previous configurations - poor on pitch up
6.2	reasonably good
6.3	about the same overall with single gain α
6.4	still poor on pitch up
6.5	a major improvement over 5.9 - due to δ_e
6.6	somewhat improved on low in close
6.7	too much throttle due to δe but OK performance
6.8	compromise δ_e gain
6.9	good low in close
6.10	excessive δ_t in turbulence with reduced time constant
6.11	near optimum shorebased
6.12	final system
6.13	pseudo V system - poor turn performance - same damping

TABLE 2

CONFIGURATION MATRIX FOR PRELIMINARY ANALYSIS

APCS FEEDBACK GAINS

Configuration	K_α	$K_{f\alpha}$	K_{n_z}	$K_{\delta e}$	K_v	K_{n_x}	K_θ
	rad/rad	rad-sec/rad	rad/fps^2	rad/rad	rad/fps	rad/fps^2	rad/rad
0'	5.47	.865	.0154	4.37	0	0	0
0A'	5.47	.865	.0154	0	0	0	0
1'	2.73	.865	.0237	4.37	0	0	0
1A'	2.73	.433	.0237	4.37	0	0	0
2'	5.47	.865	.0475	4.37	0	0	0
2A'	5.47	.865	.0475	6.55	0	0	0
3'	8.20	.865	.0712	4.37	0	0	0
3A'	8.20	1.300	.0712	4.37	0	0	0
4'	5.47	.433	.0475	4.37	0	0	0
5'	5.47	1.300	.0475	4.37	0	0	0
6'	5.47	.865	.0309	4.37	0	0	0
7'	5.47	.865	0	4.37	0	0	0
7A'	5.47	0	0	4.37	0	0	0
7B'	5.47	.433	0	4.37	0	0	0
8'	5.47	.865	0	2.18	0	0	0
8B'	5.47	.433	0	2.18	0	0	0
8C'	5.47	.433	0	6.55	0	0	0
9'	5.47	.865	.0309	6.55	0	0	0

TABLE 2 (Continued)

APCS FEEDBACK GAINS

Configuration	K_α	$K_{\int\alpha}$	K_{n_z}	$K_{\delta e}$	K_V	K_{n_x}	K_θ
	rad/rad	rad-sec/rad	rad/fps^2	rad/rad	rad/fps	rad/fps^2	rad/rad
10'	5.47	0	.0154	0	0	0	0
15'	5.47	.865	.0154	4.37	0	0	1.2
16'	5.47	.865	.0154	4.37	0	.0271	0
17'	5.47	.865	.0154	4.37	0	.0541	0
27A'	0	.865	0	4.37	.0135	0	0

Notes:

Input Filtering

τ_α = 1.0, $\tau_{\int\alpha}$ = 0, τ_{n_z} = 1.0, $\tau_{\delta e}$ = .5 with 7.0 washout, τ_V = 1.0, τ_{n_x} = 0, τ_θ = 1.0

α corrected for upwash factor of 1.4

g $\Delta T/W/\delta t$ = 26.6 ft/sec^2/rad

part we will not consider the subject of turn performance in this report; however, a brief discussion is presented on page 90. It might be noted that Configurations 0', 6' and 2' correspond to Configuration 6:12 (identically configuration 0'), -3, and 6:13 of Table 1 of the A-7E APCS development program.

Both time histories and frequency response plots (jω-Bodes) of the configurations of Table 2 were made. The time histories in Section 1 of Appendix A include the response to step inputs of δ_e, θ_c and APCS engagements with a 1 degree angle of attack offset. The attitude hold mechanization is that shown in Figure 2 and is essentially that used in the Automatic Carrier Landing System for the A-7E. Bode plots for the configurations of the γ/θ_c, γ/δ_e and V/δ_e are presented in Section 2 of Appendix A.

The following may be noted upon inspection of the analog time histories of the response to a θ command:

1. The θ_c steps result in nearly identical initial α disturbances regardless of the γ response.

2. Using the time to 0.90 γ_{ss} as an indicator of flight path response, the effectiveness of the δ_e and α feedbacks may be noted. The effect of the δ_e input is best seen from comparisons between configurations of the sets 0A'/0', 8B'/8C', and 8'/7'. For example, in the first case the ratio of the times required to reach 0.90 γ_{ss} is greater than 4/3.

3. The effective α feedback is considered as the sum of the α and pseudo α feedbacks ($K'_\alpha = K_\alpha + K^*_\alpha$). In this respect Configurations 2', 6', 0' and 7' represent a steadily increasing feedback. Again, an improvement in the response time is observed.

4. The γ response improvement between Configuration 2' and 7' is not without expense in terms of damping and γ overshoot. Configuration 7' has

near neutral damping with an initial overshoot in the γ response of about 35%. Even the current Navy system (Configuration 0') has about 25% overshoot with very light damping. The pseudo V Configuration 2' has little overshoot and good damping.

The γ/θ_c Bodes of the configuration show that the APCS feedbacks have little effect on the response above 1 rad/sec frequency. This is not surprising since the engine time lag is 1.7 seconds. The improvement in the bandwidth of control is not noticeably altered in the configuration series 2', 6', 0', 7' (steadily increasing effective α feedback). The reduction in damping with the configuration series is quite noticeable. Much of the "apparent" improvement in flight path response noted in the time histories is that associated with the light damping.

The flight tests were made with the Princeton Variable Stability Navion. An accurate simulation of the A-7E and its APCS had been demonstrated in a previous program (Reference 1). Briefly, this simulation included the nonlinear engine response to throttle (gain and time constant, average time constant of 1.7 seconds), the lift curve slope and cross lift terms, drag characteristics, stick forces and geometry, angle of attack presentation and indexer, and the dual time constant input to the APCS. The simulation corresponded to the YAW STAB "on", CONT AUG "off" mode of the flight control system (Reference 5). Closure speed and aerodynamic approach angle were duplicated. The noteable limitations of the simulation for this phase of testing were the lack of turbulence and burble simulation, and a stationary (nonheaving) carrier.

The evaluation pilot was one of the Princeton University staff pilots. This pilot had considerable experience in handling qualities evaluations and was carrier qualified, but lacked experience in APCS techniques.

Initially the pilot was reluctant to note differences in configurations; however, with additional flight experience the pilot became quite perceptive. The baseline Configuration 0' was rated as 3.5 to 4.0 on the Cooper-Harper scale. The most improvement, of the order of ½ a Cooper-Harper unit, was obtained with Configurations 2' and 27A'. This was attributed to an improvement in the smoothness of operation of the throttle and apparent closed loop damping ratio. The pilot was also aware of differences between Configurations 2' and 27A'. "In smooth air Configuration 2' is a little better than 27A'." The reason for this, based on other pilot commentary, may be related to slightly better resolution of the angle of attack sensor over that of the velocity transducer. The quoted resolution of the velocity transducer was ½ knot. Under the conditions of external turbulence Configuration 27A' was better than 2.' This effect may be explained by assuming isotropic turbulence (same vertical and horizontal disturbances) and evaluating the effect of local turbulence on the sensors.

The relation between airspeed and angle of attack for trimmed perturbations from the approach condition for the A-7 is such that 7 ft/sec is equivalent to 1 degree. If we are concerned with the steady state error due to sensor resolution, the relative measurement accuracy requirements are in the same ratio. For example, a velocity transducer of ± .7 ft/sec or an angle of attack transducer of ± .1 degree resolution would be equivalent. In the case of local turbulence disturbances a 7 ft/sec vertical gust corresponds to an angle of attack gust of 1.8 degrees at the A-7 approach speed. If the same effective feedback is used the angle of attack transducer will generally be more sensitive to turbulence disturbances since the aircraft approach speed generally exceeds the value $2g/(L_\alpha/V)$, (see p. 52 for further discussion).

A point of particular interest during these preliminary evaluations was the effect of the APCS on flight path augmentation. The pilot was questioned specifically about the relative differences in this respect of Configurations $0'$ vs either Configuration $2'$ or $27A'$ during the test. The pilot was not able to detect differences of the type attributable to augmentation of the derivative L_α/V.

Unfortunately, Patuxent (NATC) pilots were not available to evaluate the configurations. On an informal basis an A-7 pilot who was stationed nearby agreed to fly the simulator aircraft. Although this provided the opportunity for a more critical evaluation of the A-7E/APCS simulation, no analytical data was generated as the pilot could not distinguish differences between Configurations $0'$, $2'$, and $27A'$.

In the time period between these preliminary evaluations and the next phase of investigation, the analytical methods were refined and a burble and turbulence simulation were incorporated into the in-flight simulator aircraft.

The conclusions of the preliminary phase of the investigation were the following:

1. Large improvements in the overall handling qualities of the airplane (A-7E) are not likely to result from improvements in the APCS design alone.

2. Flight path controllability was the major concern of the pilot. Significant augmentation of this parameter through the APCS cannot be achieved (on the A-7E).

3. The APCS performance tradeoffs are complex and can only be established through pilot opinion with user personnel.

Although some progress could be made pursuing complete APCS design, it was felt that more thought should be given to the relative importance of the aircraft dynamics and the APCS. In the absence of NATC evaluation pilots it was decided to pursue a more theoretical approach to the overall problem of controlling flight path with a single controller. The theoretical or idealized study in the next section is concerned with systems which provide a near optimum transfer function for pilot control of altitude.

FLIGHT PATH CONTROL SYSTEMS

1. Introduction

It is apparent that the augmentation of the flight path response by the APCS is critically dependent on the basic airframe, in particular the lift to thrust ratio and the response time lags of the engine. In this section we will consider the limiting case of zero engine derived lift ($L_{\delta t}/V = 0$) and examine the possibility of flight path controllability improvement by other means. One method would be to use feedbacks or pilot inputs to a direct lift control (DLC) surface (Reference 11). Since such an option is not generally available, only changes in the pitch control (Pitch AFCS) will be considered.

Two augmentation schemes will be examined: an attitude command inner loop such as shown in Figures 1 and 2, and a washout prefilter on the pilot's stick input. A simplified outer throttle control loop or APCS will be used with both systems.

The purpose of the outer loop or APCS part of either system is to minimize the airspeed excursions. In order to maintain constant velocity when the airplane changes its flight path, the thrust has to be changed in magnitude by the gravity component of the airplane along the flight path. This decoupling feature is obtained by a $\Delta\theta$ to $\Delta\delta_t$ feedback which, in the case of the A-7E, has the following value.

$$K_\theta = \Delta\delta_t/\Delta\delta_e = -g/D_{\delta t} = 1.21 \text{ (rad/rad)}$$

A velocity feedback to the throttle is used to provide an adequate level of flight path stability and to minimize transient velocity changes caused by the transient angle of attack excursions. The level chosen, $K_V = \Delta\delta_t/\Delta V = -.0135$ (rad/fps), is equivalent to the flight path stability

level of the current APCS on the A-7E. To simplify the analysis, no filters are used on these APCS feedbacks.

2. Attitude Command System

The attitude or θ command system uses $\Delta\theta$ and $\Delta\dot{\theta}$ to $\Delta\delta_e$ feedbacks to improve the short period mode inner loop, with a simplified APCS outer loop. This system is displayed in block diagram form in Figure 4.

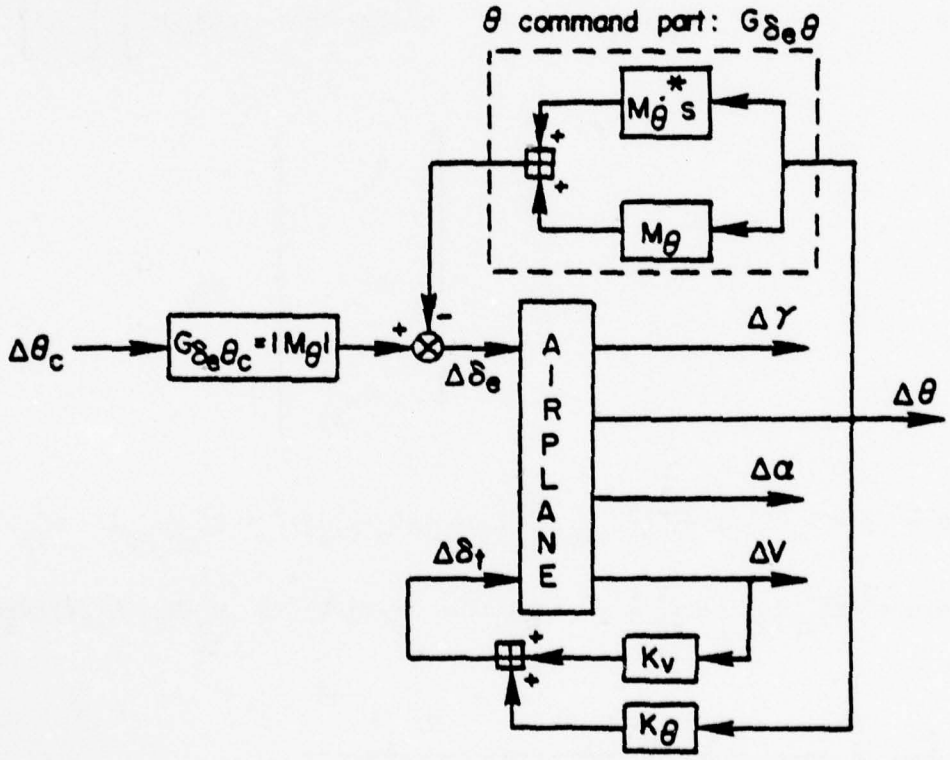

Figure 4. θ Command Configuration

The characteristic equations and the transfer functions of $\Delta\gamma$, $\Delta\theta$, and ΔV due to the control stick input or the pitch attitude command will be expressed as follows:

$$\begin{bmatrix} s+D_V+K_V D_{\delta t} & -(D_\alpha-g) & D_\alpha+(-g) \\ L_V/V & -(s+L_\alpha/V) & L_\alpha/V \\ 0 & M_{\dot\alpha}s+M_\alpha & s^2-(M_{\dot\alpha}+M_{\dot\theta}+M_{\dot\theta}^*)s-M_\alpha-M_\theta \end{bmatrix} \begin{bmatrix} \Delta V \\ \Delta\gamma \\ \Delta\theta \end{bmatrix} = \begin{bmatrix} 0 \\ 0 \\ |M_\theta|M_{\delta e} \end{bmatrix} \Delta\delta_s \tag{4}$$

$$\Delta \cong (s + L_\alpha/V)\{s + D_V+K_V D_{\delta t} - (L_V/L_\alpha)(D_\alpha-g)\}(s^2 + 2\zeta_{sp}\omega_{sp}s + \omega_{sp}^2)$$

where $s^2+2\zeta_{sp}\omega_{sp}\, s+\omega_{sp}^2 \cong s^2 + (L_\alpha/V) - M_{\dot\alpha}-M_{\dot\theta}-M_{\dot\theta}^*)s-\{M_\alpha+M_\theta+(L_\alpha/V)(M_{\dot\theta}+M_{\dot\theta}^*)\}$

$$\frac{\Delta\gamma}{\Delta\delta_s} \cong \frac{|M_\theta|M_{\delta e}\ L_\alpha/V}{(s + L_\alpha/V)(s^2 + 2\,\zeta_{sp}\omega_{sp}s + \omega_{sp}^2)} \tag{5}$$

$$\frac{\Delta\theta}{\Delta\delta_s} \cong \frac{|M_\theta|M_{\delta e}}{s^2 + 2\,\zeta_{sp}\omega_{sp}\, s + \omega_{sp}^2} \tag{6}$$

$$\frac{\Delta V}{\Delta\delta_s} \cong \frac{|M_\theta|M_{\delta e}(D_\alpha - g)s}{(s + L_\alpha/V)\{s + D_V+K_V D_{\delta t} - (L_V/L_\alpha)(D_\alpha-g)\}(s^2 + 2\zeta_{sp}\omega_{sp}s + \omega_{sp}^2)} \tag{7}$$

The corresponding approximate jω-Bode gain diagrams are shown in Figure 5.

It may be noted that the Δγ and Δθ responses are almost independent of the APCS part as noticed in equations 5 and 6. The Δγ response is nearly first order with a time constant equal to $1/(L_\alpha/V)$ (sec), and Δθ response is approximately the short period with a bandwidth of the short period frequency. The ΔV response depends on L_α/V and ω_{sp} but will effect only the higher frequency part of the diagram. In other words, the +20 db/dec slope in the lower frequency part of the ΔV diagram in Figure 5 has accomplished the steady state, or low frequency, decoupled tendency, and L_α/V and ω_{sp} affect only the transient response of ΔV. This effect will later be shown to be negligible; accordingly, the velocity response will not be discussed at this time.

Reviewing the equations 5 and 6, it will be seen that the flight path controllability will depend on L_α/V, ζ_{sp}, ω_{sp}, and $M_{\delta e}$. For the carrier approach task a wide bandwidth of flight path (Δγ) response is desired to permit precise tracking of the optical landing aid, particularly under the conditions of a heaving carrier and turbulence (Reference 3). The effect of L_α/V and ω_{sp} on the bandwidth is apparent in Figure 5. In the absence of a means of augmenting L_α/V (through DLC) some improvement in bandwidth may be possible through augmentation of ω_{sp}. In the case of the A-7E an increase in the short period frequency could be made without exceeding the boundaries of Reference 9 as shown in Figure 6. In fact, even greater values may be acceptable based on the data of Reference 8.

It might be noted that an increase in the short period frequency could also be obtained by augmenting the apparent static stability M_α rather than through M_θ. The attitude feedback case has the advantage of

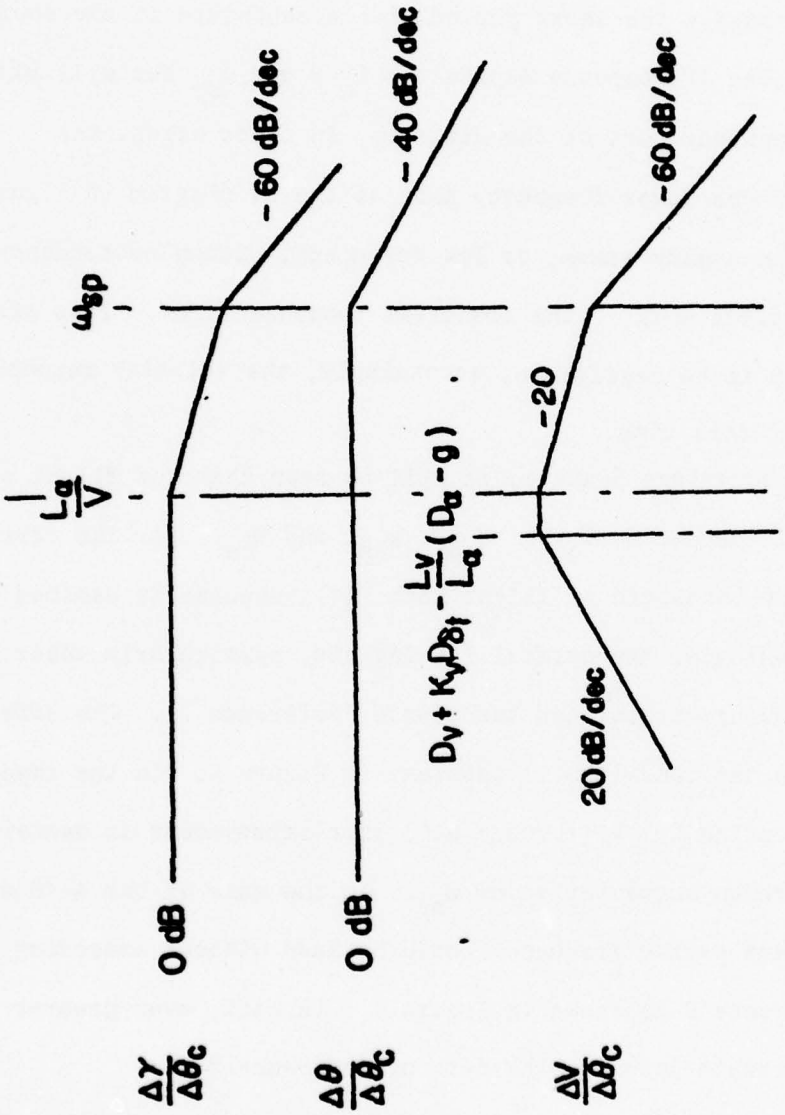

Figure 5. Approximate jω-Bode Gain Diagram of θ Command System (Asymptotic expression)

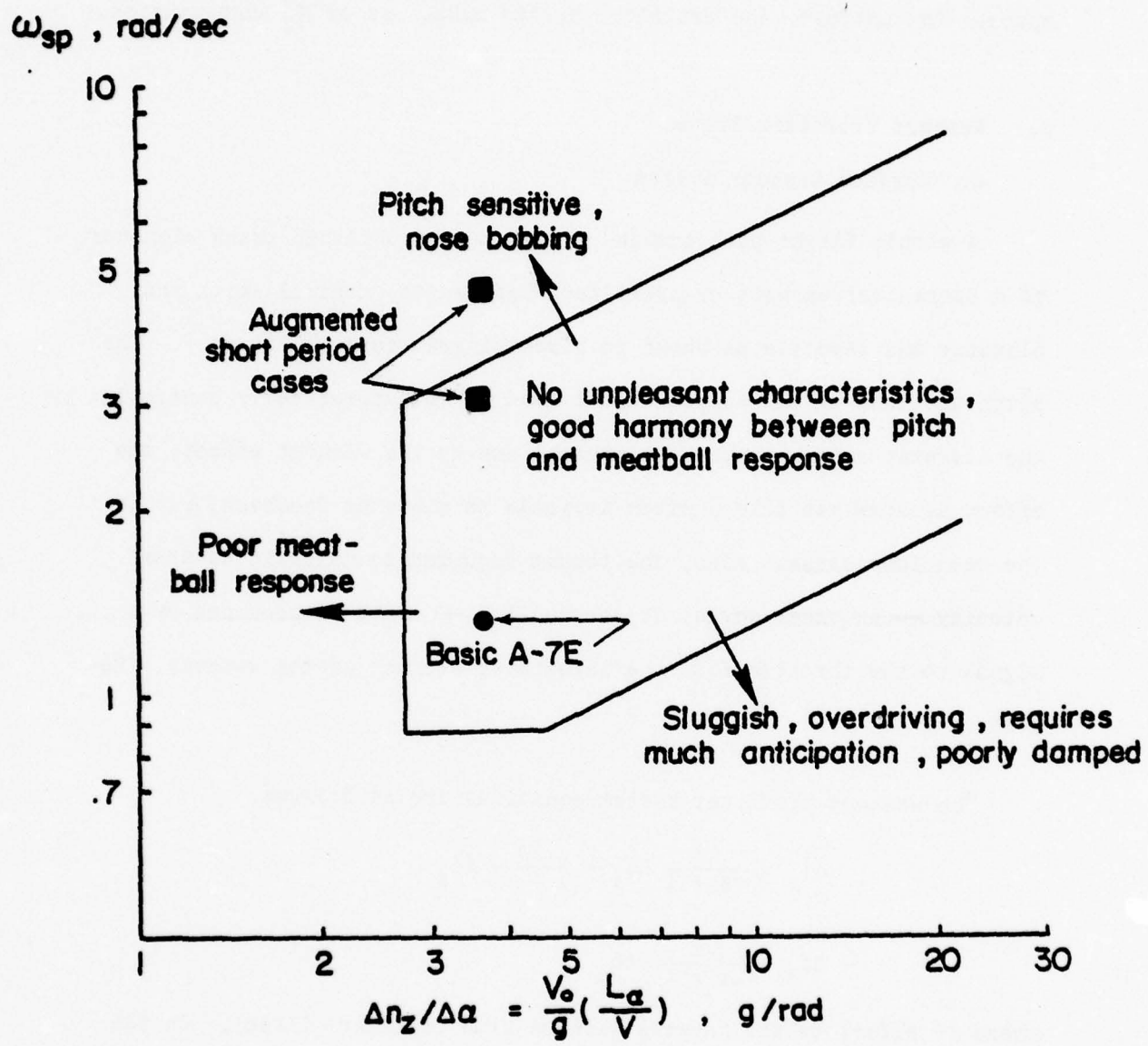

Figure 6. Effects of L_α/V and ω_{sp} to Carrier Approach Controllability (Reference 7)

gust alleviation since it stabilizes the airplane with respect to inertial space. In contrast, the prefilter system makes use of M_α augmentation.

3. Washout Prefilter System

a. Surface Washout System

A simple flight path command system can be obtained using elements of a controller washout or prefilters between the control stick and elevator and throttle as shown in block diagram form in Figure 7. The pitch attitude of the airplane will tend to be automatically controlled by the elevator being restored to neutral due to the washout effect; the effect is somewhat like a pitch attitude to elevator feedback, but in the open loop sense. Also, the thrust required to maintain constant velocity — in other words, for decoupling — could be provided by a signal to the throttle from the integrator element of the washout. (Reference 12).

The washout prefilter system equations are as follows.

$$\Delta\delta_e = \frac{\tau s}{\tau s + 1}\,\Delta\delta_s = \frac{s}{s + \tau'}\,\Delta\delta_s$$

$$\Delta\delta_t = \frac{-1}{\tau s + 1}\,\Delta\delta_s$$

where τ' refers to the inverse washout time constant (1/sec). In the APCS part a ΔV to $\Delta\delta_t$ feedback is used in order to obtain the same "frontsidedness" or flight path stability as the θ command system, and the $\Delta\theta$ to $\Delta\delta_t$ feedback, as shown by the dashed line in Figure 7, replaces the washout to the throttle (A) in order to preserve the same decoupled characteristics for comparison.

The $\Delta\alpha$ and $\Delta\dot{\theta}$ to $\Delta\delta_e$ feedback are used to maintain basically the same inner loop controllability as the θ command system. Therefore, the $\Delta\alpha$

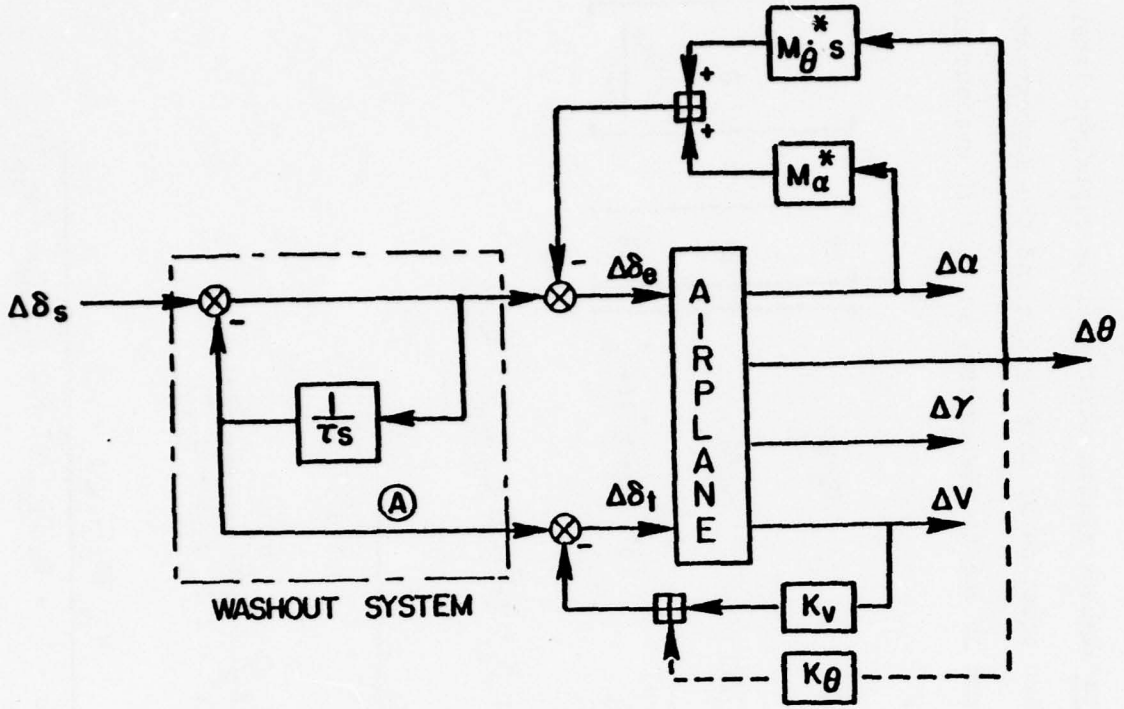

* refers to equivalent stability derivative as feedback gain

τ refers to washout time constant (sec)

– – – – refers to modified decoupled loop ($\Delta\theta \rightarrow \Delta\delta_t$) instead of loop Ⓐ

Figure 7. Surface Washout Configuration

to $\Delta\delta_e$ feedback gain (M_α^*) is chosen as numerically equal to M_θ in the θ command system, and the same $M_{\dot\theta}^*$ is used for both systems. The significant aspect of the washout system is that a given flight path response bandwidth can be obtained through selection of the washout time constant.

The system shown in Figure 7 is a surface washout system as distinguished from the force washout system which will be explained later.

The characteristic equation of this system and the approximate transfer function of $\Delta\gamma$, $\Delta\theta$, and ΔV due to the control stick with washout are expressed as follows.

$$\begin{bmatrix} s+D_V+K_V D_{\delta t} & -(D_\alpha-g) & D_\alpha-g \\ L_V/V & -(s+L_\alpha/V) & L_\alpha/V \\ 0 & M_\alpha^{\bullet}s+M_\alpha^* & s^2-(M_\alpha^{\bullet}+M_{\dot\theta}^*)s-M_\alpha^* \end{bmatrix} \begin{bmatrix} \Delta V \\ \Delta\gamma \\ \Delta\theta \end{bmatrix} = \begin{bmatrix} 0 \\ 0 \\ \dfrac{s\,M_{\delta e}}{s+\tau'} \end{bmatrix} \Delta\delta_s$$

$$\Delta \cong -s(s + D_V + K_V D_{\delta t})(s^2 + 2\zeta_{sp}\omega_{sp}s + \omega_{sp}^2) \tag{8}$$

$$\frac{\Delta\gamma}{\Delta\delta_s} \cong \frac{M_{\delta e}\, L_\alpha/V}{(s + \tau')(s^2 + 2\zeta_{sp}\omega_{sp}s + \omega_{sp}^2)} \tag{9}$$

$$\frac{\Delta\theta}{\Delta\delta_s} \cong \frac{M_{\delta e}\,(s + L_\alpha/V)}{(s + \tau')(s^2 + 2\zeta_{sp}\omega_{sp}s + \omega_{sp}^2)} \tag{10}$$

$$\frac{\Delta V}{\Delta\delta_s} \cong \frac{M_{\delta e}\,(D_\alpha - g)s}{(s + \tau')(s + D_V + K_V D_{\delta t})(s^2 + 2\zeta_{sp}\omega_{sp}s + \omega_{sp}^2)} \tag{11}$$

The corresponding approximate $j\omega$-Bode gain diagram is shown in Figure 8.

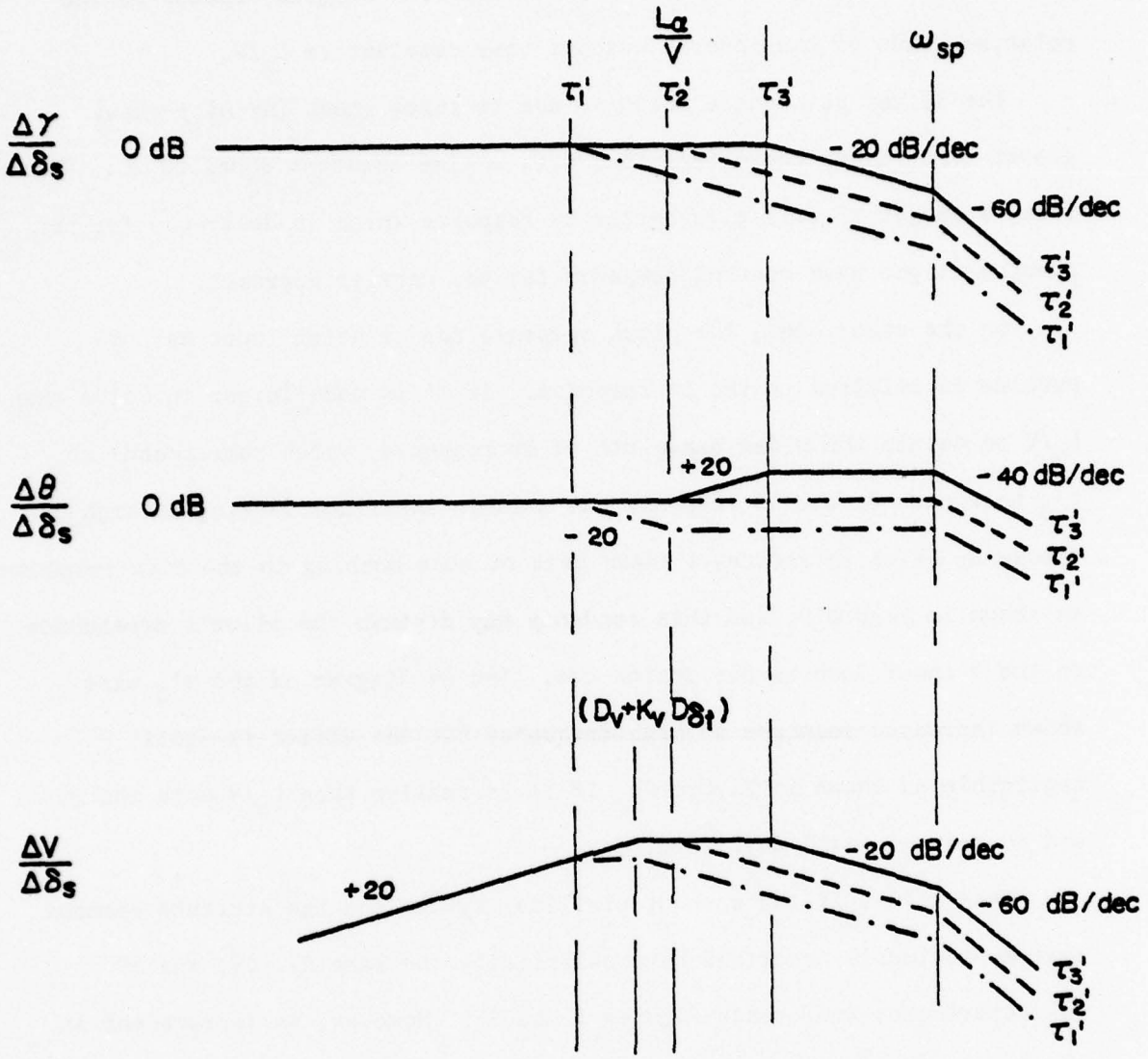

Figure 8. Approximate jω-Bode Gain Diagram of Surface Washout System for Different Inverse Washout Time Constants

As shown in Figure 8, the shape of the Bode diagram depends on the relative value of the inverse washout time constant to L_α/V.

The flight path angle response due to stick input ($\Delta\gamma/\Delta\delta_s$) shows almost first order characteristics with a time constant equal to τ'. Therefore, a larger τ' will give better $\Delta\gamma$ response which is desirable for the precise flight path control demanded for the carrier approach.

On the other hand, the pitch response due to stick input has a problem in relation to the $\Delta\gamma$ response. If τ' is made larger in value than L_α/V to obtain the wider bandwidth of $\Delta\gamma$ response, which corresponds to τ'_3 in Figure 8, the $\Delta\theta$ response has a large amplitude peaking at high frequency which introduces a sharp peak or nose bobbing in the time response. as shown in Figure 9, and this tendency may disturb the pilot's dependence on the θ inner loop as his motion cue. The ΔV diagram of the τ'_3 case shows increased response at high frequency but the effect is still negligible as shown in Figure 9. If τ' is smaller than L_α/V both the $\Delta\gamma$ and $\Delta\theta$ response will deteriorate.

When $\tau' = L_\alpha/V$ the washout prefilter system and the attitude command system previously described have essentially the same $\Delta\gamma$, $\Delta\theta$, and ΔV characteristics (reference Figures 5 and 8). However, an improvement in the $\Delta\gamma$ response is possible with the washout prefilter system at the expense of high frequency attitude control problems by increasing τ'.

b. Force Washout System

An interesting variation of the prefilter concept is obtained by replacing the surface washout by a <u>force</u> washout which has the feedback proportional to the integration of the applied force of the pilot. The block diagram is represented in Figure 10. The feedback force is provided by the mechanized hydraulic control stick servo. The system transfer

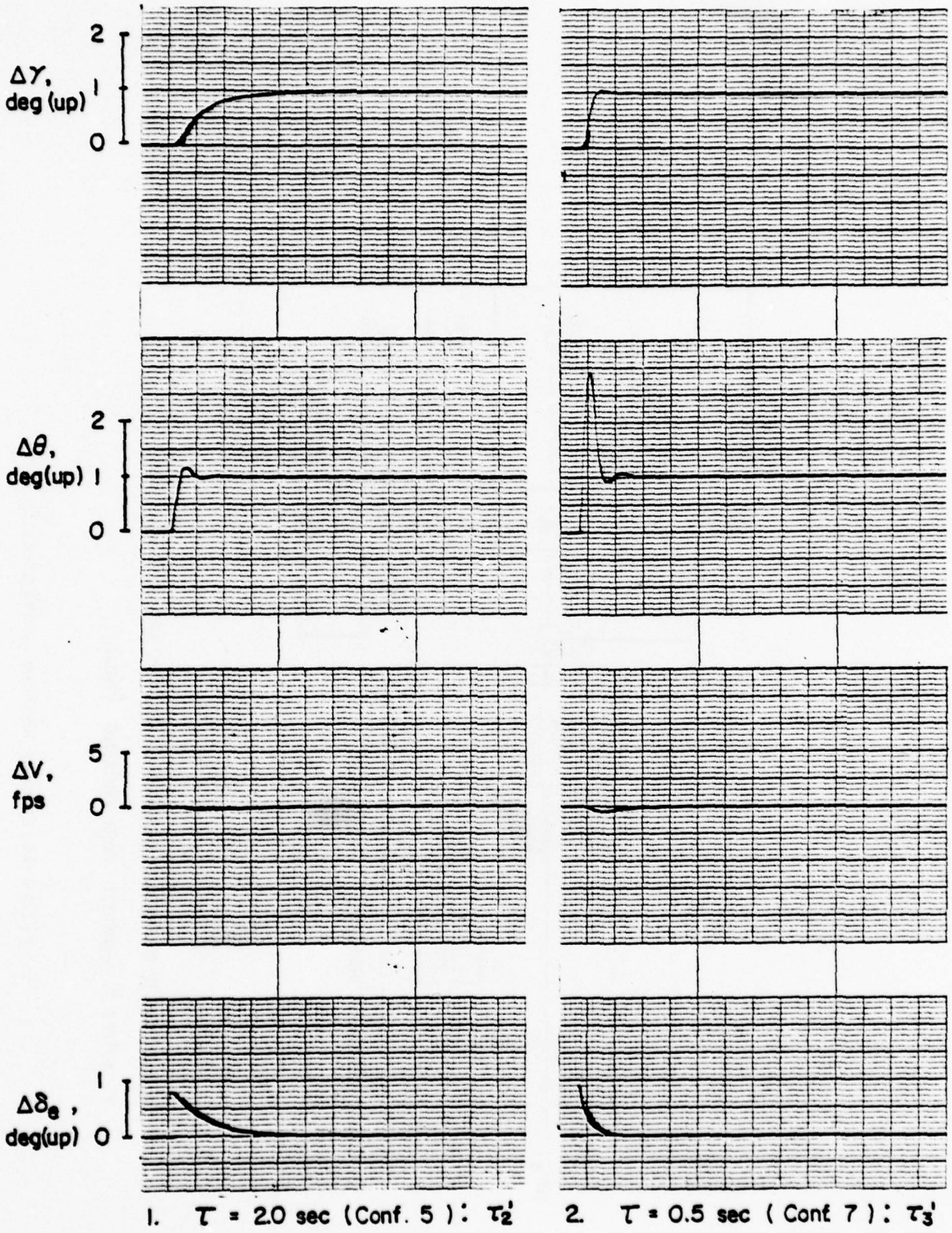

Figure 9. Effect of τ, Time Responses due to Step Stick Input of Washout Prefilter System

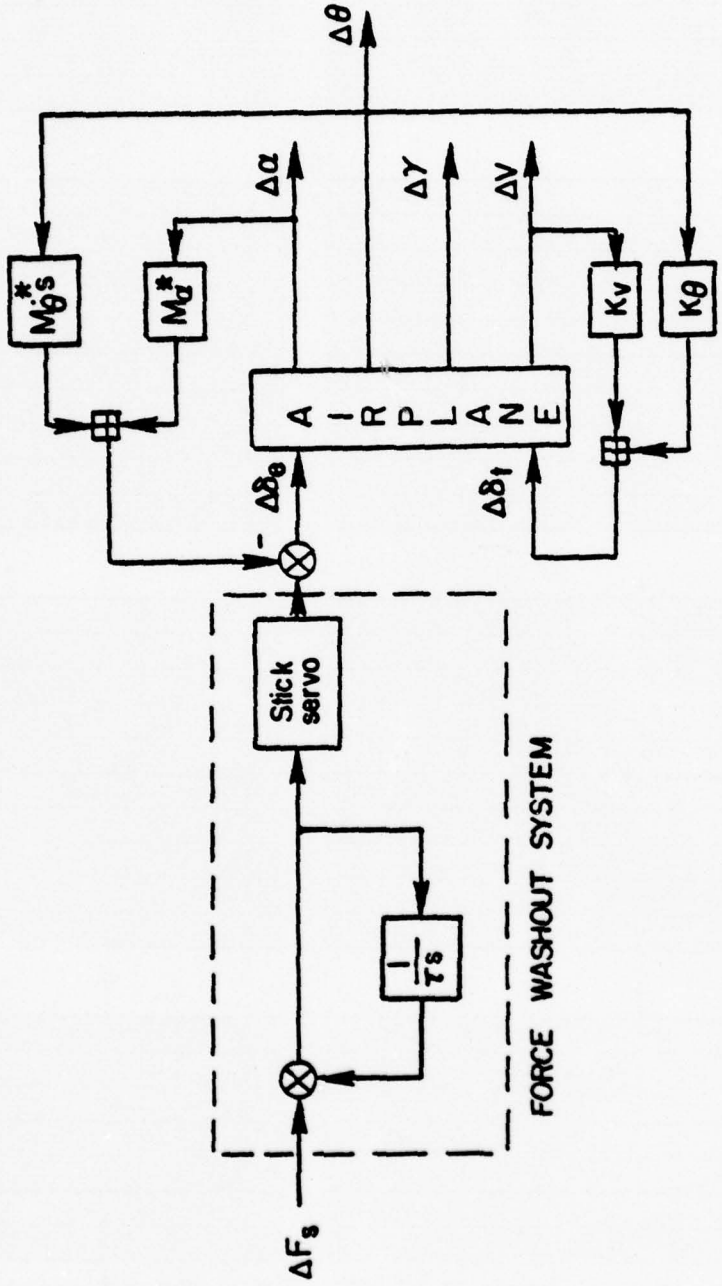

* refers to equivalent stability derivative as feedback gain

τ refers to washout time constant (sec)

Figure 10. Force Washout Configuration

function is basically the same as the surface washout case except $\Delta\delta_s$ is replaced by ΔF_s in Figure 7 and in equations 9-11. Likewise, the $j\omega$-Bode diagrams are identical.

The system behavior is such that when the pilot displaces the stick a fixed amount, he feels a steadily building force which tends to restore the stick to center. This feedback force is proportional to the integration of the stick offset from center. If the applied force is constant the stick movement is similar to the elevator movement of the surface washout. In the force washout case the movement of the control stick and surface positions are directly related, providing the pilot with a "position" indication of the input by the system akin to a parallel servo mechanization. In the surface washout case the system inputs are inserted in series between the control stick and the surface such that the pilot is not aware of the washout.

4. Speed Decoupling-System (APCS)

If the airplane is to maintain constant velocity with changes in flight path angle, the thrust must be changed in magnitude by the gravity component of the airplane weight along the flight path. This type of thrust compensation can be obtained through a K_θ feedback.
In current Navy APCS designs the thrust change is accomplished by the integration of the angle of attack error ($K_{\int\alpha}$). An analogous relationship between these two feedbacks can be shown.

Assume that the pitch attitude hold loop is tightly closed; that is, the steady state pitch angle response due to elevator can be obtained immediately. The trajectory of the flight path cannot be changed in direction abruptly because of the inertia of the airplane; consequently, the flight path will have a curvature during the transient motion as shown in Figure 11, and the velocity vector which is tangent to the flight

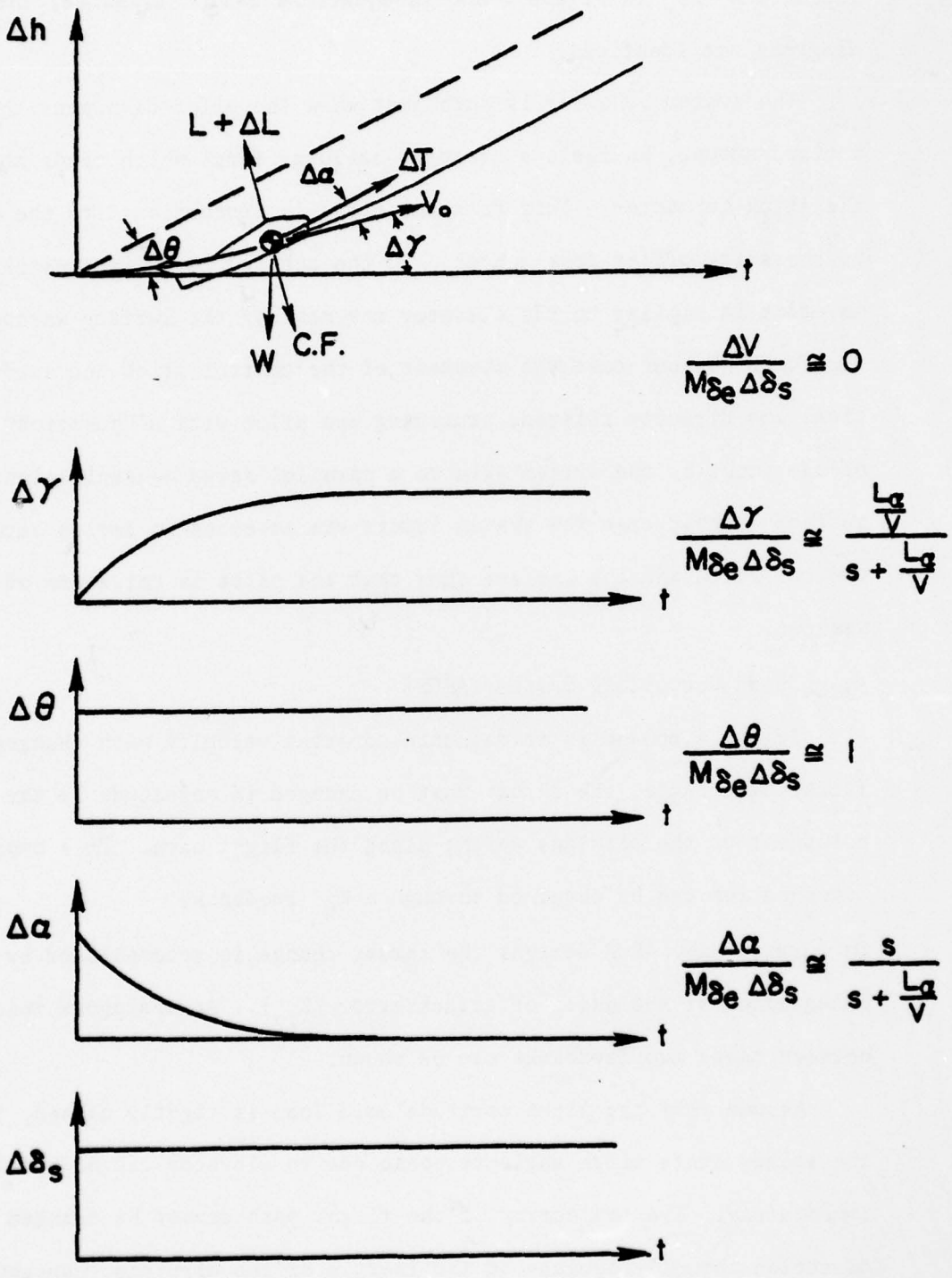

Figure 11. Transient Motion due to Flight Path Change

path will make a transient angle of attack excursion as shown in Figure 11. This $\Delta\alpha$ produces the transient lift increment ΔL which is balanced by the centrifugal force caused by the flight path curvature; that is

$$\left(\frac{\partial L}{\partial \alpha} \right) \Delta\alpha = \Delta L = C.F. = mV \frac{d(\Delta\gamma)}{dt}$$

$$\frac{d(\Delta\gamma)}{dt} = \frac{d(\Delta\theta)}{dt} - \frac{d(\Delta\alpha)}{dt}, \quad \text{since } \frac{d(\Delta\theta)}{dt} = 0$$

$$\left(\frac{L_\alpha}{V} \right) \Delta\alpha = - \frac{d(\Delta\alpha)}{dt}$$

$$\left(\frac{L_\alpha}{V} \right) \int_0^t (\Delta\alpha)\, dt = - \Delta\alpha$$

On the other hand, the force equilibrium along the thrust axis to maintain constant velocity is

$$\Delta T - W\Delta\theta + L\Delta\alpha = 0, \quad \text{since } L = W$$

$$\left(\frac{1}{m} \right) \Delta T = D_{\delta t}\, \Delta\delta_t = g\Delta\theta + g \frac{L_\alpha}{V} \int \alpha\, dt$$

$$\Delta\delta_t = \left(\frac{g}{D_{\delta t}} \right) \Delta\theta + \left(\frac{g\,(L_\alpha/V)}{D_{\delta t}} \right) \int \alpha\, dt$$

As expressed above the possible means of compensation are obtained in such a way as $\Delta\theta \rightarrow \Delta\delta_t$ or $\int\alpha\, dt \rightarrow \Delta\delta_t$, or the combination of these two. If these are used individually, each value of the feedback gain should satisfy the following numbers in the case of the A-7E.

$$K_\theta = -g/D_{\delta t} = 1.21 \text{ (rad/rad)}$$

$$K_{\int\alpha} = -g(L_\alpha/V)/D_{\delta t} = 0.642 \text{ (rad/sec-rad)}$$

The integration of the angle of attack error in effect computes the change in pitch angle of the airplane. To overwork the use of the adjective, we might say that the feedback $K_{\int\alpha}$ is a pseudo attitude feedback.

The relation between the two feedbacks could also be derived from examination of the ΔV transfer function. If the feedbacks K_v, K_θ and $K_{\int\alpha}$ are included, the ΔV transfer function becomes:

$$\frac{\Delta V}{\Delta \delta_s} \cong \frac{|M_\theta| M_{\delta e} s\left[(D_\alpha + K_\theta D_{\delta t})s + (L_\alpha/V)(g + K_\theta D_{\delta t}) + K_{\int\alpha} D_{\delta t}\right]}{(s + \frac{L_\alpha}{V})\left[s^2 + \{D_v + K_v D_{\delta t} - \frac{L_v}{L_\alpha}(D_\alpha + K_\theta D_{\delta t})\}s - \frac{L_v}{L_\alpha} K_{\int\alpha} D_{\delta t}\right](s^2 + 2\zeta_{sp}\omega_{sp}s + \omega_{sp}^2)}$$

In the above expression the denominator is approximately factored but the numerator is calculated exactly. The following points may be determined by examination of the above equation:

1. Any nonzero $K_{\int\alpha}$ will provide zero steady state velocity response since there will be a free zero in the numerator (reference examples Figures 12a and 12d).
2. If $K_{\int\alpha}$ is zero, the steady state velocity response is not automatically zero because a free zero in the numerator will be cancelled by a free zero of the denominator. In this case, only $K_\theta = -g/D_{\delta t} = 1.21$ (rad/rad) would make the steady state velocity response zero (reference Figure 12c).
3. If the decoupling value of K_θ is not used (item 2), then any nonzero value of $K_{\int\alpha}$ could be used to provide steady state decoupling. However, a reduced level of transient velocity response is suggested for values of $K_{\int\alpha}$ for which the constant part of the numerator of the transfer function is zero or

$$L_\alpha/V\ (g + K_\theta D_{\delta t}) + K_{\int\alpha} D_{\delta t} = 0$$

The above relationship corresponds to the one derived from flight path equilibrium considerations. Possible cases satisfying this condition are shown in the following figure (reference Figure 13).

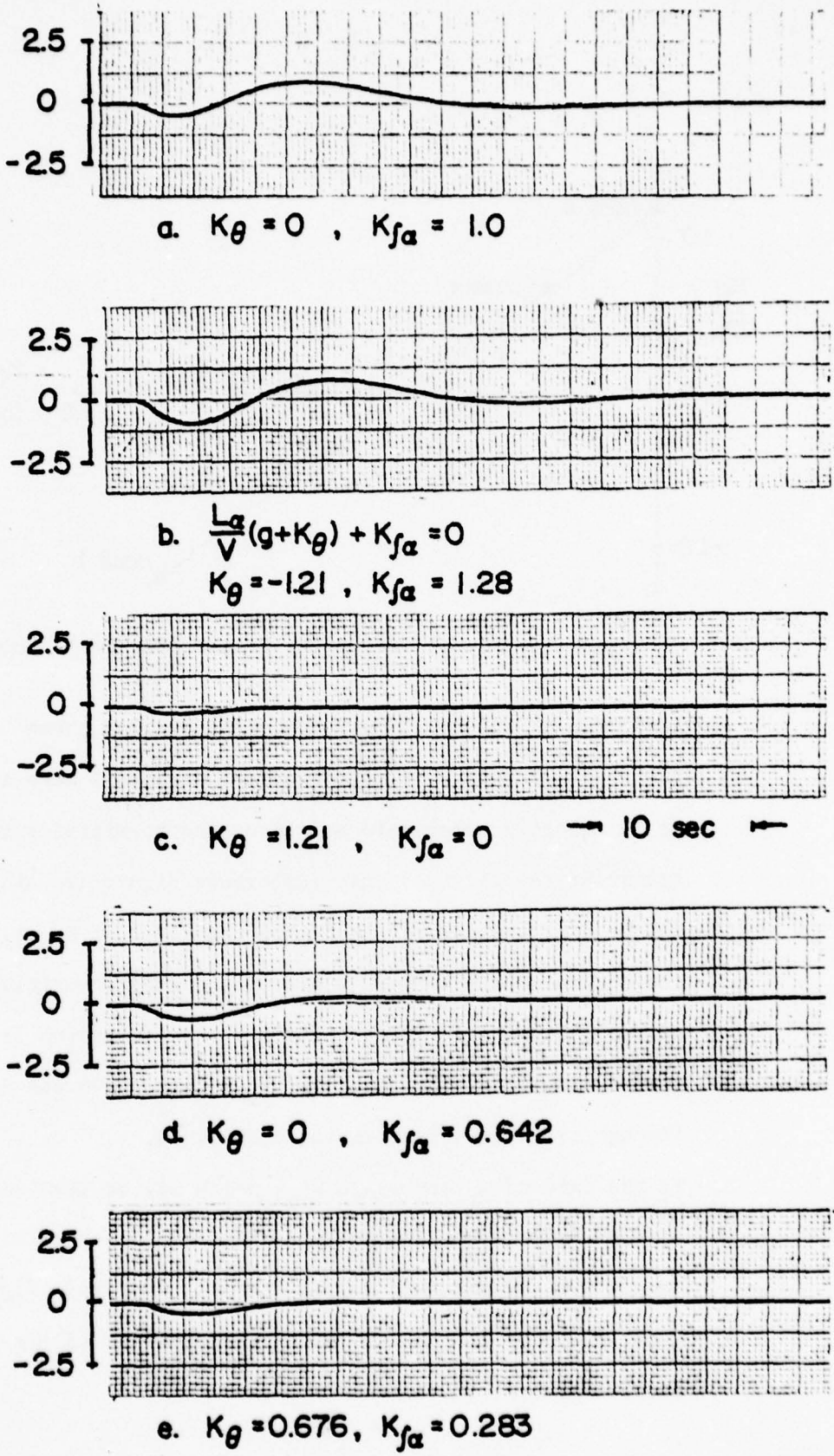

Figure 12. Comparison of Transient Velocity Responses due to Control Stick Step Input

(K_V = 0.0135 rad/fps, engine response time lag = 1.7 sec)

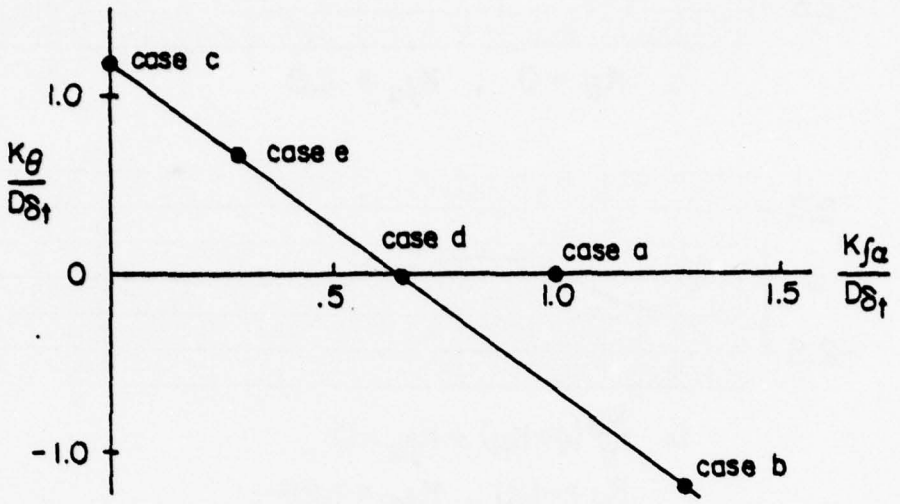

Figure 13. Cases Satisfying Flight Path Equilibrium

4. If $K_\theta = 0$ as in the current Navy APCS designs, then $K_{\int\alpha} = -L_\alpha/V \times g/D_{\delta t} = .642$ (rad/sec-rad) will make the steady state velocity error zero and also tend to minimize the transient velocity response (reference Figure 12d and 12a). In the case of the current A-7E APCS the level of $K_{\int\alpha}$ is .865 rad/sec-rad which is very close to the suggested value and corresponding velocity excitation. This situation is very interesting since the level of $K_{\int\alpha}$ for the A-7E was determined through trial and error tuning techniques.
5. In the case of a very large $K_{\int\alpha}$, which may be required for adequate turn performance as discussed later, a K_θ feedback might be used to reduce the velocity excitation (Case b, reference Figure 12 b).
6. Finally, there will be no velocity excitation if the following conditions are simultaneously met.

$$D_\alpha + K_\theta D_{\delta t} = 0$$

$$L_\alpha/V\ (g + K_\theta D_{\delta t}) + K_{\int\alpha} D_{\delta t} = 0$$

Engine and sensor time lags will alter the above relationships somewhat as might be noted in Figure 12e.

As a more general case the feedbacks K_α and K_{n_z} and engine time lag may be considered which results in the following numerator for the velocity to control stick transfer function

$$N_{\delta sV} = |M_\theta|M_{\delta e}\, s\left[\tau D_\alpha s^2 + \{\tau(L_\alpha/V)\, g + D_\alpha + (L_\alpha/V)V\, K_{n_z} D_{\delta t} + K_\alpha D_{\delta t} + K_\theta D_{\delta t}\}\, s + \{(L_\alpha/V)(g + K_\theta D_{\delta t}) + K_{\int\alpha} D_{\delta t}\}\right]$$

where the engine response lag is expressed as $1/(\tau s + 1)$. It is evident that complete decoupling cannot be obtained because of the $\tau D_\alpha s^2$ term. The conditions which probably result in small transient velocity excitation are

$$\tau(L_\alpha/V)g + D_\alpha + (L_\alpha/V)V\, K_{n_z} D_{\delta t} + K_\alpha D_{\delta t} + K_\theta D_{\delta t} = 0$$

$$(L_\alpha/V)(g + K_\theta D_{\delta t}) + K_{\int\alpha} D_{\delta t} = 0$$

The second equation dealing with flight path equilibrium is unchanged. In the first equation it may be noted that the K_{n_z} and K_α terms will cancel if they form a pseudo velocity feedback as follows:

$$K_\alpha = -K_V\ (L_\alpha/V)/(L_V/V)$$

$$V\, K_{n_z} = K_V/(L_V/V)$$

Finally, although the minimum excitation in Figure 12 corresponds to the case K_θ = 1.21, the velocity excursions for the case $K_{\int\alpha}$ = .642 are still very small, less than 1 fps for a step command resulting in one degree of flight path angle. In the real world situation the K_θ feedback case would be sensitive to engine gain ($D_{\delta t}$) with temperature, etc. and to differences in aircraft weight or drag. On the other hand, the $K_{\int\alpha}$ feedback case is not sensitive to these conditions and is compatible with the constant stall margin turn requirements.

5. Stability Considerations

Under the simplifying conditions of zero moment and lift due to thrust the APCS feedbacks will tend to influence only the phugoid mode. The effect on the stability characteristics of the phugoid mode of the APCS feedbacks K_V, K_α and K_{n_z} is shown in Figure 14. The aircraft configuration base is the A-7E without engine or sensor time lags. It may be noted that K_α feedback influences primarily the frequency while K_{n_z} feedback influences primarily the damping of the phugoid. The K_V feedback, on the contrary, affects both the frequency and damping. The ability to combine K_α and K_{n_z} feedbacks to produce a K_V feedback can be seen (reference Figure 14).

In the case of the A-7E with an attitude command system the corresponding loci are considerably distorted (reference Figure 15). The phugoid roots are no longer a complex pair but are real. The locus of roots for $K_{\int\alpha}$ is shown to the value $K_{\int\alpha}$ = .865, the level of the current A-7E APCS. As noted previously this is reasonably close to the theoretical decoupling value of .642. At this root location the effects of either K_α or K_V are shown. From the root location of K_α = 5.47 (the level of the A-7E APCS), the effect of the feedback K_{n_z} is shown. It may be noted that the current

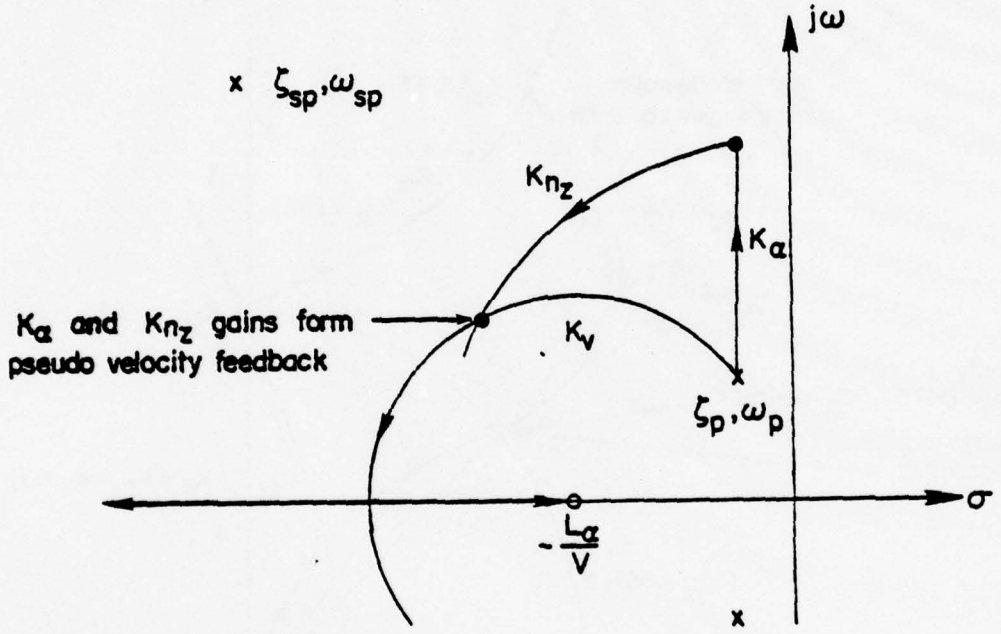

Figure 14. Effects of K_α, K_{n_z} and K_v Feedbacks on Phugoid Mode, Basic A-7E (no engine response time lag and sensor filters)

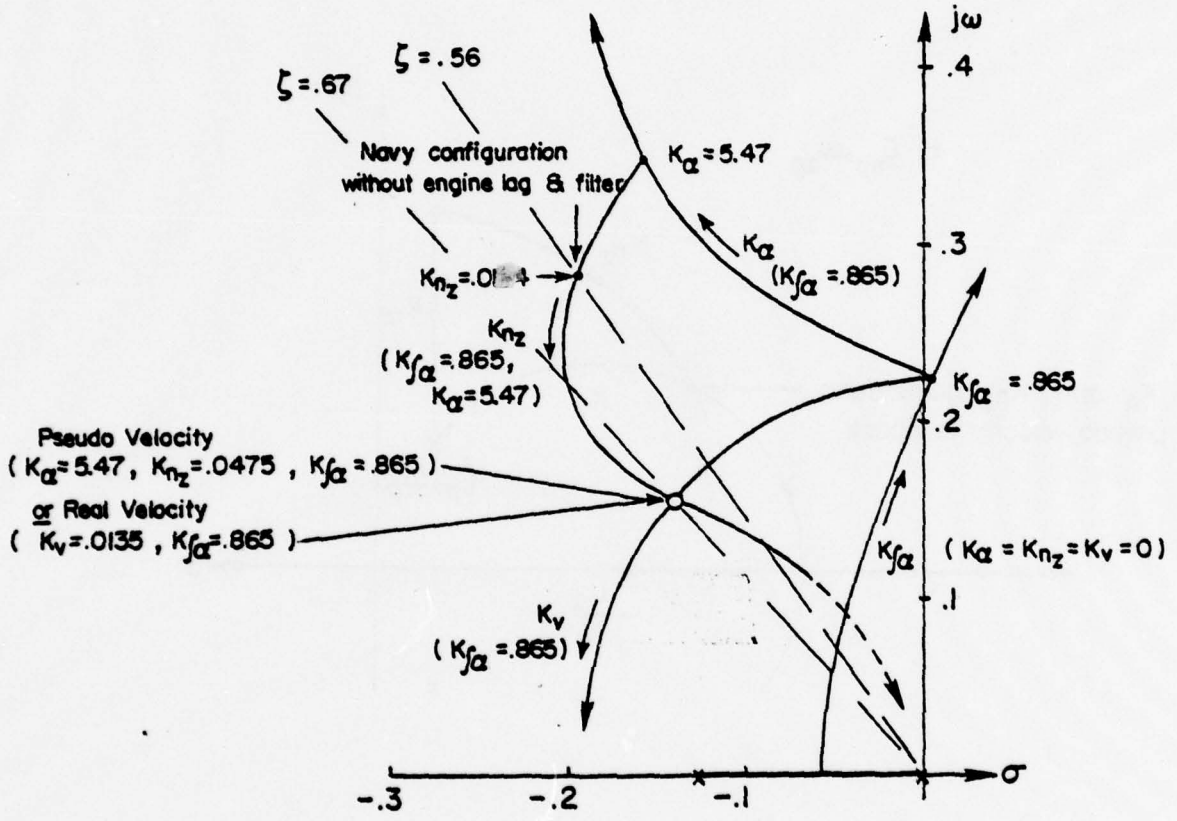

Figure 15. Effects of APCS Feedbacks on Phugoid Mode, Attitude Command System (no engine response time lag and sensor filters)

A-7E APCS level for K_{n_z} is about 1/3 of that required for a pseudo velocity mechanization.

6. Elevator to Throttle Crossfeed

A systematic study of the effect of elevator to throttle crossfeed was not done in this program. A short review will be included here since this feedback was used for the in-flight simulation and is a standard feedback of the current A-7E APCS.

The purposes of this feedback as noted in Reference 13 are:

1. "Auxiliary thrust control to manually augment the APCS functions in crucial situations such as are apparent in the burble or off-nominal flight path corrections."
2. "Airspeed and stall control during large flight path corrections such as tipover and turns."

Auxiliary thrust control provides the pilot with some flexibility and control options (use of throttle control) to replace those inherently lost through the incorporation of the APCS. The current A-7E APCS uses different time constants for each direction of stick motion and provides a temporary movement of the throttle lever due to cyclic motions of stick; that is, the cyclic stick motion tends to move the throttle forward. The transfer functions are:

nose up: $$G_{\delta t \delta e} = \frac{K_{\delta e}\ (7s)}{(7s + 1)(.1s + 1)}$$

nose down: $$G_{\delta t \delta e} = \frac{K_{\delta e}\ (7s)}{(7s + 1)(.9s + 1)}$$

7. Throttle Thrash

There are two aspects of turbulence and burble response associated with the APCS. The first is the one dealing with the aircraft perturbations. A second area is the amount of high frequency throttle activity or "thrash". Although throttle thrash does not necessarily degrade the performance of the aircraft with respect to completing the mission, "excessive" amounts are bothersome to the pilot. The APCS design may be compromised to appease the pilot by introducing additional signal filtering or by lowering the system gains. Some aspects of the throttle thrash problem are discussed herein.

The effect of local turbulence in the vicinity of the sensor on systems using a velocity transducer vs a pseudo velocity computer with an angle of attack transducer has been mentioned previously (Preliminary Flight Tests, p. 25). It was noted that a velocity transducer would generally be superior since the aircraft approach speed is usually greater than $2g/(L_\alpha/V)$. The factors involved are the ratio of airspeed to angle of attack for perturbations from trim in 1 g flight and the approach velocity of the aircraft. The former can be found thru the expression

$$L_\alpha/V \times \Delta\alpha = L_v/V \times \Delta V$$

$$\Delta V/\Delta\alpha = (L_\alpha/V)/(L_v/V)$$

In the case of the A-7 this expression gives the result

$$\Delta V/\Delta\alpha = 7 \text{ fps/deg}$$

This means that in 1 g flight one degree of angle of attack corresponds to 7 fps of airspeed. Under the condition that the two systems have the same flight path stability or "frontsideness", then:

$$K_\alpha \times \Delta\alpha = K_V \times \Delta V$$

$$K_\alpha/K_V = (L_\alpha/V)/(L_V/V)$$

If we assume that the vertical and horizontal gusts are of the same magnitude, the ratio of the velocity gusts to the angle of attack gusts is dependent on the approach velocity.

$$w_g = u_g$$

$$\alpha_g = w_g/V = u_g/V$$

$$u_g/\alpha_g = V$$

The ratio of throttle motions associated with the gusts is the following:

$$\delta t_{\alpha_g}/\delta_{u_g} = (K_\alpha \times \alpha_g)/(K_V \times u_g)$$

$$\delta t_{\alpha_g}/\delta t_{u_g} = (L_\alpha/V)/(V \times L_V/V)$$

This ratio is 1.8 for the A-7E indicating that a direct velocity measurement is preferred over a pseudo velocity computation with regard to local turbulence disturbances.

An extension of this line of reasoning suggests that a pseudo velocity configuration will have a lower level of thrash than an angle of attack configuration. Consider a system with both angle of attack and normal acceleration feedbacks. This is equivalent, of course, to an "effective" angle of attack feedback and a pseudo velocity feedback. If we assume that the gust is uniform over the entire airplane (not confined to the sensor location), then a pseudo velocity sensor combination will respond only to velocity gusts. There will be throttle motions or thrash associated with both the angle of attack and velocity disturbances. Since the disturbances in the two axes are random and uncorrelated, a reasonable

expression for the total throttle thrash is the expression

$$\sigma_{\delta_t} = \sqrt{\Sigma(\delta_{t_{\alpha_g}})^2 + \Sigma(\delta_{t_{u_g}})^2}$$

With the same level of flight path stability, the effect of varying the normal acceleration feedback will be to alter the ratio of "equivalent" angle of attack and pseudo velocity feedbacks. Using x for the percentage of equivalent angle of attack feedback and the value 1.8 for the relative sensitivity factor of the A-7, a solution for minimum thrash can be obtained.

$$\sigma_{\delta_t} = \sqrt{(1.8\ x)^2 + (1 - x)^2}$$
$$= \sqrt{4.24\ x^2 - 2x + 1}$$

Setting the derivative of this expression with respect to x equal to zero, a minimum level of thrash is indicated when

$$x = 1/(4.24) = .24$$

The minimum level of thrash is only slightly less than that obtained with $x = 0$ or an entirely pseudo velocity feedback.

The above analysis was readily verified in a simple flight test. The simulator aircraft was flown in moderate turbulence with the APCS engaged but with the "link" from the throttle handle to the engine electrically disconnected. To insure a proper airframe response to natural turbulence the A-7 was not simulated; rather, the dynamics were those of the basic aircraft. The significance of this artifice is that the normal acceleration gain required to achieve 100% pseudo velocity feedback was reduced due to the higher level of L_α/V of the test aircraft. Without sensor filtering the pseudo velocity configuration was qualitatively better than

the angle of attack configuration in terms of throttle thrash, probably by a factor of two or more. The tests also demonstrated that a velocity transducer is preferable to the pseudo velocity computation method.

The flight test verification of the reduction in throttle thrash with the pseudo velocity configuration confirms the assumption that a significant part of the turbulence is uniform over the entire aircraft. Therefore, the measured normal acceleration and angle of attack will properly compute velocity. This suggests that if different filters are used on the two sensors, the magnitude of thrash will increase since the correlation between the two signals will be altered. This hypothesis was qualitatively verified during the previously mentioned flight tests. Adding a filter to either of the sensors individually did not reduce but increased the throttle activity. With a low level of filtering (.25 to .5 second time constant) the minimum thrash appeared to occur when both filters had the same time constant. The tests also indicated that the level of filtering required on a pseudo velocity configuration can probably be reduced considerably below a 1.0 second time constant. A filter of .5 second resulted in barely detectable throttle motions in moderate turbulence. Present APCS designs use an accelerometer with mechanical filtering of about a 1.0 second time constant.

There is one other source of throttle thrash in current APCS designs, namely, the elevator input. In the A-7 this is a relatively high gain input of 4.4 degrees of throttle per degree of control surface. Since the measurement is made at the surface rather than the pilot's stick, SAS inputs are also sensed. In turbulence the stabilizing control inputs by the pilot and/or SAS probably account for the major part of the unwanted throttle activity on the A-7 aircraft.

TEST PROCEDURES

1. Ground-Based Simulation

The simulator studies were performed to compare the effects of the several decoupled controller systems prior to the actual flight evaluation. The ground based simulator of the Flight Research Laboratory of Princeton University illustrated in block diagram form in Figure 16 was used in this study.

The A-7E aircraft was used as the model for the studies because it has been extensively evaluated and documented in the past. The aircraft characteristics were generated on an analog computer by linear three degree of freedom longitudinal equations of motion. The set of longitudinal stability derivatives which correspond to the approach configuration of the A-7E at 129 kt, the engine response characteristics, and the APCS gains are given in Table 3. The nonlinear stick force gradient of the A-7E which is shown in Figure 17 was mechanized through a hydraulic force feel stick system.

The primary display simulated the pilot's view of the Fresnel lens system (or other mirror system) currently used on aircraft carriers and is illustrated in Figure 18. This display consisted of the Fresnel Lens Optical Landing System (FLOLS) datum bar and meatball which were represented on the two-gun cathode-ray tube (CRT) as depicted in Figure 19. The parallel movement of both bar and meatball indicated the pitch attitude changes, and the relative movement of the meatball about the datum bar indicated the altitude deviation from the FLOLS beam reference. This display had a time/range varying characteristic; that is, real time was

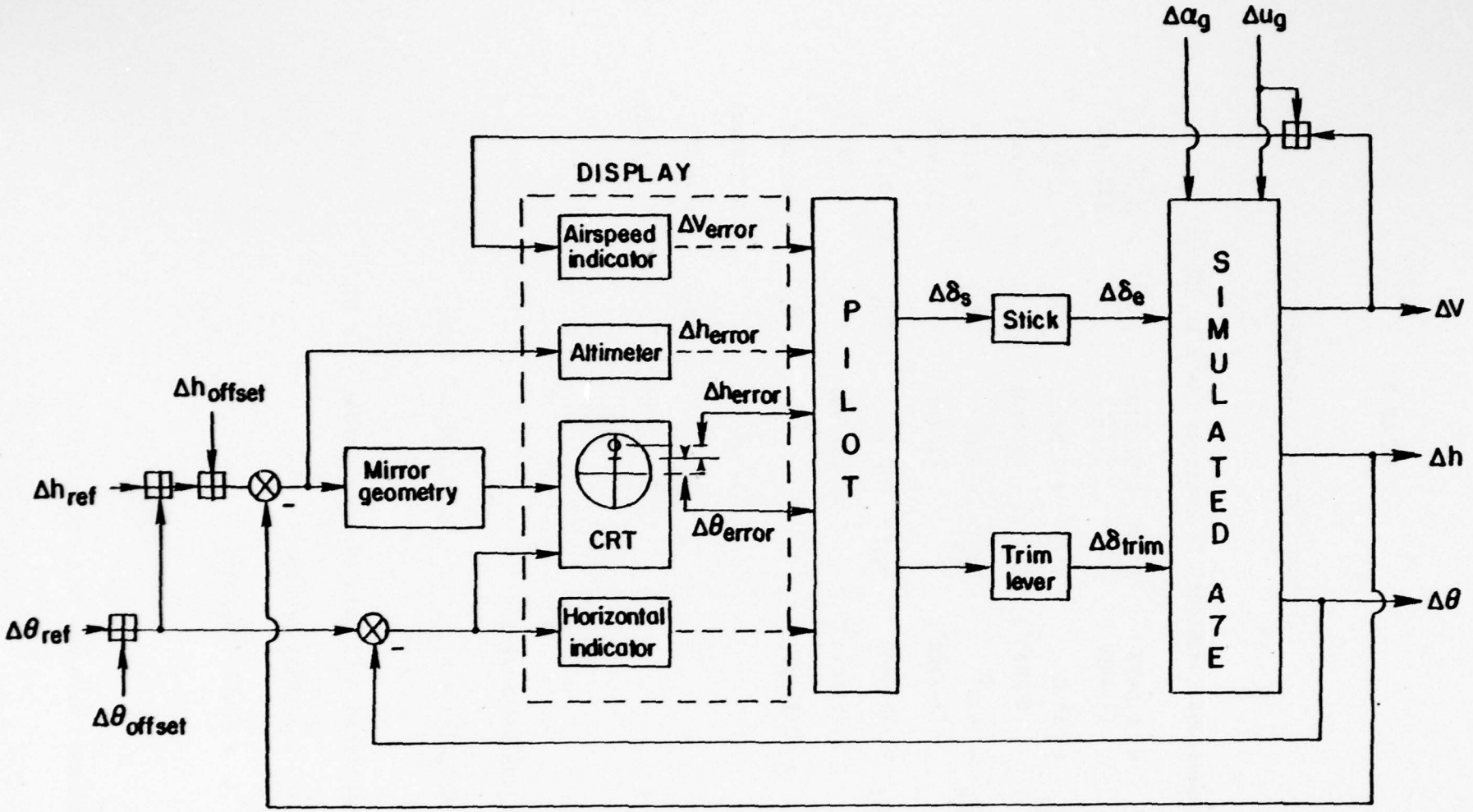

Figure 16. Block Diagram Representation of the Simulated Carrier Approach System

TABLE 3

LONGITUDINAL CHARACTERISTICS

A. Dimensional Stability Derivatives (A-7E at 129 kt)

D_v	= 0.0493 (1/sec)	L_v/V	= 0.00132 (1/ft)	M_v	= 0.0* (ft/sec)
D_α	= 18.0 (ft/sec^2)	L_α/V	= 0.531 (1/sec)	M_α	= - 1.74 ($1/sec^2$)
$D_{\delta e}$	= 0.0* (ft/sec^2)	$L_{\delta e}/V$	= 0.0* (1/sec)	$M_{\delta e}$	= - 2.167 ($1/sec^2$)
$D_{\delta t}$	= -26.6445 (ft/sec^2)	$L_{\delta t}/V$	= 0.0* (1/sec)	$M_{\delta t}$	= 0.0* ($1/sec^2$)
V	= 218 fps			$\dot{M}_\alpha$	= -0.063 (1/sec)
				$\dot{M}_\theta$	= -0.327 (1/sec)

B. Engine Response Lag

$(D/\delta_t)(s) = D_{\delta t}/(\tau_E s + 1)$; $\tau_E = 1.7$ (sec)

C. Simplified APCS Gain (Configurations 1 to 13)

$K_v = 0.0135$ (rad/fps)

$K_\theta = 1.21$ (rad/rad)

*Assumed zero for this test program.

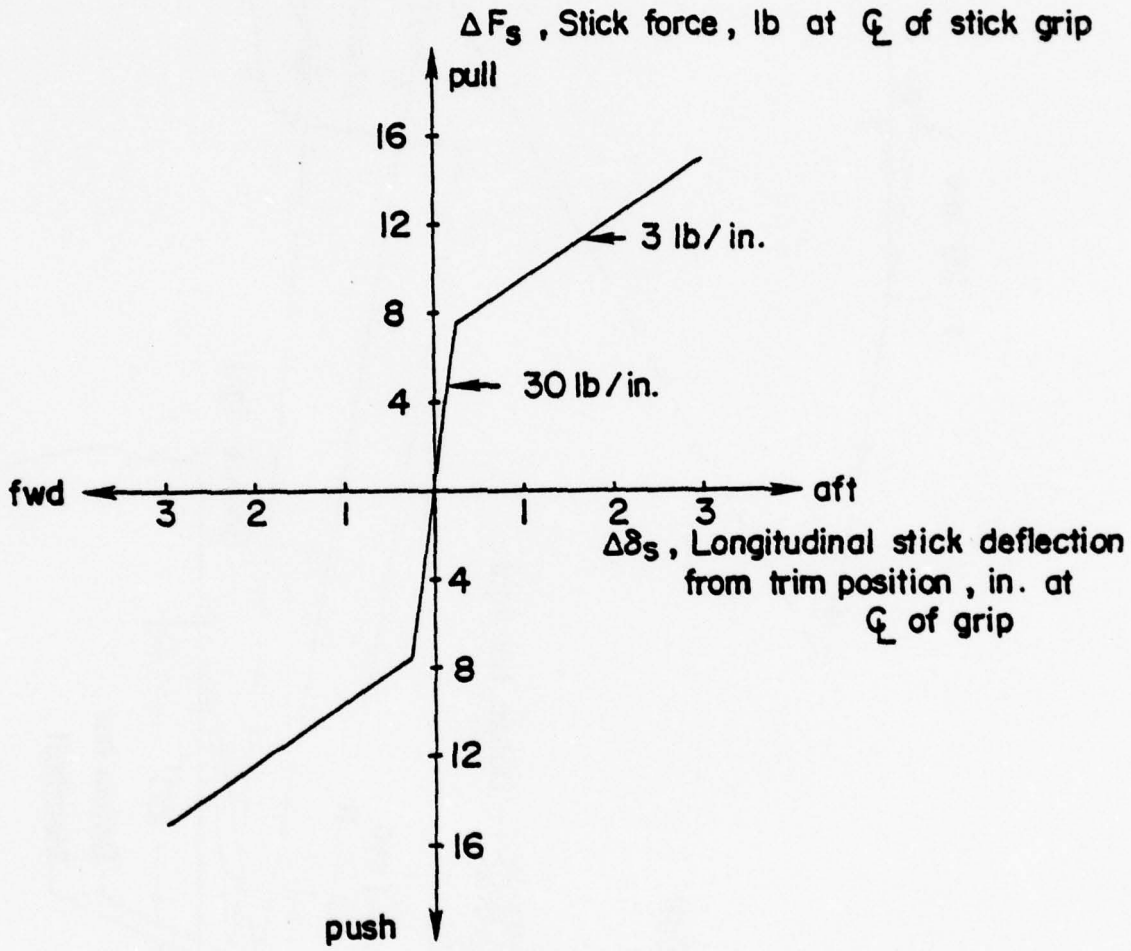

Figure 17. Simulated Stick Force Gradient of A-7E

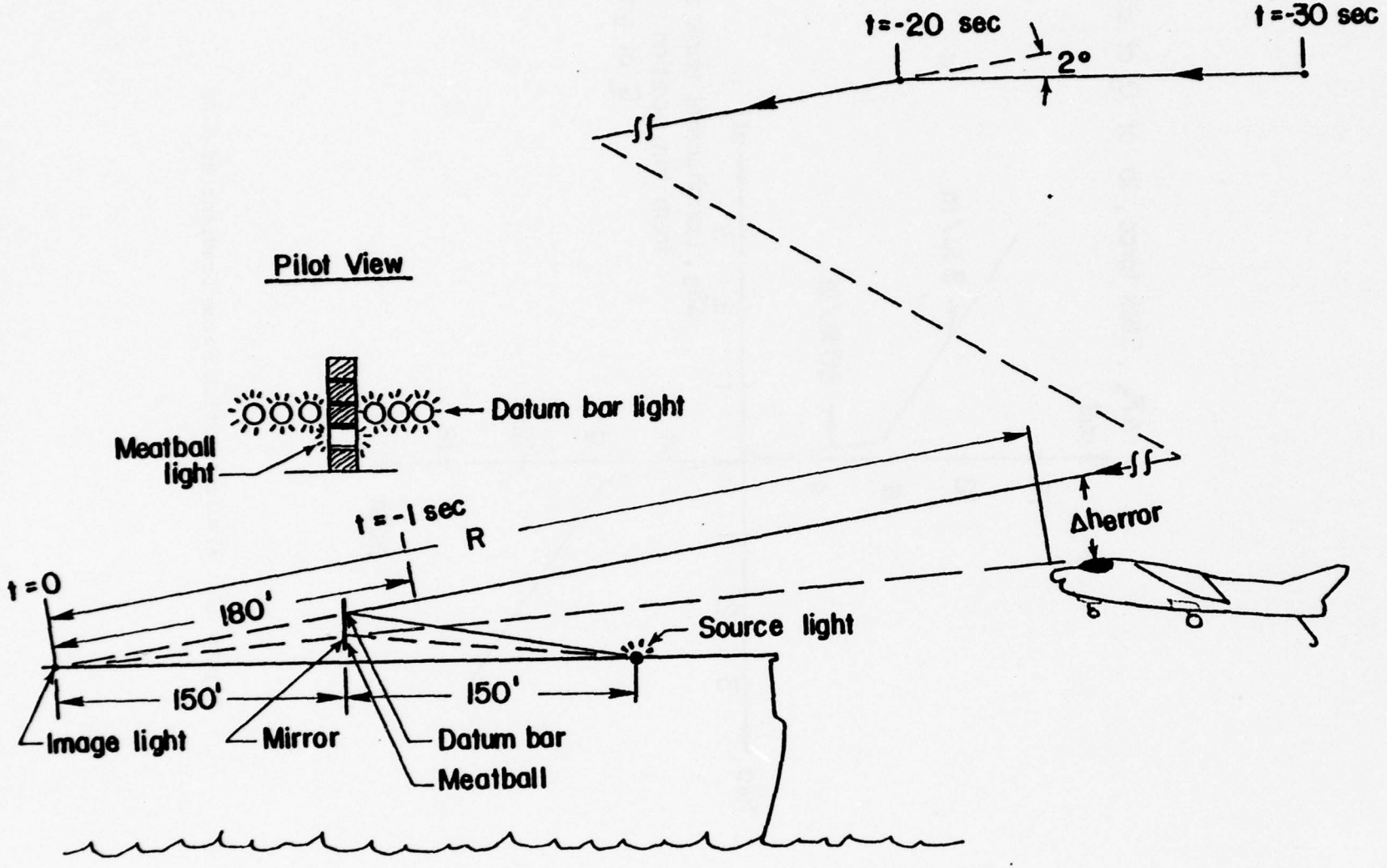

Figure 18. Geometry of Ground Based Simulation

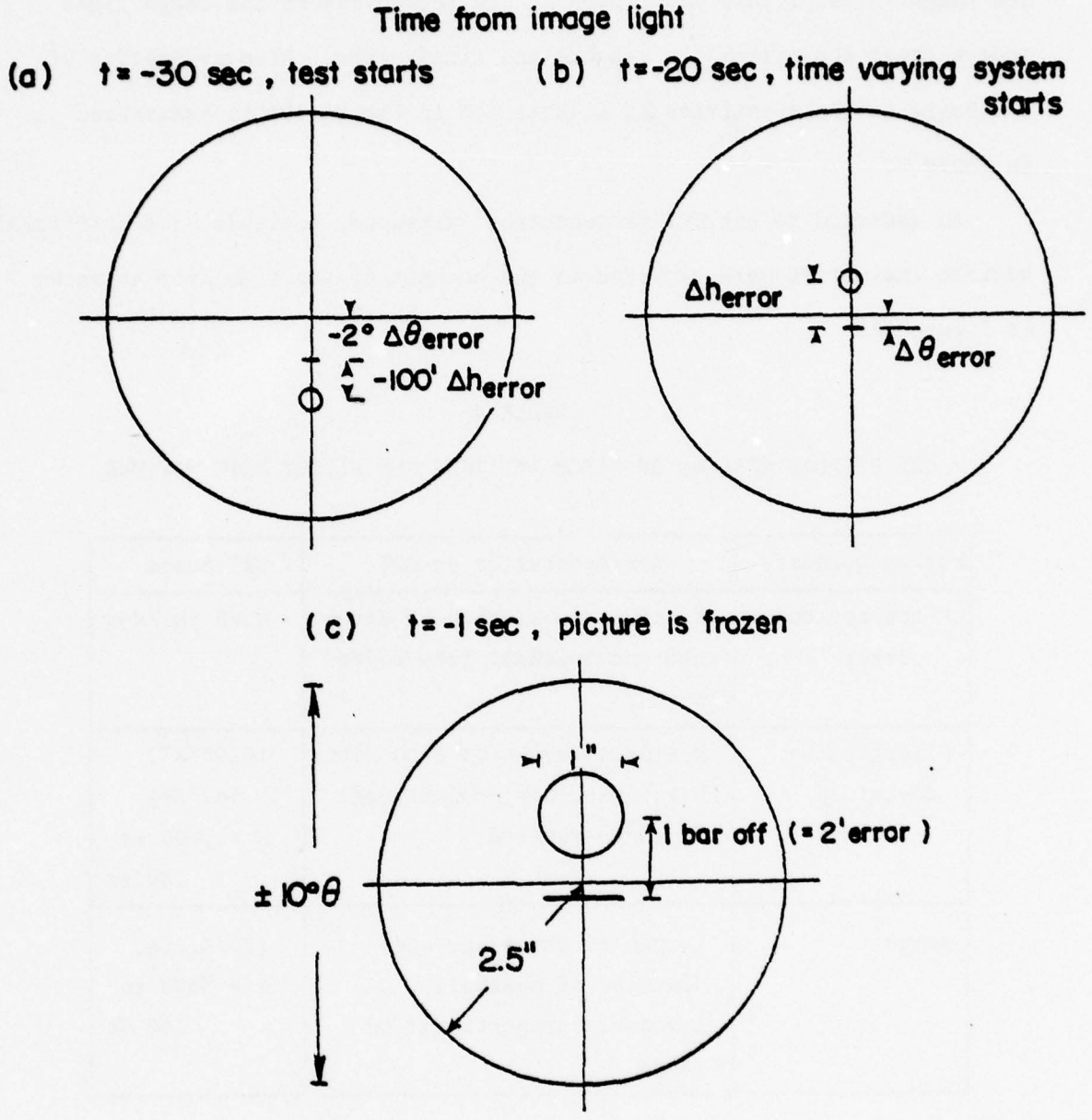

Figure 19. Cathode Ray Tube Display of FLOLS

used and the size of the picture was enlarged inversely proportional to the range. The picture was frozen at one second before the image light source (near the mirror) to measure the final error. Display scaling of the basic motion quantities as illustrated in Figure 19c is summarized in Table 4.

In addition to the CRT presentation, airspeed, altitude, and artificial horizon indicators were provided in the cockpit of the simulator as shown in Figure 16.

TABLE 4

CRT DISPLAY SCALING OF PITCH ATTITUDE AND FLIGHT PATH MOTIONS

Motion Quantity	Representation on CRT	CRT Scale
Pitch attitude error	Up-down translation of datum bar and meatball from center of CRT	0.25 in./deg
Flight path deviation	Meatball deviation from datum bar, inversely proportional to range squared	$16200/R^2$, in./deg R = 3600 to 180 ft*
Range	Length of datum bar and diameter of meatball, inversely proportional to range	180/R, in. R = 3600 to 180 ft*

*R = 180 ft from Image Light Source, reference Figure 18.

Equivalent sharp edge gusts representing the atmospheric disturbance associated with the carrier air wake were used in the tests. That is, u_g = -3 fps and α_g = ± .5 degree gusts were applied at 6 and 9 seconds before the mirror point respectively. These numerical values are a sharp-edge gust approximation of the random gust data of North American Aviation (Reference 14 and Figure 22). Ship motions were not provided in the tests.

The following mission task of the simulated carrier landing approach was required of the pilots.

a. Commence flying on a shallow descent about one mile behind the carrier and 100 feet below the FLOLS beam.

b. Perform a smooth pitch-over maneuver to "capture" the proper glideslope. A 2 degree flight path angle correction from the starting condition was required. Depending on the test configuration, throttle or a pitch (attitude) trim controller lever could be used in coordination with stick inputs.

c. Track meatball using apparent size as an indication of range. Minimize the effects of u_g and α_g gusts and attitude errors up to the simulated touchdown indicated by a frozen display one second before reaching the image light source.

Eleven configurations were tested in the ground based investigation. Parameters of these configurations are listed in Table B-1 of Appendix B. Configurations 1 to 4 were chosen in order to compare the effect of APCS and/or the attitude command system with the unaugmented A-7E. Configurations 5 to 9, washout systems, were selected: first, to examine the possibility of bandwidth improvement and second, to determine the preferred method of

implementation (force or surface washout). Configurations 10 and 11 were used for comparison with the high bandwidth washout configurations. The APCS or the throttle parts of all configurations had the same setting as tabulated in Table 3. These same configurations were used in Phase I in-flight simulation.

2. In-Flight Simulation

The airplane used in the flight tests was the Princeton Variable Stability Navion (N91566) shown in Figure 20. The airplane was capable of independent variation of the stability derivatives associated with the six degrees of freedom in flight. Side force control was not used but the installed side force vane was used to simulate the side force derivatives (for example Y_β). The lateral and directional stability derivatives were adjusted to simulate an A-7E with yaw axis control augmentation. Stability derivatives and parameters of the lateral-directional configuration are listed in Table 5.

High performance hydraulic servos are utilized in the variable stability systems to deflect elevator, flaps, etc., in proportion to pilot control inputs as well as to sensed angular rate, rate of surface deflection, angle of attack, and velocity. A standard APCS electrical servo was used to move the throttle lever in proportion to sensed angle of attack, vertical acceleration, velocity, pitch attitude, etc.

The evaluation pilot occupied the right seat of the aircraft. His flight control instruments, typical of high performance, jet aircraft, are shown in Figure 21. Stick force gradients were generally consistent with the artificial feel systems of contemporary jet fighters and were 4.0 lb/in. longitudinally and 4.5 lb/in. laterally. The rudder pedal force gradient was 25 lb/in.

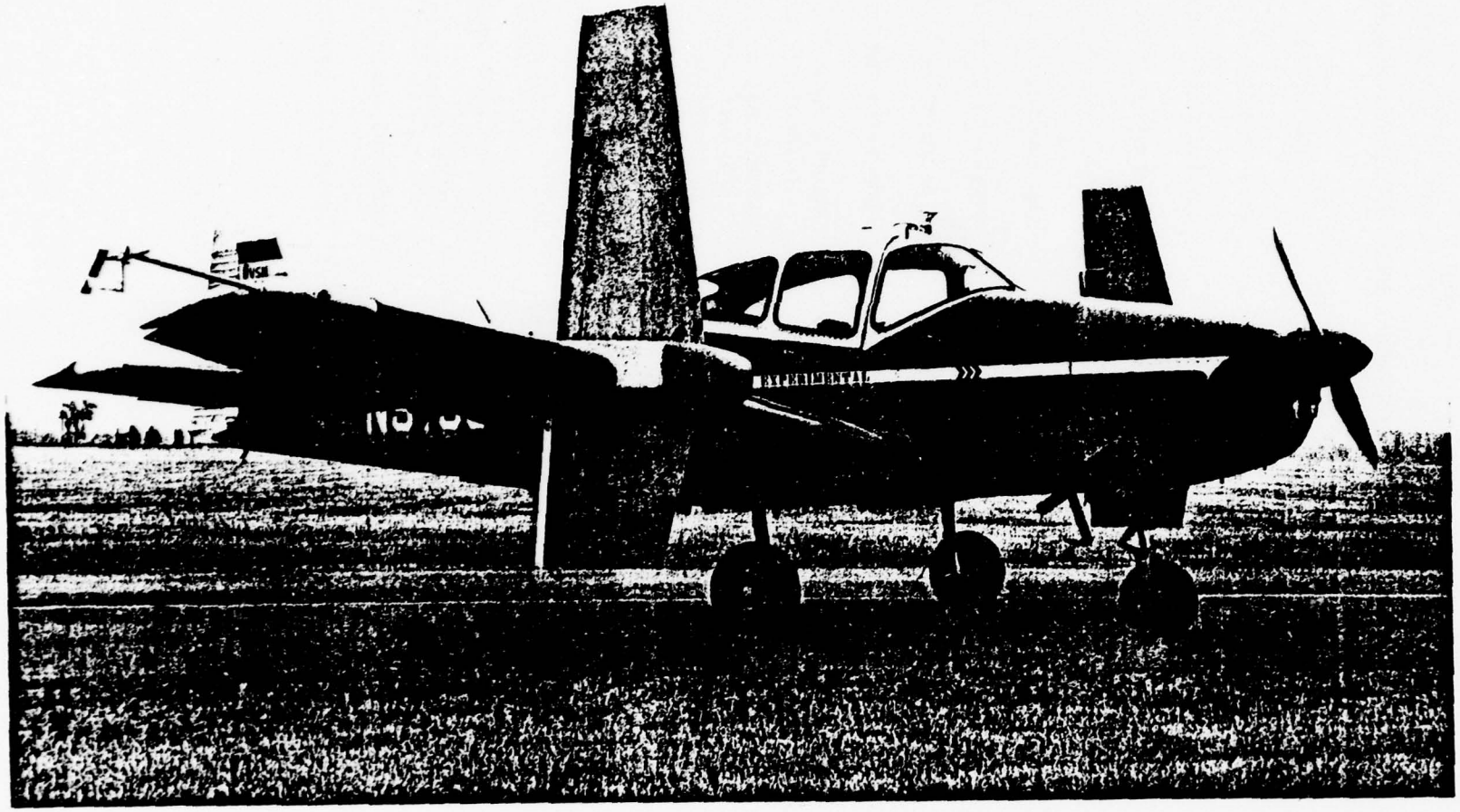

Figure 20. Princeton Variable Stability Navion

TABLE 5

A-7E LATERAL-DIRECTIONAL DERIVATIVES AND PARAMETERS

L_β	=	-7.96	dihedral effect ($1/sec^2$)
L_p	=	-1.43	roll damping (1/sec)
L_r	=	+1.013	overbanking tendency (1/sec)
N_β	=	1.84	directional stability ($1/sec^2$)
N_p	=	-0.209	adverse yaw due to roll (1/sec)
N_r	=	-0.800*	yaw damping (1/sec)
Y_β/V	=	+ .187	crosswind force (1/sec)
Y_p/V	=	0.0045	side force due to rolling velocity
Y_r/V	=	0.0054	side force due to yaw velocity
$L_{\delta a}$	=	-9.13	lateral control sensitivity ($1/sec^2$ per in.)
$N_{\delta r}$	=	-1.197	directional control sensitivity ($1/sec^2$ per in.)
$Y_{\delta r}/V$	=	0.0335	side force due to rudder (s/sec)
$Y_{\delta a}/V$	=	0.0244	side force due to aileron (1/sec)
$N_{\delta a}/L_{\delta a}$	=	0.0716*	aileron yaw-roll ratio
$L_{\delta r}/N_{\delta r}$	=	-0.414	rudder roll-yaw ratio
τ_{rm}	=	0.527	rolling time constant (sec)
τ_{sp}	=	7.50	spiral time constant (sec)
ω_d	=	1.6056	undamped Dutch roll frequency (1/sec)
ζ_d	=	0.1198	Dutch roll damping ratio (1/sec)

*Approximately for YAW STAB on (Reference 1)

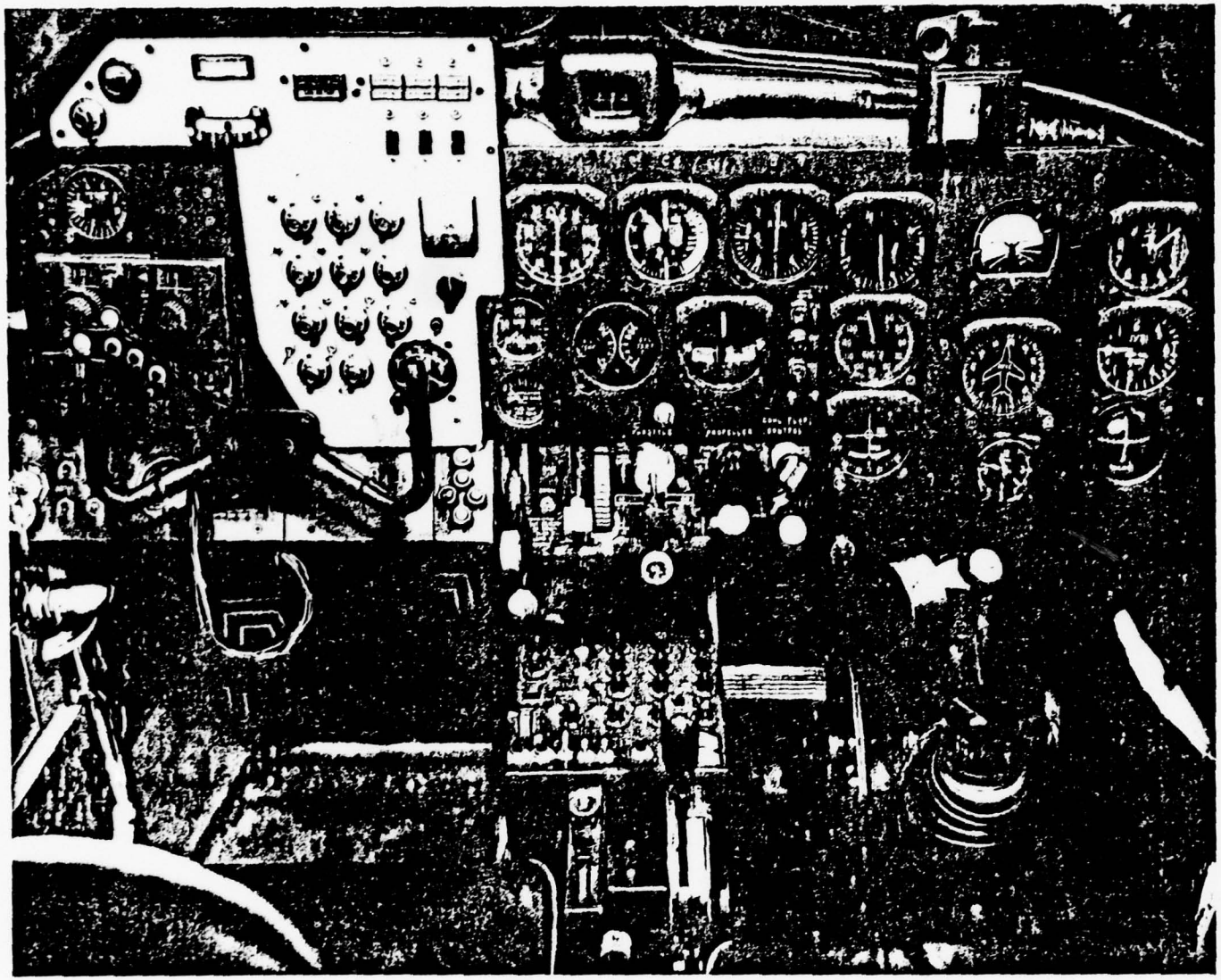

Figure 21. Cockpit Layout of Navion

The safety pilot occupied the left seat and performed the task of overall system performance monitoring and configuration setup.

An onboard turbulence simulation system simulated isotropic disturbances along three axes and a carrier wake (burble model) to add realism to the approach task. The intensities of the isotropic disturbances were 1.42 fps root mean square in all axes. The simulated burble model, expressed as a function of the time to touchdown point, is shown in Figure 22. This simulation system was turned on by the safety pilot 8 seconds before simulated touchdown.

The task for the flight evaluations was a visual simulated power approach to a carrier landing under moderately turbulent conditions. The simulated approaches were made to the Princeton runway, whose 70 feet width corresponds to the landing area on a carrier deck. Glideslope information was provided by an optical landing aid, as shown in Figure 23, developed for the Marine Corps for advanced field use and was installed at the right hand side of the runway. An approach speed of 105 knots was used to match the closure speed of the A-7E flying at 129 knots IAS, approaching a carrier with 24 knots of wind over the deck. Approaches were terminated at 20 to 30 feet above ground level by the safety pilot. This altitude was considered by the evaluation pilots as approximately the point in the approach after which almost no control movements are made. A test run sequence is illustrated in Figure 24. All runs were made in early morning smooth air so that the response of the simulated configuration to the calibrated artificial turbulence would not be distorted.

Two Princeton pilots served as evaluation pilots during the ground based and in-flight simulations. One of the two pilots had carrier

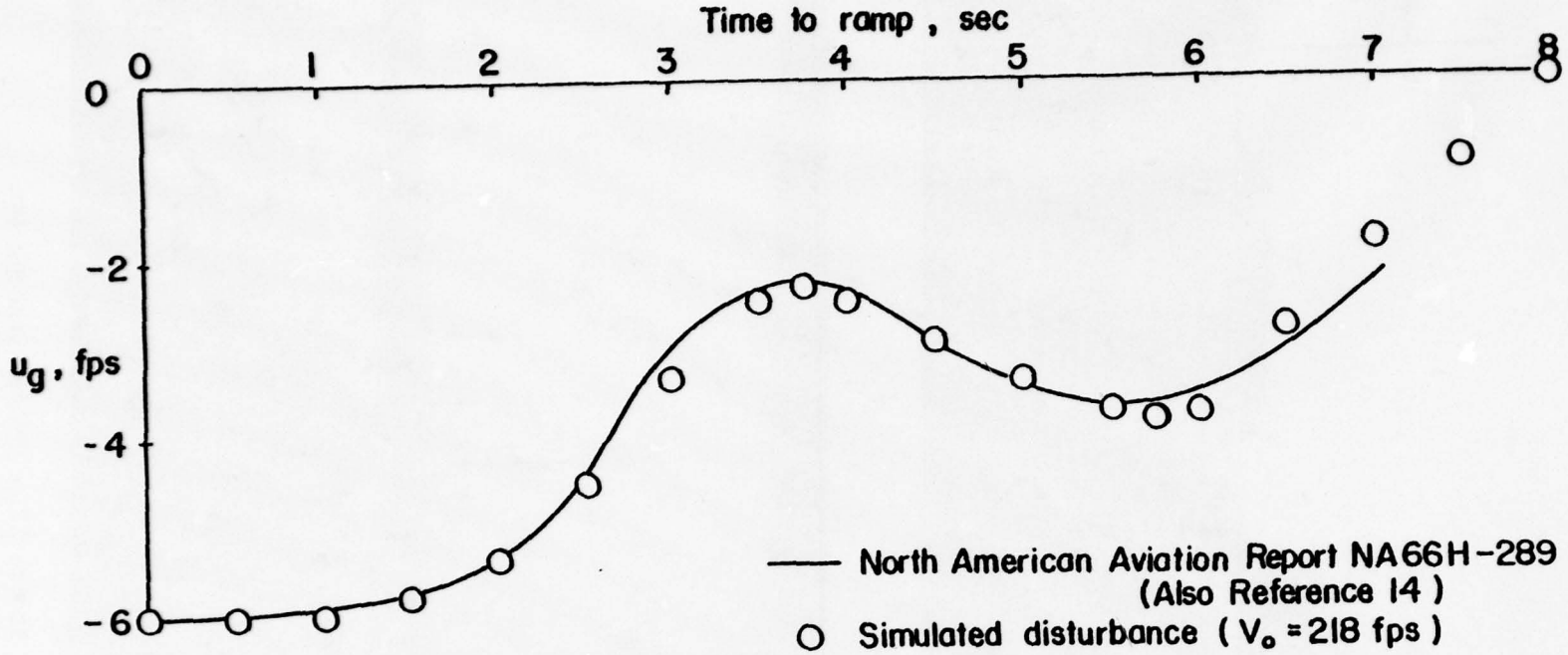

Figure 22. Horizontal Gust Velocity Turbulence for A-7E

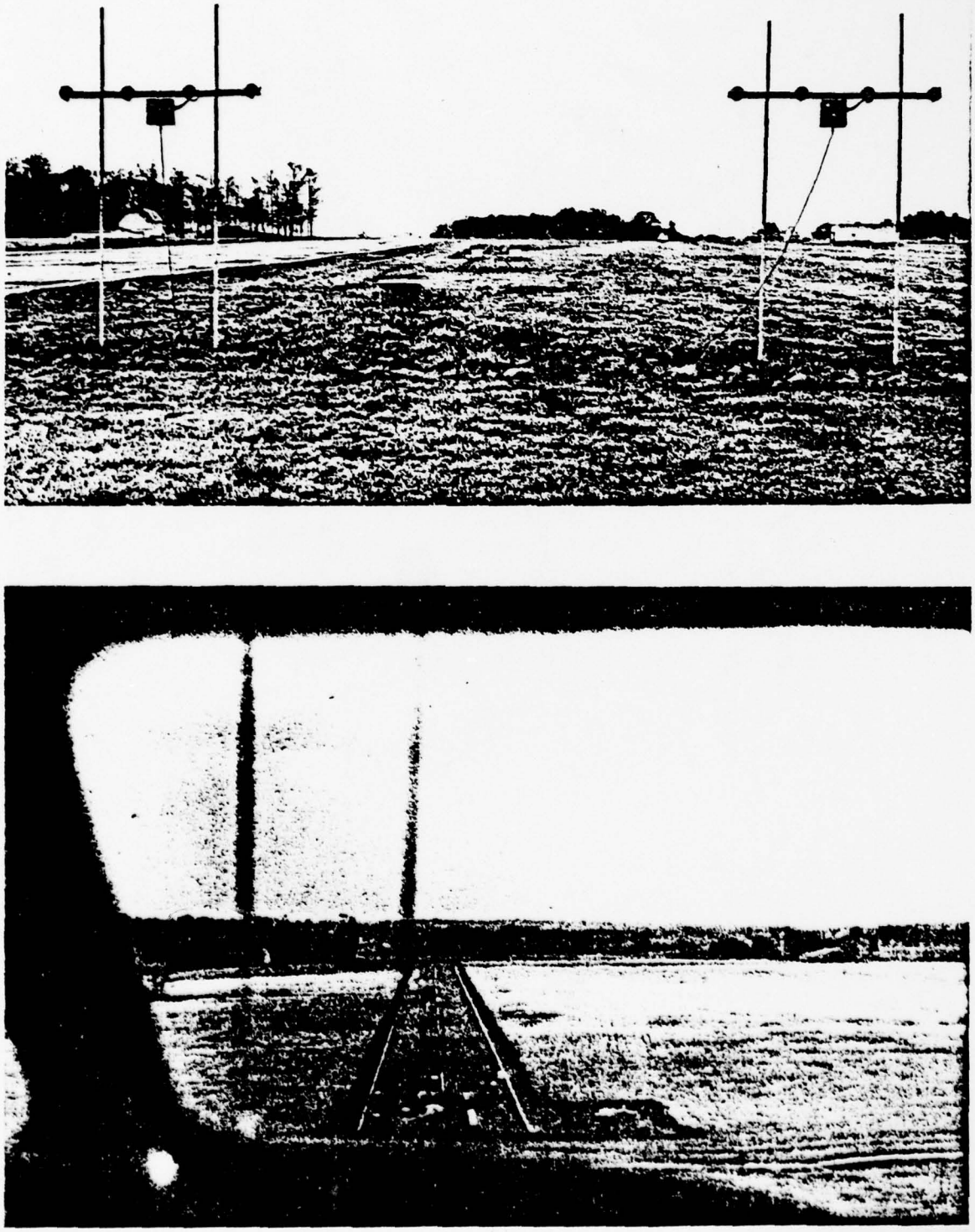

Figure 23. Optical Landing Aid

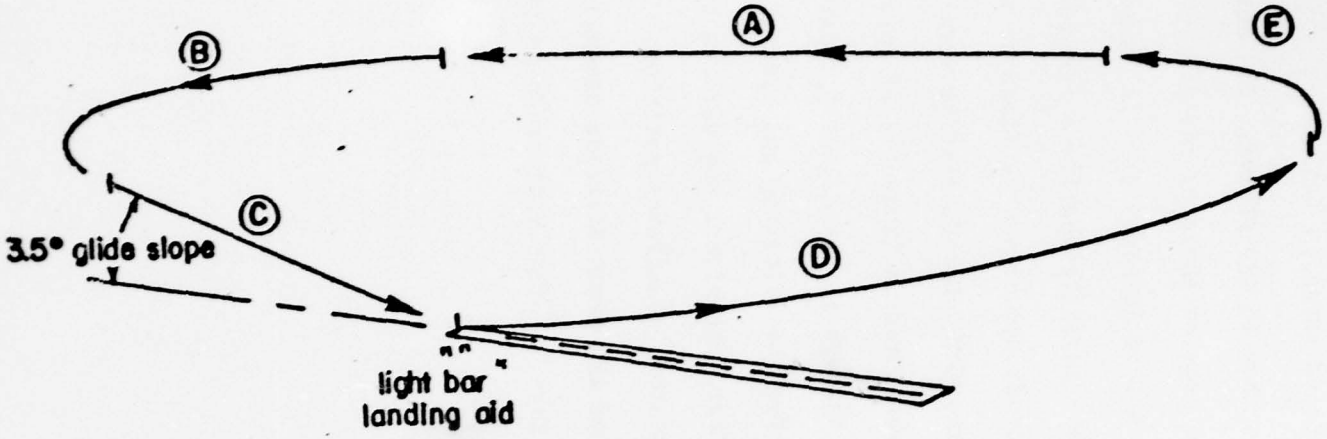

RACETRACK FLIGHT PATTERN PHASES

(A) Downwind leg, 800' alt. – evaluation pilot takes over and feels out airplane

(B) 180° turn by evaluation pilot

(C) Final approach begins approximately one mile out at the discretion of the evaluation pilot. 3.5° glide slope and configuration approach speed maintained by the evaluation pilot.

(D) Waveoff and climbout – evaluation pilot transmits rating and comments

(E) Safety pilot re-configures airplane for next approach

Figure 24. Flight Pattern

experience. The pilots were informed beforehand of the test variables and were asked to use the rating system shown in Table 6,

The in-flight simulation tests were made in two phases. The Phase I test configurations were essentially the same as those of the previously discussed ground simulation (reference Table B-1 of Appendic B). In this phase aspects of the aircraft dynamics were investigated for a fixed simplified APCS design. In Phase II, the aircraft dynamics were fixed to those of either Configuration 3 or 4 while the APCS characteristics were altered. The configurations of this phase are listed in Table B-2 of Appendix B. The items examined were decoupling through either $K_{\int\alpha}$ or K_{θ}, pseudo velocity and true velocity feedbacks, the effect of filtering and control stick crossfeed. With respect to the latter, the signal was derived from the control stick rather than the (simulated) stabilator position. Thus, the crossfeed did not contain elements of the pitch attitude command feedbacks as shown in the block diagram of Figure 1. This difference is important with respect to Configuration 15 only.

TABLE 6

Cooper-Harper Pilot Rating System

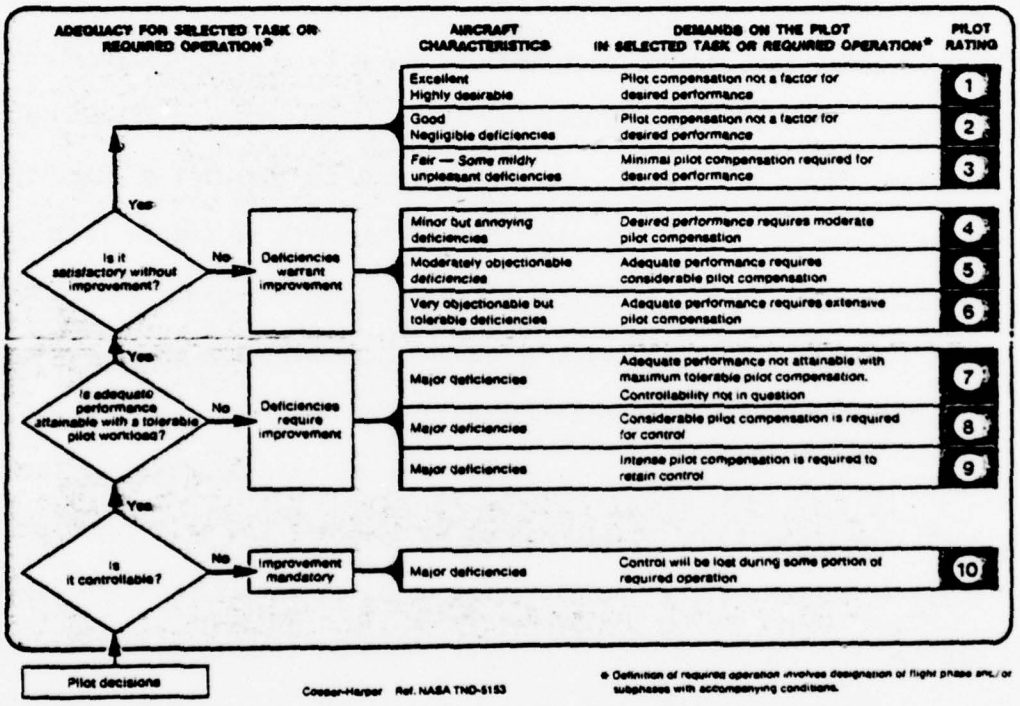

Cooper-Harper Ref. NASA TND-5153

* Definition of required operation involves designation of flight phase and/or subphase with accompanying conditions.

RESULTS AND DISCUSSIONS

1. Ground Simulation

The distinguishing flight path response characteristics of the configurations of the ground based simulations are shown in Figure 25. With respect to the flight path response of the basic A-7E, Configuration 4, the other configurations have low frequency flight path angle command characteristics and an increased short period frequency break point. It may be noted that Configurations 3,5, and 6 have essentially identical responses. In the case of Configuration 3 the improved flight path response is obtained by an attitude feedback whereas in the case of Configurations 5 and 6 similar results are achieved by an angle of attack feedback and a prefilter washout of the control input. Further improvement in the flight path response bandwidth is obtained by increasing the short period frequency (Configuration 10) or by increasing the low frequency break point (Configurations 7, 8, 9, and 11). In the latter group this is achieved through the prefilter washout on Configurations 7, 8, and 9 and by increasing the aircraft lift curve slope on Configuration 11. Finally, the configuration sets 5/6 and 7/8 differ only in the pilots control feel (surface/force washout).

Approximately 120 test runs were made for the ground based simulations. Individual pilot ratings and the average values of these are listed in Table 7. The pilot rating comparisons of the first four configurations are shown in Figure 26. As expected, a significant improvement in pilot rating was obtained on Configuration 3 relative to the unaugmented pitch responses of Configuration 4. Comparatively, the attitude command control system offered a greater reduction of pilot workload than that provided by an APCS (reference Configurations 1, 2, and 4).

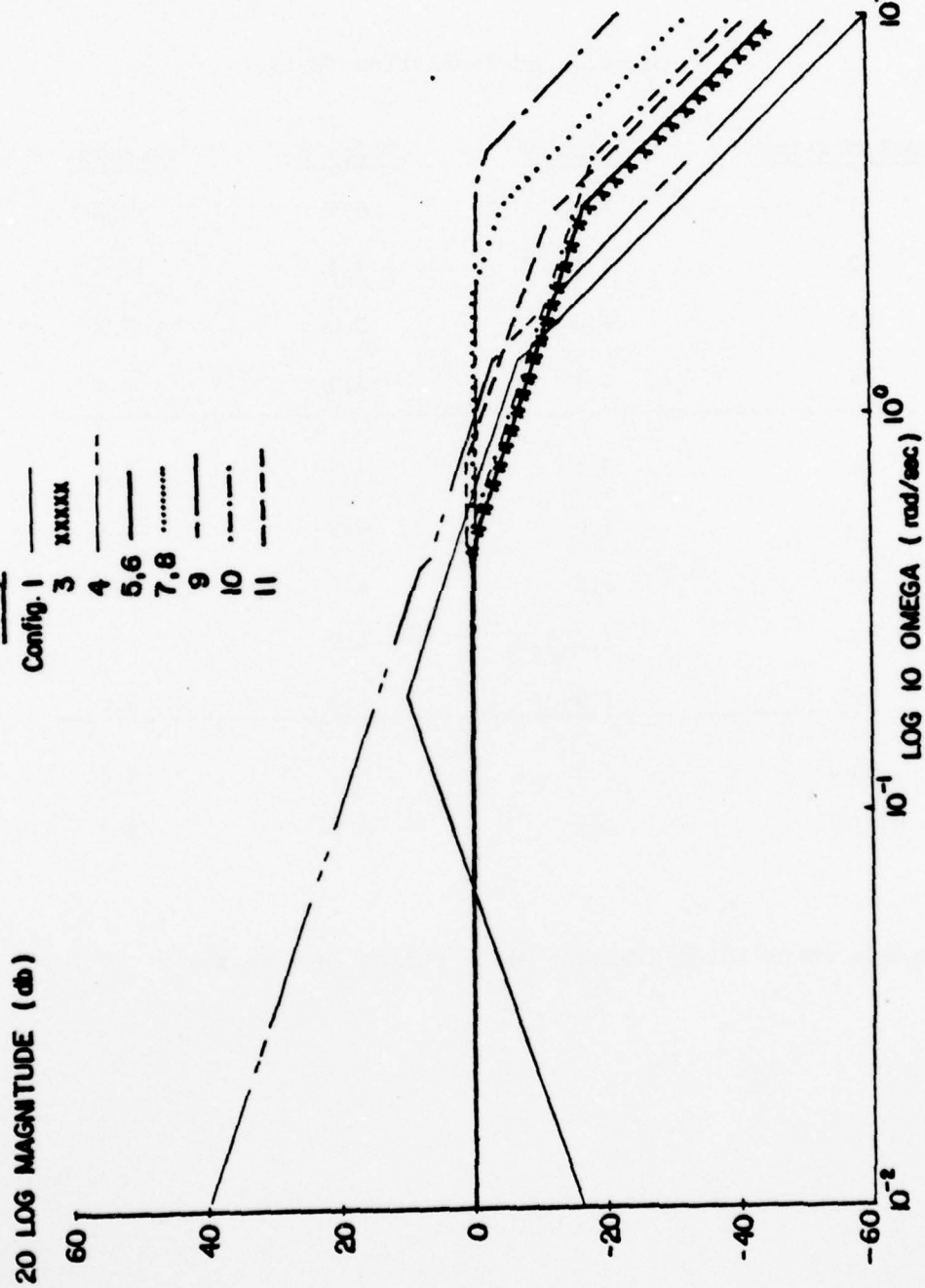

Figure 25. Flight Path Response of Phase I Configurations

TABLE 7

PILOT RATINGS

Ground Based Simulation Tests

Configuration	Pilot A	Pilot B	Average
1	5.1	6.7	5.9
2	3.1	4.1	3.6
3	3.6	3.0	3.3
4	4.4	4.4	4.4
5	3.1	3.7	3.4
6	4.9	4.0	4.5
7	3.3	3.7	3.5
8	3.8(3.0)*	4.5	4.2
9	2.9	4.3	3.6
10	2.5	-	2.5
11	2.8	2.7	2.7

*Linear stick force gradient pilot rating (see text)

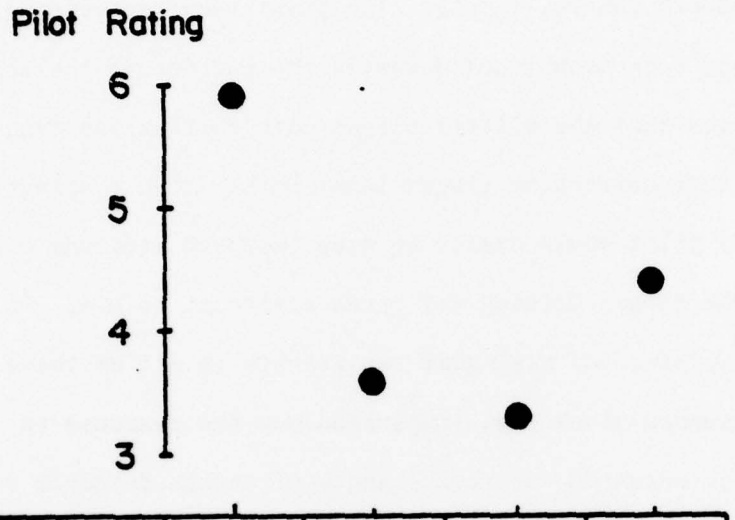

θ command	off	on	on	off
APC	off	off	on	on
Configuration	1	2	3	4

Figure 26. Comparison of Basic Feedback Concept in Ground Based Simulation

Configuration 5, which had nearly the same flight path response as Configuration 3, received about the same pilot rating. However, further improvement in the flight path bandwidth (Configurations 7 and 9) resulted in a slight degradation in pilot opinion. This was due to the pitch attitude overshoot characteristics of these configurations. The pilot felt compelled to close a pitch attitude loop to suppress the attitude excursions or use very slow, smooth control inputs. The first required considerable lead compensation and both techniques defeated the purpose of the configurations. It was obvious that the pilot's flight path corrections tend to take the form of an attitude correction (inner loop) rather than a direct control of flight path. The pilot would prefer to have improved attitude response and that we leave the (over) driving (of pitch attitude) to him. In addition, the pilots complained of high gust sensitivity in all of these cases. Fore-and-aft gusts seemed to be well suppressed but the response to vertical gusts was accentuated due to the angle of attack feedback in pitch. The pilots were forced to change their control technique from small delicate control inputs in the early stages of the approach to large coarse corrections in the final seconds to overcome the disturbances.

In contrast to the prefilter washout configurations, increasing the bandwidth of flight path control through augmentation of L_α/V on Configuration 11 offered a significant improvement in pilot rating and performance. The wider bandwidth of flight path control with good pitch attitude characteristics gave the pilots confidence in the specified task. Less lead compensation was required in the final portion of the approach. Pilots did not complain of the expected higher gust sensitivity associated with the increased level of L_α/V.

An improvement was also obtained by extending the bandwidth of attitude, and consequently flight path, control. The increase in short period frequency of Configuration 10 resulted in markedly improved pitch response and better tracking and was rated somewhat better than the high L_α/V case (Configuration 11). The pilot did not comment about the expected nose bobbing due to the medium damping of the short period mode ($\zeta_{sp} \tilde{=} 0.4$). The final errors at touchdown were quite small with this configuration.

Pilot preference for the surface washout (Configurations 5 and 7) over a force washout (Configurations 6 and 8) was clearly demonstrated. In the stick force washout system the centering or restoring force which the pilot feels is modified by the integration of the stick offset. This force feedback resulted in unfamiliar feelings to the pilot since the force was not the normal function of stick displacement. A trimming problem was also noted due to the interaction of the nonlinear stick force gradient (reference Figure 17). This was alleviated and the pilot rating was improved (as shown in the parentheses of Configuration 8, pilot A in Table 7) when a linear stick force gradient was substituted.

2. Flight Simulation, Phase I

Six of the configurations of the ground simulation studies were selected for flight testing. During the course of the experiments Configuration 12, having both high short period frequency and lift curve slope, and Configuration 13, having improved short period damping, were added. The optimum control sensitivity ($M_{\delta e}$) for each configuration was selected by the pilots in preliminary practice runs. A total of 76 data runs were flown by two Princeton test pilots, and their ratings are presented in Table 8 along with

TABLE 8

PILOT RATINGS

Phase I In-Flight Simulation Tests

Configuration	Pilot A	Pilot B	Flt Average	(Grd. Average)
3	2.3	2.5	2.4	(3.3)
4	3.2	3.8	3.5	(4.4)
5	2.8	3.0	2.9	(3.4)
7	3.5	5.0	4.3	(3.5)
10	2.5	2.5	2.5	(2.5)
11	2.0	-	2.0	(2.7)
12	2.0	2.5	2.3	-
13	-	1.8	1.8	-

the previous ground simulation results (in parentheses). As a whole the ratings were better than those obtained in the simple ground based simulation because of the increased realism and better kinematic and visual cues.

Both pilots again felt the attitude command control system of Configuration 3 was a significant improvement over the basic pitch dynamics of Configuration 4. As before, Configuration 5 was rated slightly worse than its flight path response twin, Configuration 3, due to its response to turbulence. The high flight path bandwidth Configuration 7 was much more annoying and required considerably more pilot compensation than the unaugmented basic pitch dynamics. The pilots were less inclined to ignore the pitch overshoots noted in the ground simulation in the actual flight

situation. This response was particularly bothersome in the final portions of the approach where the inability to control pitch attitude precisely far outweighed the merit of increased flight path response. Even this latter characteristic was not achieved as the pilots were reluctant to use other than low frequency control inputs for fear of adversely disturbing the pitch attitude. The spikelike pitch overshoot in Configuration 7 seemed to be amplified by turbulence more so than in the ground based simulation.

Although some improvement in flying qualities was seen in the ground simulation for a further increase in the short period frequency, a similar result was not found in the flight tests. The pilots did feel that Configuration 10 had acceptable characteristics but that the response was more than that required to do the job. Since no improvement in tracking performance was obtained, the smoother control response of Configuration 3 was verbally preferred although the rating of the two configurations was about the same. This same verbal comment was made for the high lift curve slope of Configurations 11 and 12.

The combination of a medium frequency attitude command system and high lift curve slope was the best configuration of the test group. This configuration was rated a 2.0 by Pilot A. Partly in response to Pilot B's comments the short period damping ratio was increased (Configuration 13). Pilot B rated this improved configuration a 1.8.

Five of the Phase I Flight Simulation configurations are plotted with the boundaries of the Mil. Spec. (Reference 9) and Grumman requirements (Reference 7) for a precise tracking task in Figure 27. All configurations tested satisfied the minimum boundaries of both references, and even

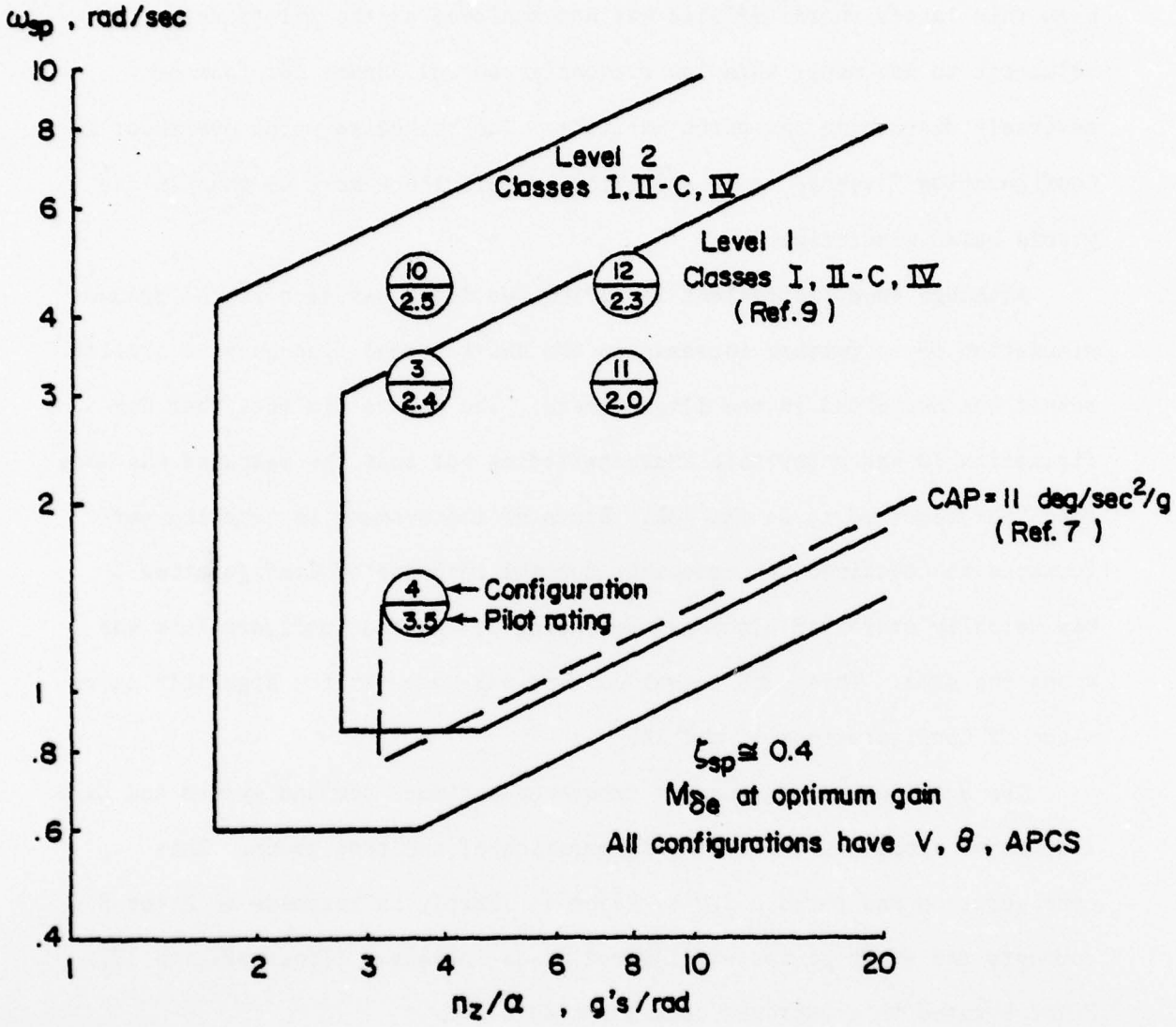

Figure 27. Compliance of Configurations of Phase I In-Flight Simulation with Requirements of References 7 and 9.

Configuration 10 which exceeded the upper boundary for Level 1 of the Mil. Spec., received a good rating. It should be noted that the prefilter washout Configurations 5 and 7, rated 2.9 and 4.3 respectively, which are not shown, would be plotted in the same location as Configuration 3.

3. Flight Simulation, Phase II

In the first phase of testing the APCS part of the system was fixed and the short period dynamics, in particular the flight path response, was investigated. The APCS mechanization consisted of an attitude to throttle decoupling feedback and a velocity feedback for flight path stability. No sensor filter was used; however, the engine time lag was simulated.

In Phase II the flight path response was fixed to either that of the basic aircraft or the favorable attitude command control system while the APCS was studied. Six APCS variations were tested. As a base APCS configuration the aforementioned simplified system of the ground and Phase I simulations was used (reference Table B2 of Appendix B, Configurations 3 and 4). In Configuration 16A an integral of the angle of attack error was substituted as the decoupling feedback. The gain used was the value of that of the present A-7E APCS, which is about 34% higher than the theoretical value. Next, the velocity feedback was replaced with a pseudo velocity feedback in Configuration 17 and filtering of the pseudo velocity signal was added in Configuration 20. For comparison the current A-7E APCS was mechanized in Configurations 14 and 15. In Configuration 15A the stick crossfeed signal was removed.

The characteristic low frequency roots of the Phase II configurations are plotted on the complex plane of Figure 28 with the loci of the APCS

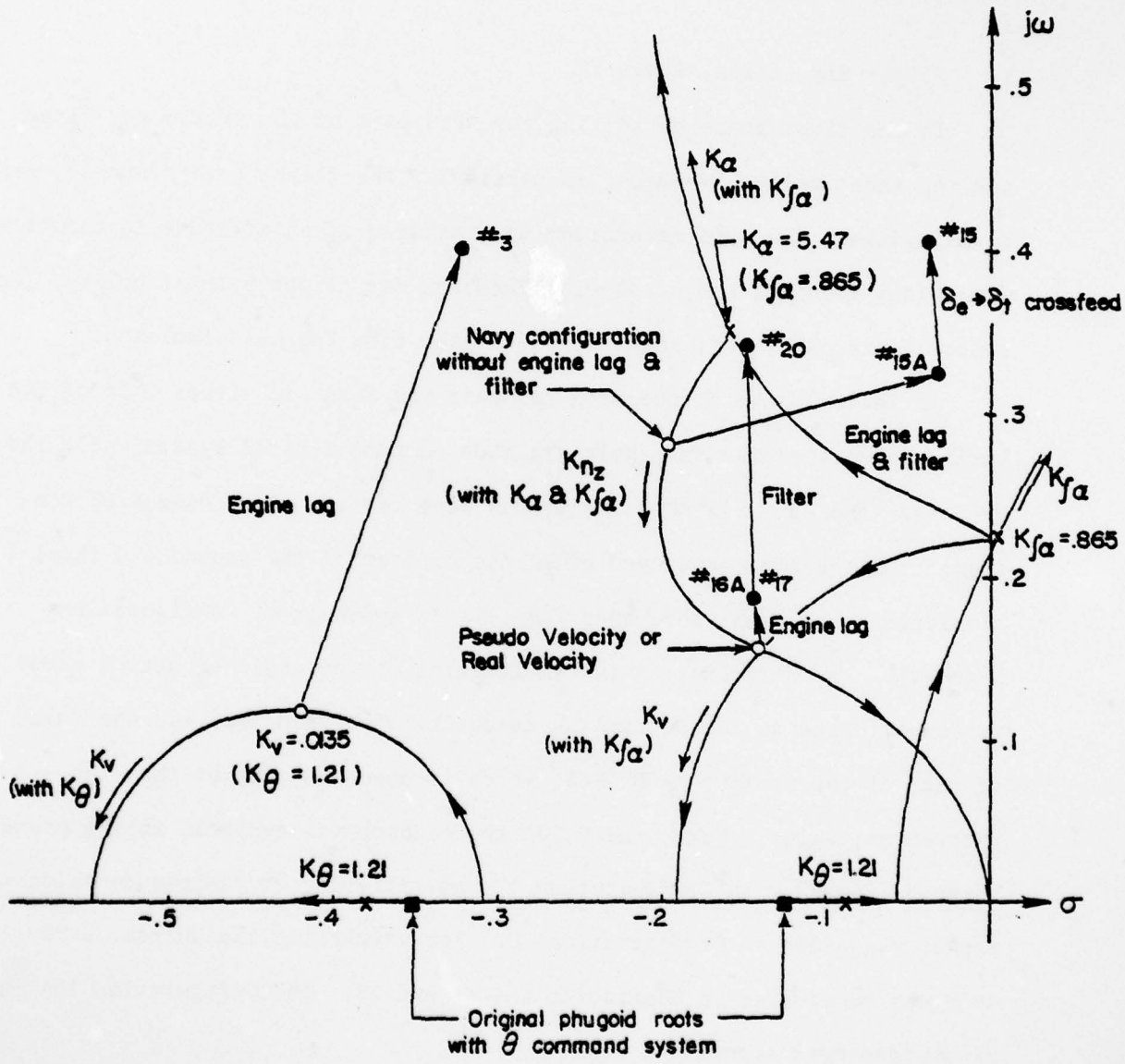

Figure 28. Predominant Lower Frequency Roots of Configurations in Phase II In-Flight Simulation

AD-A055 892 PRINCETON UNIV N J DEPT OF AEROSPACE AND MECHANICAL--ETC F/G 1/2
THE INFLUENCE OF THROTTLE AUGMENTED STABILITY (APCS) AND SHORT --ETC(U)
MAR 78 G E MILLER, S SEMBONGI, E SECKEL N00019-75-C-0528

UNCLASSIFIED AMS-1325 NL

2 OF 2
AD
A055 892

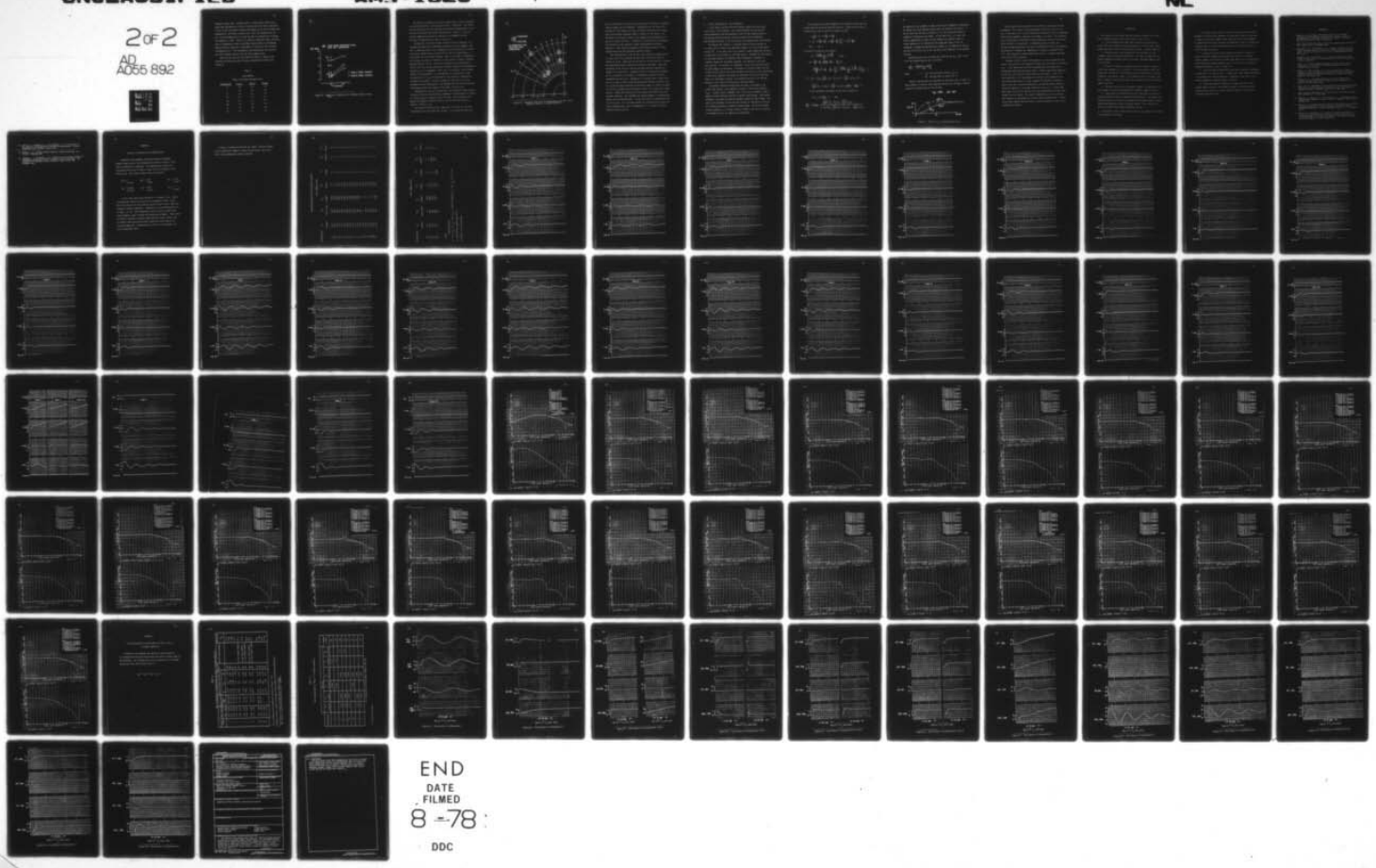

END
DATE FILMED
8-78
DDC

feedbacks without lags. Although there is a large adverse effect due to engine lag, Configuration 3 used in the ground and both flight simulations is seen to have the highest frequency and damping of the test configurations. Comparatively, the effect of engine lag is small for Configurations 16A and 17 and the damping ratio is about the same as Configuration 3 although the frequency is lower. However, the effect of additional sensor filtering used in Configuration 20 has a noticeably adverse effect on the damping. Engine and sensor lags have a large effect in the case of the A-7E APCS (Configuration 15). This configuration and Configuration 15A, which has the stick crossfeed removed, have the lowest damping ratio.

About 140 data runs were made during the Phase II studies by two Princeton test pilots and their ratings are presented in Table 9 and Figure 29.

TABLE 9

PILOT RATINGS

Phase II In-Flight Simulation Tests

Configuration	Pilot A	Pilot B	Average
3	2.5	2.5	2.5
4	4.5	3.5	4.0
14	5.3	5.3	5.3
15	4.7	4.7	4.7
15A	4.7	5.5	5.1
16A	2.8	2.8	2.8
17	2.7	3.3	3.0
20	3.2	4.7	4.0

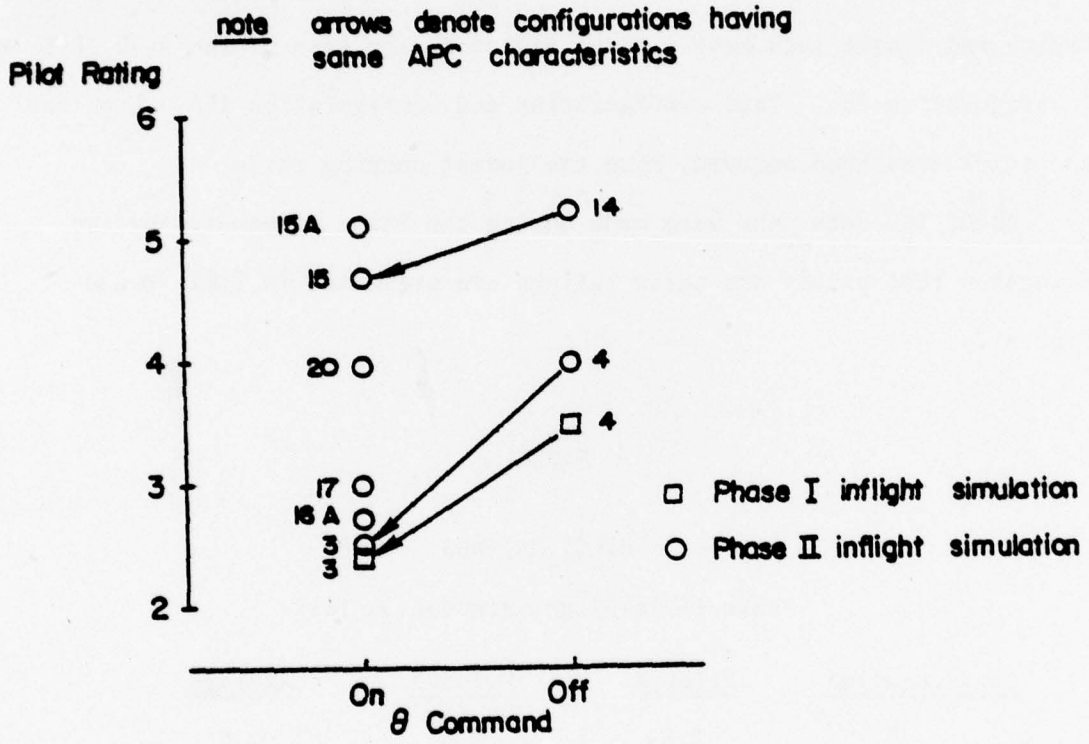

Figure 29. Comparison of Importance of θ Command System in Flight Test

The effect of providing an attitude command control system is favorable as was found previously in the ground and Phase I simulations. This effect was more pronounced with the simplified APCS design (Configurations 4 and 3) than with the current APCS design (Configurations 14 and 15). With the attitude command system the pilot ratings are in agreement with the frequency and damping effects shown in Figure 30.

Configuration 3 received the best rating as would be expected. This configuration exhibited no undesirable characteristics once engaged. However, as mentioned before, this configuration (also Configuration 4 without the attitude command control system) does not have an inherent means of establishing the trim throttle setting. That is, the effect of temperature, gross weight, variations in headwind (or WOD) require a slightly different approach throttle setting. For the test program this was determined in initial trial runs and the airplane was carefully trimmed to the premeasured conditions prior to engagement. While this was acceptable in the academic context of the experiment, it is unacceptable as an operational system. The substitution of $K_{\int\alpha}$ as the decoupler in the remaining configurations overcomes this problem. As shown in Figure 29, there was very little difference between Configuration 3 and Configuration 16A which has inherent autotrimming through the integral of the angle of attack error.

Configurations 16A and 17 theoretically have identical dynamic behavior. The pilots could not distinguish any difference in controllability in smooth air tests and their ratings are nearly the same. Some differences did appear with respect to throttle activity and was described previously (Throttle Thrash, p. 52).

The current APCS Specification (Reference 2) dictates the use of an accelerometer with one second time constant. As was shown previously the

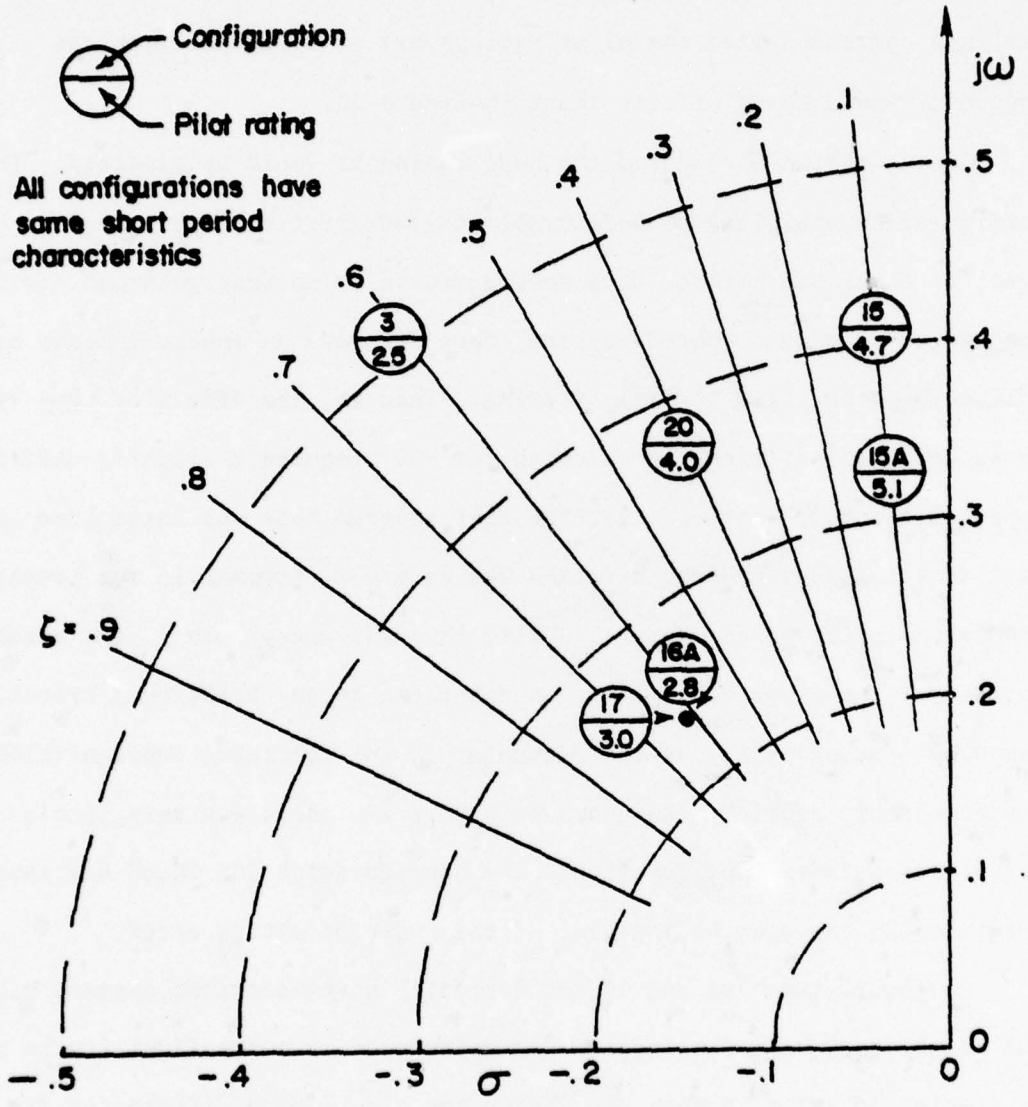

Figure 30. Predominant Mode Roots of Configurations and Their Pilot Ratings in Phase II In-Flight Simulation

angle of attack sensor should be filtered equally to maintain a correlated response between the two feedbacks. Although this was not done in the original A-7E APCS design, the final "optimized" design does have nearly equal time constants (Reference Table 1, History of A-7E APCS, p. 19). The effect of filtering is shown in the comparison of Configurations 17 and 20 in Figures 28 and 30. As expected, the filtering was unfavorable. Time histories of the response of these configurations are shown in Appendix B. Some additional thoughts on the filtering aspect of these configurations have been presented (Throttle Thrash).

Both Configurations 15 and 15A have lower long period damping due to the lower level of K_{n_z} feedback and the sensor filtering as shown in Figures 28 and 30. Large velocity oscillations (of the order of $\pm$ 5 knots) were experienced during flight path tracking in both cases. These were bothersome to the pilots in that the airspeed deviations resulted in a change in the flight path. Although this type of flight path disturbance was of a relatively low frequency, it nonetheless required additional compensation by the pilot. Configuration 15 required small, smooth stick motions in order to avoid large throttle motions from the crossfeed. However, with the proper technique the additional degree of control available to the pilot by modulating the frequency content of his inputs was of some benefit. Flight path corrections could be made with slightly less pitch attitude excursions. The crossfeed also helped somewhat in countering the effects of the simulated burble. On the other hand, the configuration was still very poor. It is not known whether the crossfeed would improve the better configurations, such as Configuration 17, or detract from their decoupled characteristics.

4. Further Considerations, Turn Performance

In this report attention has been directed towards the final wings-level portion of the approach. Turn related problems and any required system compromises have been bypassed so that the more important phase of the approach and APCS operation could be studied without encumbrance. Some thoughts pertinent to the turn portion of the approach are now presented.

The present APCS concept is to maintain angle of attack constant at all times, and as a result, the speed must change in the turn by the factor $(\text{secant } \phi)^{\frac{1}{2}}$. In the case of the A-7E airplane, a speed change from 129 knots at wings-level to 139 knots at a 30^{o} bank results. Although the time required for the speed change is not specified (MIL-C-23866A(WP), Reference 2), sluggish changes are considered a problem. This applies to both turn entry and exit. An overshoot (or undershoot) of the trim condition during the speed change is undesireable. Performance of the APCS during turn exit is more critical than for turn entry because slow recovery to trim necessitates a longer final approach, and because any undershoot of the trim speed will result in a high angle of attack, low airspeed situation at low altitude, possibly in the vicinity of the carrier turbulence burble.

The primary mechanism through which the speed is increased in the current APCS design is the integration of angle of attack error feedback ($K_{\int\alpha}$). A pseudo velocity feedback, like a true velocity feedback, tends to maintain a given reference velocity or oppose a speed change. From another standpoint, the normal acceleration feedback opposes the speed change. The sense of this feedback is such that the increase of load factor in the turn will retard the throttle or oppose the speed change. The level of pseudo velocity feedback is, of course, directly related to the level of acceleration feedback and the two viewpoints are equivalent.

The influence of the APCS feedbacks on the dynamics during turns can be seen from the following simplified analysis. Assume that the turn or recovery from a turn is made at a constant altitude.

$$L = \frac{W}{\cos\phi} = W + \Delta V \frac{\partial L}{\partial V} + \Delta\alpha \frac{\partial L}{\partial \alpha}$$

$$D = D_o + \Delta V\left(\frac{\partial D}{\partial V} + \frac{\partial T}{\partial V}\right) + \Delta\alpha\left(\frac{\partial D}{\partial \alpha} + \frac{\partial T}{\partial \alpha}\right) + \left[\int_o^t \Delta\alpha\, dt\right]^{\dagger} \frac{\partial T}{\partial [\,]^{\dagger}}$$

$$m\Delta\dot{V} + \Delta D = 0$$

solving for $\Delta\alpha$ from the lift equation

$$\Delta\alpha = \frac{W\left(\frac{1}{\cos\phi} - 1\right) - \Delta V \frac{\partial L}{\partial V}}{\frac{\partial L}{\partial \alpha}} \qquad \text{hence}$$

$$m\Delta\dot{V} + \left[\frac{\partial D}{\partial V} + \frac{\partial T}{\partial V} - \left(\frac{\partial L/\partial V}{\partial L/\partial \alpha}\right)\left(\frac{\partial D}{\partial \alpha} + \frac{\partial T}{\partial \alpha}\right)\right]\Delta V$$

$$+ \frac{W\left(\frac{1}{\cos\phi} - 1\right)}{\frac{\partial L}{\partial \alpha}}\left(\frac{\partial D}{\partial \alpha} + \frac{\partial T}{\partial \alpha}\right) + \left[\int_o^t \frac{W\left(\frac{1}{\cos\phi} - 1\right) - \Delta V \frac{\partial L}{\partial V}}{\frac{\partial L}{\partial \alpha}}\, dt\right] \frac{\partial T}{\partial [\,]^{\dagger}} = 0$$

$$\left\{s^2 + \left[D_v + K_v^* D_{\delta t} - \frac{L_v/V}{L_\alpha/V}\left(D_\alpha + K_\alpha' D_{\delta t}\right)\right] s - \frac{L_v/V}{L_\alpha/V} K_{\int\alpha} D_{\delta t}\right\} \Delta V =$$

$$- \left\{\frac{L_v/V}{L_\alpha/V}\left(D_\alpha + K_\alpha' D_{\delta t}\right) s + \frac{L_v/V}{L_\alpha/V} K_{\int\alpha} D_{\delta t}\right\} \frac{g}{(L_v/V)\, V} \Delta\left(\frac{1}{\cos\phi} - 1\right)$$

If the incremental load factor in the turn is defined as

$$\Delta n_{zt} = g\, \Delta\left(\frac{1}{\cos\phi} - 1\right) \qquad \text{then}$$

$$\frac{\Delta V}{\Delta n_{zt}} = \left(\frac{1}{V\, L_v/V}\right) \frac{- \frac{L_v/V}{L_\alpha/V}\left(D_\alpha + K_\alpha' D_{\delta t}\right) - \frac{L_v/V}{L_\alpha/V} K_{\int\alpha} D_{\delta t}}{s^2 + \left[D_v + K_v^* D_{\delta t} - \frac{L_v/V}{L_\alpha/V}\left(D_\alpha + K_\alpha' D_{\delta t}\right)\right] s - \frac{L_v/V}{L_\alpha/V} K_{\int\alpha} D_{\delta t}}$$

The addition of the integral of angle of attack error feedback is responsible for making the system response second order, and typically oscillatory. It may be noted that the term in brackets [ ] is the flight path stability parameter or front/back side effect. If the level of K_{n_z} is varied, the relative magnitudes of pseudo velocity feedback and effective angle of attack feedback will be altered but the flight path stability will be unchanged. Although the characteristic equation is not effected by the proportion of K_V^* and K_α', such is not the case for the numerator of the transfer function.

Substituting the level of flight path stability and $K_{\int\alpha}$ values of the A-7E, the transfer function may be evaluated

$$\frac{\Delta V}{\Delta n_{zt}} = \frac{3.48\ (A\ s + .057)}{s^2 + .36\ s + .057}$$

where $A = -.045$ for pure pseudo velocity ($K_\alpha' = 0$)

$+.317$ for pure angle of attack ($K_V^* = 0$)

Velocity time histories are presented for the above cases in Figure 31. Some overshoot is shown by this simplified analysis for the angle of attack relative to a pseudo velocity type of APCS.

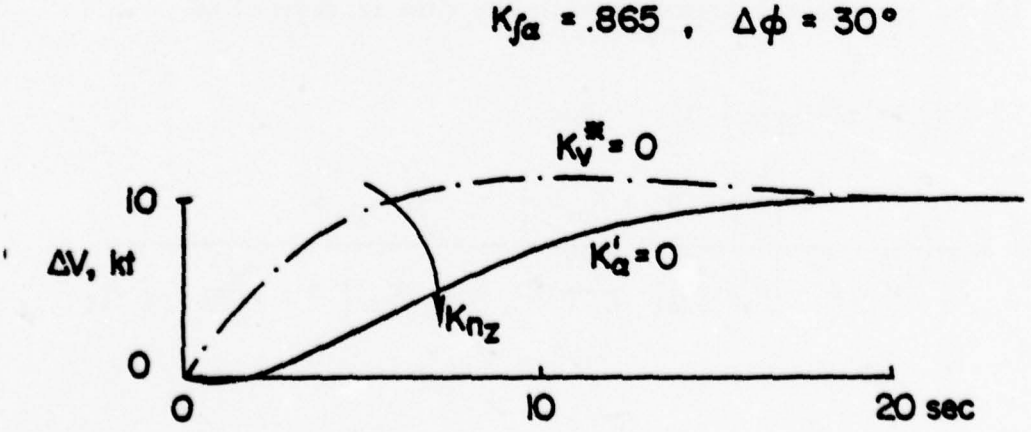

Figure 31. Effect of K_{n_z} on Speed Increase Turns

The available throttle authority of the APCS also influences the turn performance. With respect to the speed change required at turn exit, the A-7E, in particular, has a limited deceleration capability which is exaggerated under some environmental conditions (for example, cold days). This deceleration is determined by the minimum allowable engine rpm (thrust) and the drag of the aircraft on the approach. Disregarding engine time lags, the absolute minimum deceleration time from a 30 degree bank turn on the approach glideslope for a standard day (temperature) is nearly six seconds for the A-7E. This theoretical minimum deceleration time is a sizeable percentage of the typical final approach.

Although no formal study of APCS operation in turns was made for this report, some results of the exploratory flight tests are worthy of consideration. In the exploratory tests APCS configurations were tested which incorporated additional bank angle inputs. Constant speed turns mechanized by the bias of the angle of attack error with bank angle ($(\text{secant } \phi)^{\frac{1}{2}}$) were rated about 1/2 a Cooper-Harper unit better by the Princeton pilot. The constant speed turn, of course, bypasses the problems of increasing speed in the turn, overshoots/undershoots, and limited throttle authority which were apparent in the flight simulation of the A-7E. A direct bank angle input (or one which does not alter the constant angle of attack turn concept) was also tested. This type of compensation is used on the S-3A APCS; however, no improvement was noted in the exploratory tests. Finally, the attitude command system was found to function properly in turns and no problems were observed.

CONCLUSIONS

1. With respect to APCS design, the following are concluded for aircraft with an effective engine lift to thrust ratio of 20% or less:

a. Pilot evaluations show that speed excursions are undersirable because they cause flight path tracking problems. For this reason lightly damped long period velocity modes should be avoided (reference page 89).

b. Pseudo velocity type configurations were preferred over predominantly angle of attack configurations. The former configurations had improved damping and smaller velocity excursions (reference pages 48 thru 50, 87 and 88).

c. There is a theoretical optimum value for an integral of angle of attack error feedback ($K_{\int\alpha}$) of an APCS. This value decouples speed from flight path corrections. Decoupling may also be obtained with an attitude feedback to the throttle, alone, or in combination with the integral feedback. Formulae to calculate the gains are presented in the text (reference pages 41 thru 48).

d. Throttle activity due to turbulence (thrash) is significantly less with (pseudo) velocity type configurations (reference pages 52 thru 55).

e. Equal sensor filtering should be used on the angle of attack and normal acceleration sensors to minimize throttle thrash. Considerably less filtering than the 1.0 second time constant of the present normal accelerometers seems adequate in terms of throttle thrash. Less filtering will provide increased system damping (reference page 55).

2. With respect to the aircraft short period mode and flight control system, the following are concluded.

a. For typical static stability levels, increasing the short period frequency to provide wider bandwidths in flight path response is desirable. A simple pitch attitude command system using attitude and rate feedbacks to improve the short period frequency and damping was found to be sufficient (reference page 74, also compare Configuration 4 with configurations 3, 5 and 10 on pages 76 and 80).

b. Increasing the short period frequency by means of an angle of attack to elevator feedback was verified to be inferior to the pitch attitude command system because of higher gust sensitivity, and additionally, lower long period damping (reference pages 78 and 80, and the comparison between Configurations 3 and 5 on page 154).

c. If the aircraft has appreciable short period frequency and damping (of the order of 3.0 rad/sec and .7 respectively), then further improvement in the flight path response bandwidth is dependent on some form of lift control augmentation (reference pages 79 thru 81).

d. Flight path bandwith augmentation through prefilter or feed-forward washout systems is undesireable because of pitch attitude over-shoots and the inability to control attitude precisely near touchdown (reference pages 80 and 81).

REFERENCES

1. Brown, P. W., "In-Flight Simulation of the A-7E in a Manually Controlled Landing Approach, APC ON and OFF," Master's thesis of the Department of Aerospace and Mechanical Sciences of Princeton University, Report No. 1156-T, April 1974.

2. Anon, "Military Specification, Control Set, Approach Power AN/ASN-54(V), MIL-C-23866A (WP)," 15 September 1965.

3. Stapleford, R. L. and Ashkenas, I. L., "Effects of Manual Altitude Control and Other Factors on Short-Period Handling Quality Requirements," Journal of Aircraft, Vol. 5, No. 1, January-February 1968, pp. 41-48.

4. Cromwell, C. H. and Ashkenas, I. L., "A Systems Analysis of Longitudinal Piloted Control in Carrier Approach," Systems Technology, Inc. TR 124-1, June 1962.

5. Jeske, R. A., "Final Engineering Report Automatic Flight Control System for A-7D/E Aircraft," LTV Aerospace Corporation Report 2-53560/9R-5448 (no date).

6. Miller, G. E. and Traskos, R. L., "Flight Evaluation of Engine Response, Flight Path Stability, Tail Lift, and Direct Lift Control," Princeton University Aerospace and Mechanical Sciences Department Report No. 888, August 1971.

7. Bihrle, W., Jr., "Aircraft Characteristics that Influence the Longitudinal Handling Qualities during a Carrier Approach," AIAA Paper No. 69-894, August 1969.

8. Eney, John A., "Comparative Flight Evaluation of Longitudinal Handling Qualities in Carrier Approach," Princeton University Aerospace and Mechanical Sciences Department Report No. 777, May 1966.

9. Anon, "Military Specification, Flying Qualities of Piloted Airplanes, MIL-F-8785B(ASG)," 7 August 1969.

10. Bowes, W. C., Schust, A. P., and Griffith, J. L., "Evaluation of the Approach Power Compensator System in the A-7E Airplane," NATC FT-16R-71, 19 March 1971.

11. Mooij, H. A., "Flight Evaluation of Direct Lift Control and Its Effects on Handling Qualities in Carrier Approach," Princeton University Aerospace and Mechanical Sciences Department Report No. 814, December 1 1967.

12. Joslin, R. G. and Ohmiya, H., "A Study of an Open-Loop System for Decoupling Airspeed and Flight Path Angle Control," Master's thesis of the Department of Aerospace and Mechanical Sciences of Princeton University, Report No. 1234-T, March 1977.

13. Craig, S. J., Ringland, R. F., and Ashkenas, I. L., "An Analysis of Navy Approach Power Compensator Problems and Requirements," Systems Technology, Inc., TR-197-1, January 1971.

14. Durand, T. S., "Carrier Landing Analyses," Systems Technology, Inc., TR-137-2, February 1967.

15. Ashkenas, I. L. and Durand, T. S., "Simulator and Analytical Studies of Fundamental Longitudinal Control Problems in Carrier Approach," AIAA Simulation for Aerospace Flight Conference, August 26-28, 1963. Columbus, Ohio.

APPENDIX A

Analysis of Preliminary Test Configurations

Presented in this appendix are time histories and frequency response (Bode) plots of the configurations of Table 2, page 21. This table is repeated for convenience. The configurations use the A-7E longitudinal derivatives of Table 3, page 58 with the exception of the control terms. The assumed control terms are as follows:

$D_{\delta e} = 0$ (ft/sec) $\quad L_{\delta e}/V = .0672$ (1/sec) $\quad M_{\delta e} = -2.167$ ($1/sec^2$)

$D_{\delta t} = -26.6445$ (ft/sec^2) $\quad L_{\delta t}/V = .0232$ (1/sec) $\quad M_{\delta t} = 0$ ($1/sec^2$)

A first order engine time constant of 1.7 seconds is used. Sensor filtering time constants are noted on the configuration table except that in the case of the time histories the non-linear elevator input time constant is properly mechanized (Reference p. 51 and Configuration 6:12 of Table I, p. 19). The configurations use the attitude command inner loop of Figure 2, page 6 (without the acceleration feedback). The elevator to throttle crossfeed is properly taken from the elevator (rather than the control stick) position and thus contains the inputs made by the attitude command SAS. Configuration 0' is the case of the present A-7E and its operational APCS.

Finally, it should be noted that the symbol ' has been affixed to the configuration numbers to denote the preliminary test series and to avoid configuration identity problems.

CONFIGURATION MATRIX FOR PRELIMINARY ANALYSIS

APCS FEEDBACK GAINS

Configuration	K_{α}	$K_{f\alpha}$	K_{n_z}	$K_{\delta e}$	K_{v}	K_{n_x}	K_{θ}
	rad/rad	rad-sec/rad	rad/fps^2	rad/rad	rad/fps	rad/fps^2	rad/rad
0'	5.47	.865	.0154	4.37	0	0	0
0A'	5.47	.865	.0154	0	0	0	0
1'	2.73	.865	.0237	4.37	0	0	0
1A'	2.73	.433	.0237	4.37	0	0	0
2'	5.47	.865	.0475	4.37	0	0	0
2A'	5.47	.865	.0475	6.55	0	0	0
3'	8.20	.865	.0712	4.37	0	0	0
3A'	8.20	1.300	.0712	4.37	0	0	0
4'	5.47	.433	.0475	4.37	0	0	0
5'	5.47	1.300	.0475	4.37	0	0	0
6'	5.47	.865	.0309	4.37	0	0	0
7'	5.47	.865	0	4.37	0	0	0
7A'	5.47	0	0	4.37	0	0	0
7B'	5.47	.433	0	4.37	0	0	0
8'	5.47	.865	0	2.18	0	0	0
8B'	5.47	.433	0	2.18	0	0	0
8C'	5.47	.433	0	6.55	0	0	0
9'	5.47	.865	.0309	6.55	0	0	0

APCS FEEDBACK GAINS

Configuration	K_{α}	$K_{\int\alpha}$	K_{n_z}	$K_{\delta e}$	K_{v}	K_{n_x}	K_{θ}
	rad/rad	rad-sec/rad	rad/fps^2	rad/rad	rad/fps	rad/fps^2	rad/rad
10'	5.47	0	.0154	0	0	0	0
15'	5.47	.865	.0154	4.37	0	0	1.2
16'	5.47	.865	.0154	4.37	0	.0271	0
17'	5.47	.865	.0154	4.37	0	.0541	0
27A'	0	.865	0	4.37	.0135	0	0

Notes:

Input Filtering

$\tau_{\alpha} = 1.0$, $\tau_{\int\alpha} = 0$, $\tau_{n_z} = 1.0$, $\tau_{\delta e} = .5$ with 7.0 washout, $\tau_{v} = 1.0$, $\tau_{n_x} = 0$, $\tau_{\theta} = 1.0$

α corrected for upwash factor of 1.4

g $\Delta T/W/\delta t = 26.6$ ft/sec^2/rad

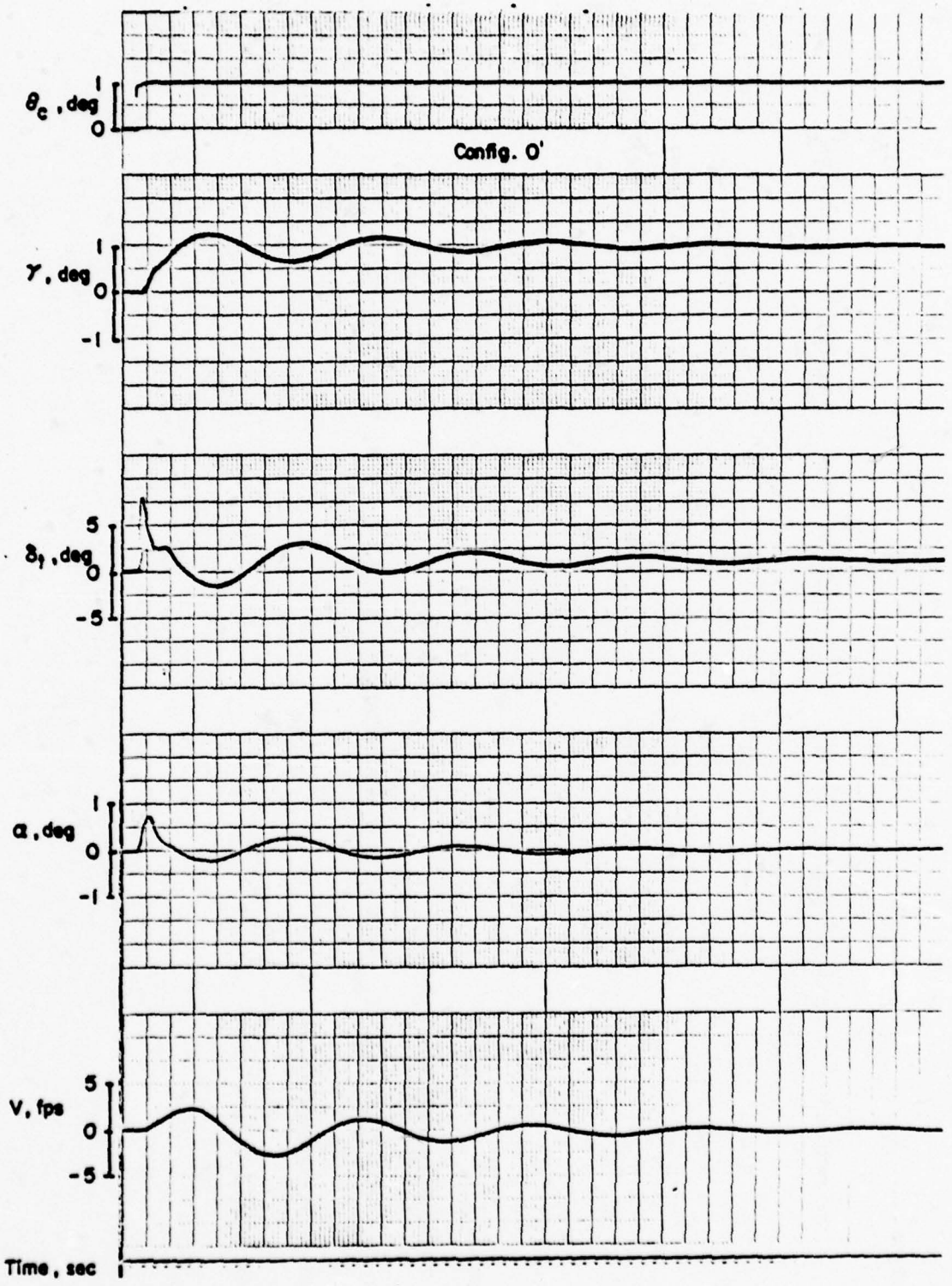
Config. O'
θ_c, deg
1
0
γ, deg
1
0
-1
δ_t, deg
5
0
-5
α, deg
1
0
-1
V, fps
5
0
-5
Time, sec

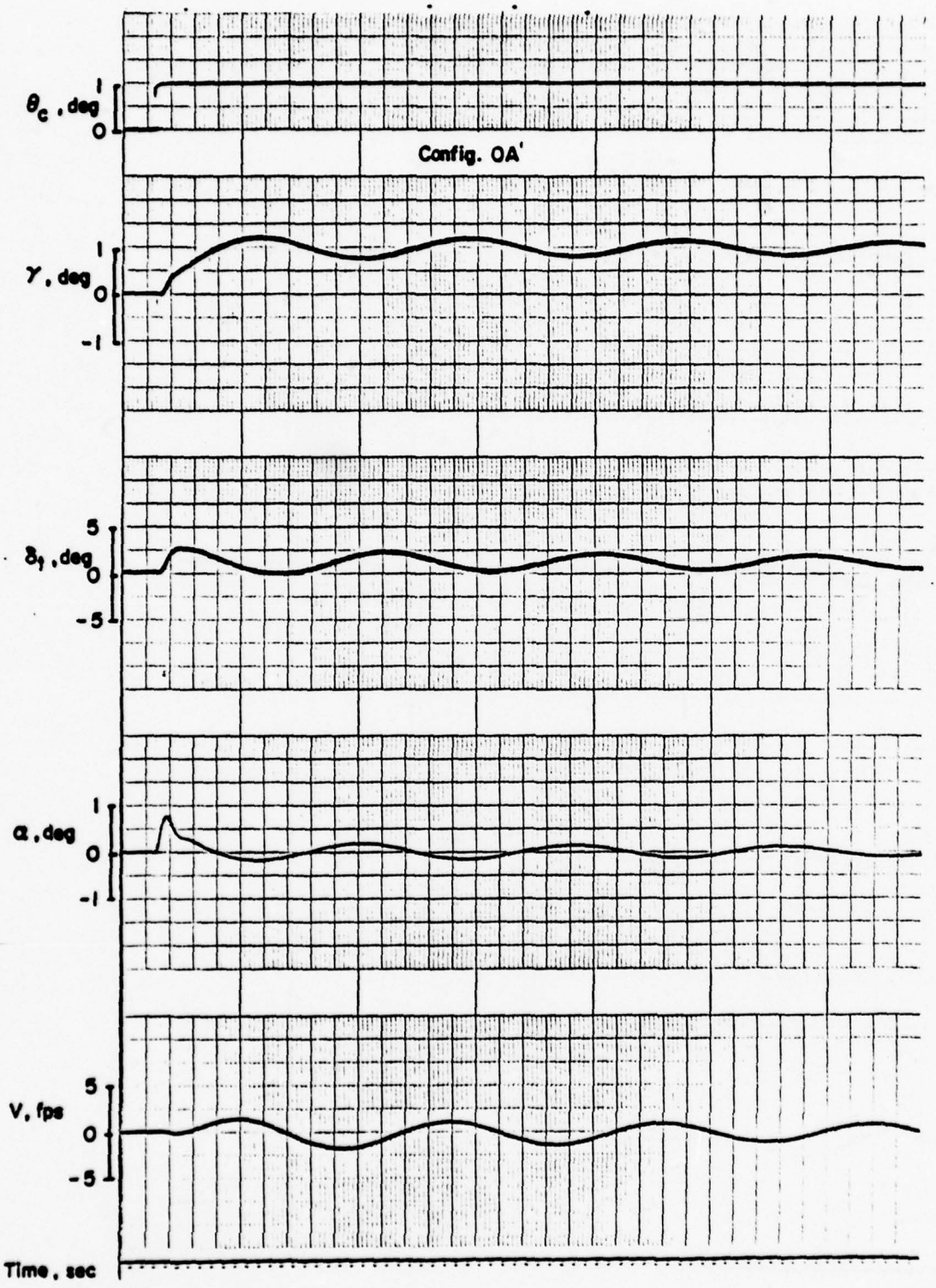
Config. OA'
θc, deg
1
0
γ, deg
1
0
-1
δf, deg
5
0
-5
α, deg
1
0
-1
V, fps
5
0
-5
Time, sec

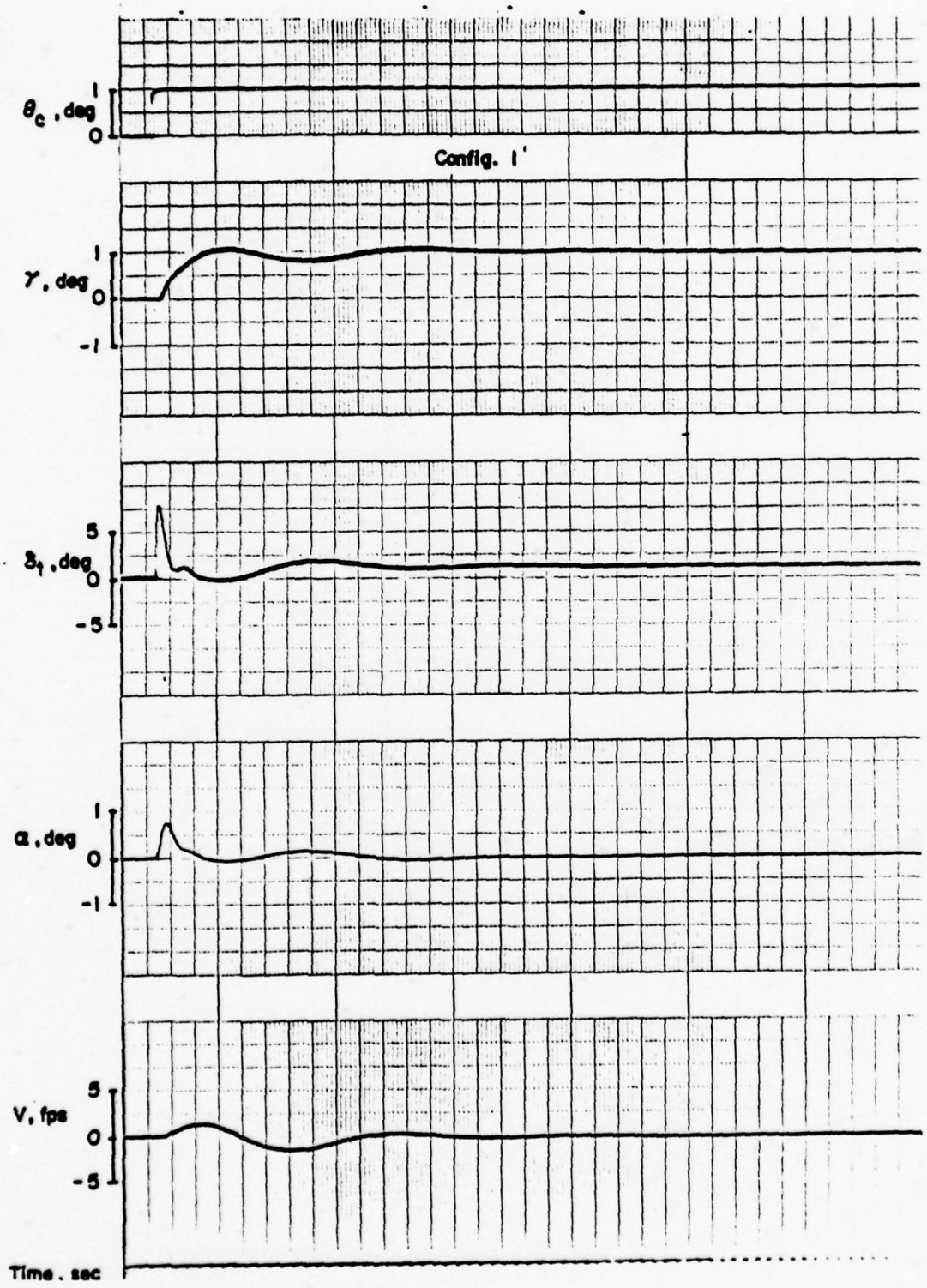
Config. 1'
θ_c, deg
1
0
γ, deg
1
0
-1
δ_f, deg
5
0
-5
α, deg
1
0
-1
V, fps
5
0
-5
Time, sec

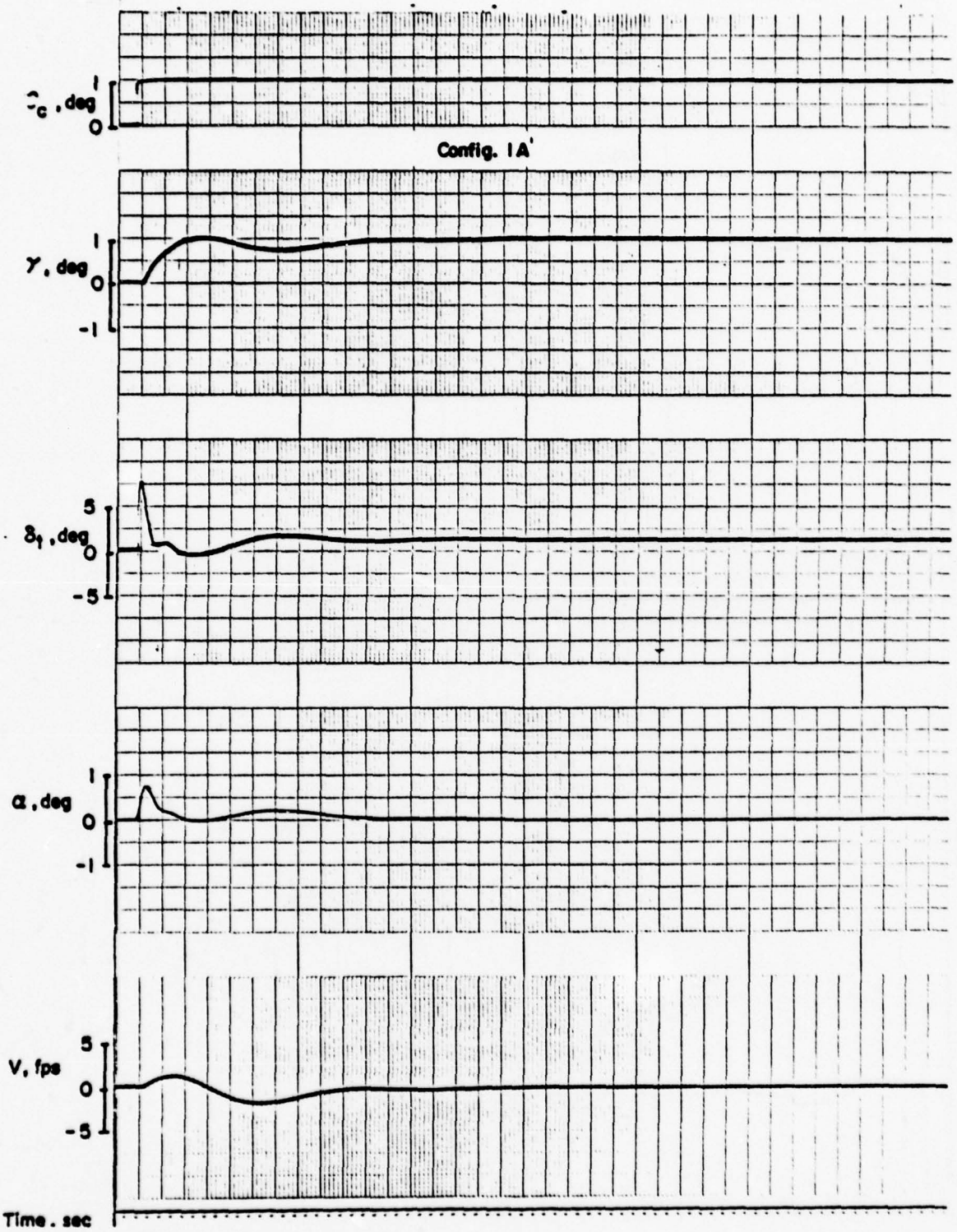
Config. 1A'
γ_c, deg
1
0
γ, deg
1
0
-1
δ_t, deg
5
0
-5
α, deg
1
0
-1
V, fps
5
0
-5
Time, sec

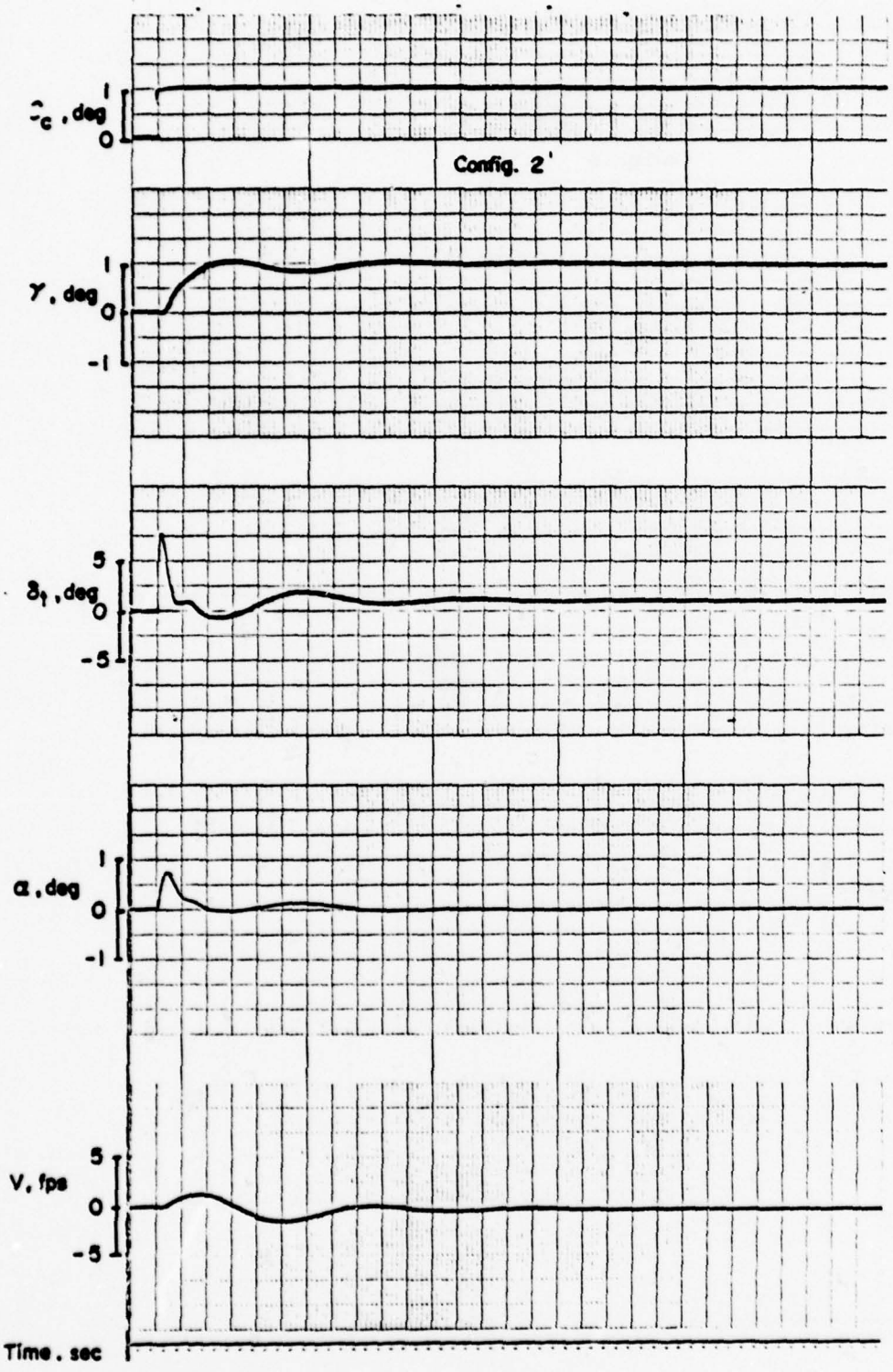
γ_c, deg
1
0
Config. 2'
γ, deg
1
0
-1
δ_t, deg
5
0
-5
α, deg
1
0
-1
V, fps
5
0
-5
Time, sec

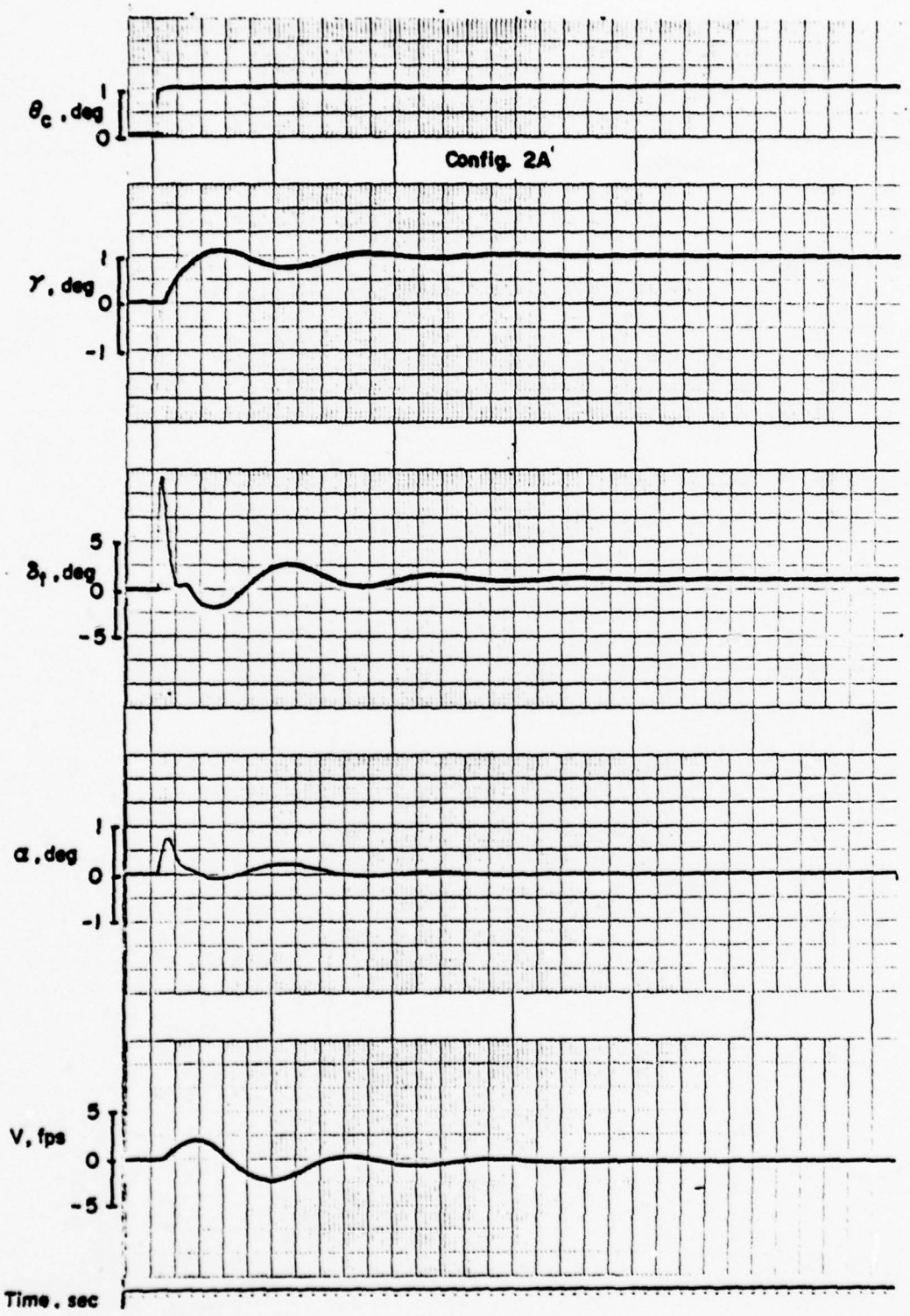
θ_c, deg
1
0
Config. 2A'
γ, deg
1
0
-1
δ_t, deg
5
0
-5
α, deg
1
0
-1
V, fps
5
0
-5
Time, sec

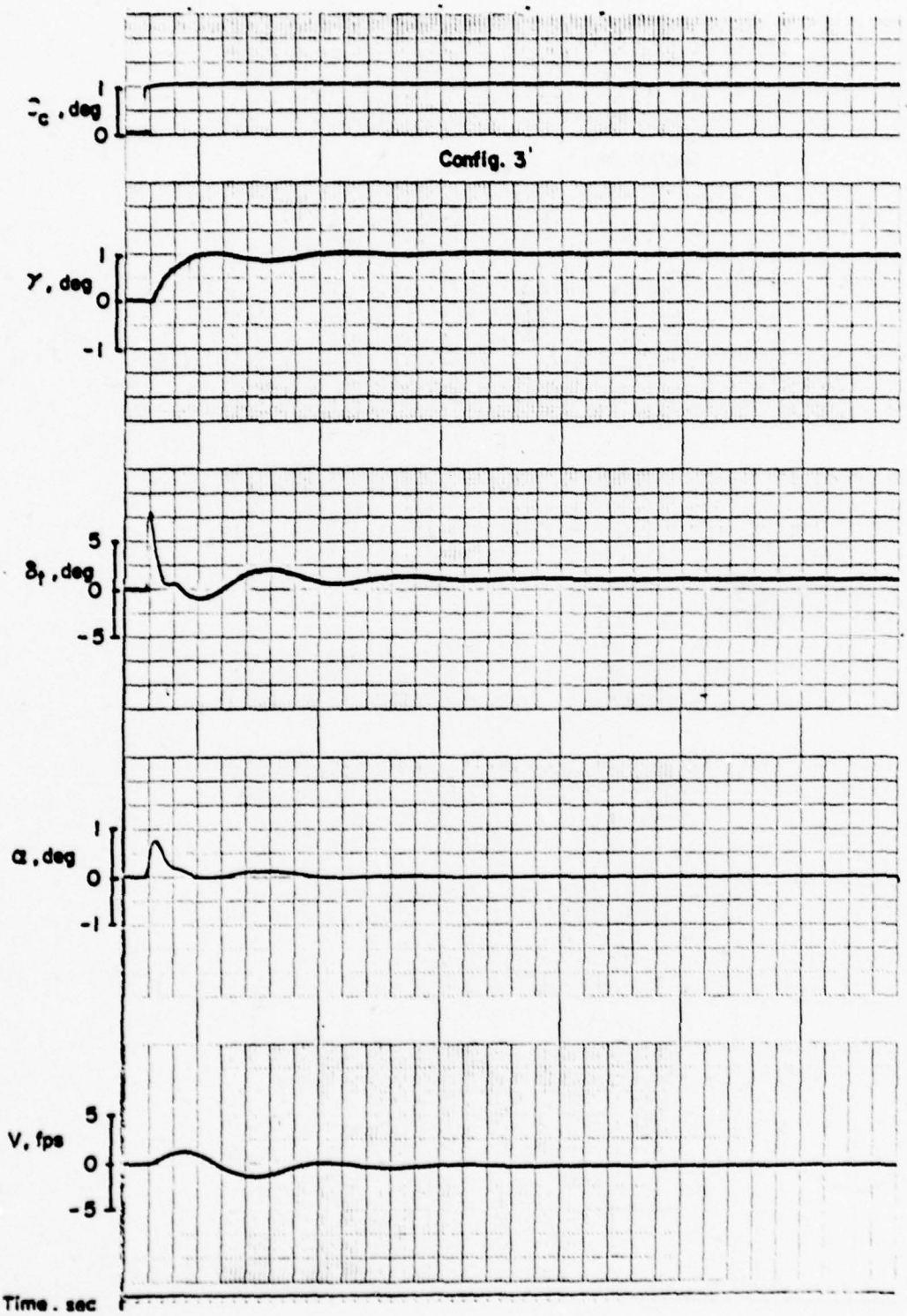
γ_c, deg
1
0
Config. 3'
γ, deg
1
0
-1
δ_t, deg
5
0
-5
α, deg
1
0
-1
V, fps
5
0
-5
Time, sec

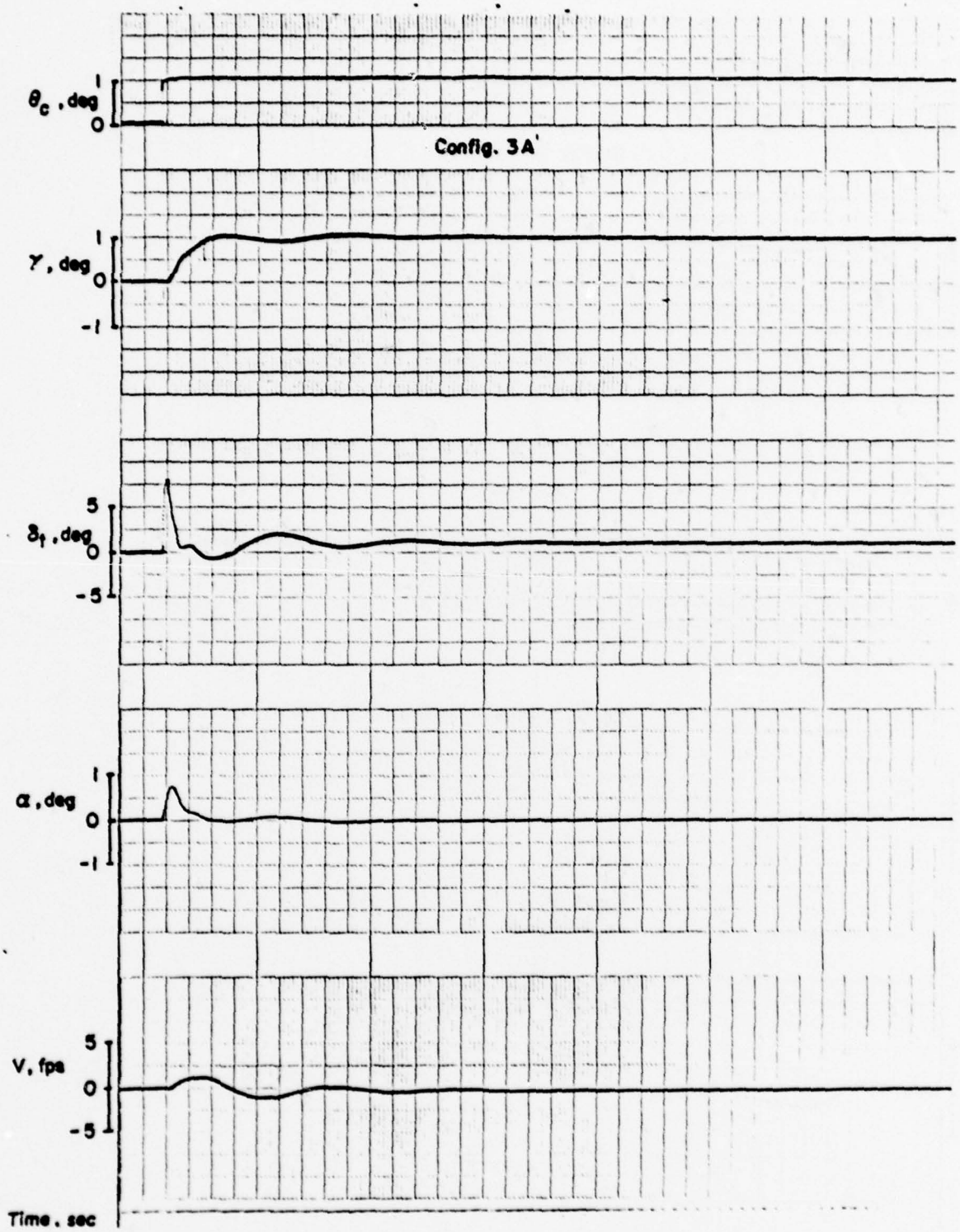
Config. 3A'
θ_c, deg
1
0
γ, deg
1
0
-1
δ_t, deg
5
0
-5
α, deg
1
0
-1
V, fps
5
0
-5
Time, sec

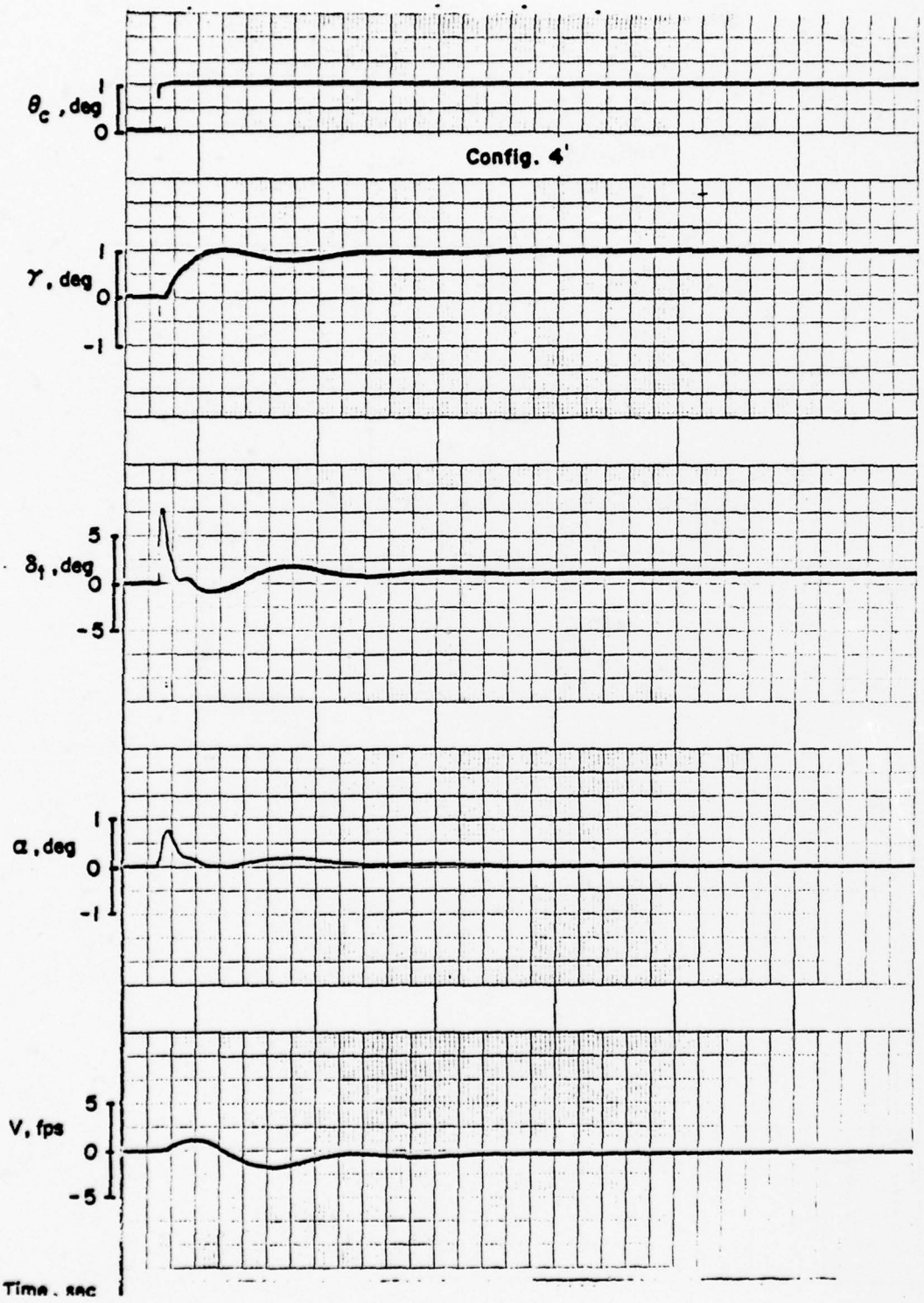
Config. 4'
θ_c, deg
1
0
γ, deg
1
0
-1
δ_t, deg
5
0
-5
α, deg
1
0
-1
V, fps
5
0
-5
Time, sec

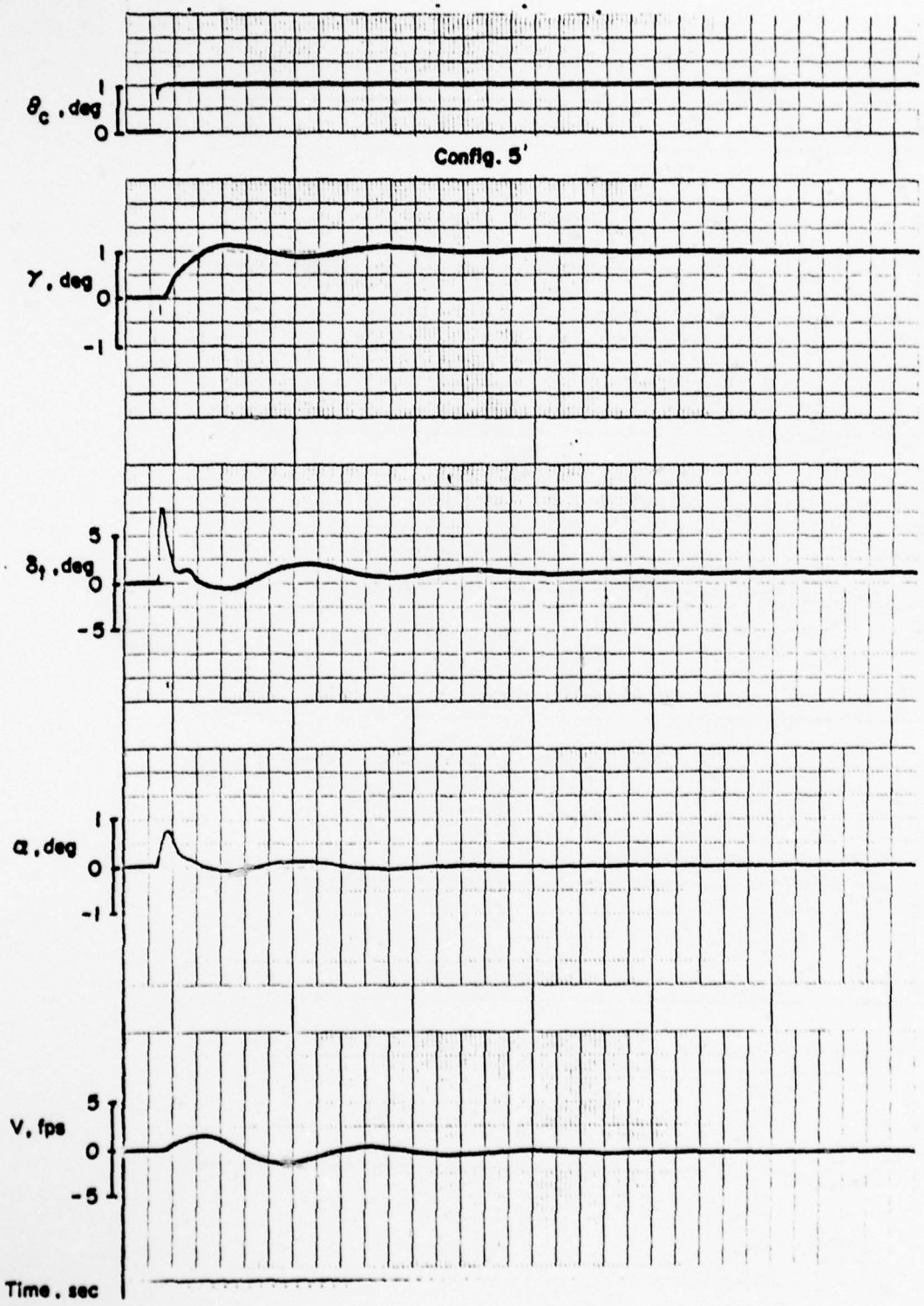
Config. 5'
θ_c, deg
1
0
γ, deg
1
0
-1
δ_f, deg
5
0
-5
α, deg
1
0
-1
V, fps
5
0
-5
Time, sec

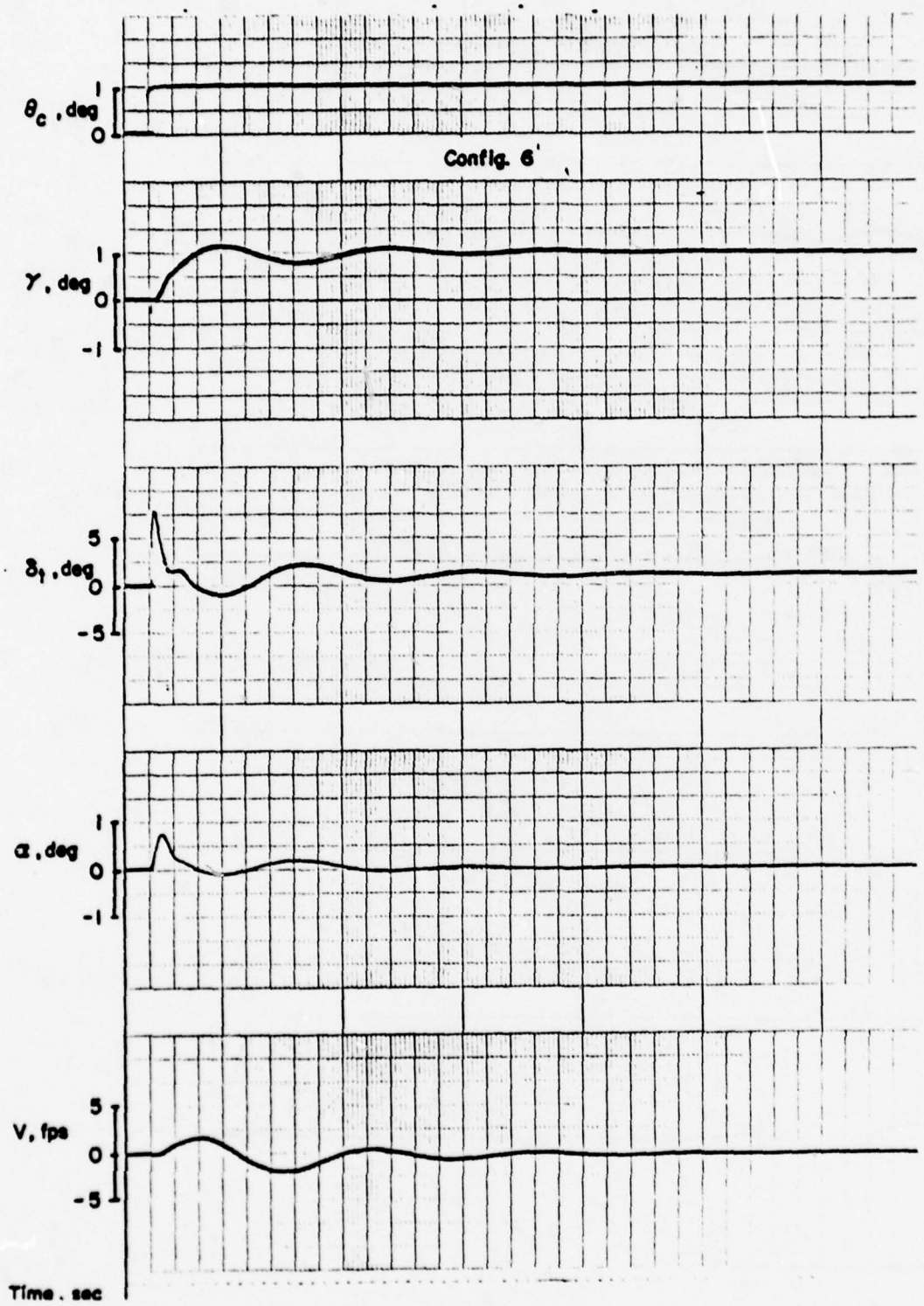
Config. 6'
θ_c, deg
1
0
γ, deg
1
0
-1
δ_t, deg
5
0
-5
α, deg
1
0
-1
V, fps
5
0
-5
Time, sec

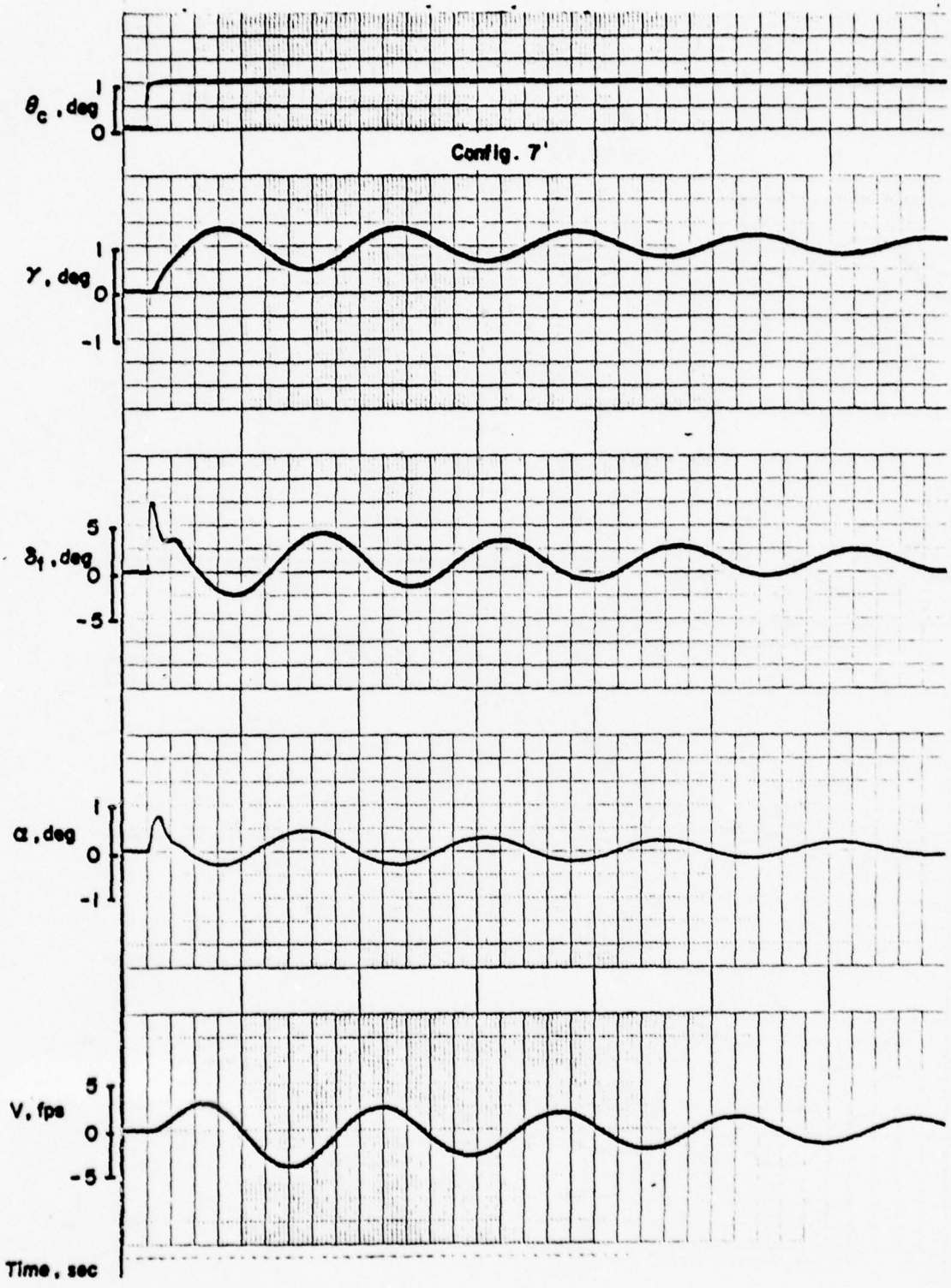
Config. 7'
θ_c, deg
1
0
γ, deg
1
0
-1
δ_f, deg
5
0
-5
α, deg
1
0
-1
V, fps
5
0
-5
Time, sec

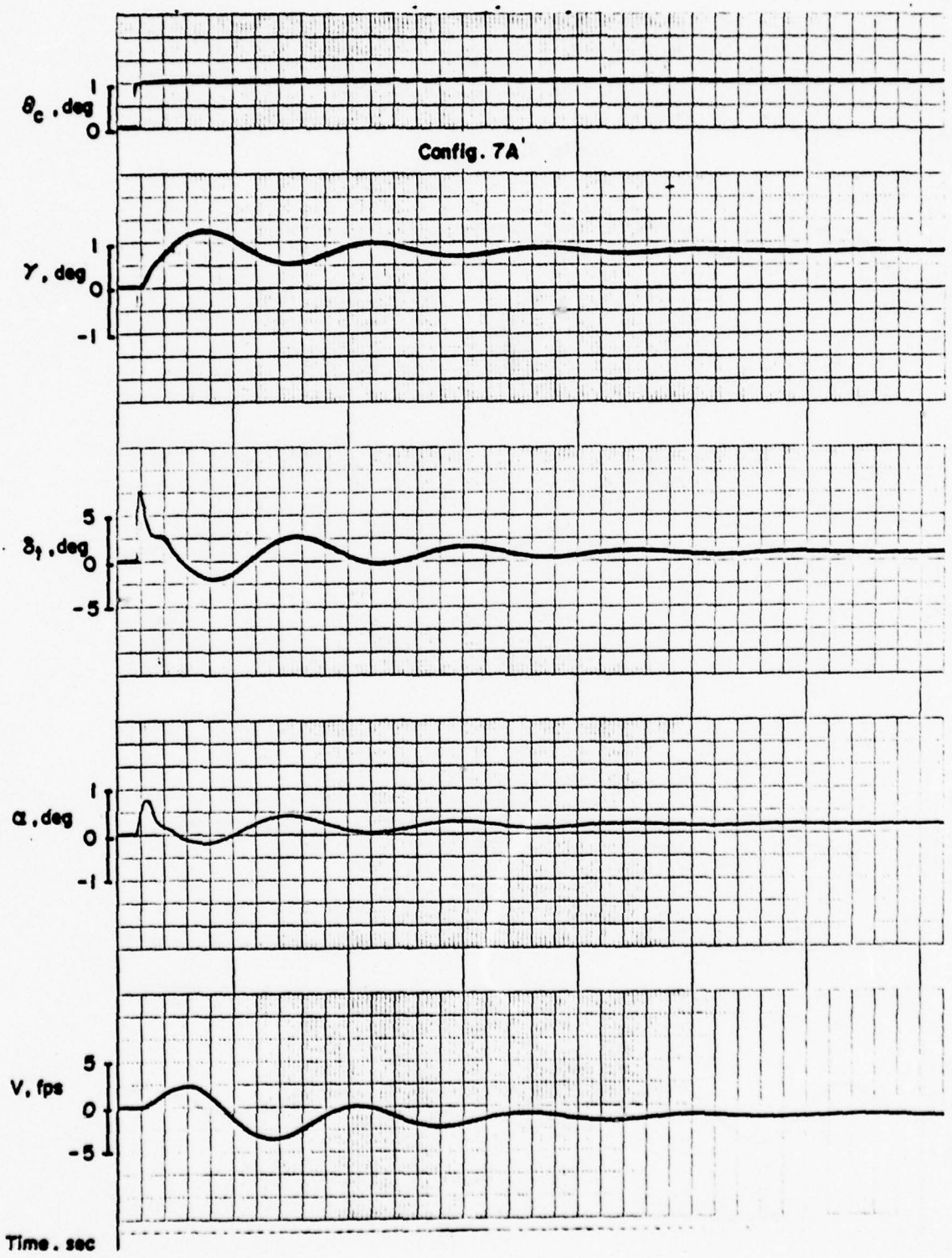
Config. 7A'
θ_c, deg
1
0
γ, deg
1
0
-1
δ_t, deg
5
0
-5
α, deg
1
0
-1
V, fps
5
0
-5
Time, sec

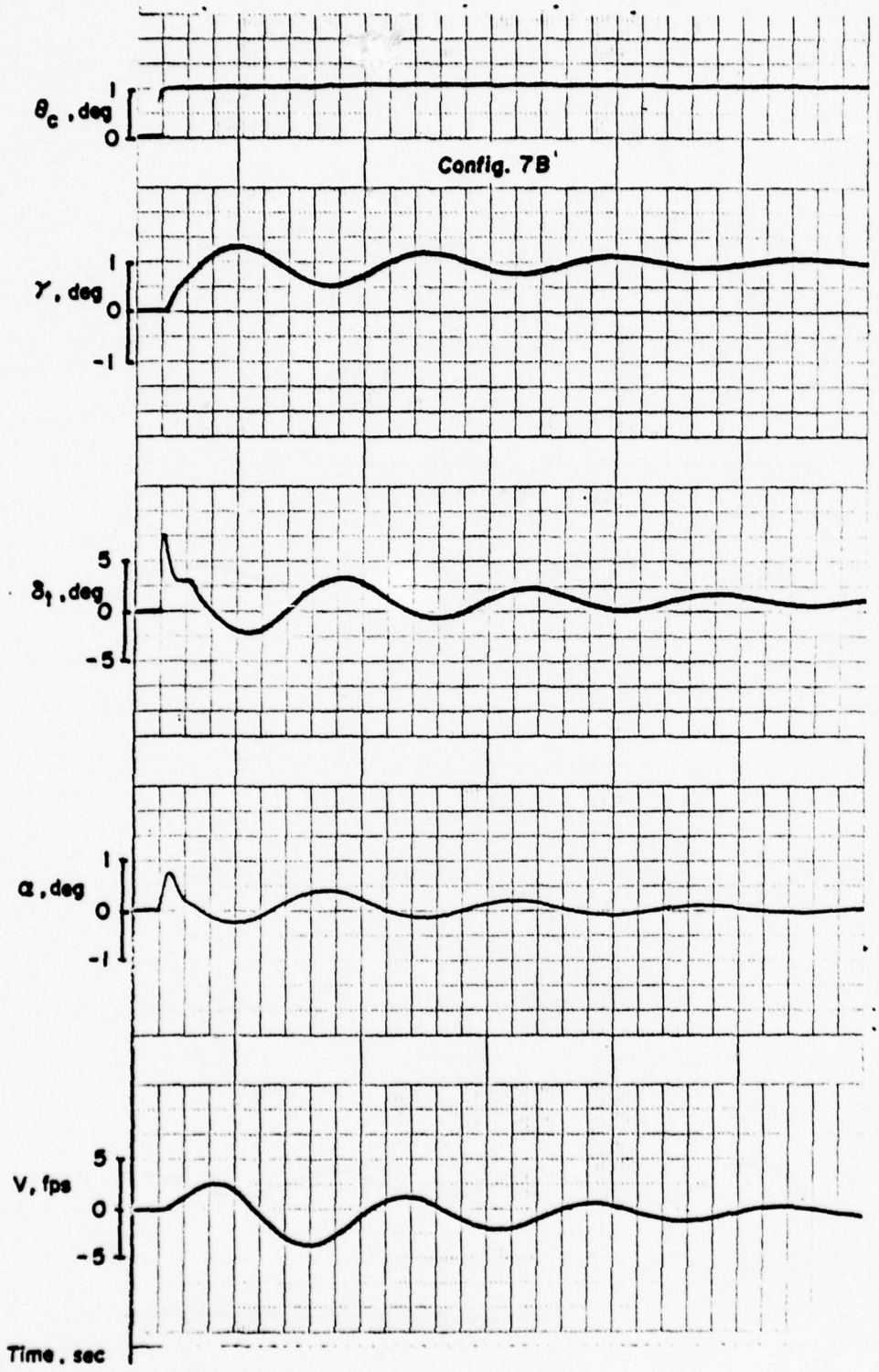
Config. 7B'
θ_c, deg
1
0
γ, deg
1
0
-1
δ_f, deg
5
0
-5
α, deg
1
0
-1
V, fps
5
0
-5
Time, sec

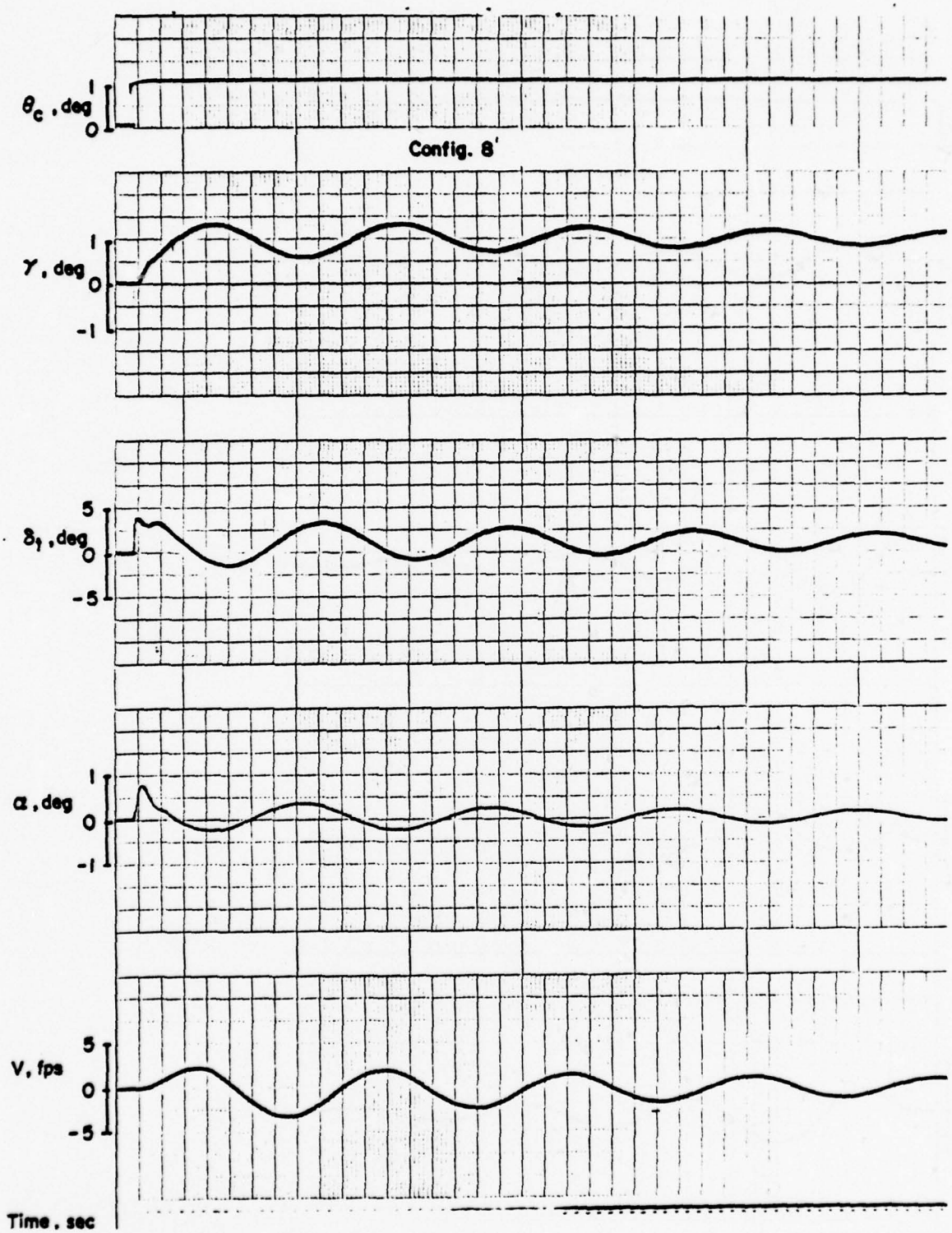
Config. 8'
θ_c, deg
1
0
γ, deg
1
0
-1
δ_t, deg
5
0
-5
α, deg
1
0
-1
V, fps
5
0
-5
Time, sec

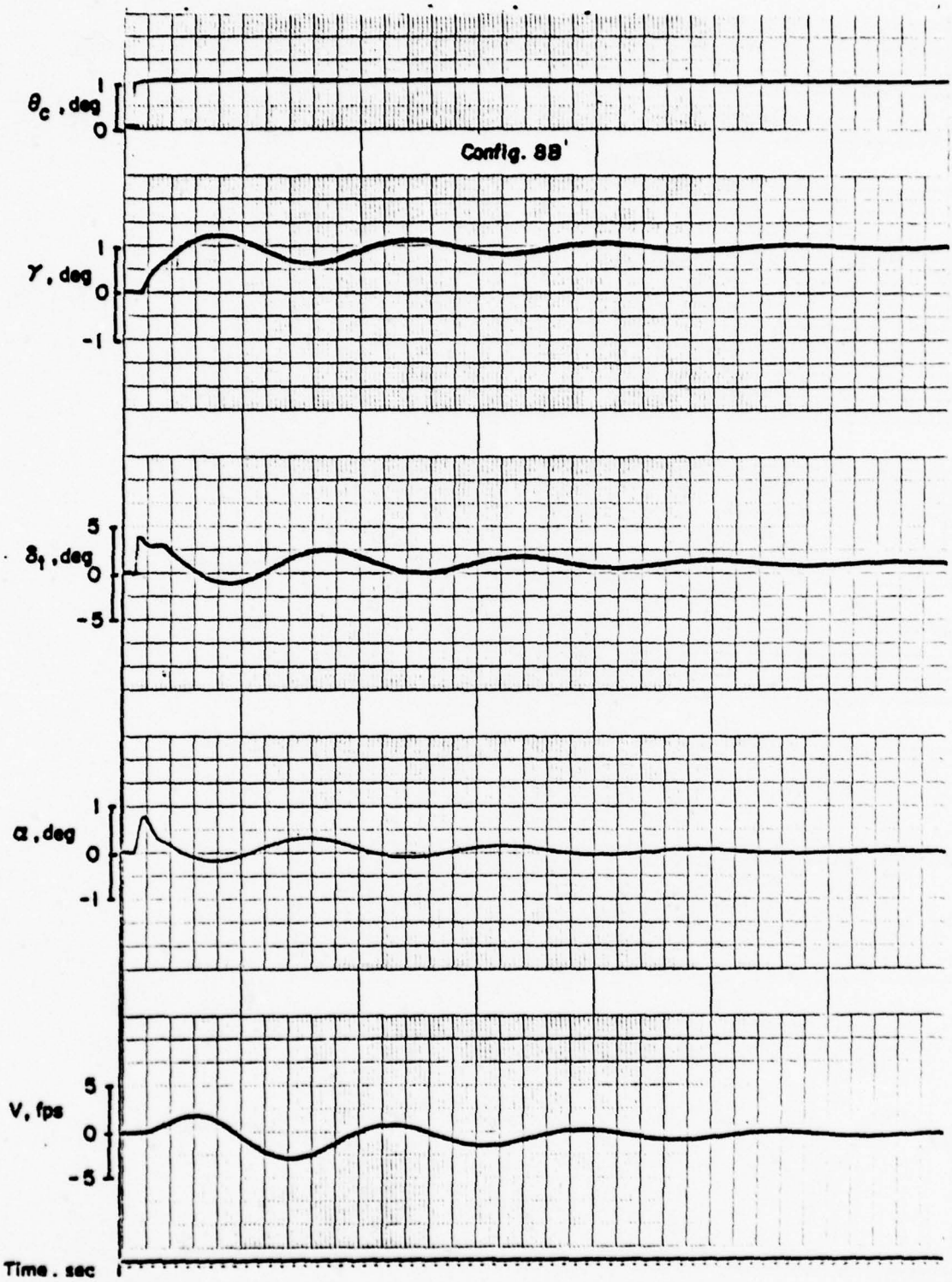
Config. 8B'
θ_c, deg
1
0
γ, deg
1
0
-1
δ_t, deg
5
0
-5
α, deg
1
0
-1
V, fps
5
0
-5
Time, sec

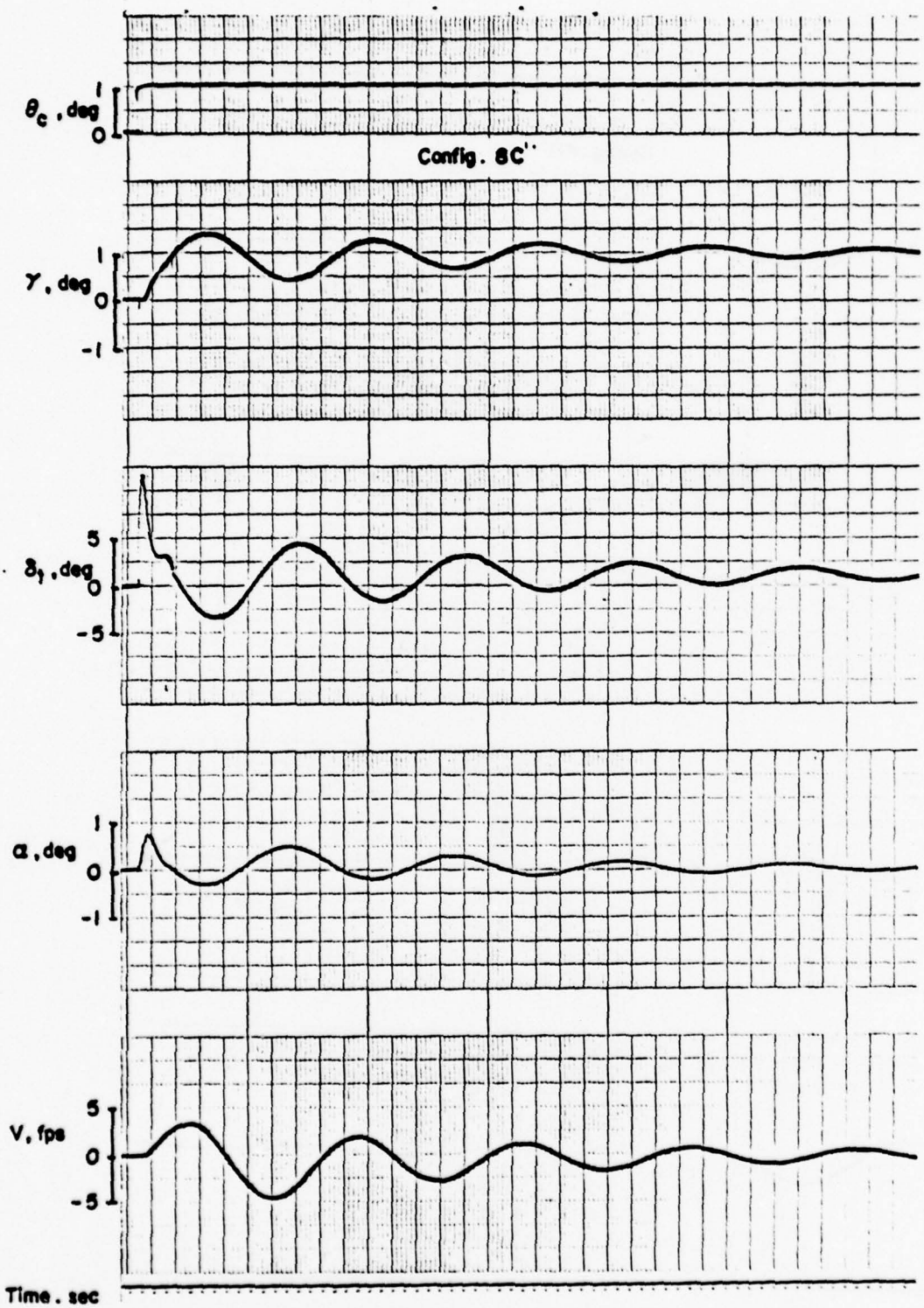
Config. 8C'
θ_c, deg
1
0
γ, deg
1
0
-1
δ_t, deg
5
0
-5
α, deg
1
0
-1
V, fps
5
0
-5
Time. sec

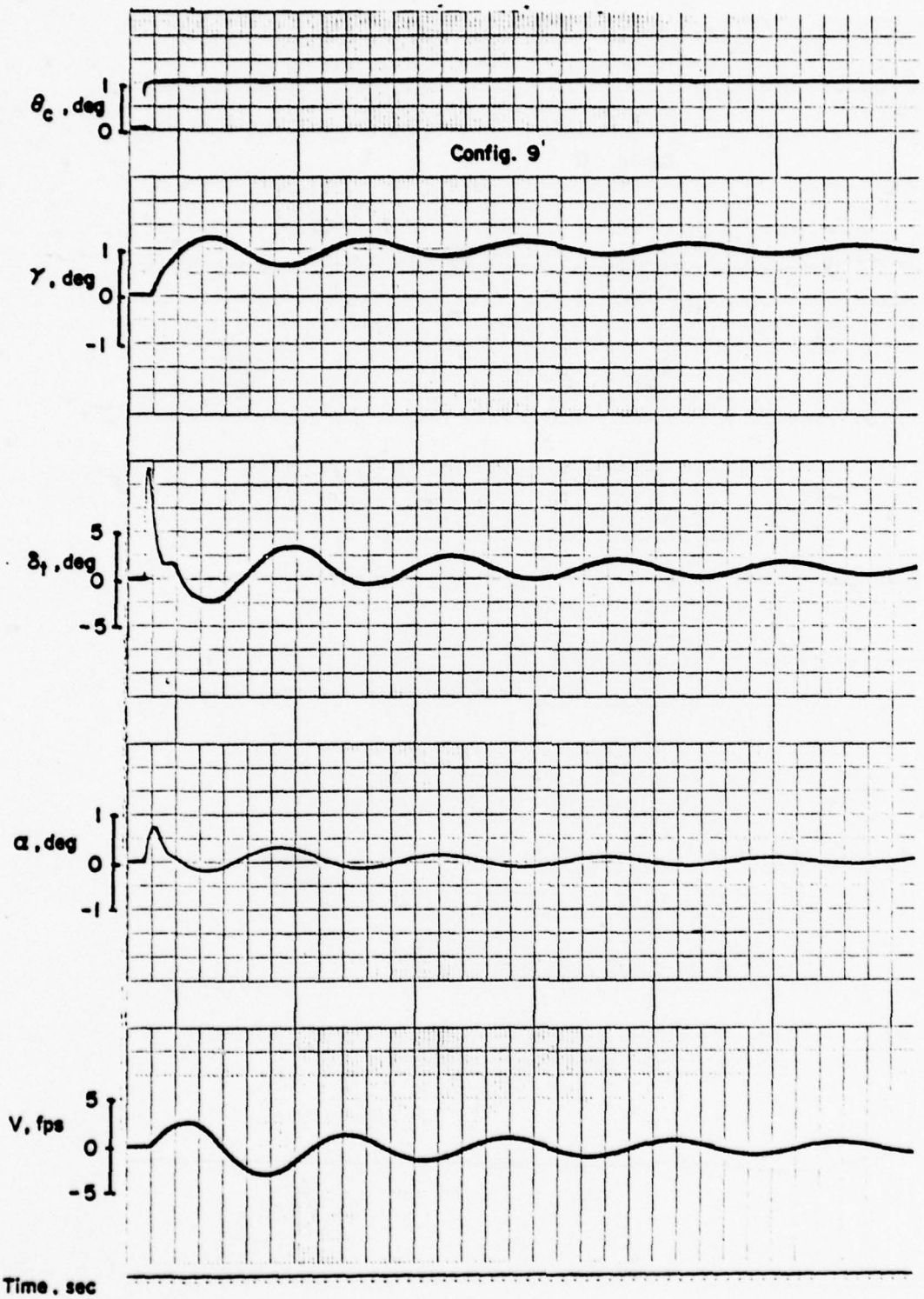
Config. 9'
θc , deg
1
0
γ, deg
1
0
-1
δf , deg
5
0
-5
α, deg
1
0
-1
V, fps
5
0
-5
Time, sec

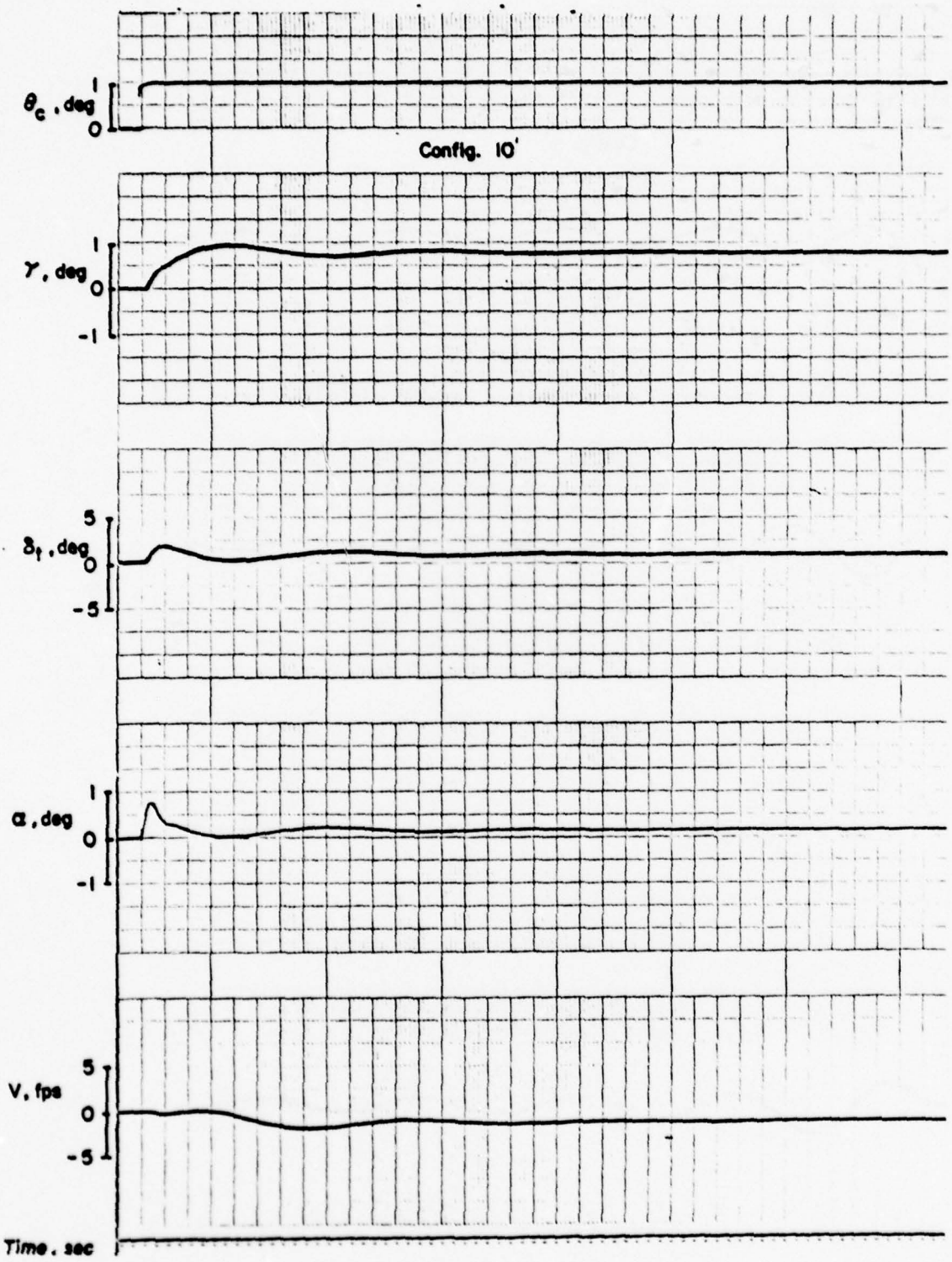
Config. 10'
θ_c, deg
1
0
γ, deg
1
0
-1
δ_t, deg
5
0
-5
α, deg
1
0
-1
V, fps
5
0
-5
Time, sec

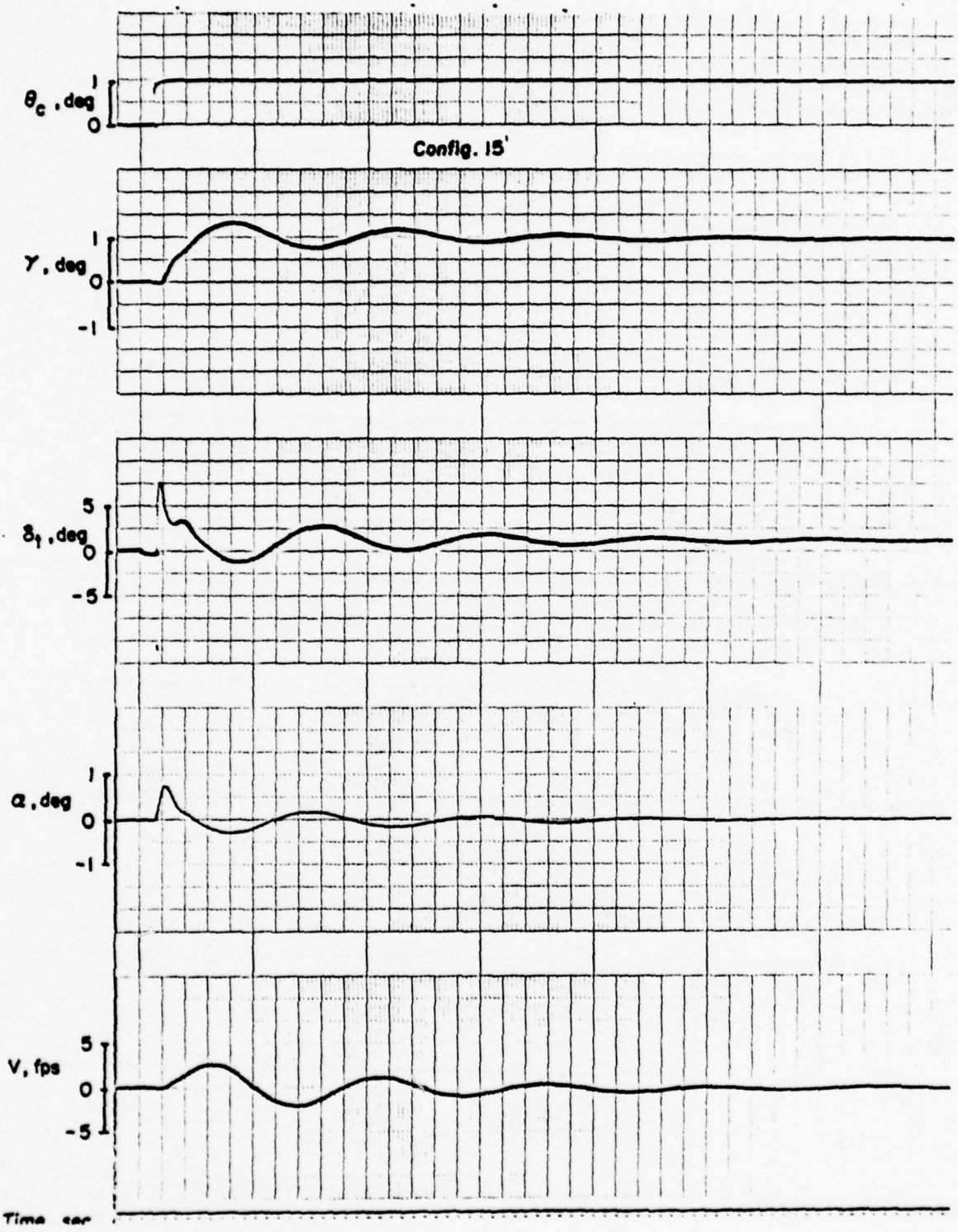
θ_c, deg
1
0
Config. 15'
γ, deg
1
0
-1
δ_t, deg
5
0
-5
α, deg
1
0
-1
V, fps
5
0
-5
Time, sec

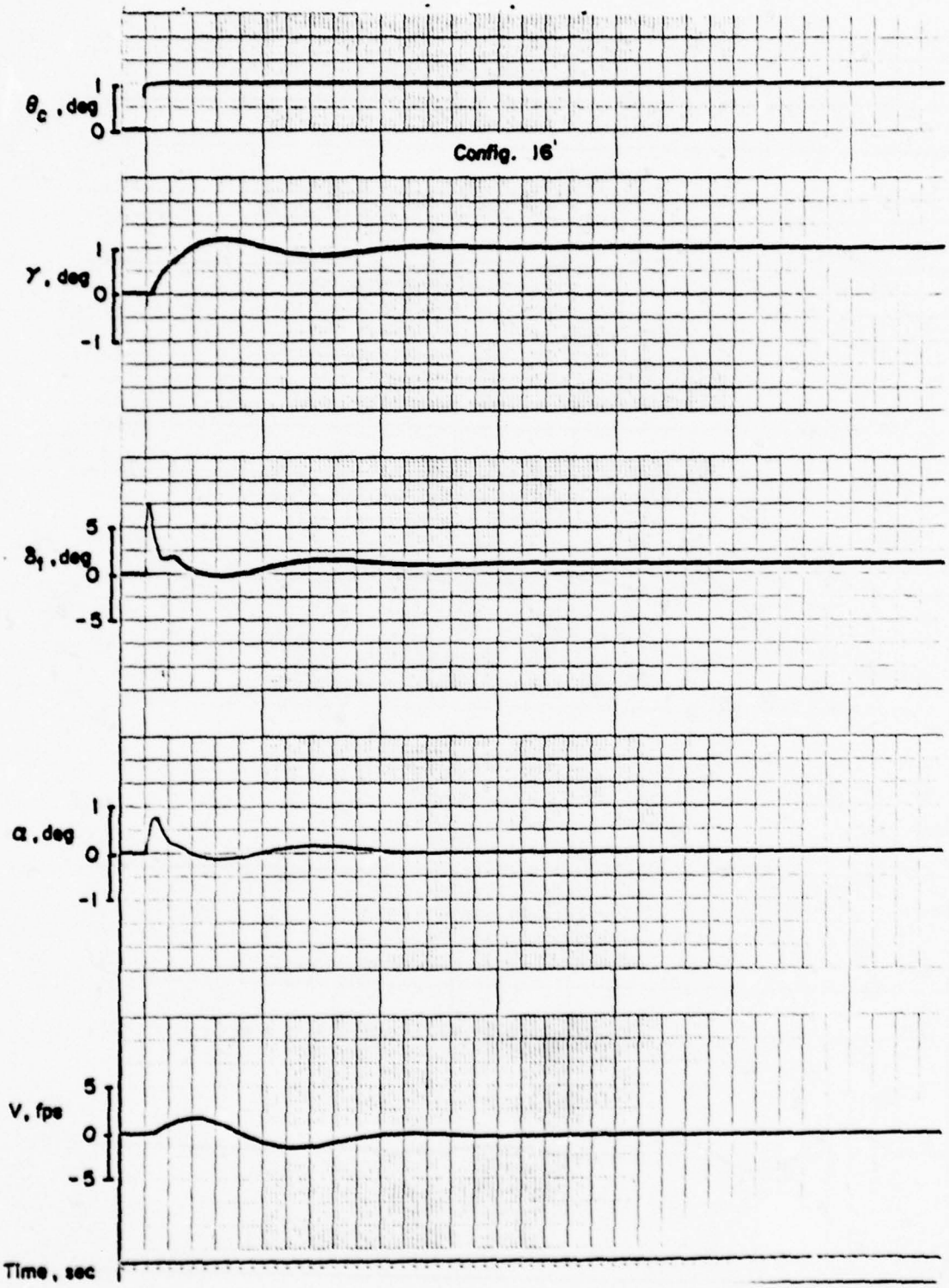
Config. 16'
θ_c, deg
1
0
γ, deg
1
0
-1
δ_t, deg
5
0
-5
α, deg
1
0
-1
V, fps
5
0
-5
Time, sec

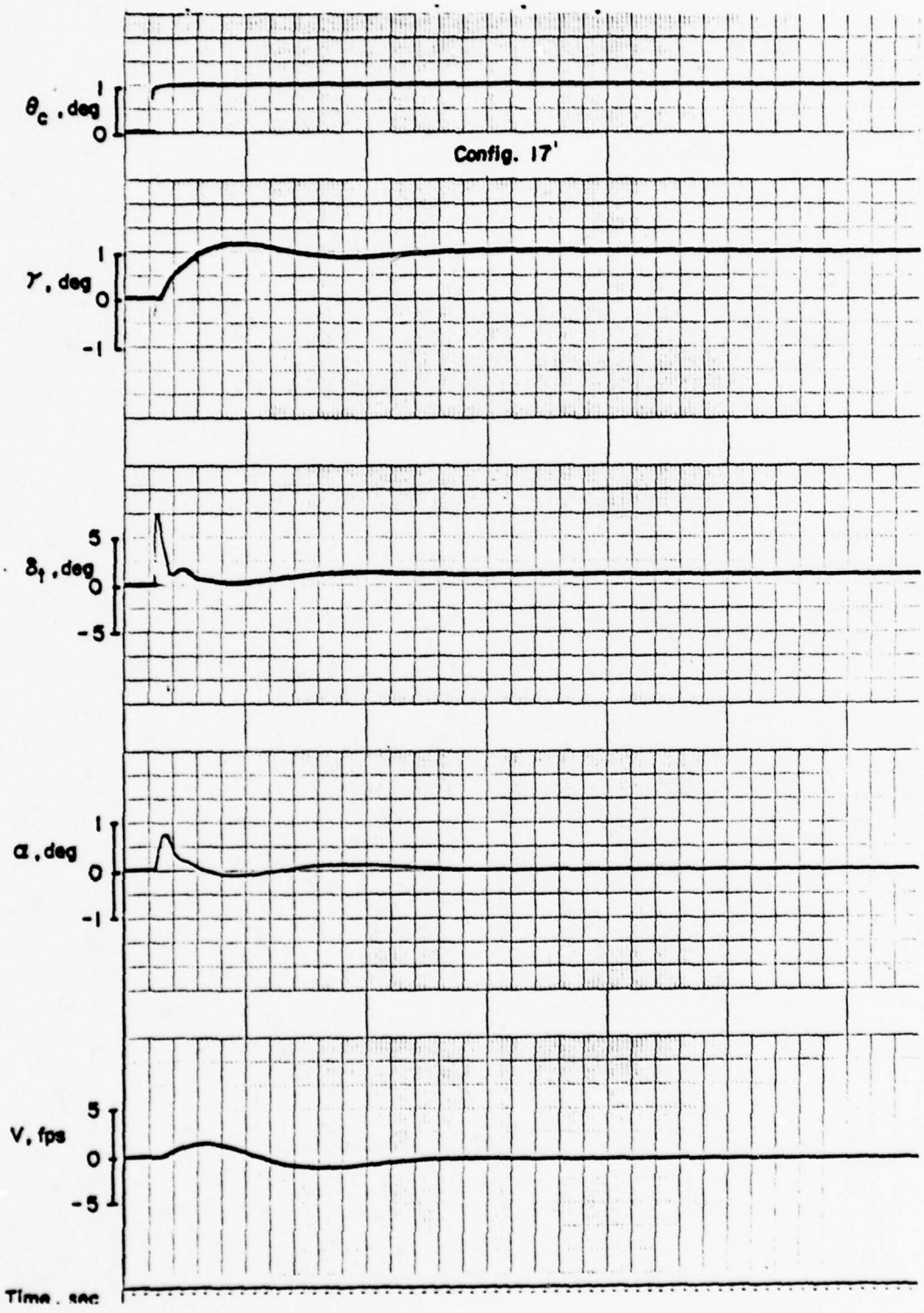
θ_c, deg
1
0
Config. 17'
γ, deg
1
0
-1
δ_t, deg
5
0
-5
α, deg
1
0
-1
V, fps
5
0
-5
Time, sec

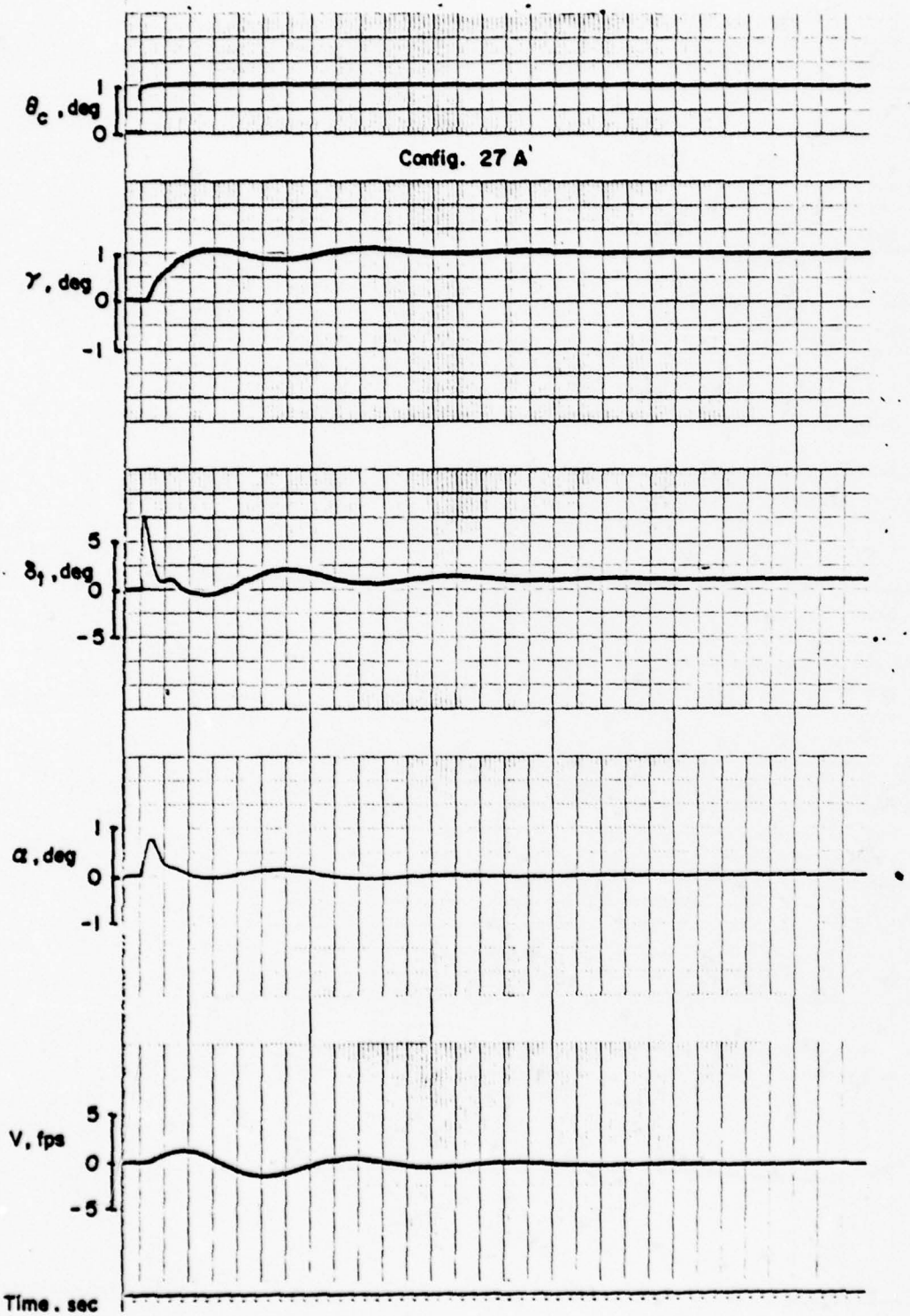
Config. 27 A'
θ_c, deg
1
0
γ, deg
1
0
-1
δ_t, deg
5
0
-5
α, deg
1
0
-1
V, fps
5
0
-5
Time, sec

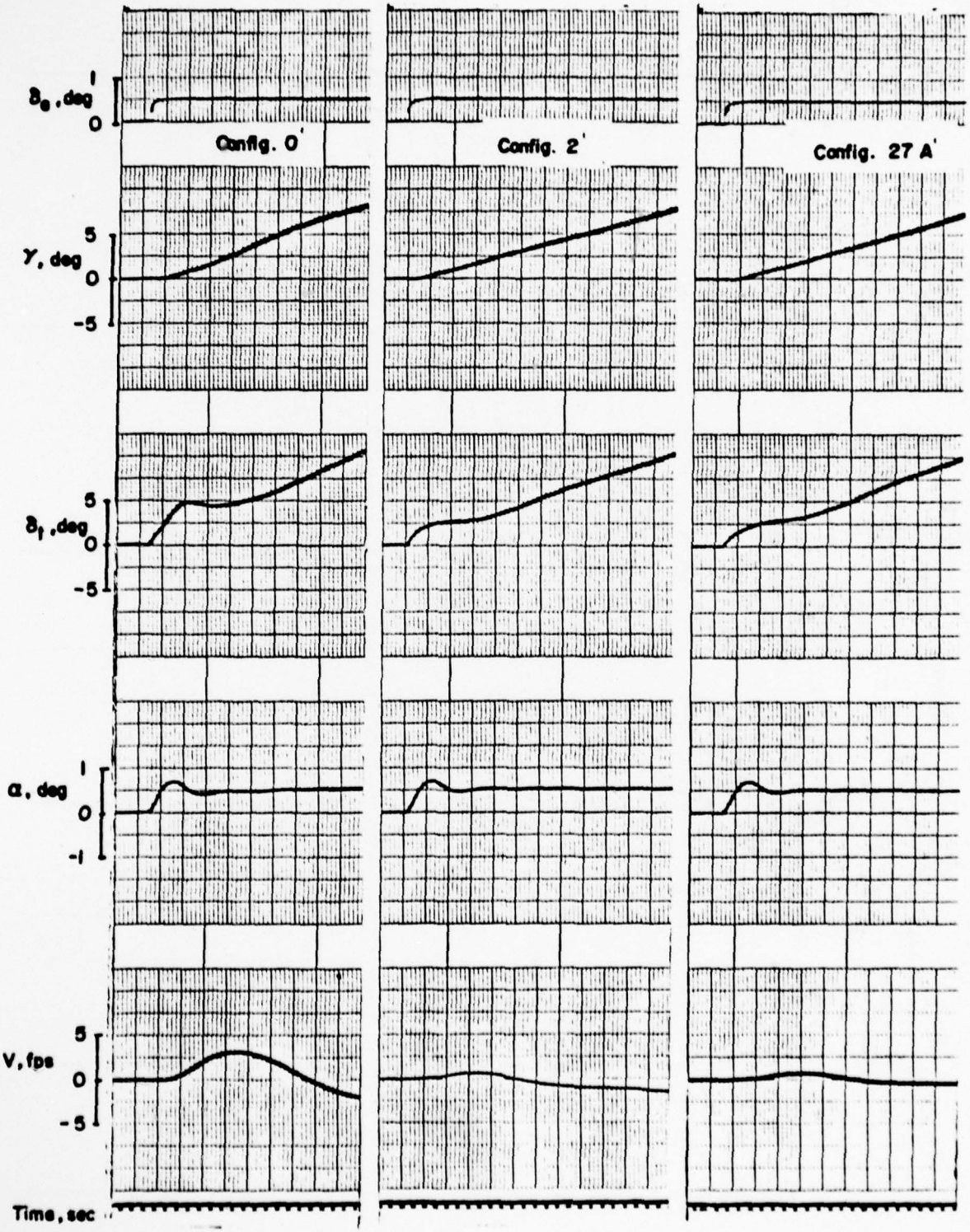
Config. 0'
Config. 2'
Config. 27 A'
δ_e, deg
1
0
γ, deg
5
0
-5
δ_f, deg
5
0
-5
α, deg
1
0
-1
V, fps
5
0
-5
Time, sec

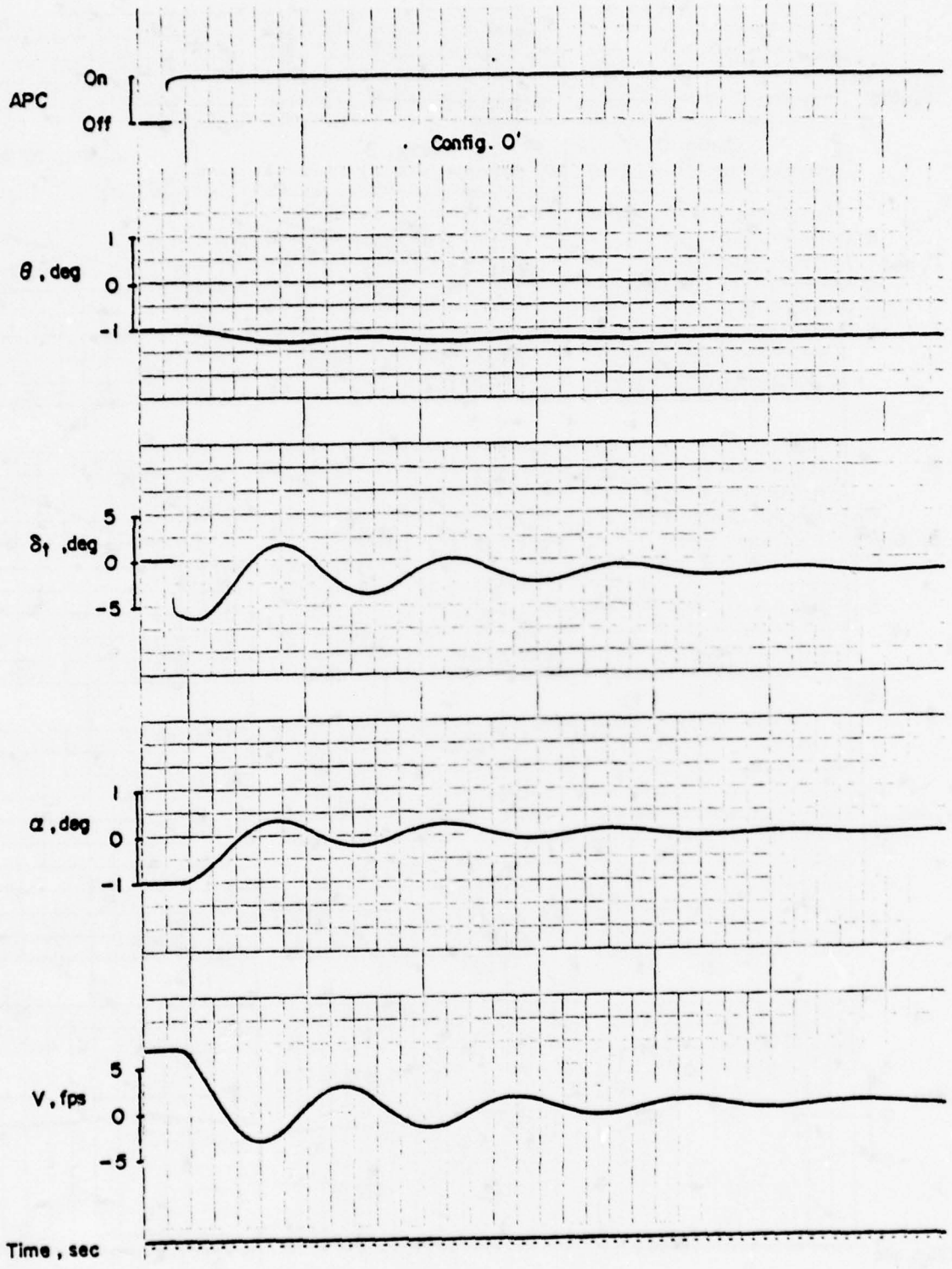
APC
On
Off
Config. O'
θ, deg
1
0
-1
δf, deg
5
0
-5
α, deg
1
0
-1
V, fps
5
0
-5
Time, sec

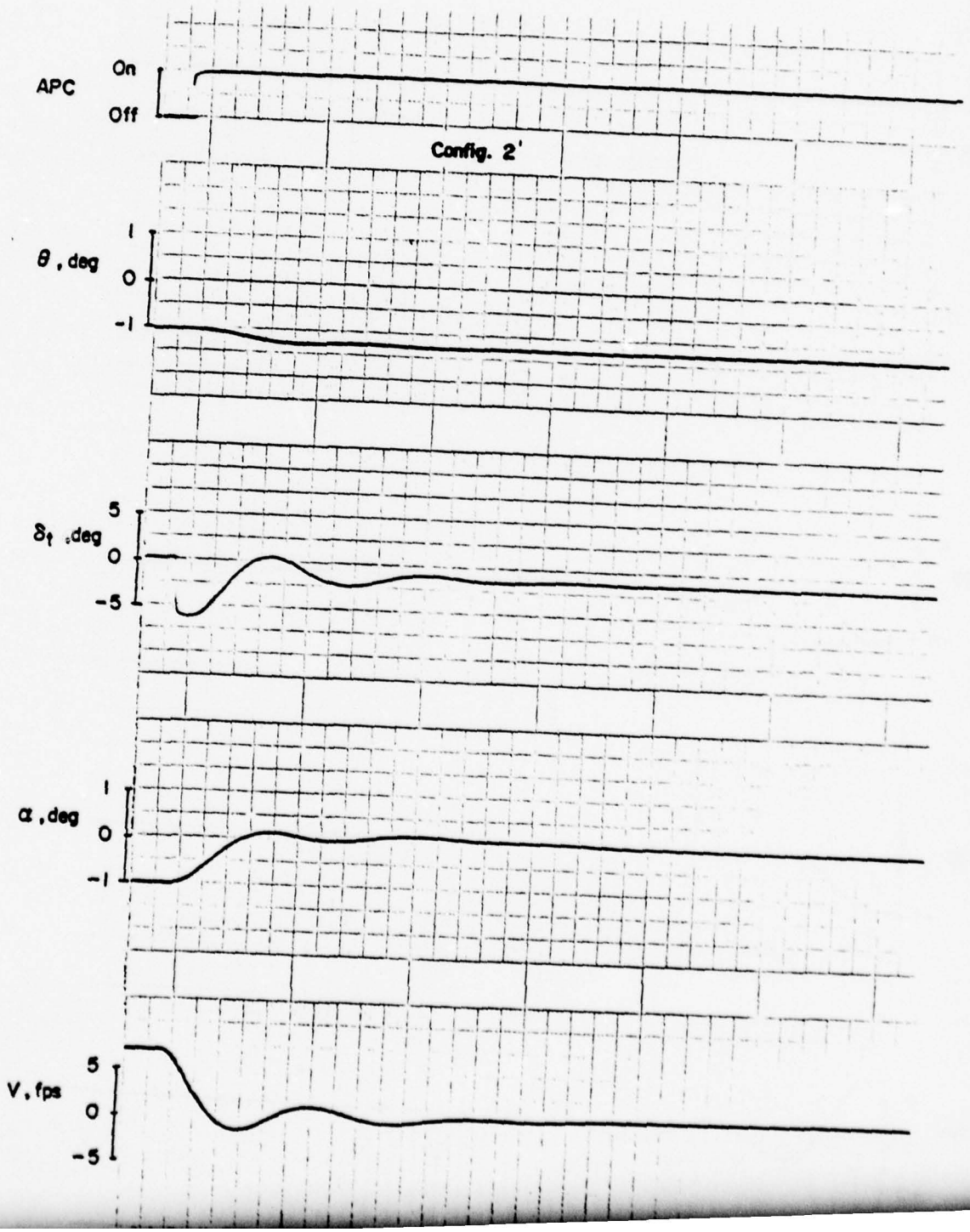
APC
On
Off
Config. 2'
θ, deg
1
0
-1
δt, deg
5
0
-5
α, deg
1
0
-1
V, fps
5
0
-5

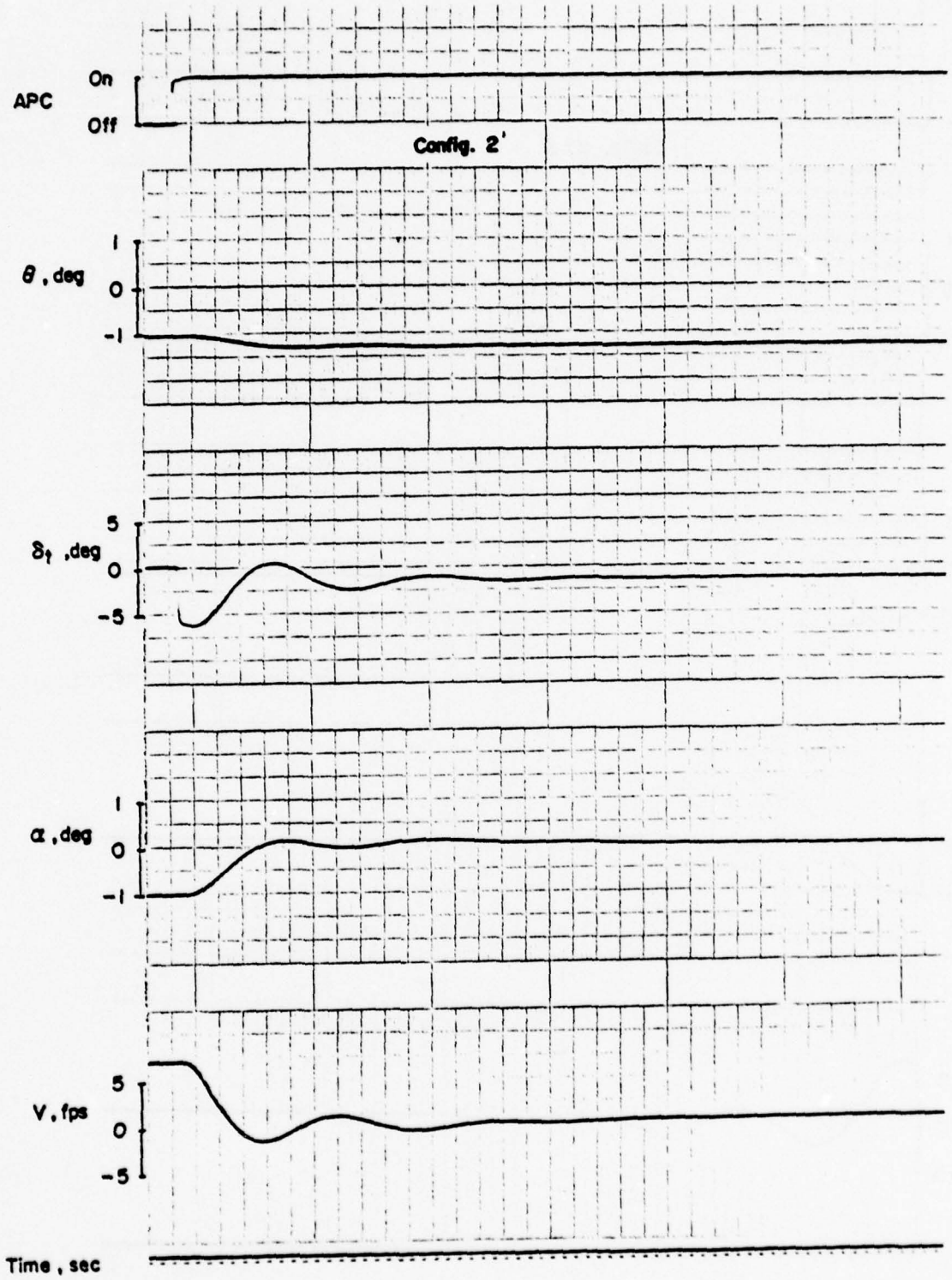
APC
On
Off
Config. 2'
θ, deg
1
0
-1
δf, deg
5
0
-5
α, deg
1
0
-1
V, fps
5
0
-5
Time, sec

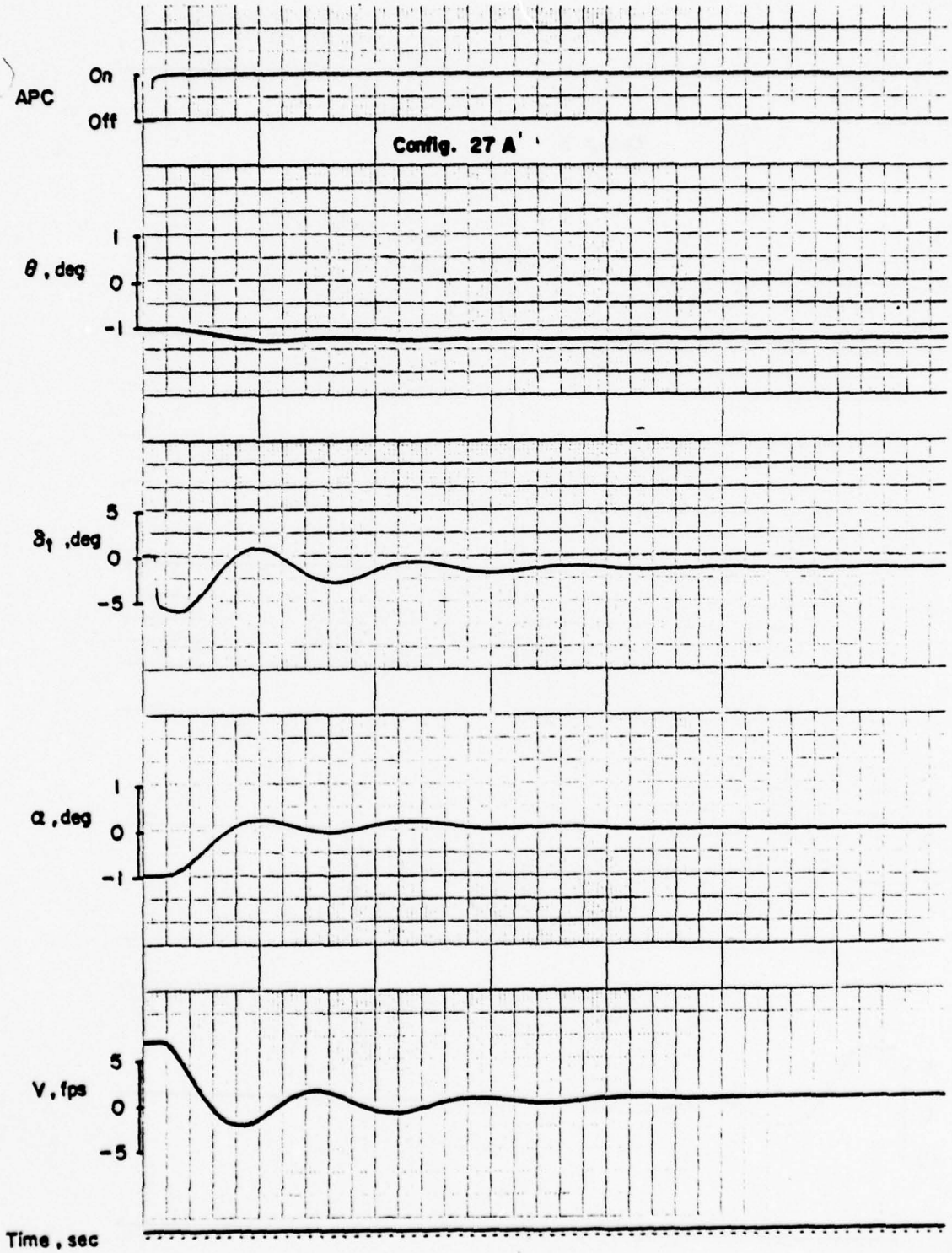
APC
On
Off
Config. 27 A'
θ, deg
1
0
-1
δf, deg
5
0
-5
α, deg
1
0
-1
V, fps
5
0
-5
Time, sec

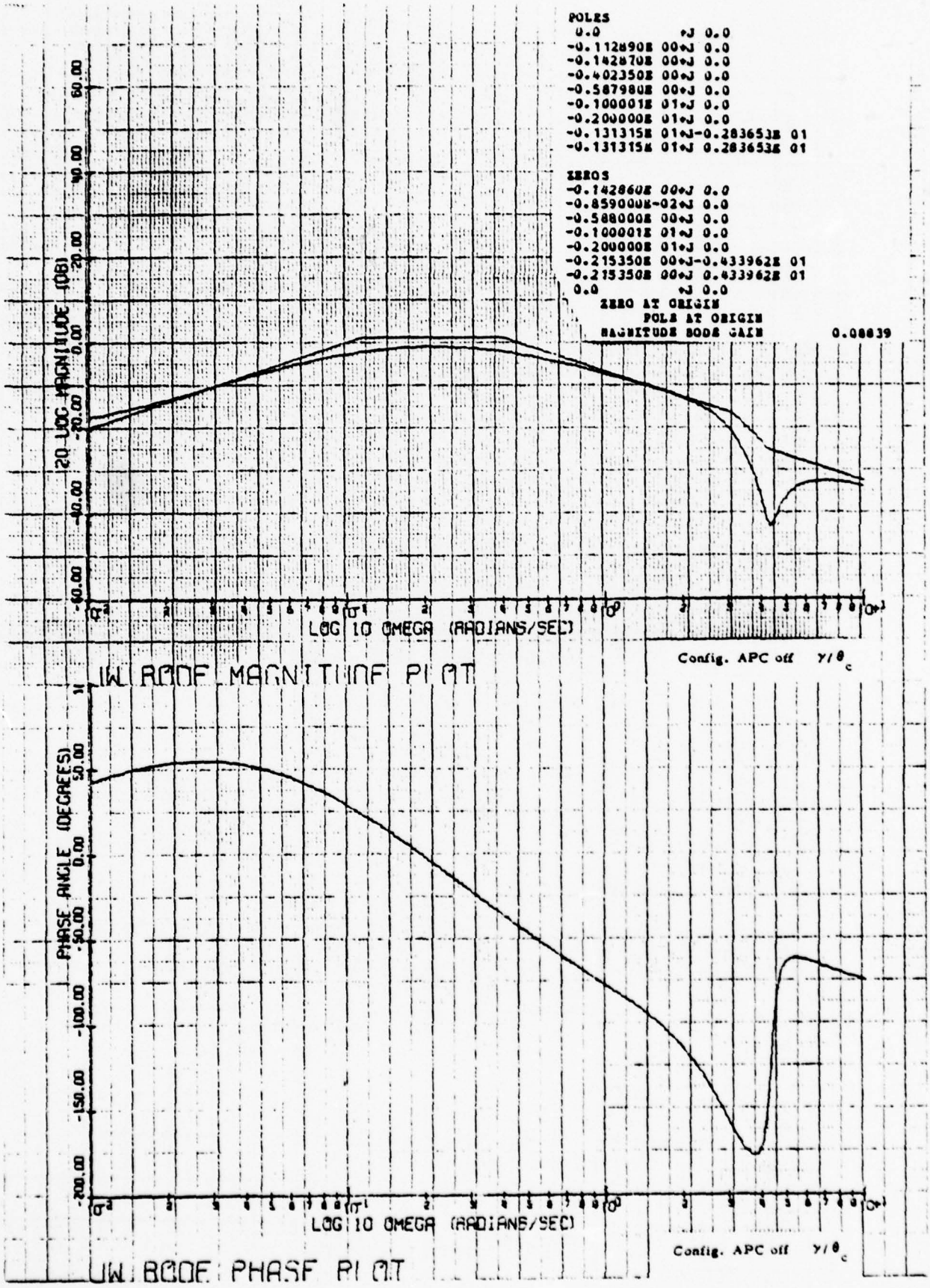
POLES
0.0 +J 0.0
-0.112890E 00+J 0.0
-0.142870E 00+J 0.0
-0.402350E 00+J 0.0
-0.587980E 00+J 0.0
-0.100001E 01+J 0.0
-0.200000E 01+J 0.0
-0.131315E 01+J-0.283653E 01
-0.131315E 01+J 0.283653E 01
ZEROS
-0.142860E 00+J 0.0
-0.859000E-02+J 0.0
-0.588000E 00+J 0.0
-0.100001E 01+J 0.0
-0.200000E 01+J 0.0
-0.215350E 00+J-0.433962E 01
-0.215350E 00+J 0.433962E 01
0.0 +J 0.0
ZERO AT ORIGIN
POLE AT ORIGIN
MAGNITUDE BODE GAIN 0.08839
60.00
40.00
20.00
0.00
-20.00
-40.00
-60.00
20 LOG MAGNITUDE (DB)
LOG 10 OMEGA (RADIANS/SEC)
Config. APC off γ/θ_c
UW BODE MAGNITUDE PLOT
50.00
0.00
-50.00
-100.00
-150.00
-200.00
PHASE ANGLE (DEGREES)
LOG 10 OMEGA (RADIANS/SEC)
Config. APC off γ/θ_c
UW BODE PHASE PLOT

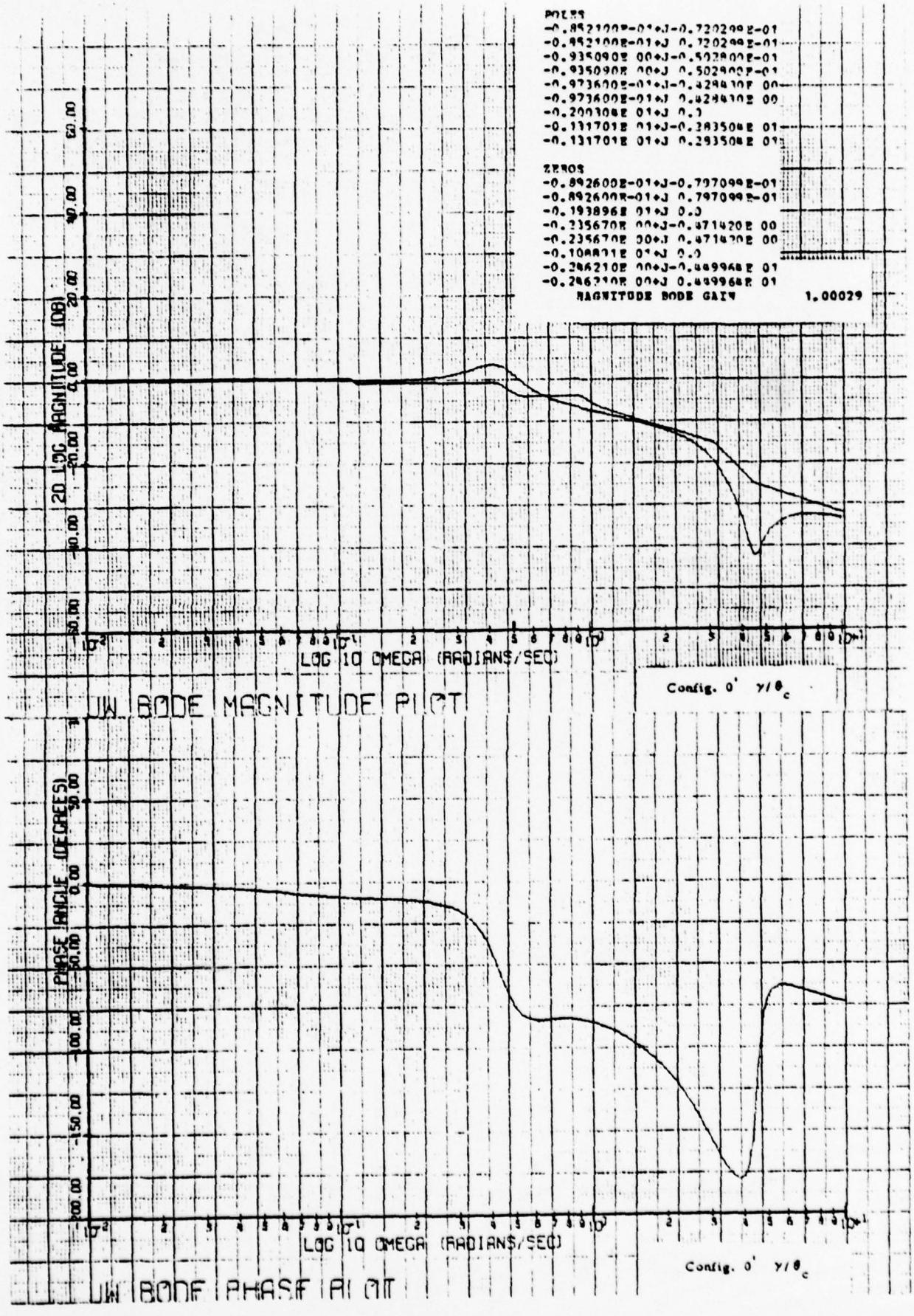
POLES
-0.8921000E-01+J-0.7202998E-01
-0.8921000E-01+J 0.7202998E-01
-0.9350900E 00+J-0.5029000E-01
-0.9350900E 00+J 0.5029000E-01
-0.9736000E-01+J-0.4294810E 00
-0.9736000E-01+J 0.4294810E 00
-0.2003088E 01+J 0.0
-0.1317018E 01+J-0.2835088E 01
-0.1317018E 01+J 0.2835088E 01
ZEROS
-0.8926000E-01+J-0.7970998E-01
-0.8926000E-01+J 0.7970998E-01
-0.1938968E 01+J 0.0
-0.2356708E 00+J-0.4714208E 00
-0.2356708E 00+J 0.4714208E 00
-0.1088711E 01+J 0.0
-0.2862108E 00+J-0.4899688E 01
-0.2862108E 00+J 0.4899688E 01
MAGNITUDE BODE GAIN 1.00029
20 LOG MAGNITUDE (DB)
LOG 10 OMEGA (RADIANS/SEC)
Config. 0' Y/θc
UW BODE MAGNITUDE PLOT
PHASE ANGLE (DEGREES)
LOG 10 OMEGA (RADIANS/SEC)
Config. 0' Y/θc
UW BODE PHASE PLOT

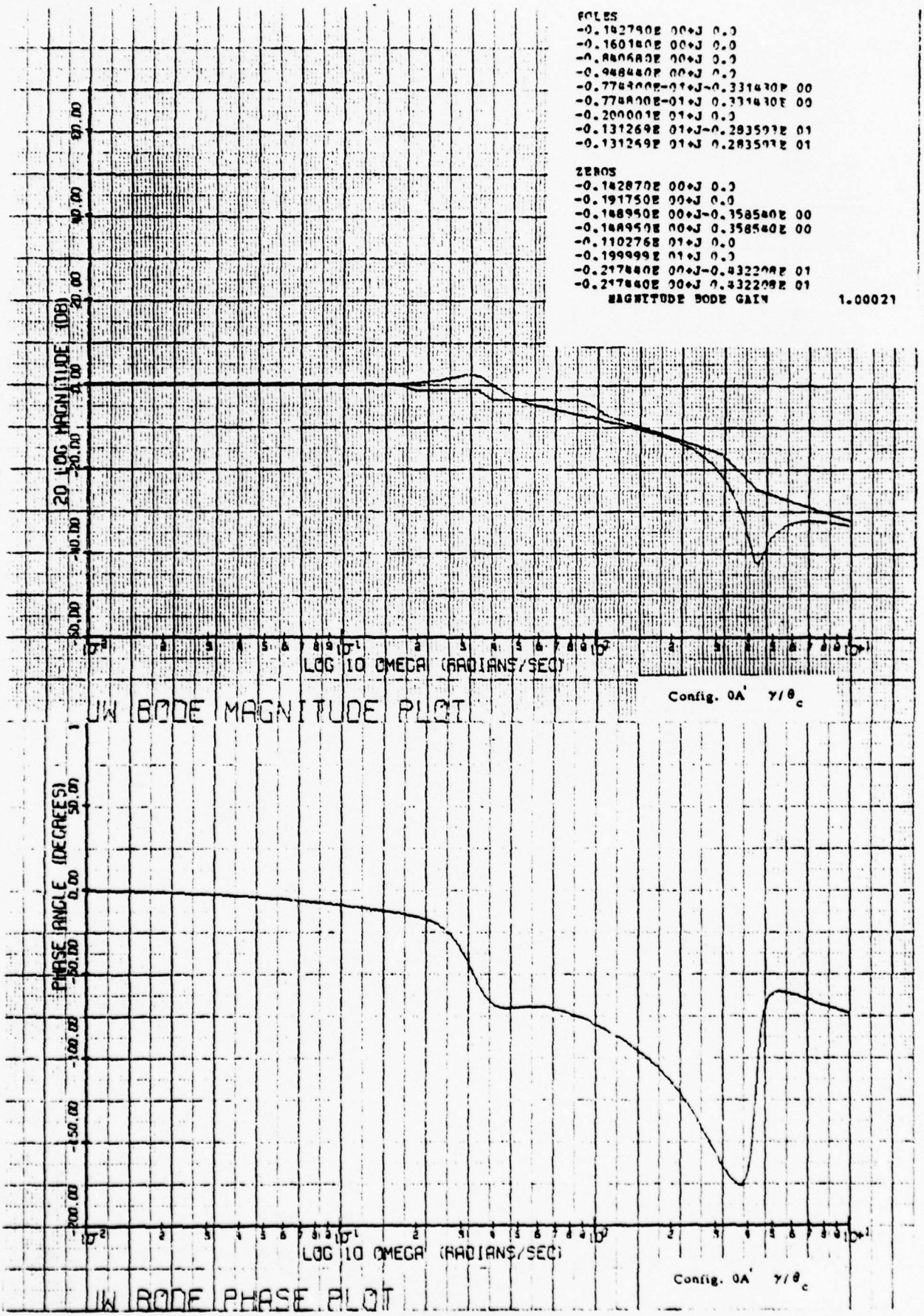
POLES
-0.1427908 00+J 0.0
-0.1601808 00+J 0.0
-0.8806808 00+J 0.0
-0.9488408 00+J 0.0
-0.7788008-01+J-0.3314308 00
-0.7788008-01+J 0.3314308 00
-0.2000018 01+J 0.0
-0.1312698 01+J-0.2835938 01
-0.1312698 01+J 0.2835938 01
ZEROS
-0.1428708 00+J 0.0
-0.1917508 00+J 0.0
-0.1488958 00+J-0.3585408 00
-0.1488958 00+J 0.3585408 00
-0.1102768 01+J 0.0
-0.1999998 01+J 0.0
-0.2178408 00+J-0.8322088 01
-0.2178408 00+J 0.8322088 01
MAGNITUDE BODE GAIN 1.00021
20 LOG MAGNITUDE (DB)
80.00
40.00
20.00
4.00
-20.00
-40.00
-80.00
LOG 10 OMEGA (RADIANS/SEC)
Config. 0A' γ/θc
UW BODE MAGNITUDE PLOT
PHASE ANGLE (DEGREES)
50.00
0.00
-50.00
-100.00
-150.00
-200.00
LOG 10 OMEGA (RADIANS/SEC)
Config. 0A' γ/θc
UW BODE PHASE PLOT

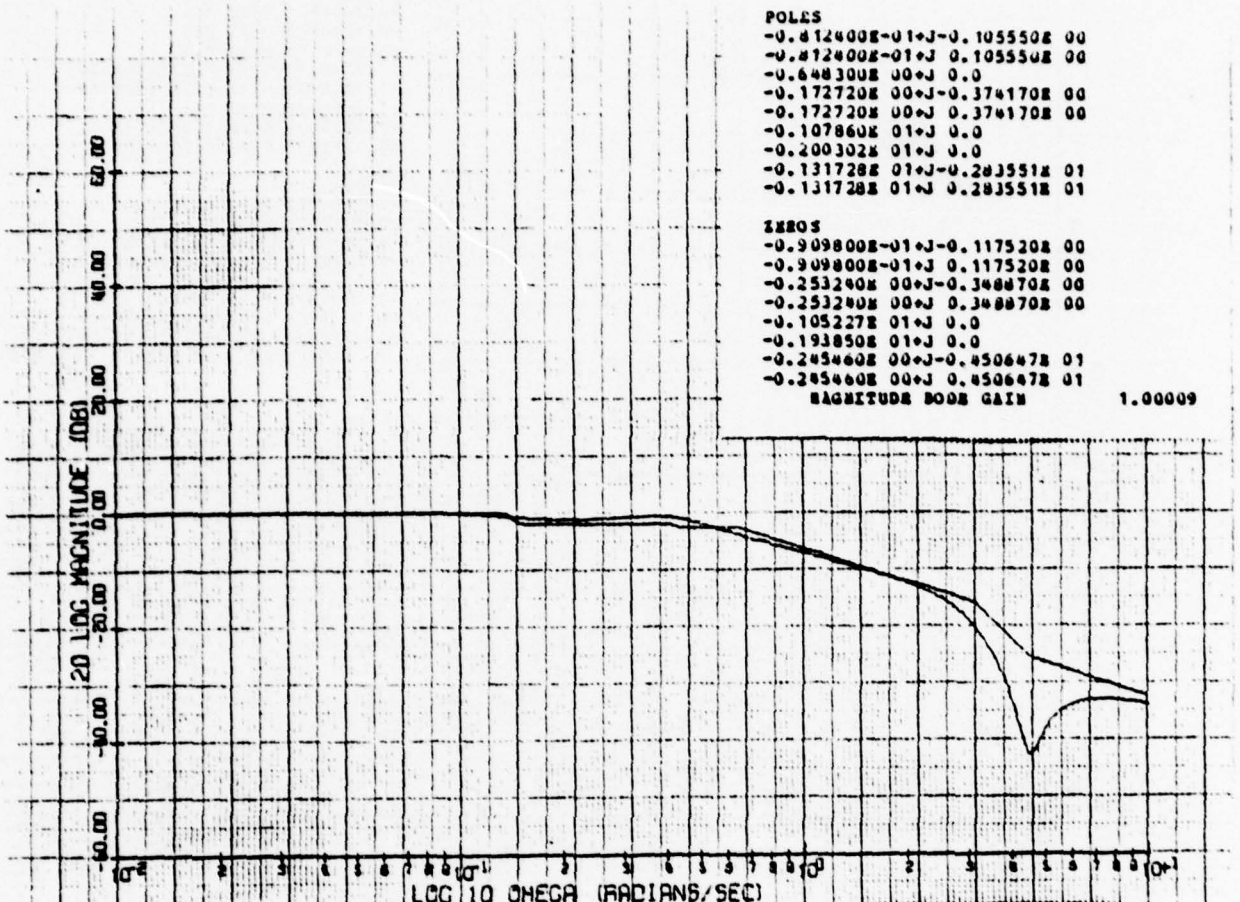

UW BODE MAGNITUDE PLOT

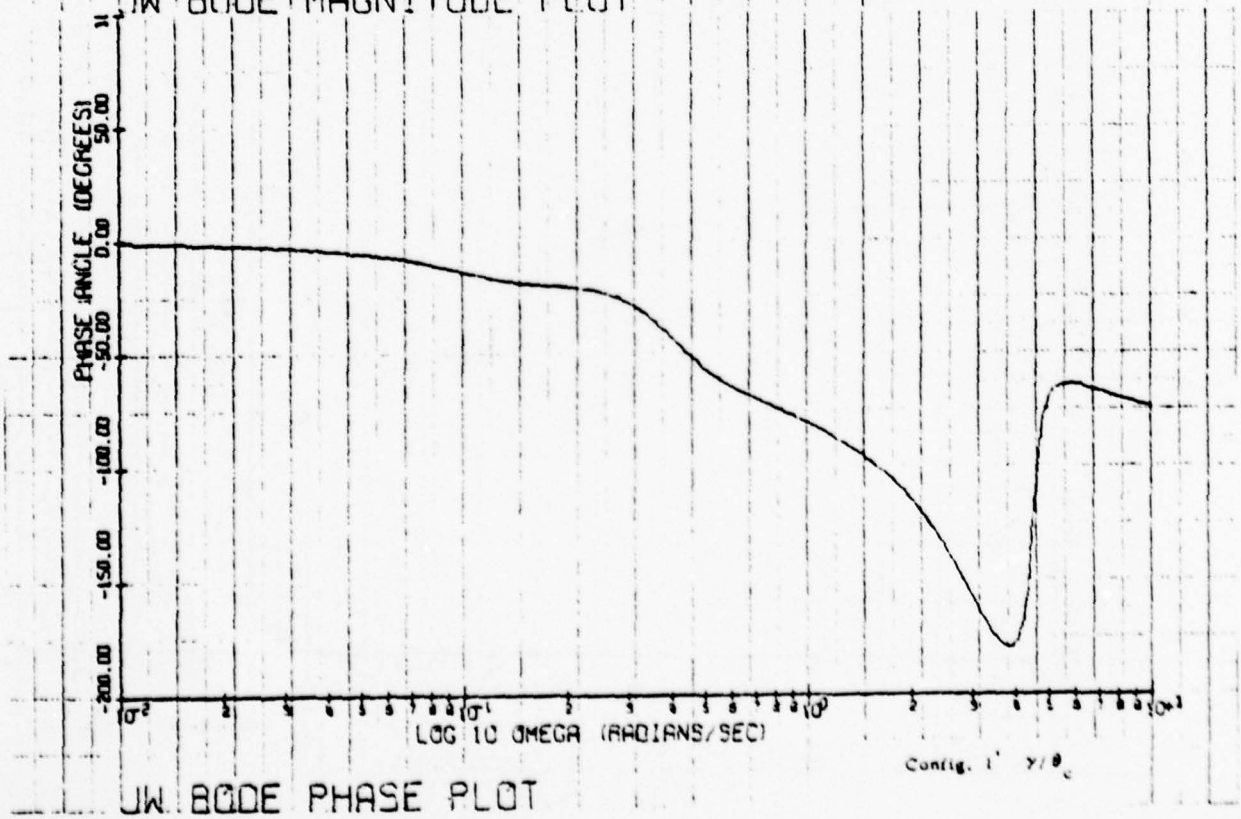

UW BODE PHASE PLOT

POLES
-0.533500E-01+J-0.663100E-01
-0.533500E-01+J 0.663100E-01
-0.661390E 00+J 0.0
-0.107897E 01+J 0.0
-0.193860E 00+J-0.398950E 00
-0.193860E 00+J 0.398950E 00
-0.200302E 01+J 0.0
-0.131730E 01+J-0.283556E 01
-0.131730E 01+J 0.283556E 01

ZEROS
-0.547100E-01+J-0.801899E-01
-0.547100E-01+J 0.801899E-01
-0.105194E 01+J 0.0
-0.290060E 00+J-0.365930E 00
-0.290060E 00+J 0.365930E 00
-0.193847E 01+J 0.0
-0.245110E 00+J-0.450750E 01
-0.245110E 00+J 0.450750E 01
MAGNITUDE BODE GAIN 1.00003

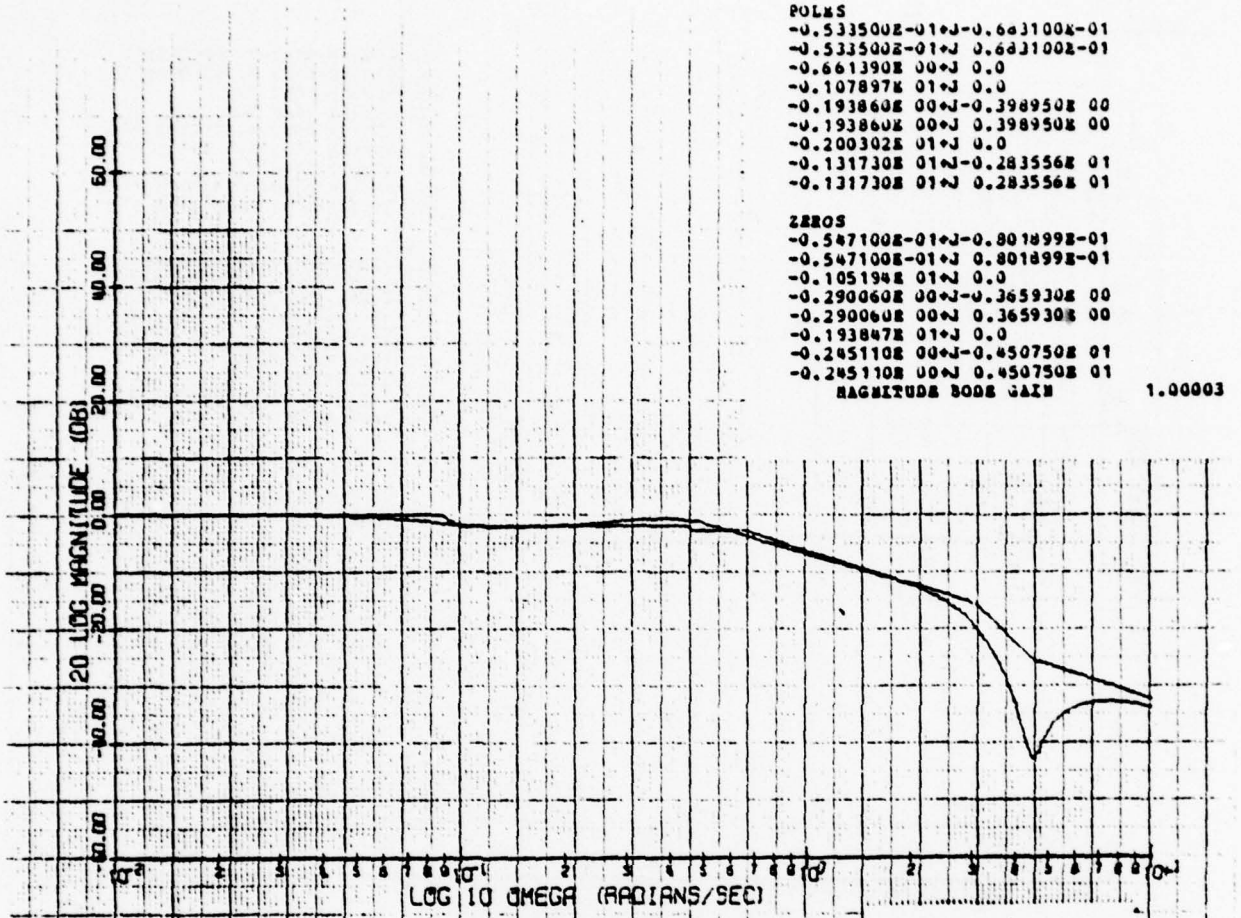

JW BODE MAGNITUDE PLOT

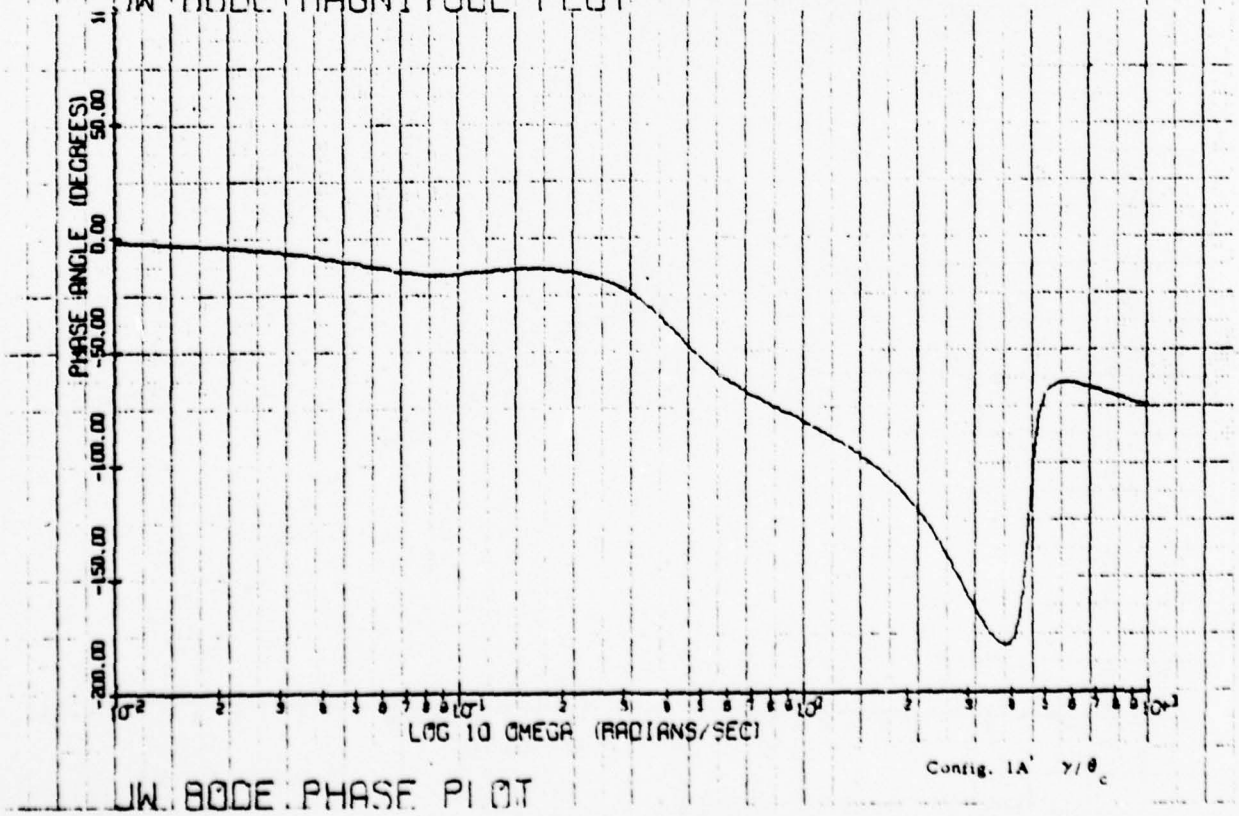

JW BODE PHASE PLOT

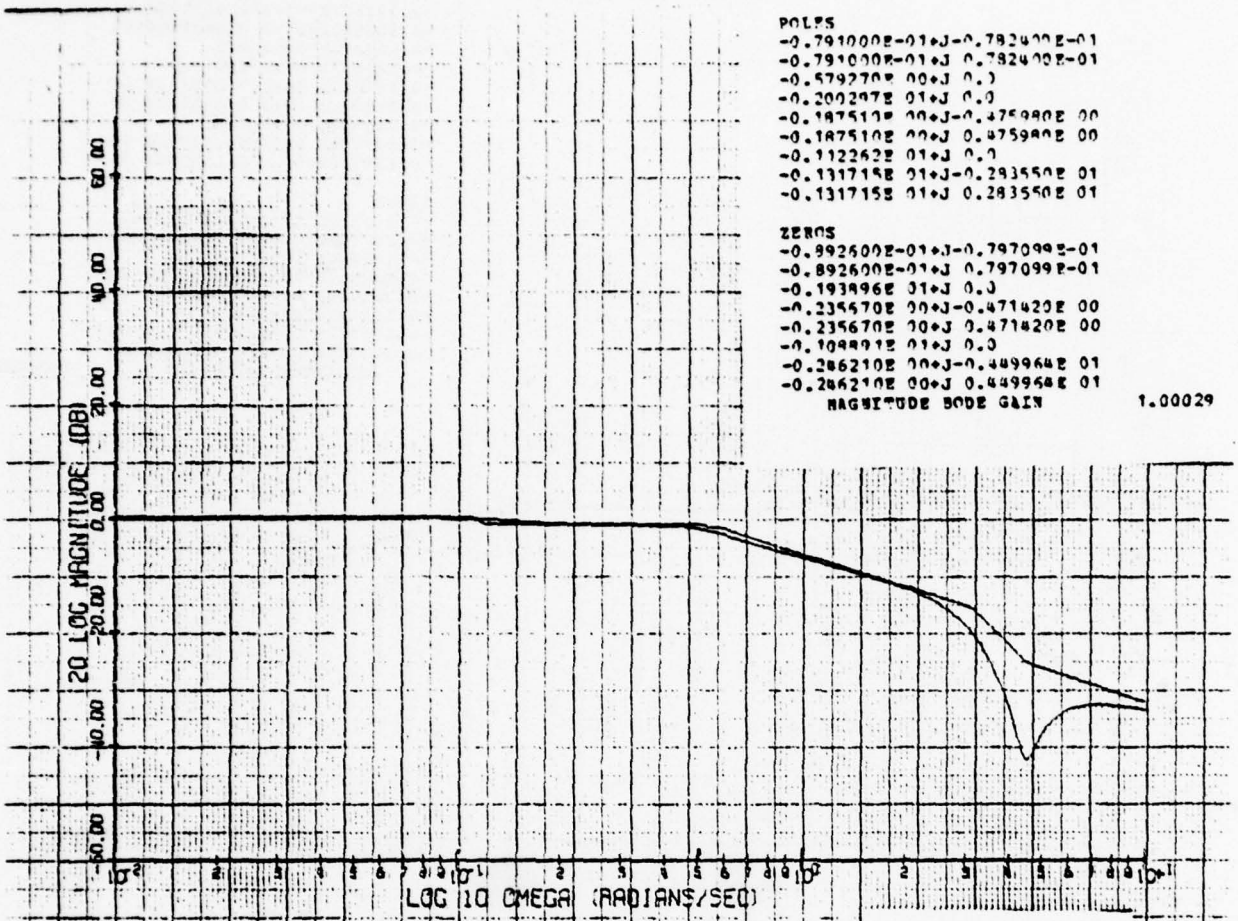
POLES
-0.791000E-01+J-0.782400E-01
-0.791000E-01+J 0.782400E-01
-0.579270E 00+J 0.0
-0.200297E 01+J 0.0
-0.187511E 00+J-0.475980E 00
-0.187511E 00+J 0.475980E 00
-0.112262E 01+J 0.0
-0.131715E 01+J-0.283550E 01
-0.131715E 01+J 0.283550E 01
ZEROS
-0.892600E-01+J-0.797099E-01
-0.892600E-01+J 0.797099E-01
-0.193896E 01+J 0.0
-0.235670E 00+J-0.471420E 00
-0.235670E 00+J 0.471420E 00
-0.108891E 01+J 0.0
-0.286210E 00+J-0.449964E 01
-0.286210E 00+J 0.449964E 01
MAGNITUDE BODE GAIN 1.00029
20 LOG MAGNITUDE (DB)
60.00
40.00
20.00
0.00
-20.00
-40.00
-60.00
LOG 10 OMEGA (RADIANS/SEC)
Config. 2' γ/θc
JW BODE MAGNITUDE PLOT
PHASE ANGLE (DEGREES)
50.00
0.00
-50.00
-100.00
-150.00
-200.00
LOG 10 OMEGA (RADIANS/SEC)
Config. 2' γ/θc
JW BODE PHASE PLOT

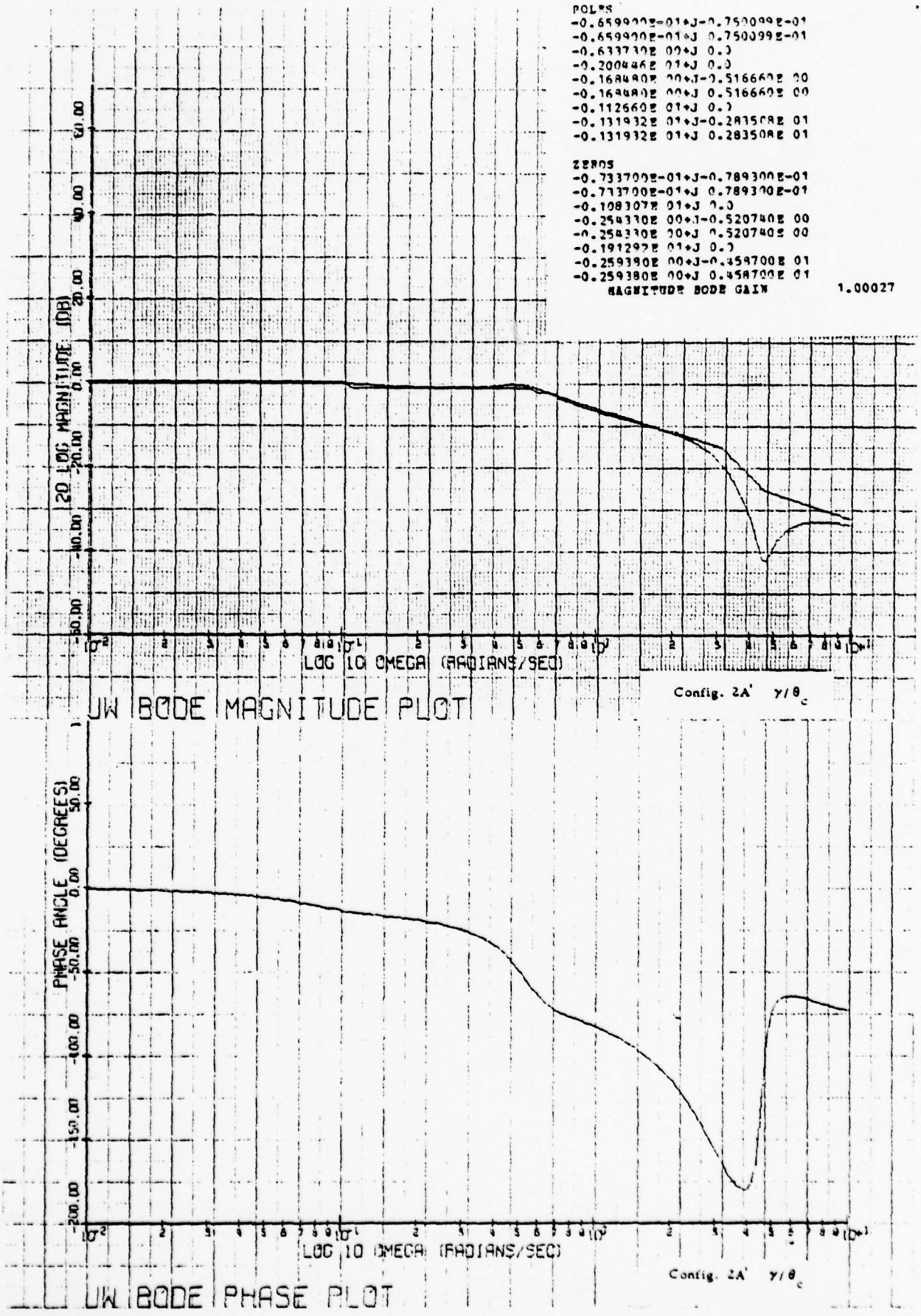
POLES
-0.6599990E-01+J-0.7500990E-01
-0.6599990E-01+J 0.7500990E-01
-0.6337330E 00+J 0.0
-0.2004460E 01+J 0.0
-0.1684980E 00+J-0.5166600E 00
-0.1684980E 00+J 0.5166600E 00
-0.1126600E 01+J 0.0
-0.1319320E 01+J-0.2835080E 01
-0.1319320E 01+J 0.2835080E 01
ZEROS
-0.7337000E-01+J-0.7893000E-01
-0.7337000E-01+J 0.7893000E-01
-0.1083070E 01+J 0.0
-0.2543300E 00+J-0.5207400E 00
-0.2543300E 00+J 0.5207400E 00
-0.1912920E 01+J 0.0
-0.2593900E 00+J-0.4587000E 01
-0.2593900E 00+J 0.4587000E 01
MAGNITUDE BODE GAIN 1.00027
20 LOG MAGNITUDE (DB)
LOG 10 OMEGA (RADIANS/SEC)
Config. 2A' Y/θc
UW BODE MAGNITUDE PLOT
PHASE ANGLE (DEGREES)
LOG 10 OMEGA (RADIANS/SEC)
Config. 2A' Y/θc
UW BODE PHASE PLOT

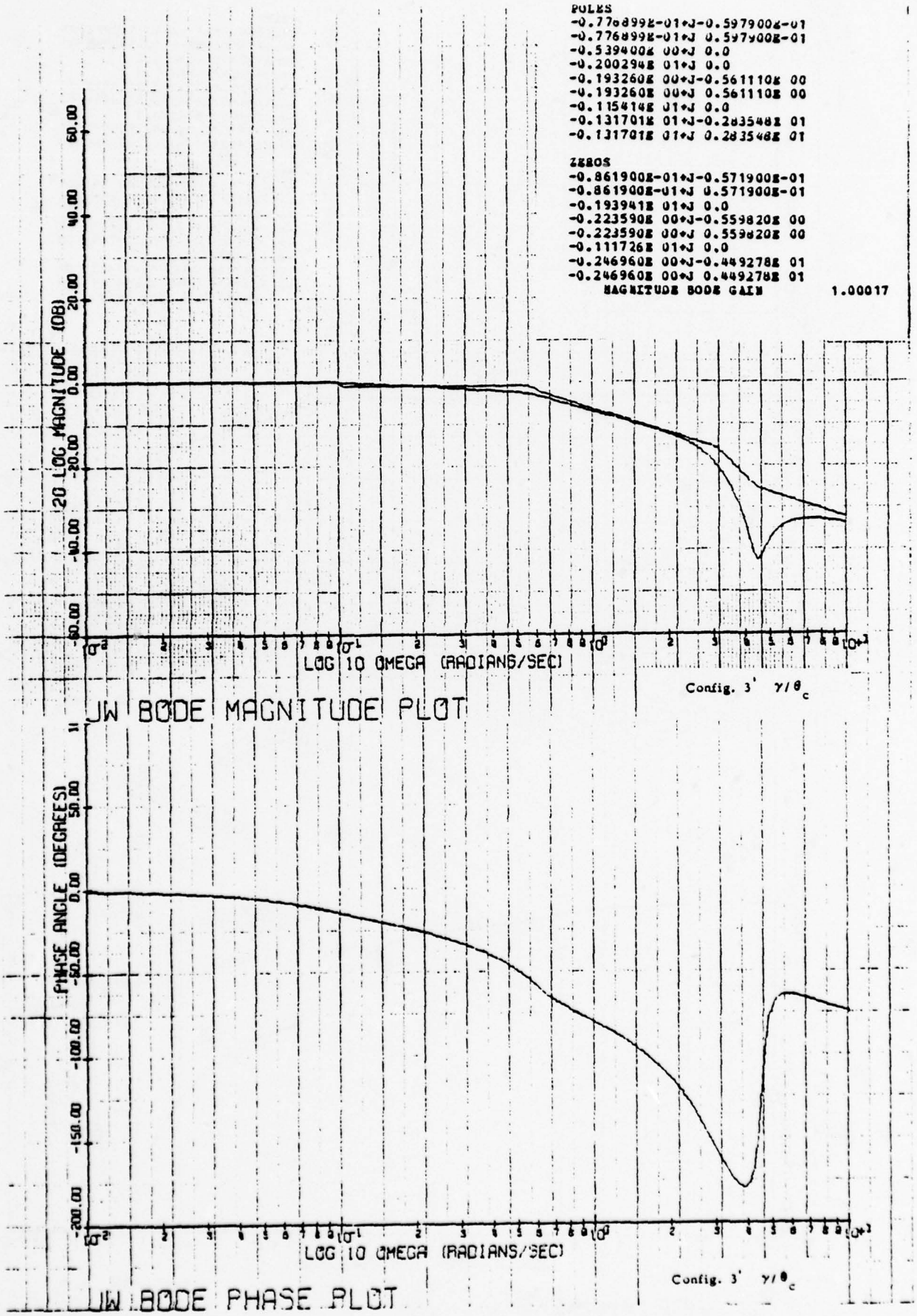
POLES
-0.776899E-01+J-0.597900E-01
-0.776899E-01+J 0.597900E-01
-0.539400E 00+J 0.0
-0.200294E 01+J 0.0
-0.193260E 00+J-0.561110E 00
-0.193260E 00+J 0.561110E 00
-0.115414E 01+J 0.0
-0.131701E 01+J-0.283548E 01
-0.131701E 01+J 0.283548E 01
ZEROS
-0.861900E-01+J-0.571900E-01
-0.861900E-01+J 0.571900E-01
-0.193941E 01+J 0.0
-0.223590E 00+J-0.559820E 00
-0.223590E 00+J 0.559820E 00
-0.111726E 01+J 0.0
-0.246960E 00+J-0.449278E 01
-0.246960E 00+J 0.449278E 01
MAGNITUDE BODE GAIN 1.00017
60.00
40.00
20.00
0.00
-20.00
-40.00
-60.00
20 LOG MAGNITUDE (DB)
LOG 10 OMEGA (RADIANS/SEC)
Config. 3' γ/θc
JW BODE MAGNITUDE PLOT
50.00
0.00
-50.00
-100.00
-150.00
-200.00
PHASE ANGLE (DEGREES)
LOG 10 OMEGA (RADIANS/SEC)
Config. 3' γ/θc
JW BODE PHASE PLOT

POLES
-0.962500E-01+J-0.795799E-01
-0.962500E-01+J 0.795799E-01
-0.523330E 00+J 0.0
-0.200295E 01+J 0.0
-0.182900E 00+J-0.550280E 00
-0.182900E 00+J 0.550280E 00
-0.115382E 01+J 0.0
-0.131699E 01+J-0.283542E 01
-0.131699E 01+J 0.283542E 01

ZEROS
-0.105880E 00+J-0.714200E-01
-0.105880E 00+J 0.714200E-01
-0.193944E 01+J 0.0
-0.111769E 01+J 0.0
-0.203310E 00+J-0.562940E 00
-0.203310E 00+J 0.562940E 00
-0.247320E 00+J-0.449173E 01
-0.247320E 00+J 0.449173E 01
MAGNITUDE BODE GAIN 1.00013

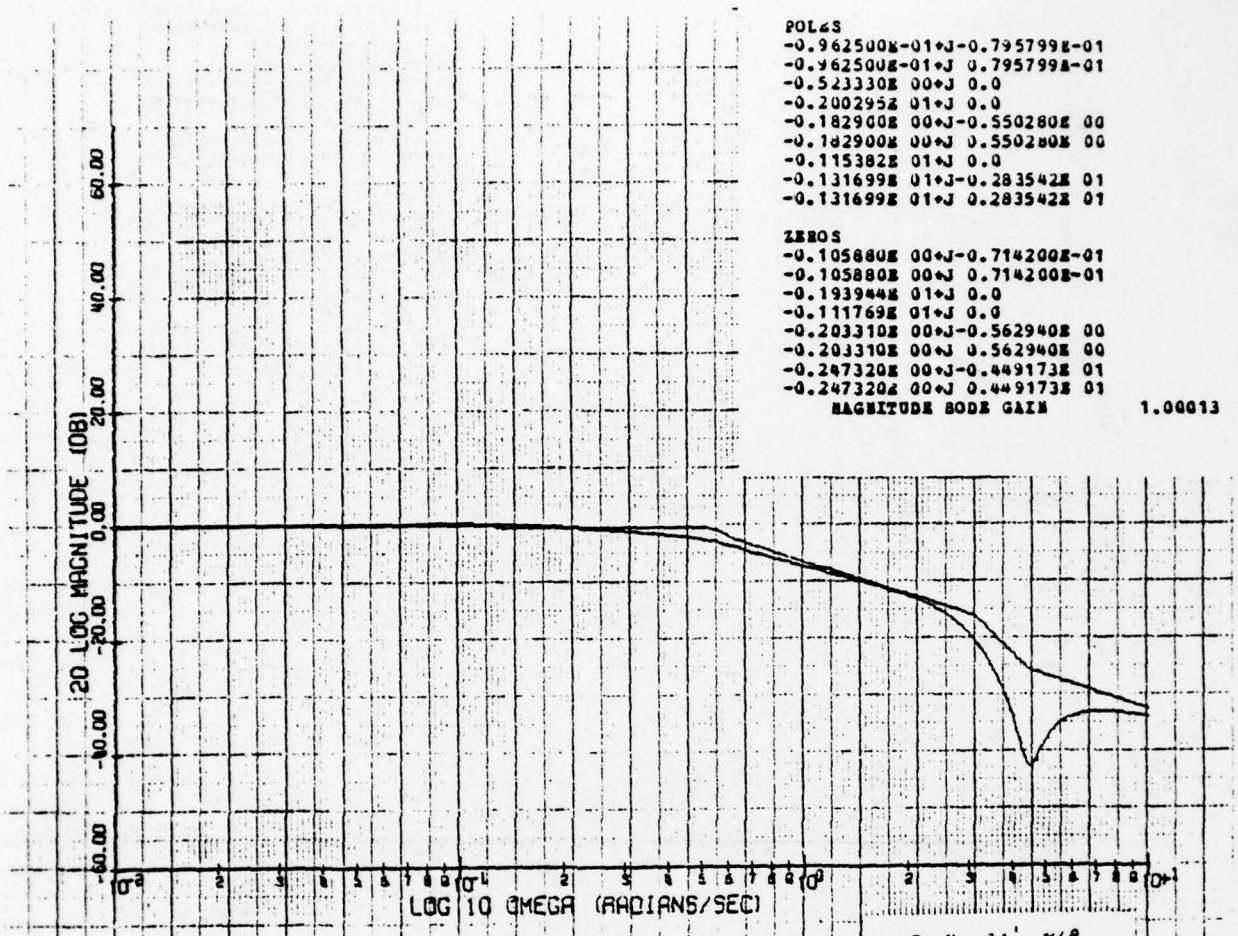

IW RAMF MAGNITUDE PLOT

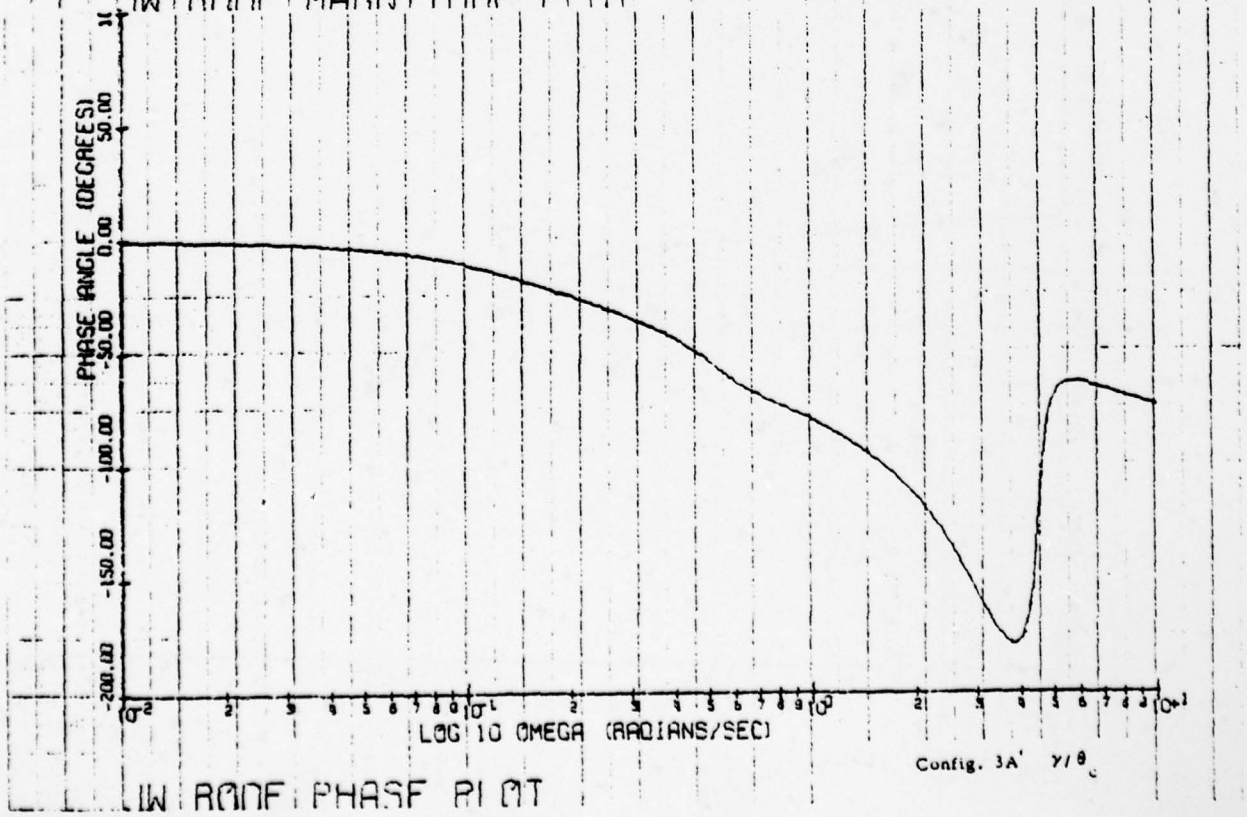

IW RAMF PHASE PLOT

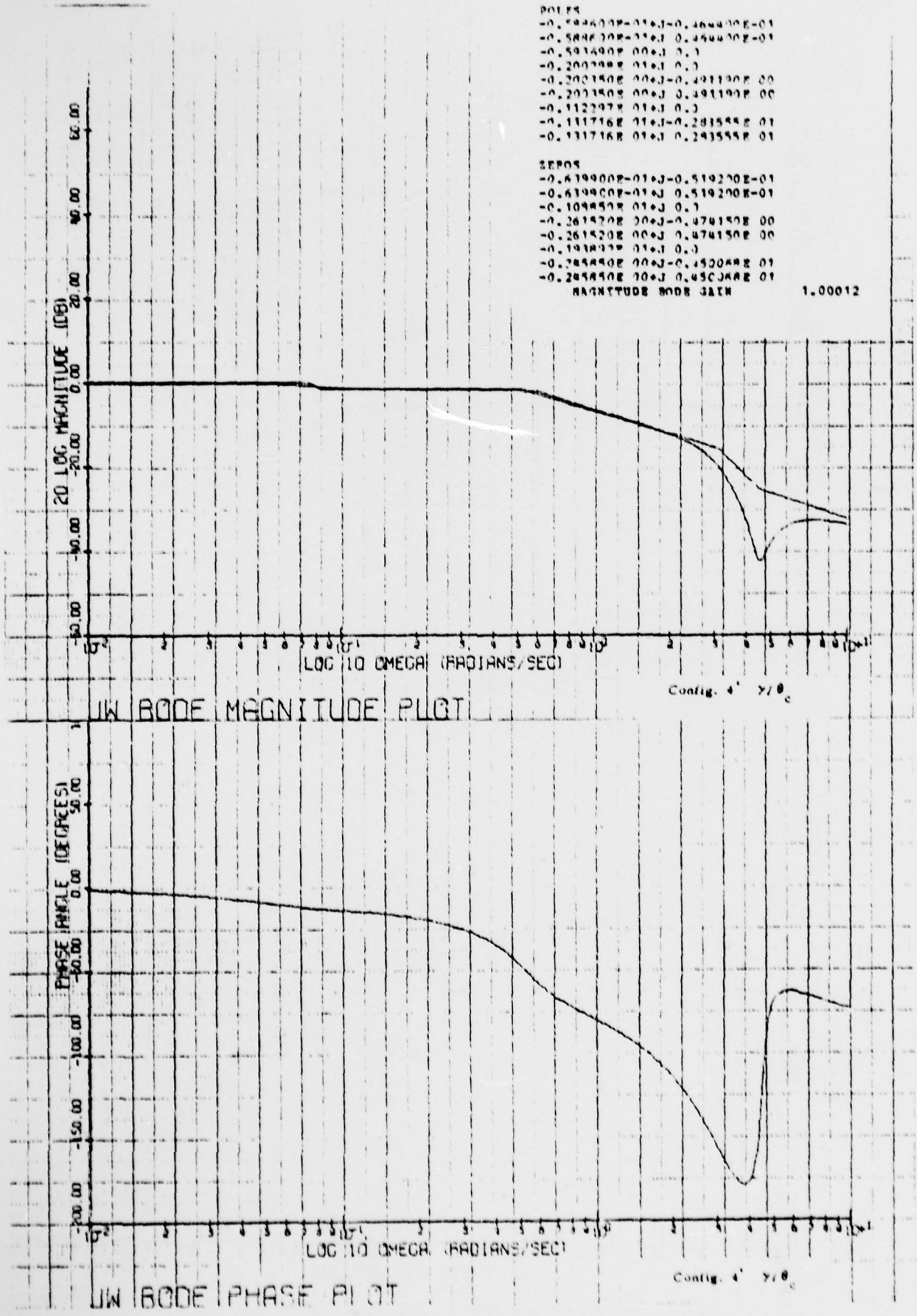
POLES
-0.5199000E-01+J-0.5192700E-01
-0.5199000E-01+J 0.5192700E-01
-0.1098500E 01+J 0.0
-0.2615200E 00+J-0.4781500E 00
-0.2615200E 00+J 0.4781500E 00
-0.1938000E 01+J 0.0
-0.2858500E 00+J-0.4500400E 01
-0.2858500E 00+J 0.4500400E 01
MAGNITUDE BODE GAIN 1.00012
20 LOG MAGNITUDE (DB)
50.00
30.00
20.00
0.00
-20.00
-30.00
-50.00
LOG 10 OMEGA (RADIANS/SEC)
Config. 4' Y/θc
UW BODE MAGNITUDE PLOT
PHASE ANGLE (DEGREES)
50.00
0.00
-50.00
-100.00
-150.00
-200.00
LOG 10 OMEGA (RADIANS/SEC)
Config. 4' Y/θc
UW BODE PHASE PLOT

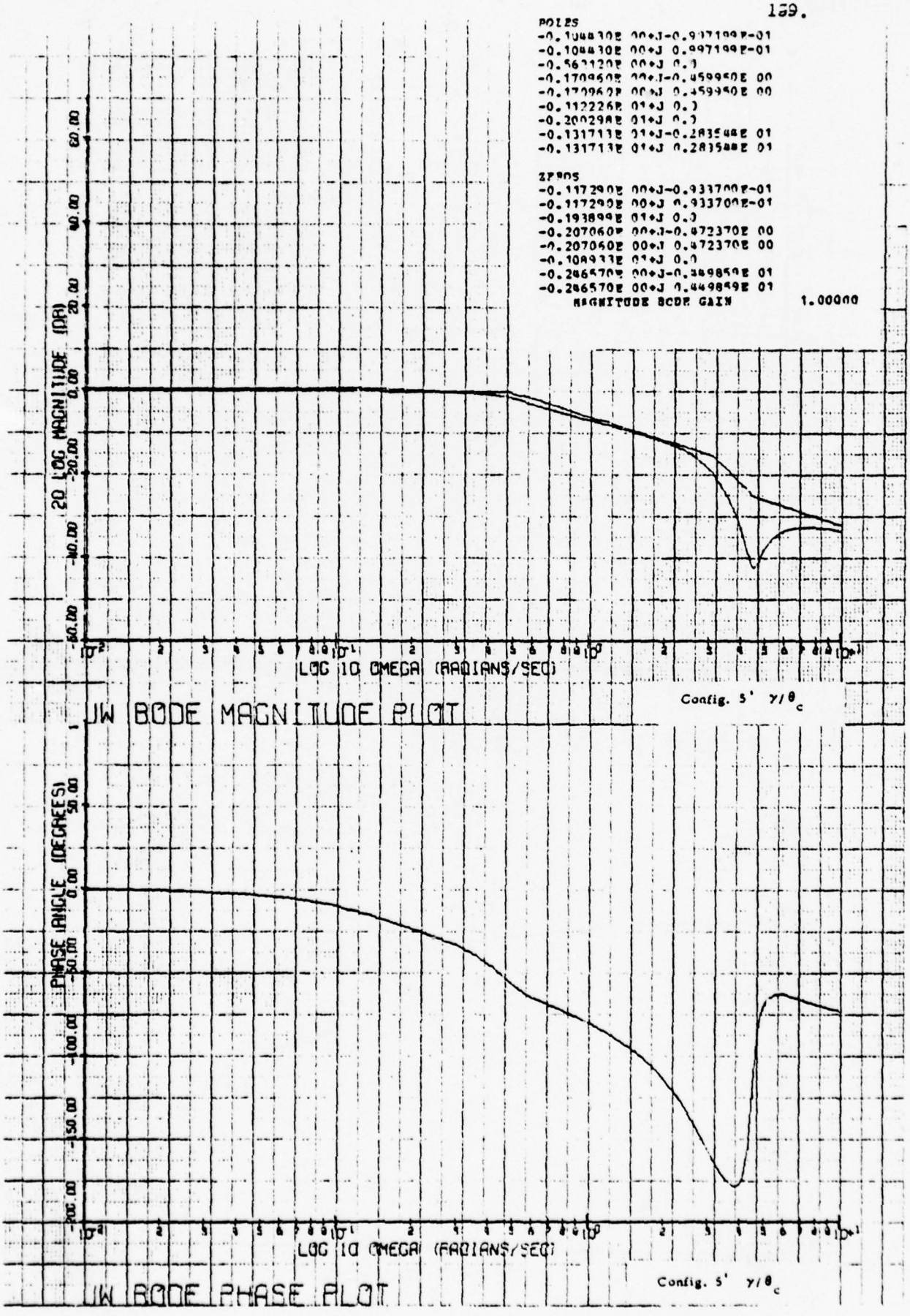
POLES
-0.1044302 00+J-0.9971992-01
-0.1044302 00+J 0.9971992-01
-0.5621202 00+J 0.0
-0.1709602 00+J-0.4599502 00
-0.1709602 00+J 0.4599502 00
-0.1122262 01+J 0.0
-0.2002982 01+J 0.0
-0.1317132 01+J-0.2835482 01
-0.1317132 01+J 0.2835482 01
ZEROS
-0.1172902 00+J-0.9337002-01
-0.1172902 00+J 0.9337002-01
-0.1938992 01+J 0.0
-0.2070602 00+J-0.4723702 00
-0.2070602 00+J 0.4723702 00
-0.1089932 01+J 0.0
-0.2865702 00+J-0.3498592 01
-0.2865702 00+J 0.3498592 01
MAGNITUDE SCOPE GAIN 1.00000
20 LOG MAGNITUDE (DB)
60.00
40.00
20.00
0.00
-20.00
-40.00
-60.00
LOG 10 OMEGA (RADIANS/SEC)
JW BODE MAGNITUDE PLOT
Config. 5' γ/θ_c
PHASE ANGLE (DEGREES)
50.00
0.00
-50.00
-100.00
-150.00
-200.00
LOG 10 OMEGA (RADIANS/SEC)
JW BODE PHASE PLOT
Config. 5' γ/θ_c

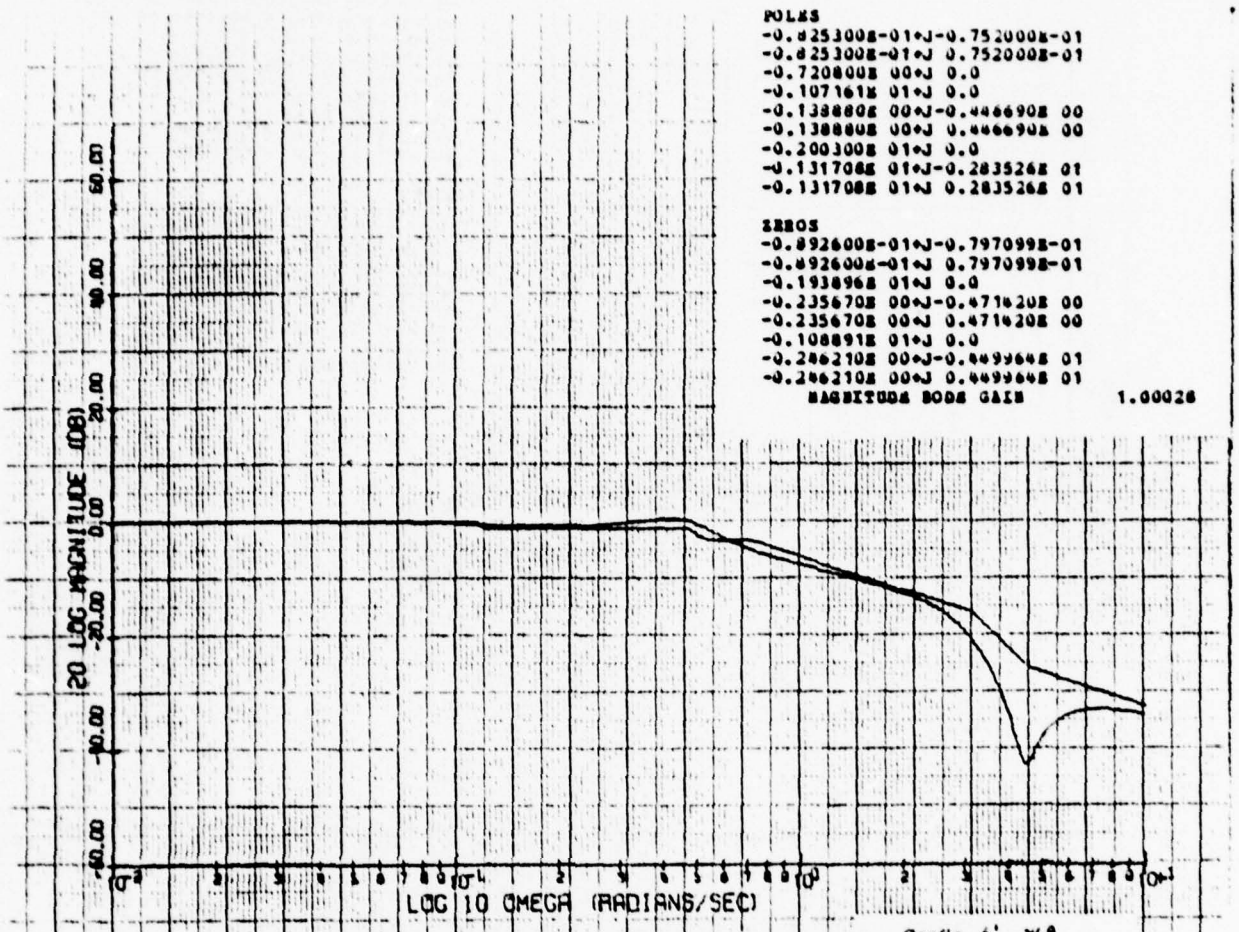

JW BODE MAGNITUDE PLOT

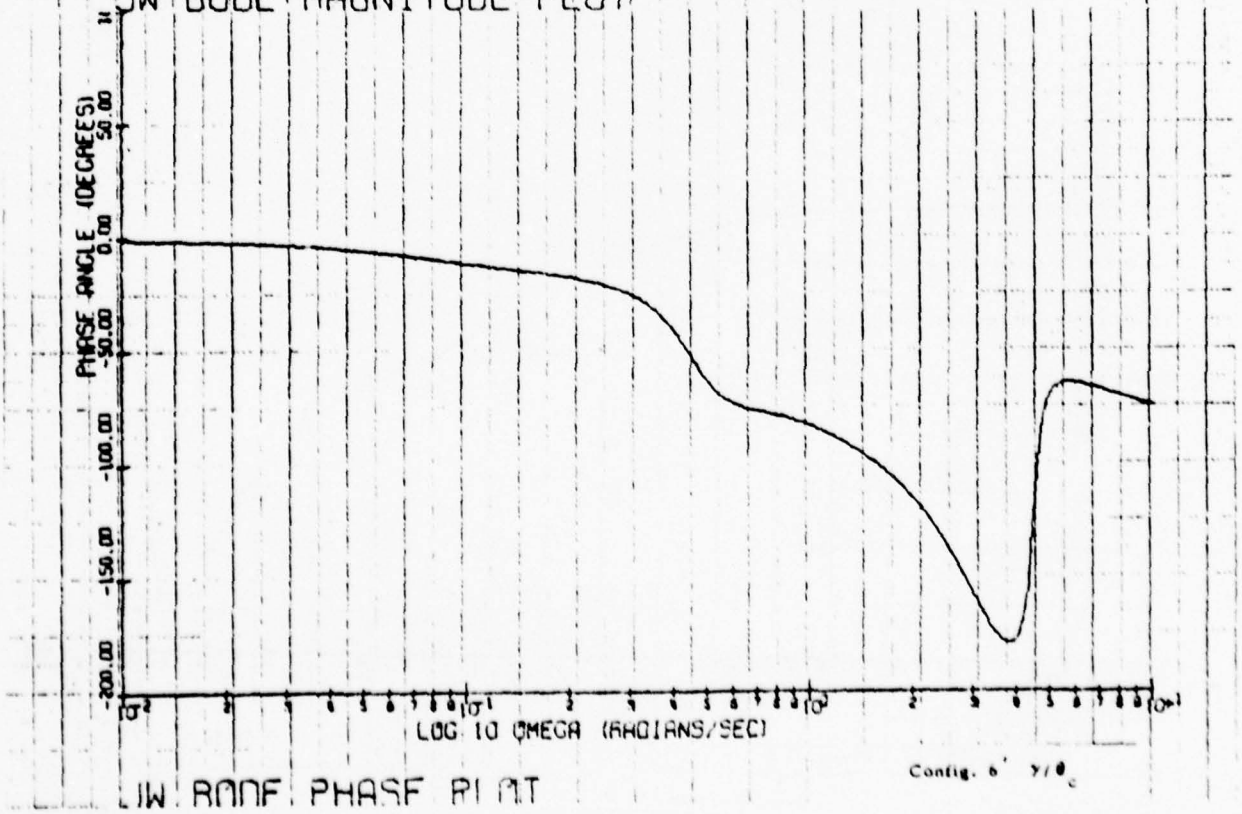

JW BODE PHASE PLOT

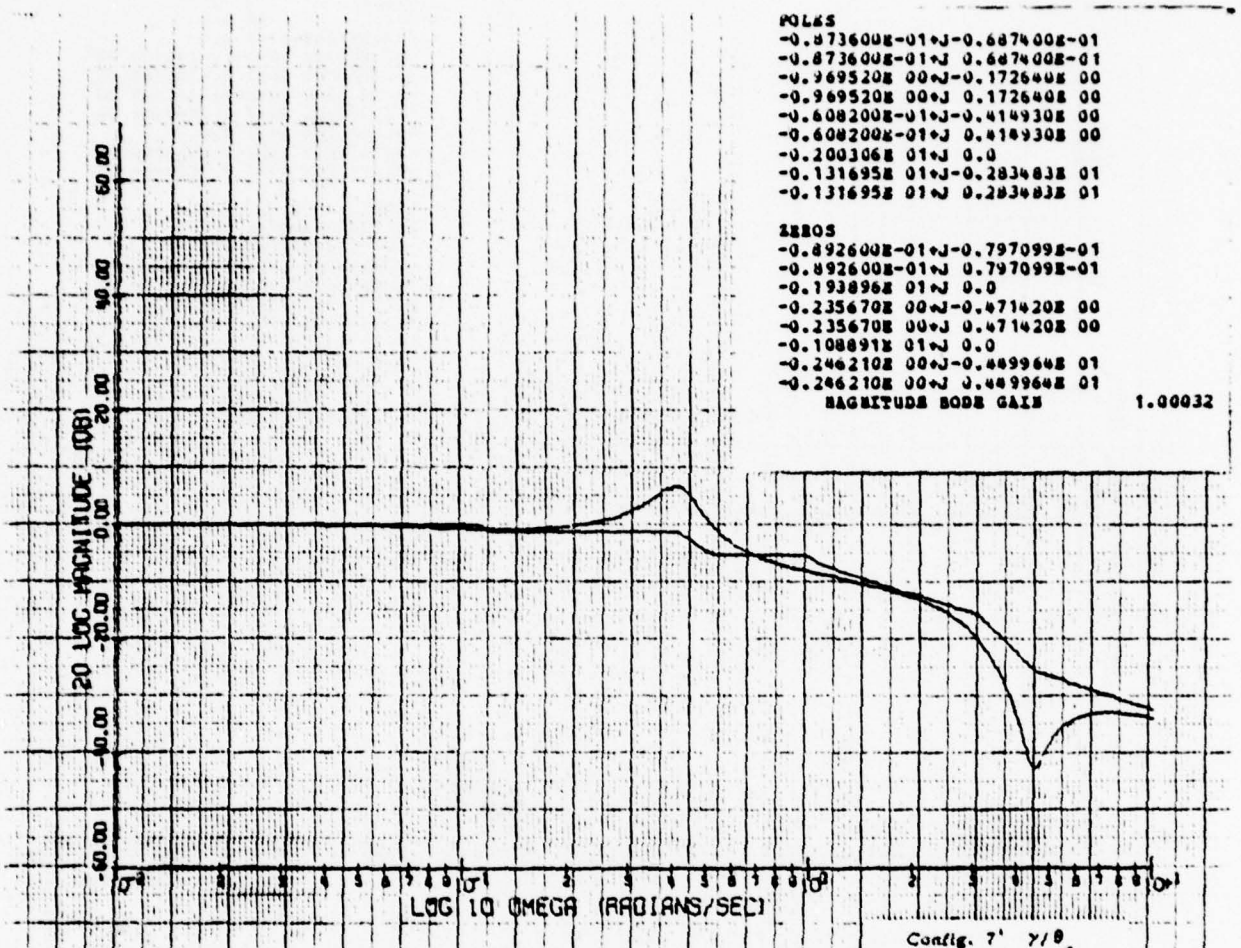

JW RODF MAGNITUDE PLOT

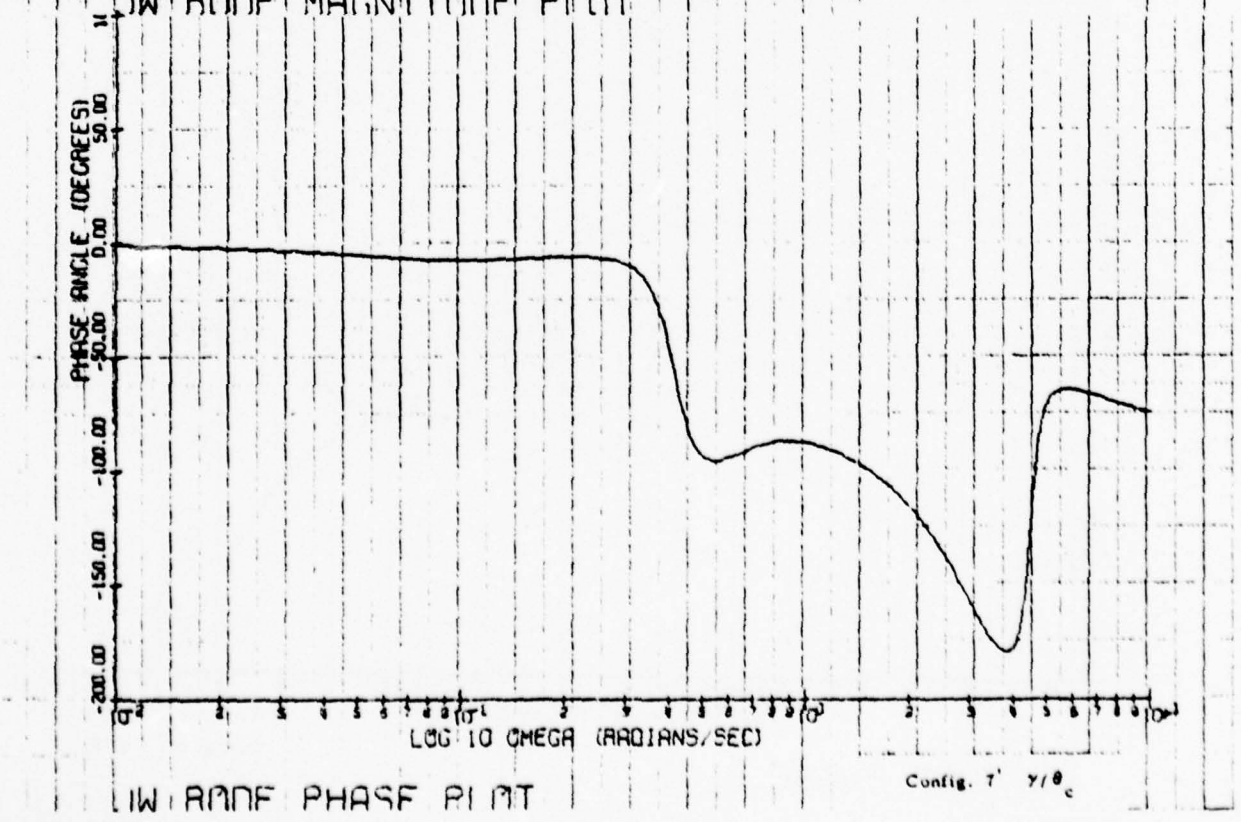

JW RODF PHASE PLOT

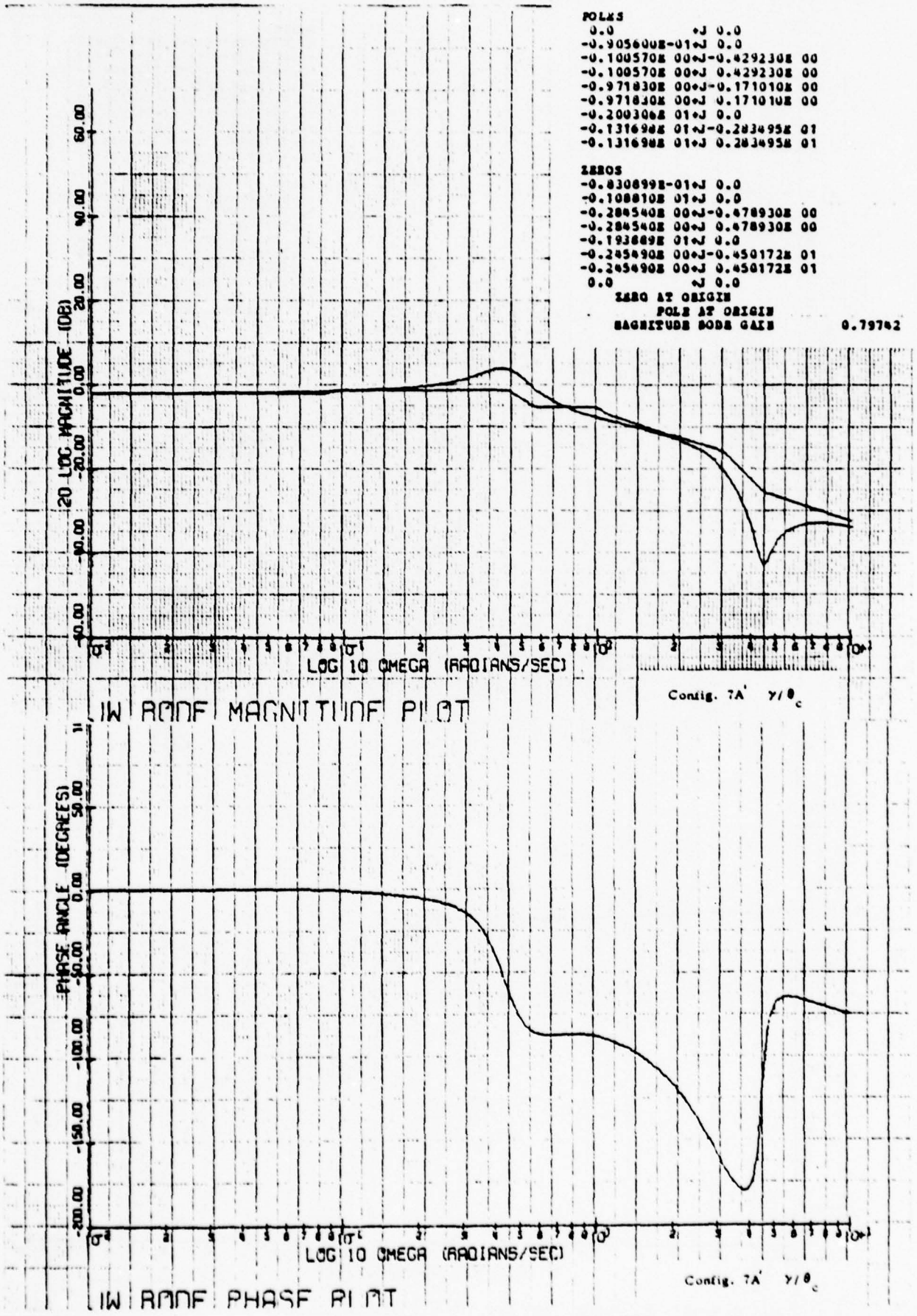
POLES
0.0 +J 0.0
-0.905600E-01+J 0.0
-0.100570E 00+J-0.429230E 00
-0.100570E 00+J 0.429230E 00
-0.971830E 00+J-0.171010E 00
-0.971830E 00+J 0.171010E 00
-0.200306E 01+J 0.0
-0.131698E 01+J-0.283495E 01
-0.131698E 01+J 0.283495E 01
ZEROS
-0.830899E-01+J 0.0
-0.108810E 01+J 0.0
-0.284540E 00+J-0.678930E 00
-0.284540E 00+J 0.678930E 00
-0.193869E 01+J 0.0
-0.265490E 00+J-0.450172E 01
-0.265490E 00+J 0.450172E 01
0.0 +J 0.0
ZERO AT ORIGIN
POLE AT ORIGIN
MAGNITUDE BODE GAIN 0.79762
60.00
40.00
20.00
0.0
-20.00
-40.00
-60.00
20 LOG MAGNITUDE (DB)
LOG 10 OMEGA (RADIANS/SEC)
Config. 7A' Y/θc
LW RDDF MAGNITUDE PLOT
90.00
0.0
-90.00
-180.00
-270.00
PHASE ANGLE (DEGREES)
LOG 10 OMEGA (RADIANS/SEC)
Config. 7A' Y/θc
LW RDDF PHASE PLOT

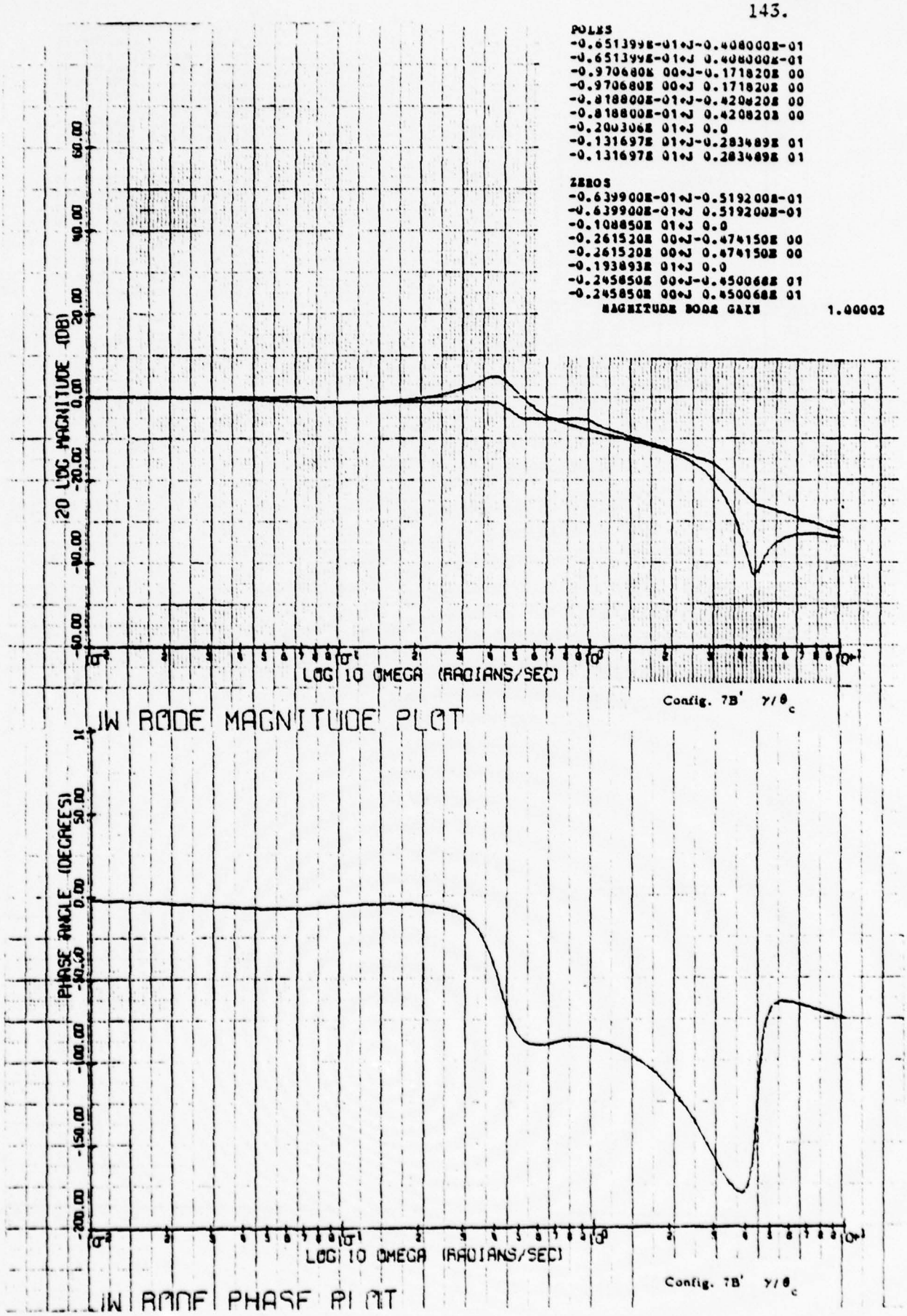
POLES
-0.651399E-01+J-0.408000E-01
-0.651399E-01+J 0.408000E-01
-0.970680E 00+J-0.171820E 00
-0.970680E 00+J 0.171820E 00
-0.818800E-01+J-0.420820E 00
-0.818800E-01+J 0.420820E 00
-0.200306E 01+J 0.0
-0.131697E 01+J-0.283489E 01
-0.131697E 01+J 0.283489E 01
ZEROS
-0.639900E-01+J-0.519200E-01
-0.639900E-01+J 0.519200E-01
-0.108850E 01+J 0.0
-0.261520E 00+J-0.474150E 00
-0.261520E 00+J 0.474150E 00
-0.193893E 01+J 0.0
-0.245850E 00+J-0.450068E 01
-0.245850E 00+J 0.450068E 01
MAGNITUDE BODE GAIN 1.00002
60.00
40.00
20.00
0.00
-20.00
-40.00
-60.00
20 LOG MAGNITUDE (DB)
LOG 10 OMEGA (RADIANS/SEC)
Config. 7B' γ/θc
JW BODE MAGNITUDE PLOT
50.00
0.00
-50.00
-100.00
-150.00
-200.00
PHASE ANGLE (DEGREES)
LOG 10 OMEGA (RADIANS/SEC)
Config. 7B' γ/θc
JW BODE PHASE PLOT

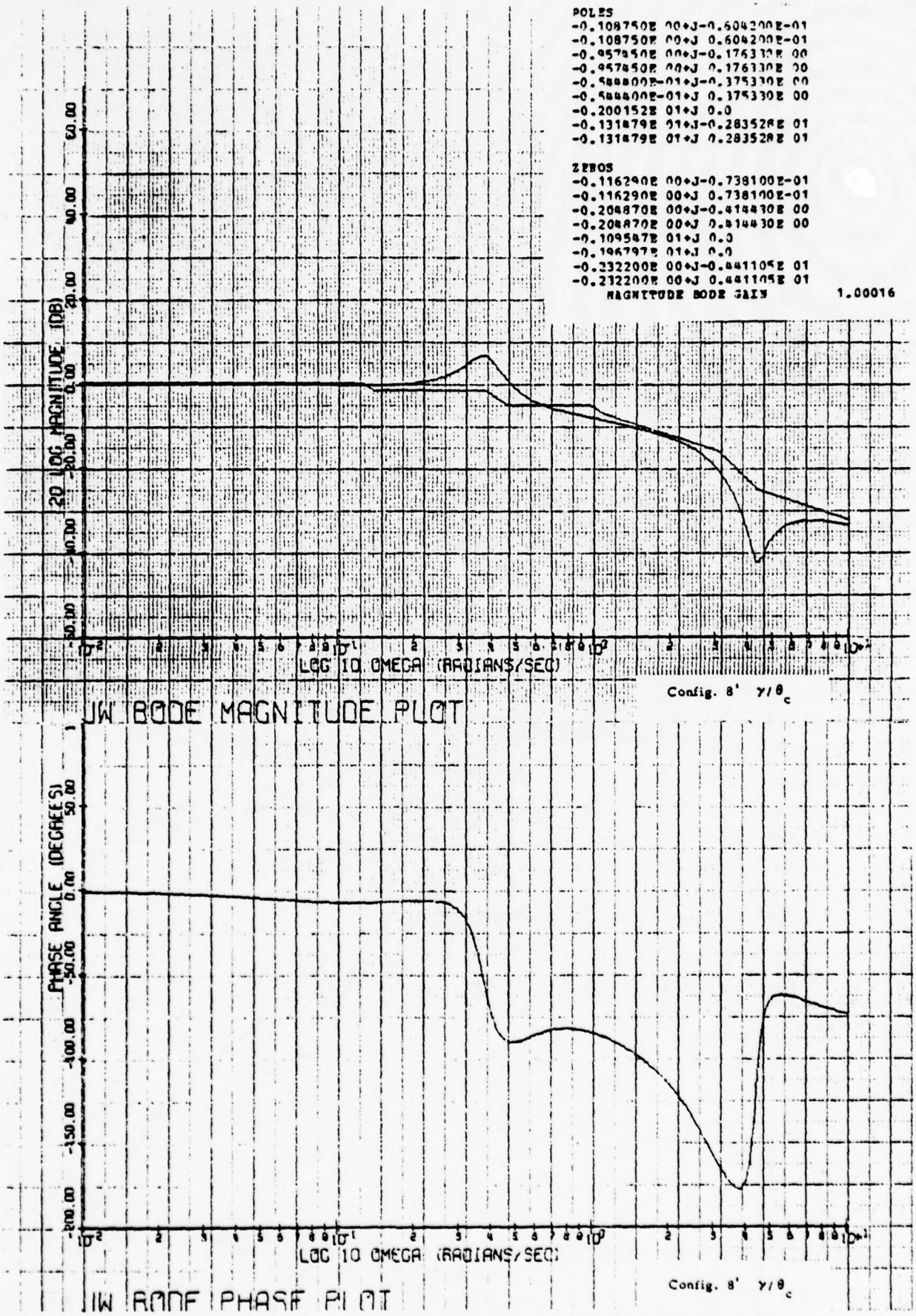
POLES
-0.108750E 00+J-0.604200E-01
-0.108750E 00+J 0.604200E-01
-0.957850E 00+J-0.176330E 00
-0.957850E 00+J 0.176330E 00
-0.588800E-01+J-0.375330E 00
-0.588800E-01+J 0.375330E 00
-0.200152E 01+J 0.0
-0.131879E 01+J-0.283528E 01
-0.131879E 01+J 0.283528E 01
ZEROS
-0.116290E 00+J-0.738100E-01
-0.116290E 00+J 0.738100E-01
-0.204870E 00+J-0.414430E 00
-0.204870E 00+J 0.414430E 00
-0.109587E 01+J 0.0
-0.196797E 01+J 0.0
-0.232200E 00+J-0.441105E 01
-0.232200E 00+J 0.441105E 01
MAGNITUDE BODE GAIN
1.00016
20 LOG MAGNITUDE (DB)
LOG 10 OMEGA (RADIANS/SEC)
Config. 8' Y/θc
JW BODE MAGNITUDE PLOT
PHASE ANGLE (DEGREES)
LOG 10 OMEGA (RADIANS/SEC)
Config. 8' Y/θc
JW BODE PHASE PLOT

POLES
-0.803100E-01+J-0.360500E-01
-0.803100E-01+J 0.360500E-01
-0.958800E 00+J-0.175440E 00
-0.958800E 00+J 0.175440E 00
-0.815099E-01+J-0.380150E 00
-0.815099E-01+J 0.380150E 00
-0.200153E 01+J 0.0
-0.131481E 01+J-0.283533E 01
-0.131481E 01+J 0.283533E 01

ZEROS
-0.814800E-01+J-0.462400E-01
-0.814800E-01+J 0.462400E-01
-0.109502E 01+J 0.0
-0.240290E 00+J-0.416530E 00
-0.240290E 00+J 0.416530E 00
-0.196795E 01+J 0.0
-0.231820E 00+J-0.441216E 01
-0.231820E 00+J 0.441216E 01

MAGNITUDE BODE GAIN 1.00022

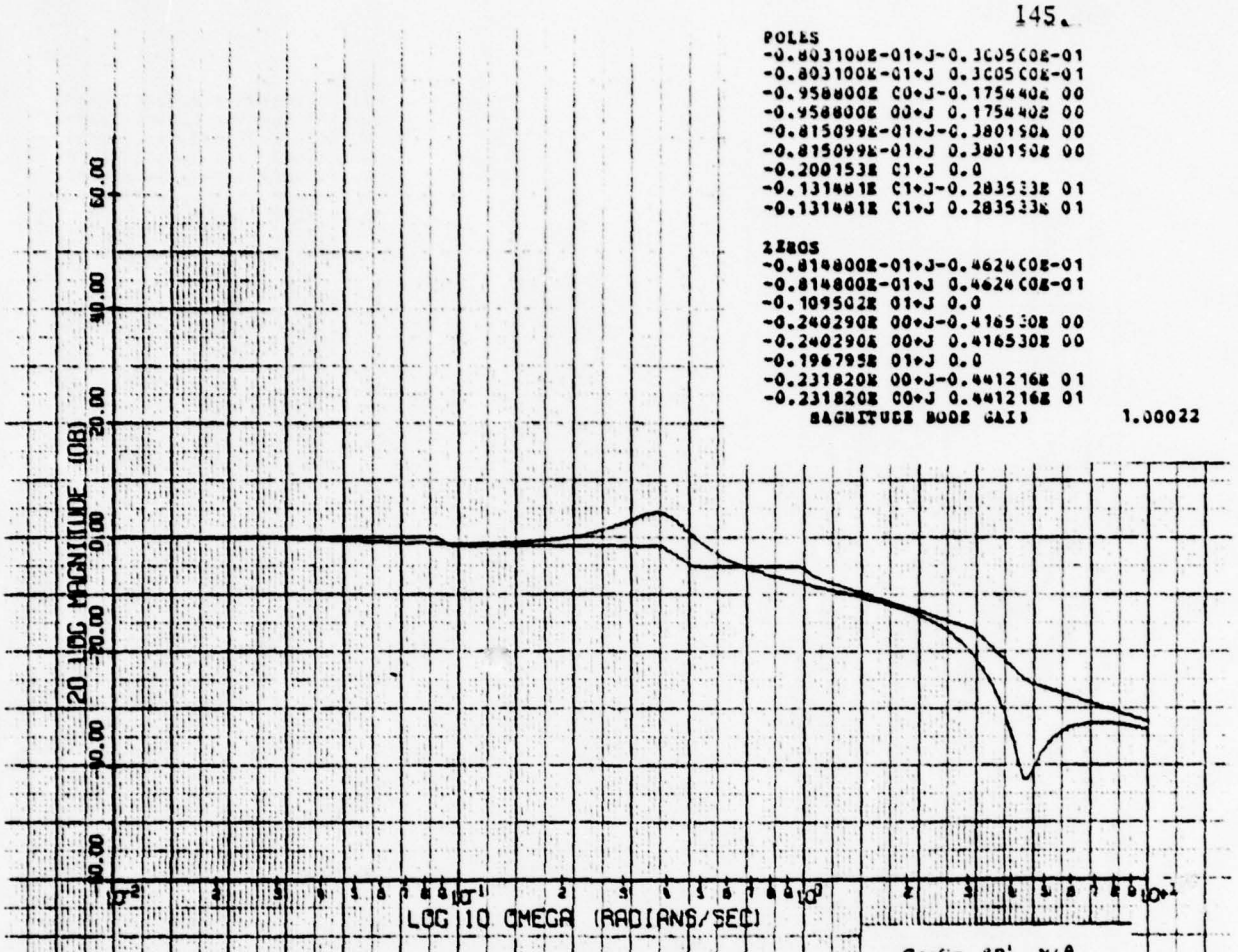

Config. 8B' γ/θ_c

IW BODE MAGNITUDE PLOT

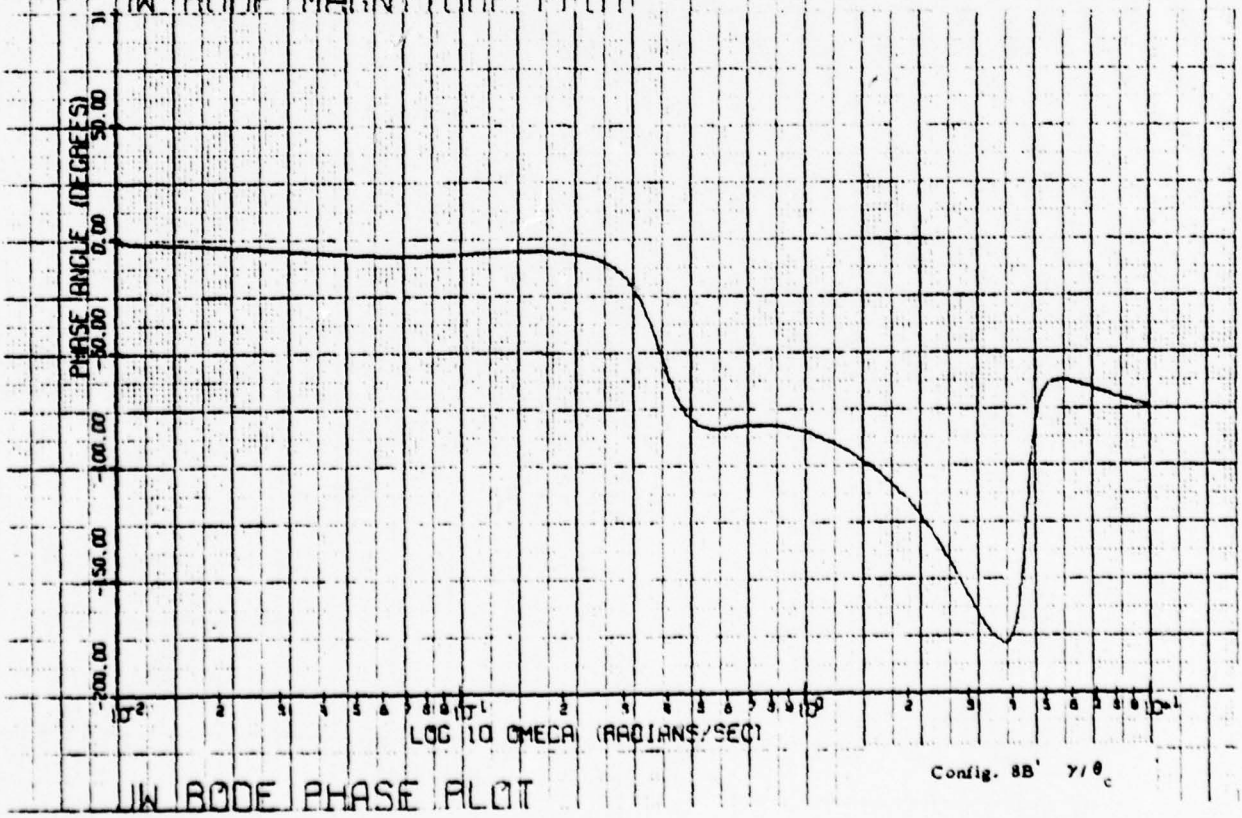

Config. 8B' γ/θ_c

IW BODE PHASE PLOT

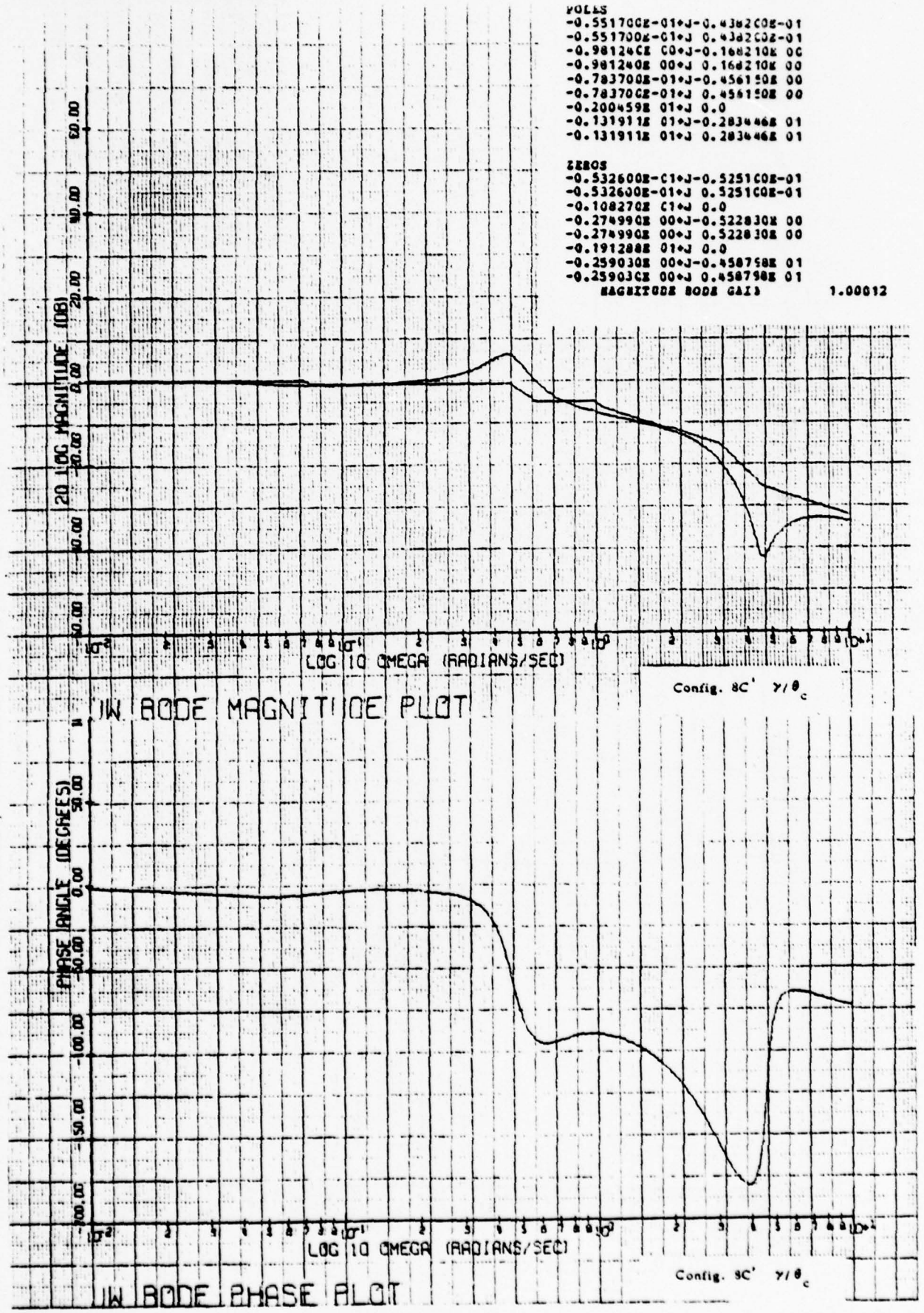
POLES
-0.551700E-01+J-0.438260E-01
-0.551700E-01+J 0.438260E-01
-0.981240E 00+J-0.168210E 00
-0.981240E 00+J 0.168210E 00
-0.783700E-01+J-0.456150E 00
-0.783700E-01+J 0.456150E 00
-0.200459E 01+J 0.0
-0.131911E 01+J-0.283446E 01
-0.131911E 01+J 0.283446E 01
ZEROS
-0.532600E-01+J-0.525100E-01
-0.532600E-01+J 0.525100E-01
-0.108270E 01+J 0.0
-0.274990E 00+J-0.522830E 00
-0.274990E 00+J 0.522830E 00
-0.191288E 01+J 0.0
-0.259030E 00+J-0.458758E 01
-0.259030E 00+J 0.458758E 01
MAGNITUDE BODE GAIN 1.00012
20 LOG MAGNITUDE (DB)
60.00
40.00
20.00
0.00
-20.00
-40.00
-60.00
LOG 10 OMEGA (RADIANS/SEC)
Config. 8C' Y/θc
1W BODE MAGNITUDE PLOT
PHASE ANGLE (DEGREES)
50.00
0.00
-50.00
-100.00
-150.00
-200.00
LOG 10 OMEGA (RADIANS/SEC)
Config. 8C' Y/θc
1W BODE PHASE PLOT

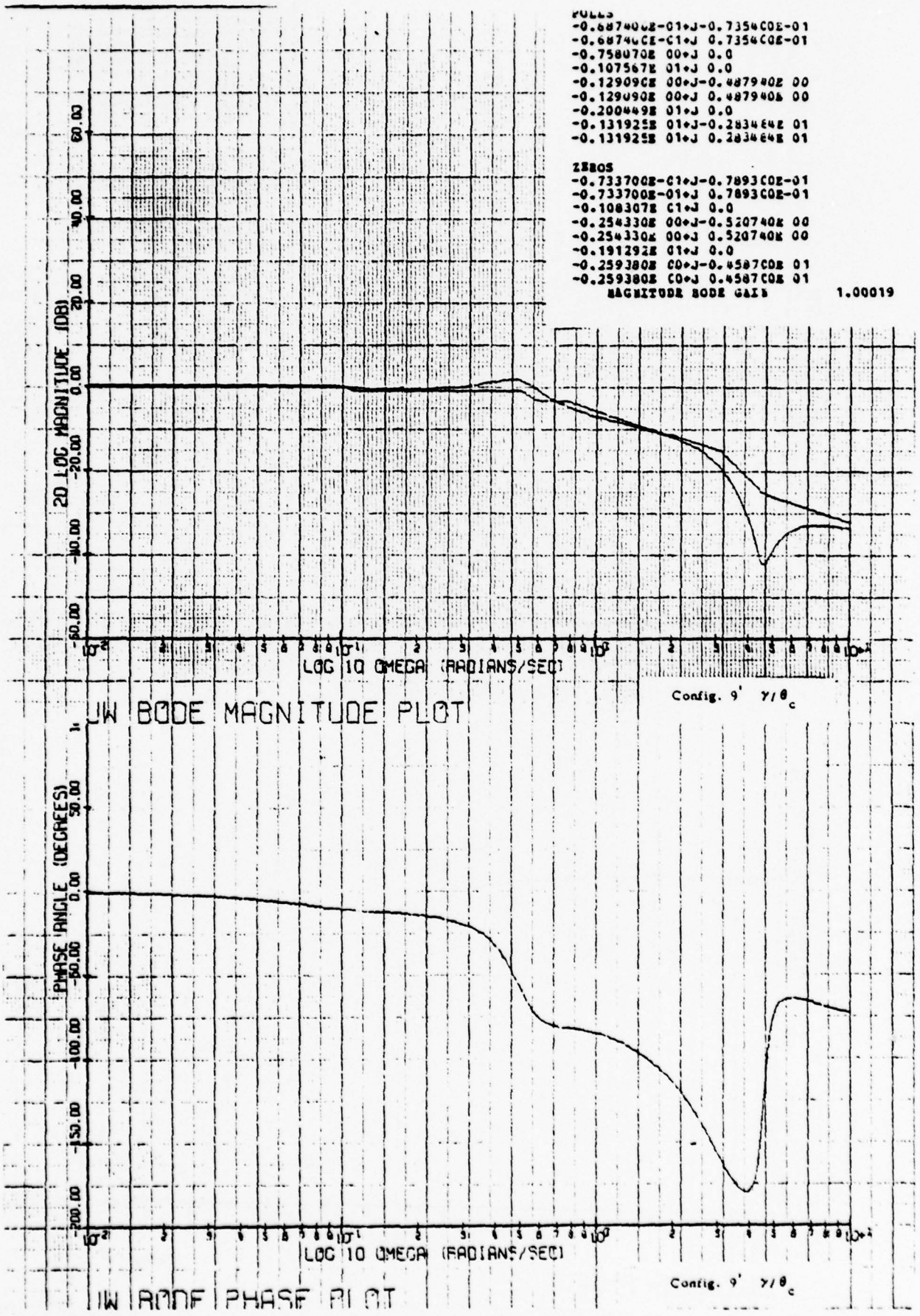
POLES
-0.687406E-01+J-0.735406E-01
-0.687406E-01+J 0.735406E-01
-0.758070E 00+J 0.0
-0.107567E 01+J 0.0
-0.129090E 00+J-0.487940E 00
-0.129090E 00+J 0.487940E 00
-0.200449E 01+J 0.0
-0.131925E 01+J-0.283464E 01
-0.131925E 01+J 0.283464E 01
ZEROS
-0.733700E-01+J-0.789300E-01
-0.733700E-01+J 0.789300E-01
-0.108307E 01+J 0.0
-0.254330E 00+J-0.520740E 00
-0.254330E 00+J 0.520740E 00
-0.191292E 01+J 0.0
-0.259380E 00+J-0.458700E 01
-0.259380E 00+J 0.458700E 01
MAGNITUDE BODE GAIN 1.00019
20 LOG MAGNITUDE (DB)
60.00
40.00
20.00
0.00
-20.00
-40.00
-60.00
LOG 10 OMEGA (RADIANS/SEC)
Config. 9' γ/θc
JW BODE MAGNITUDE PLOT
PHASE ANGLE (DEGREES)
50.00
0.00
-50.00
-100.00
-150.00
-200.00
LOG 10 OMEGA (RADIANS/SEC)
Config. 9' γ/θc
JW BODE PHASE PLOT

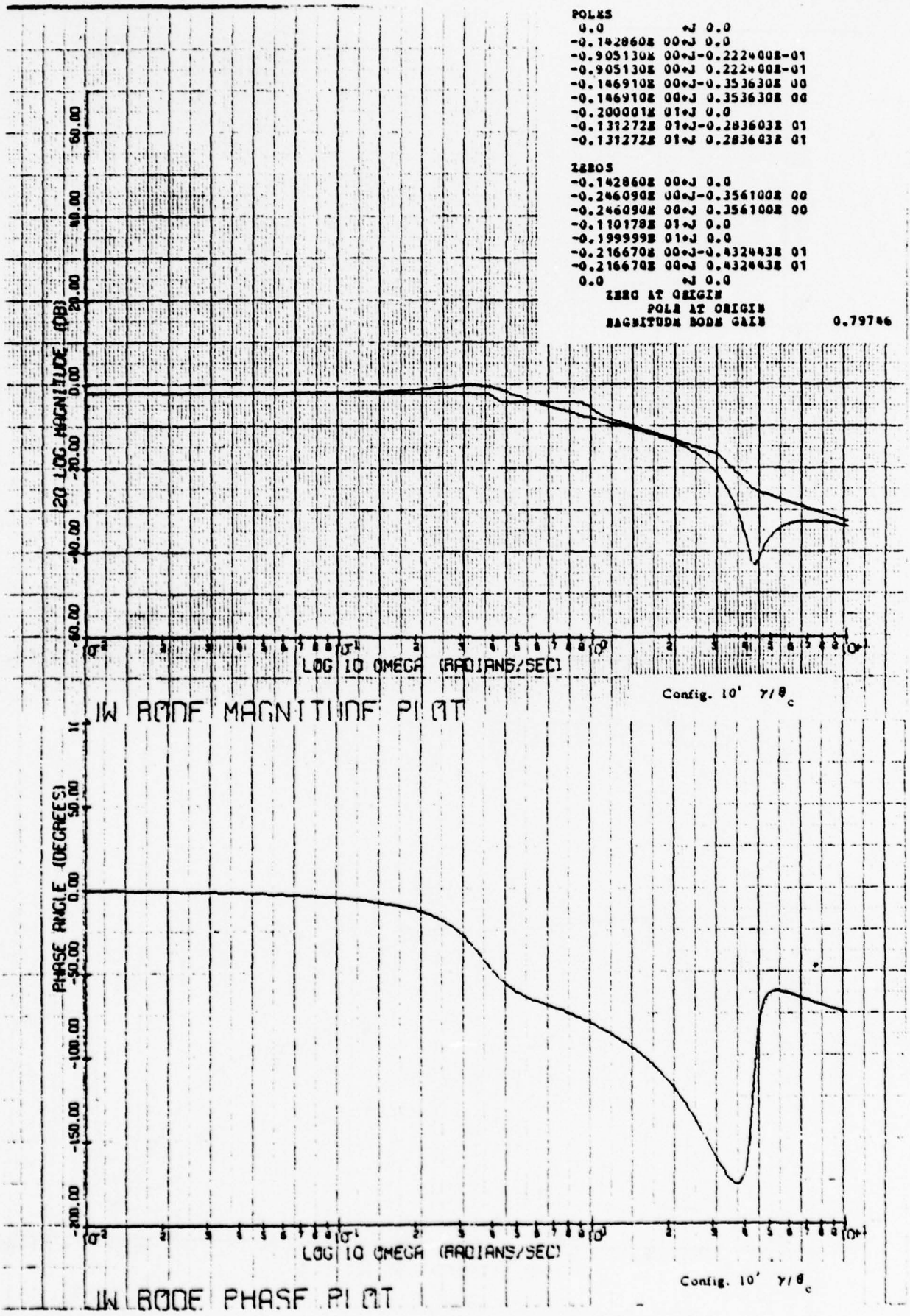
POLES
0.0 +J 0.0
-0.142860E 00+J 0.0
-0.905130E 00+J-0.222400E-01
-0.905130E 00+J 0.222400E-01
-0.146910E 00+J-0.353630E 00
-0.146910E 00+J 0.353630E 00
-0.200001E 01+J 0.0
-0.131272E 01+J-0.283603E 01
-0.131272E 01+J 0.283603E 01
ZEROS
-0.142860E 00+J 0.0
-0.246090E 00+J-0.356100E 00
-0.246090E 00+J 0.356100E 00
-0.110178E 01+J 0.0
-0.199999E 01+J 0.0
-0.216670E 00+J-0.432443E 01
-0.216670E 00+J 0.432443E 01
0.0 +J 0.0
ZERO AT ORIGIN
POLE AT ORIGIN
MAGNITUDE BODE GAIN 0.79746
20 LOG MAGNITUDE (DB)
60.00
40.00
20.00
0.00
-20.00
-40.00
-60.00
LOG 10 OMEGA (RADIANS/SEC)
Config. 10' Y/θc
W BODE MAGNITUDE PLOT
PHASE ANGLE (DEGREES)
50.00
0.00
-50.00
-100.00
-150.00
-200.00
LOG 10 OMEGA (RADIANS/SEC)
Config. 10' Y/θc
W BODE PHASE PLOT

POLES
-0.854599E-01+J-0.742500E-01
-0.854599E-01+J 0.742500E-01
-0.933080E 00+J-0.419700E-01
-0.933080E 00+J 0.419700E-01
-0.992000E-01+J-0.422680E 00
-0.992000E-01+J 0.422680E 00
-0.200304E 01+J 0.0
-0.131693E 01+J-0.283489E 01
-0.131693E 01+J 0.283489E 01

ZEROS
-0.878200E-01+J-0.688500E-01
-0.878200E-01+J 0.688500E-01
-0.193916E 01+J 0.0
-0.230070E 00+J-0.512910E 00
-0.230070E 00+J 0.512910E 00
-0.110214E 01+J 0.0
-0.246540E 00+J-0.449663E 01
-0.246540E 00+J 0.449663E 01
MAGNITUDE BODE GAIN 1.00025

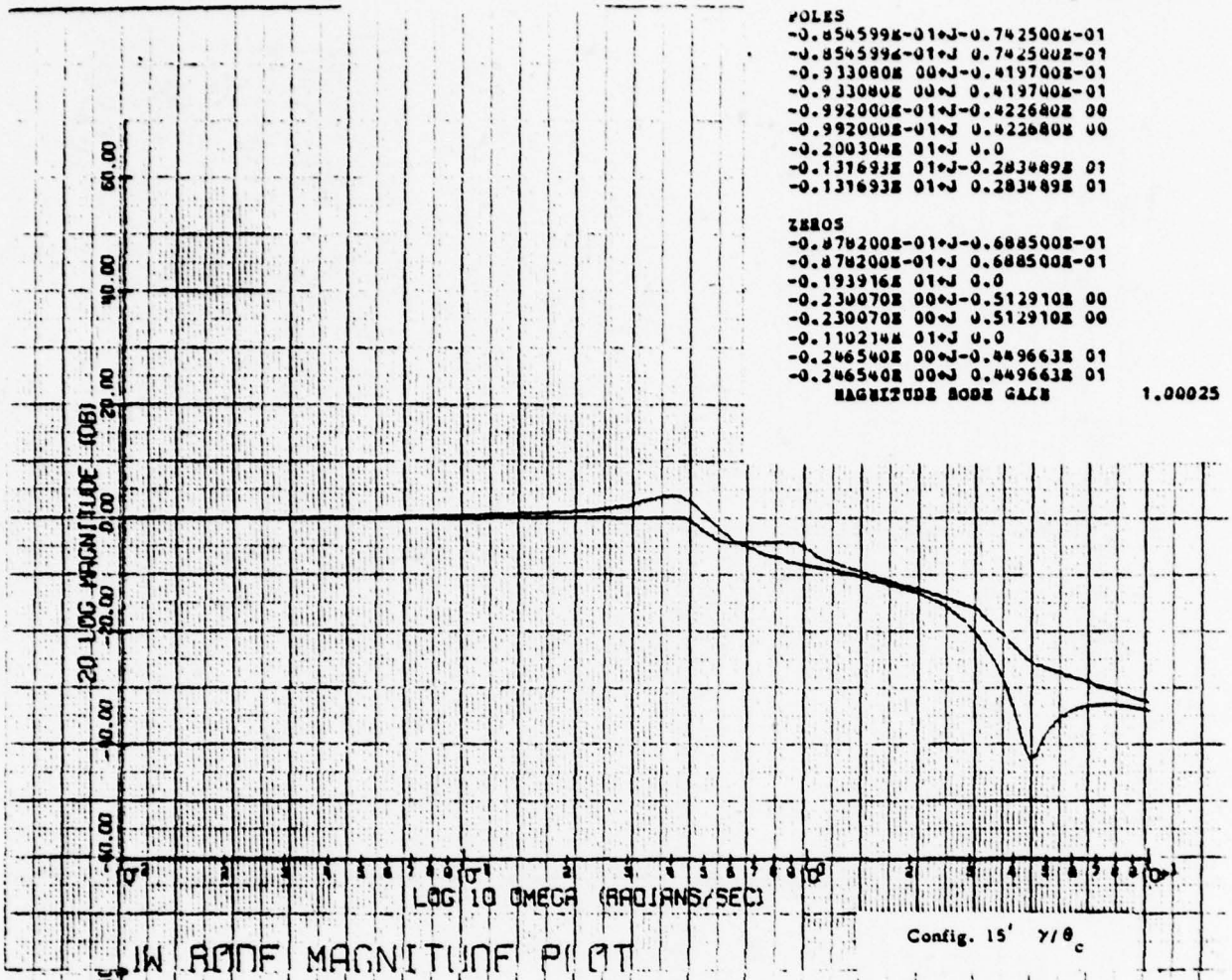

JW BODE MAGNITUDE PLOT

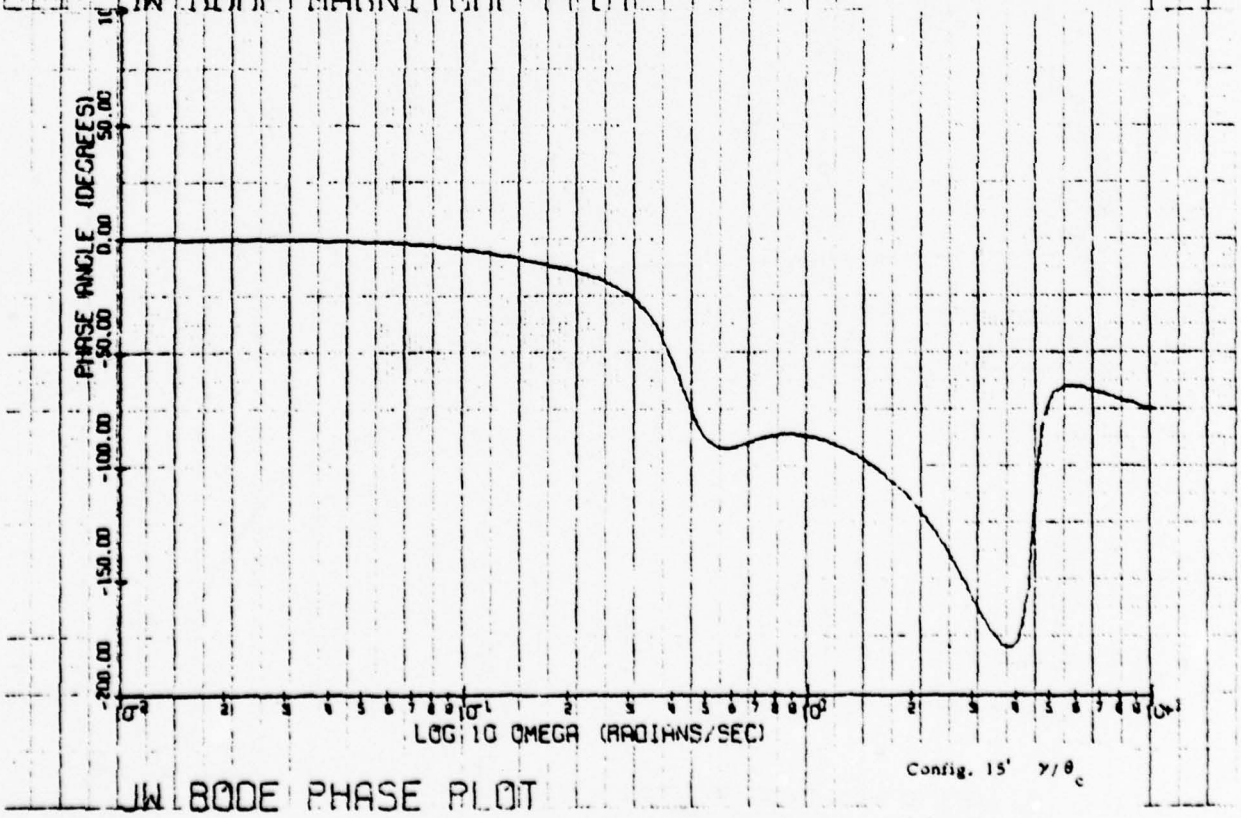

JW BODE PHASE PLOT

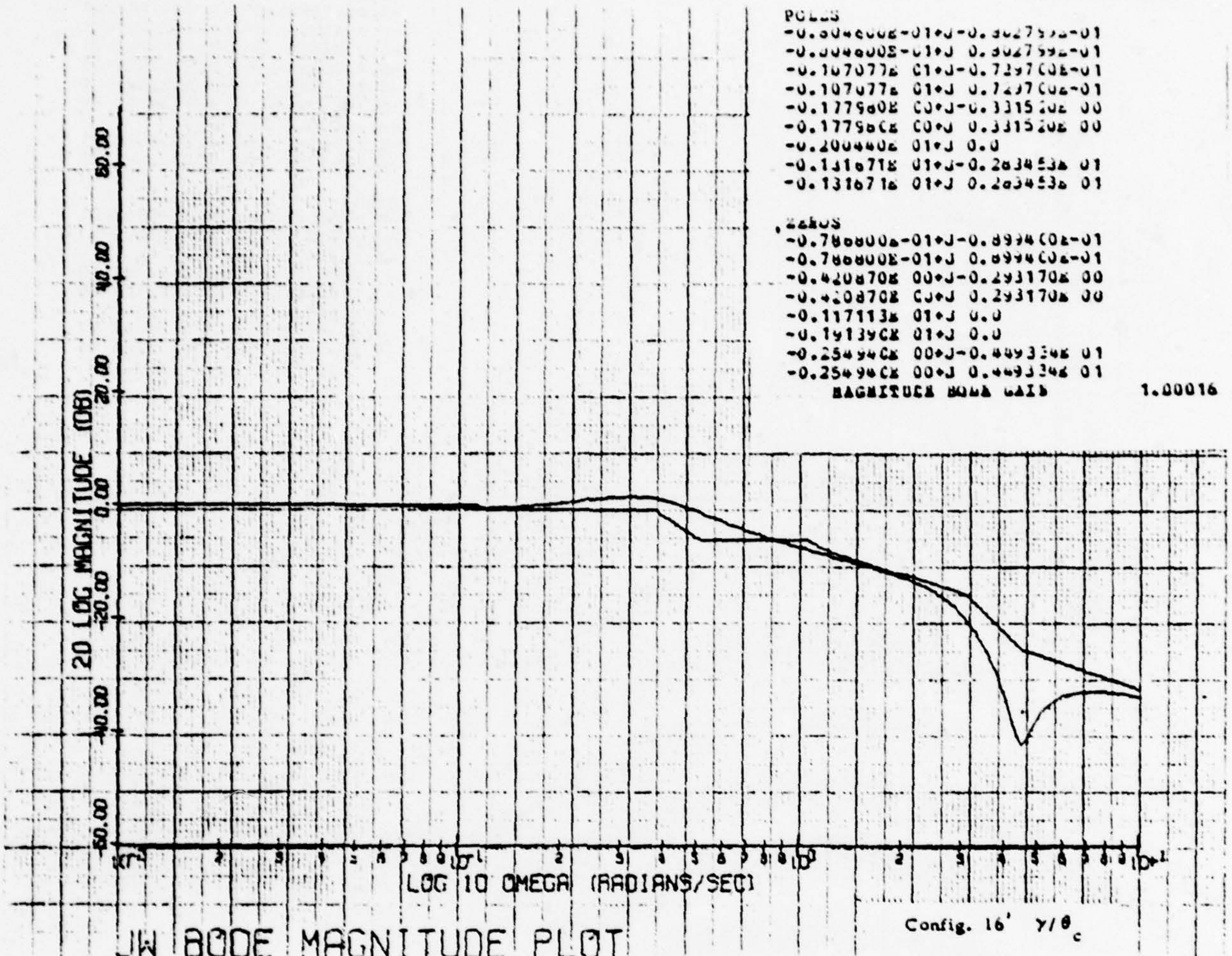

Config. 16' γ/θ_c

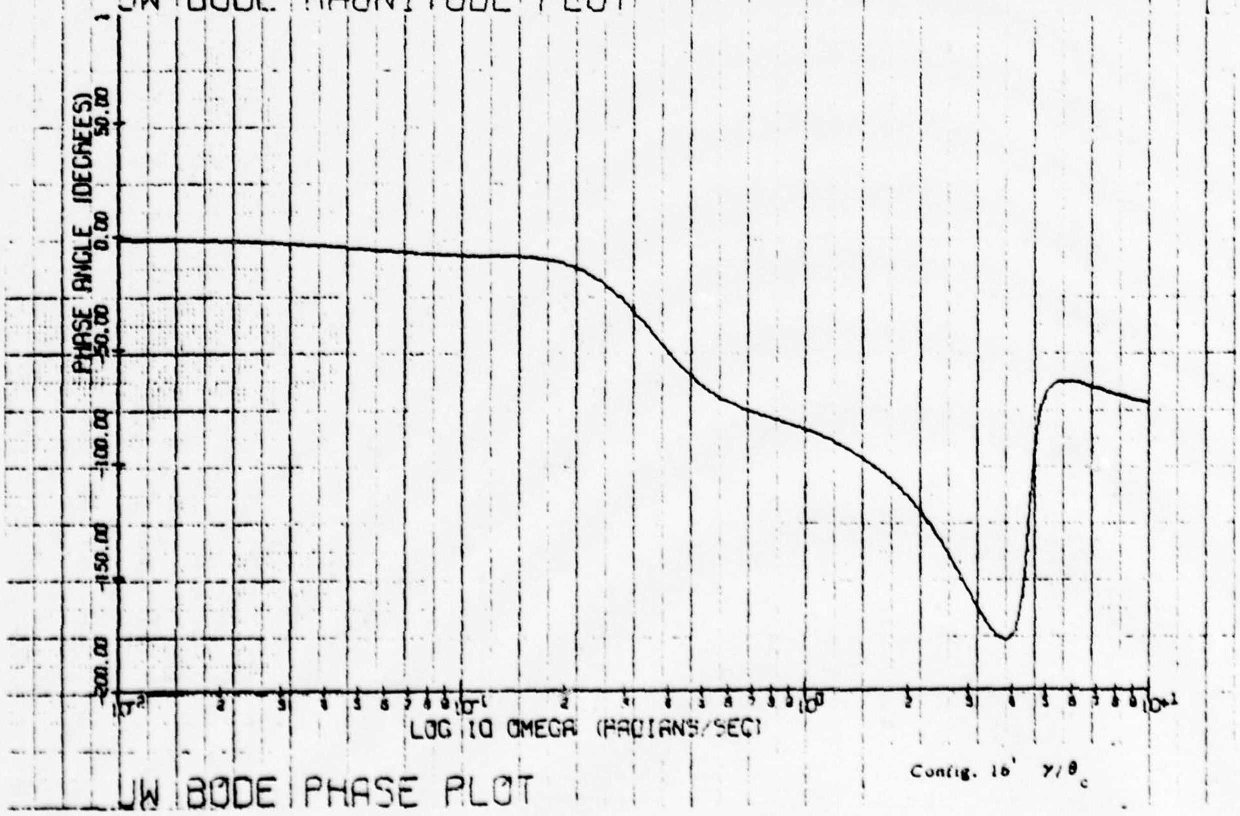

Config. 16' γ/θ_c

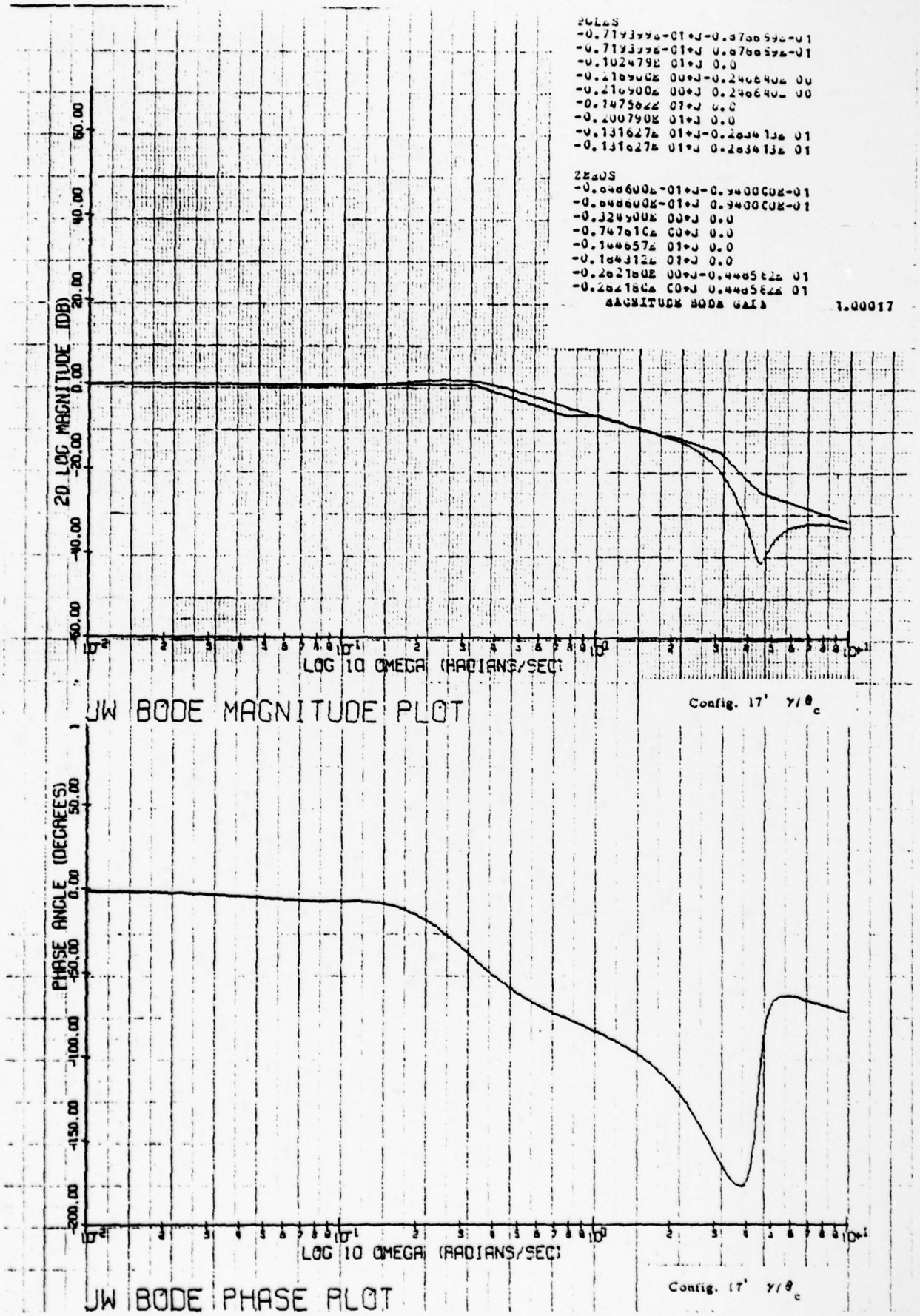
ZEROS
-0.7193998-01+J-0.6786592-01
-0.7193998-01+J 0.6786592-01
-0.1024798 01+J 0.0
-0.2169008 00+J-0.2466408 00
-0.2169008 00+J 0.2466408 00
-0.1475822 01+J 0.0
-0.2007908 01+J 0.0
-0.1316478 01+J-0.2834138 01
-0.1316478 01+J 0.2834138 01
ZEROS
-0.9486008-01+J-0.9400208-01
-0.9486008-01+J 0.9400208-01
-0.3249008 00+J 0.0
-0.7476128 00+J 0.0
-0.1446578 01+J 0.0
-0.1843128 01+J 0.0
-0.2821808 00+J-0.4465828 01
-0.2821808 00+J 0.4465828 01
MAGNITUDE BODE GAIN 1.00017
20 LOG MAGNITUDE (DB)
60.00
40.00
20.00
0.00
-20.00
-40.00
-60.00
LOG 10 OMEGA (RADIANS/SEC)
JW BODE MAGNITUDE PLOT
Config. 17' γ/θc
PHASE ANGLE (DEGREES)
50.00
0.00
-50.00
-100.00
-150.00
-200.00
LOG 10 OMEGA (RADIANS/SEC)
JW BODE PHASE PLOT
Config. 17' γ/θc

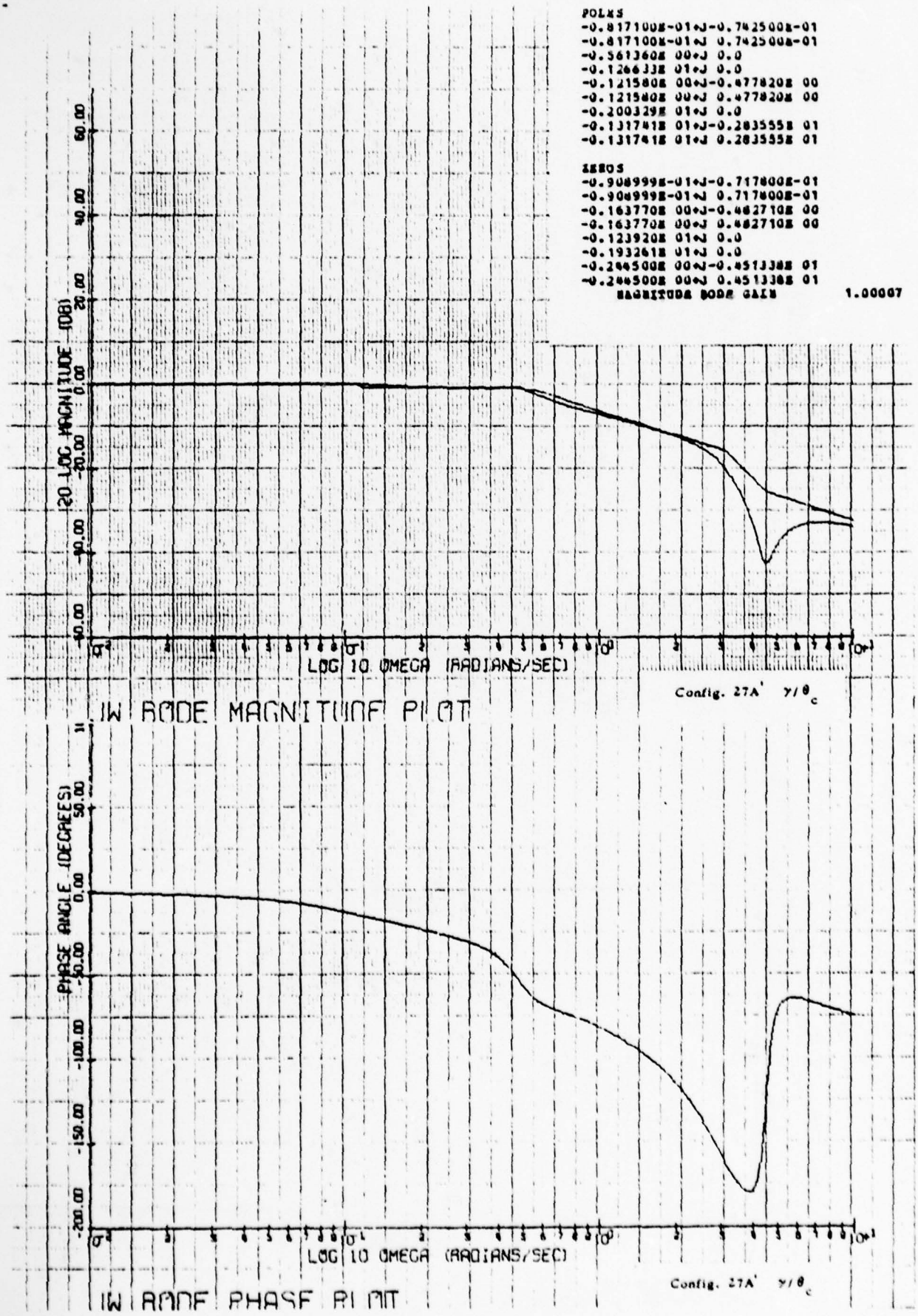
POLES
-0.817100E-01+J-0.742500E-01
-0.817100E-01+J 0.742500E-01
-0.561360E 00+J 0.0
-0.126633E 01+J 0.0
-0.121580E 00+J-0.477820E 00
-0.121580E 00+J 0.477820E 00
-0.200329E 01+J 0.0
-0.131741E 01+J-0.283555E 01
-0.131741E 01+J 0.283555E 01
ZEROS
-0.908999E-01+J-0.717800E-01
-0.908999E-01+J 0.717800E-01
-0.163770E 00+J-0.482710E 00
-0.163770E 00+J 0.482710E 00
-0.123920E 01+J 0.0
-0.193261E 01+J 0.0
-0.244500E 00+J-0.451338E 01
-0.244500E 00+J 0.451338E 01
MAGNITUDE BODE GAIN 1.00007
MAGNITUDE (DB)
LOG 10 OMEGA (RADIANS/SEC)
Config. 27A' γ/θc
1W BODE MAGNITUDE PLOT
PHASE ANGLE (DEGREES)
LOG 10 OMEGA (RADIANS/SEC)
Config. 27A' γ/θc
1W BODE PHASE PLOT

APPENDIX B

Test Configurations of Ground Based and Phase I and II In-Flight Simulations

Presented in this appendix are tables and time histories of the configurations discussed under Flight Path Control Systems, page 28, and thereafter. The configurations use the "simplified" A-7E airframe having zero cross control terms, that is:

$$L_{\delta e}/V = L_{\delta t}/V = M_{\delta t} = D_{\delta e} = 0$$

TABLE B 1

Test Configurations of Ground Based and Phase I In-Flight Simulation

Configuration	Short Period		Phugoid Roots (no engine lag)	Effective Moment Derivatives**			APCS***	Control System Dynamics	Equivalent
	ω_{sp}	ζ_{sp}		M_α	M_θ	$M_{\dot{\theta}}$			$M_{\delta e}$
1	1.38	0.34	-.017±.194i	-1.74	0.0	- .327	OFF	-	-2.17
2	3.12	0.43	-.11,-.40	-1.74	-7.80	-2.49	OFF	-	-7.80
3	3.12	0.43	-.41 ±.12i	-1.74	-7.80	-2.49	ON	-	-7.80
4	1.39	0.33	0,-.40	-1.74	0.0	- .327	ON	-	-2.17
5	3.30	0.47	0,-.40	-9.54	0.0	-2.49	ON	2.0 sec surface washout	-9.21
6	3.30	0.47	0,-.40	-9.54	0.0	-2.49	ON	2.0 sec force washout	-9.21
7	3.30	0.47	0,-.40	-9.54	0.0	-2.49	ON	0.5 sec surface washout	-36.8
8	3.30	0.47	0,-.40	-9.54	0.0	-2.49	ON	0.5 sec force washout	-36.8
9	4.71	0.45	0,-.38	-20.3	0.0	-3.73	ON	0.25 sec surface washout	-73.7
10	4.51	0.42	-.44±.12i	-1.74	-18.5	-3.73	ON	-	-18.5
11*	3.14	0.44	-.44,-.75	-1.74	-7.80	-2.49	ON	-	-7.80
12*	4.51	0.42	- -	-1.74	-18.5	-3.73	ON	-	-18.5
13*	3.12	0.70	- -	-1.74	-7.80	-3.77	ON	-	-7.80

*This configuration was mechanized by high L_α/V (L_α/V = 1.0)

**Different values as listed in the above table include the effective feedback gain

***"OFF" refers to a basic A-7E with manual throttle inputs
"ON" refers to a simplified APCS with $\Delta\theta$ and ΔV feedbacks

TABLE B 2

Test Configurations of Phase II In-Flight Simulation

Configuration	APC GAIN						θ Command System
	K_{α} (rad/rad)	K_{n_z} (rad/fps^2)	K_{v} (rad/fps)	$K_{\int\alpha}$ (rad/sec-rad)	K_{θ} (rad/rad)	$K_{\delta e}$ (rad/rad)	
3	-	-	0.0135	-	1.21	-	ON
4	-	-	0.0135	-	1.21	-	OFF
14	5.47*	0.0154*	-	0.865	-	4.37	OFF
15	5.47*	0.0154*	-	0.865	-	4.37	ON
15A	5.47*	0.0154*	-	0.865	-	-	ON
16A	-	-	0.0135	0.865	-	-	ON
17	5.47	0.0475	-	0.865	-	-	ON
20	5.47*	0.0475*	-	0.865	-	-	ON

All configurations include engine response time lag

*1.0 first order filter

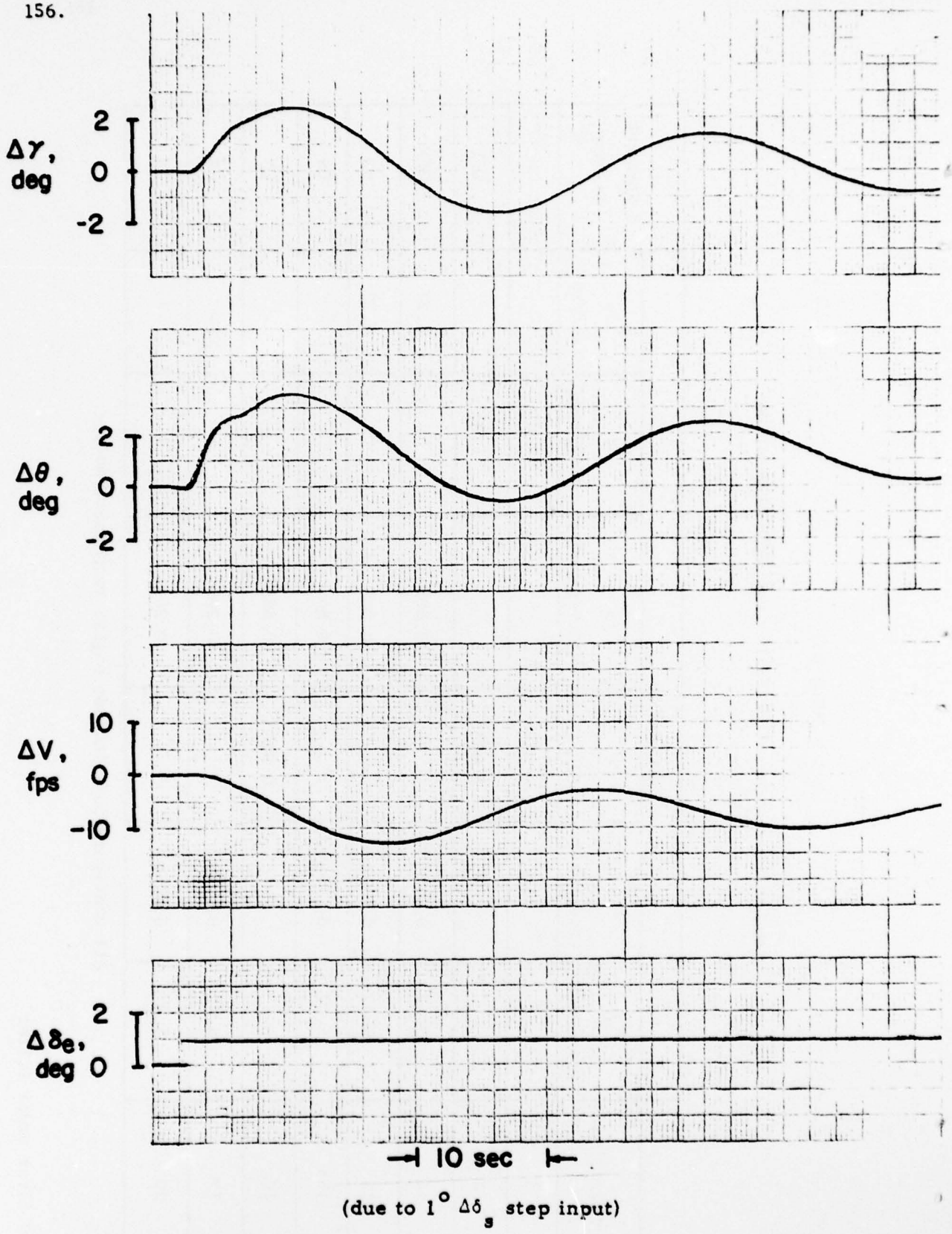

(due to 1° $\Delta\delta_s$ step input)

Figure B-1 Time History of Configuration 1

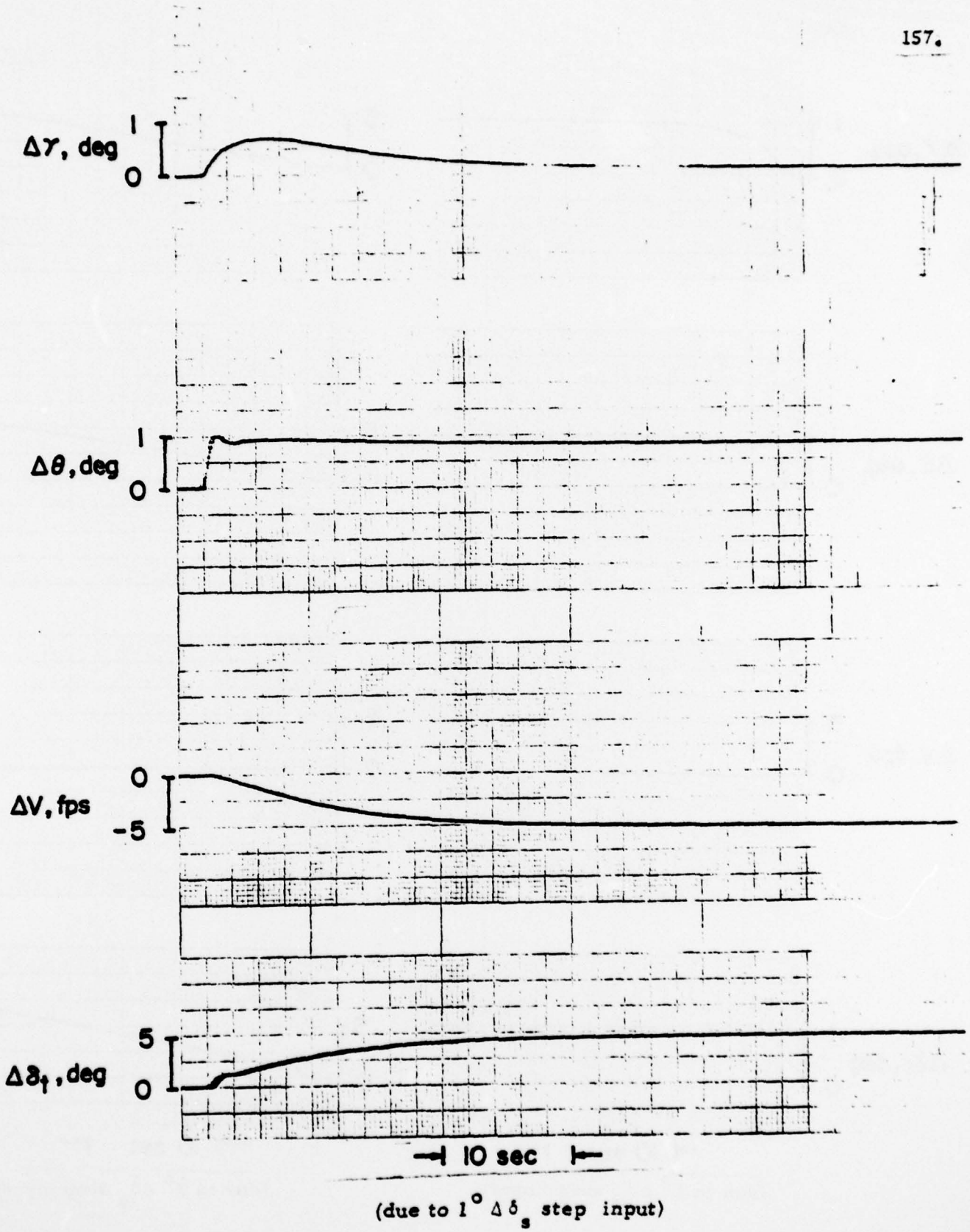

(due to 1° $\Delta\delta_s$ step input)

Figure B-2 Time History of Configuration 2

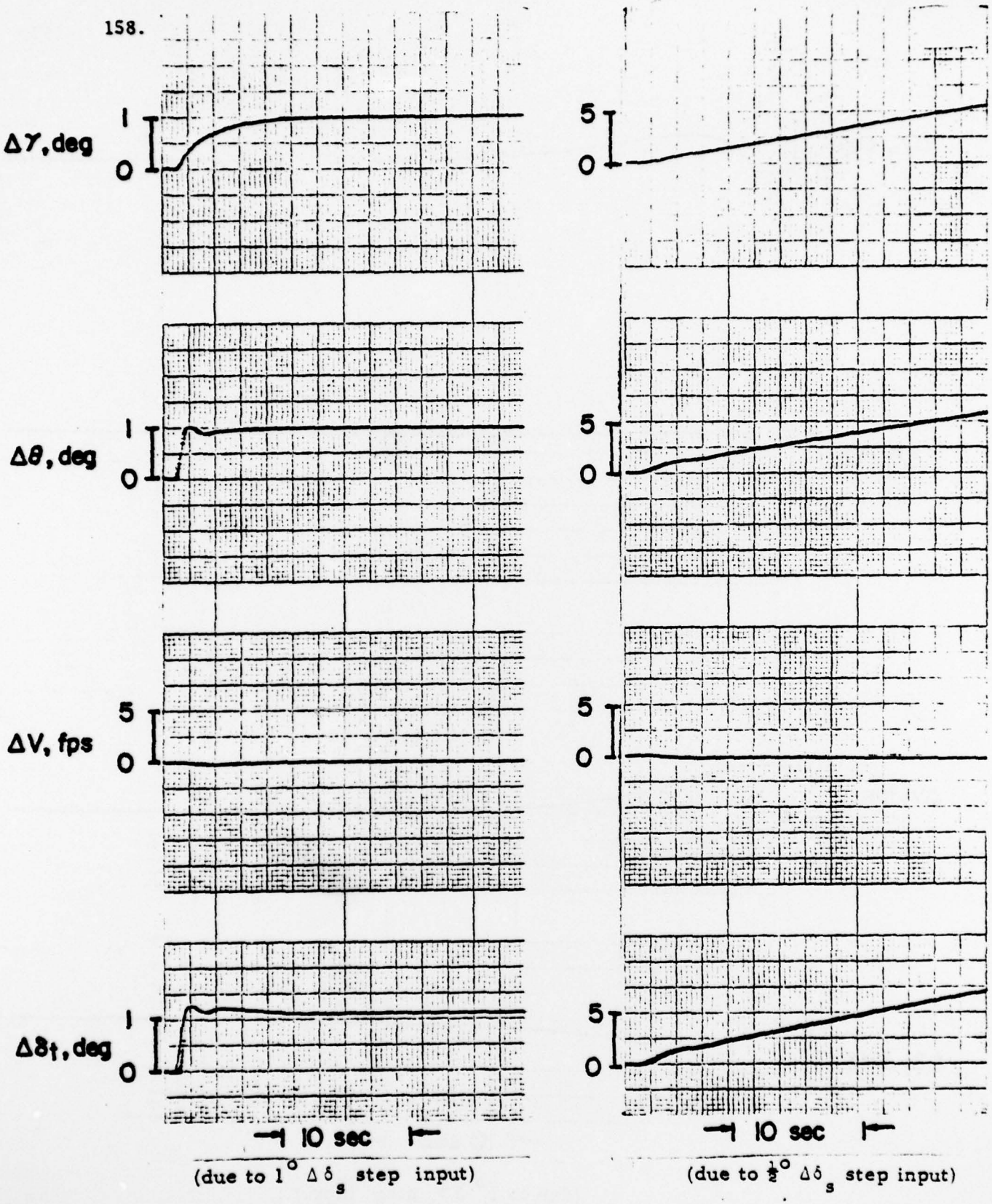

Figure B-3 Time History of Configurations 3 and 4

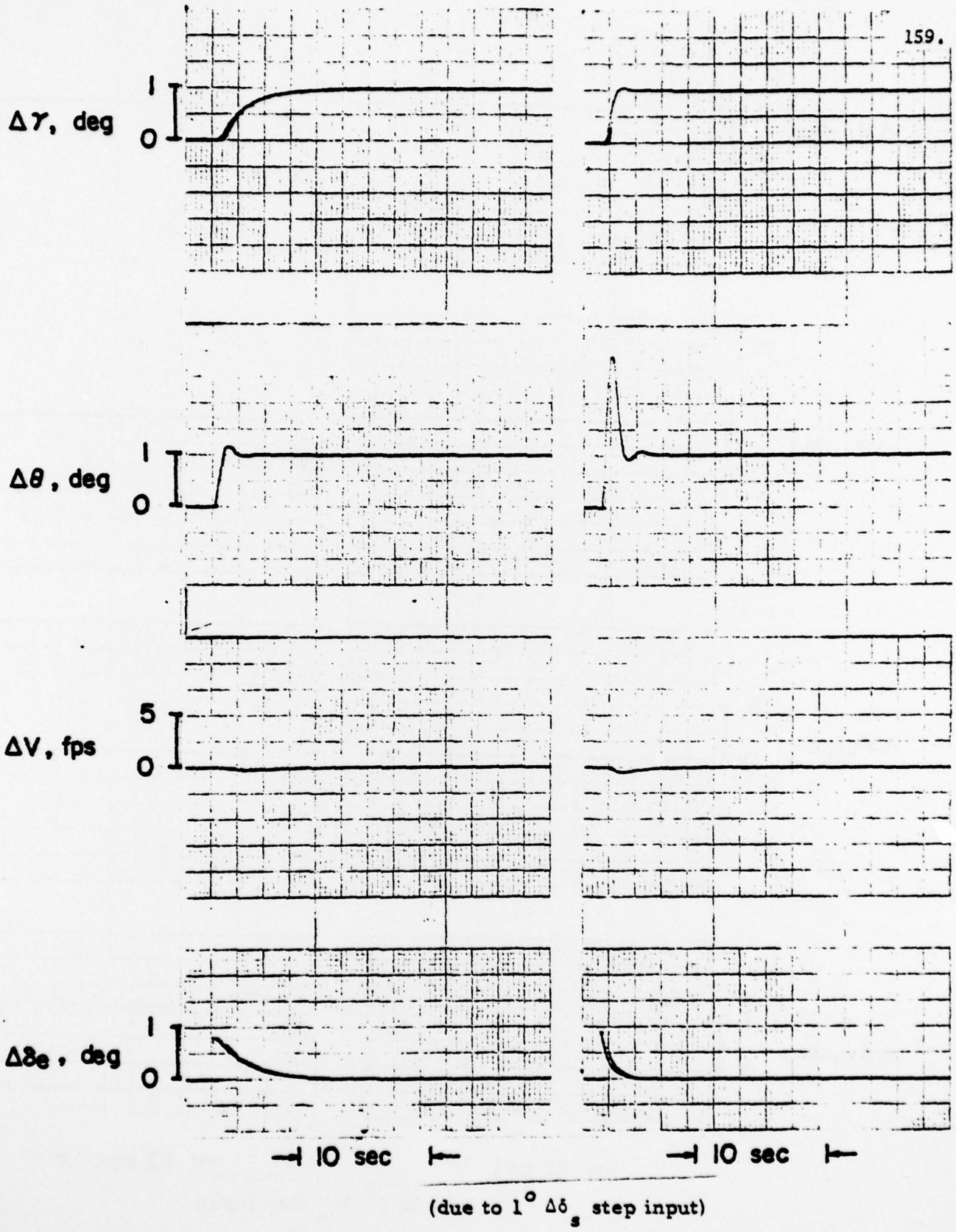

Figure B-4 Time History of Configurations 5 and 7

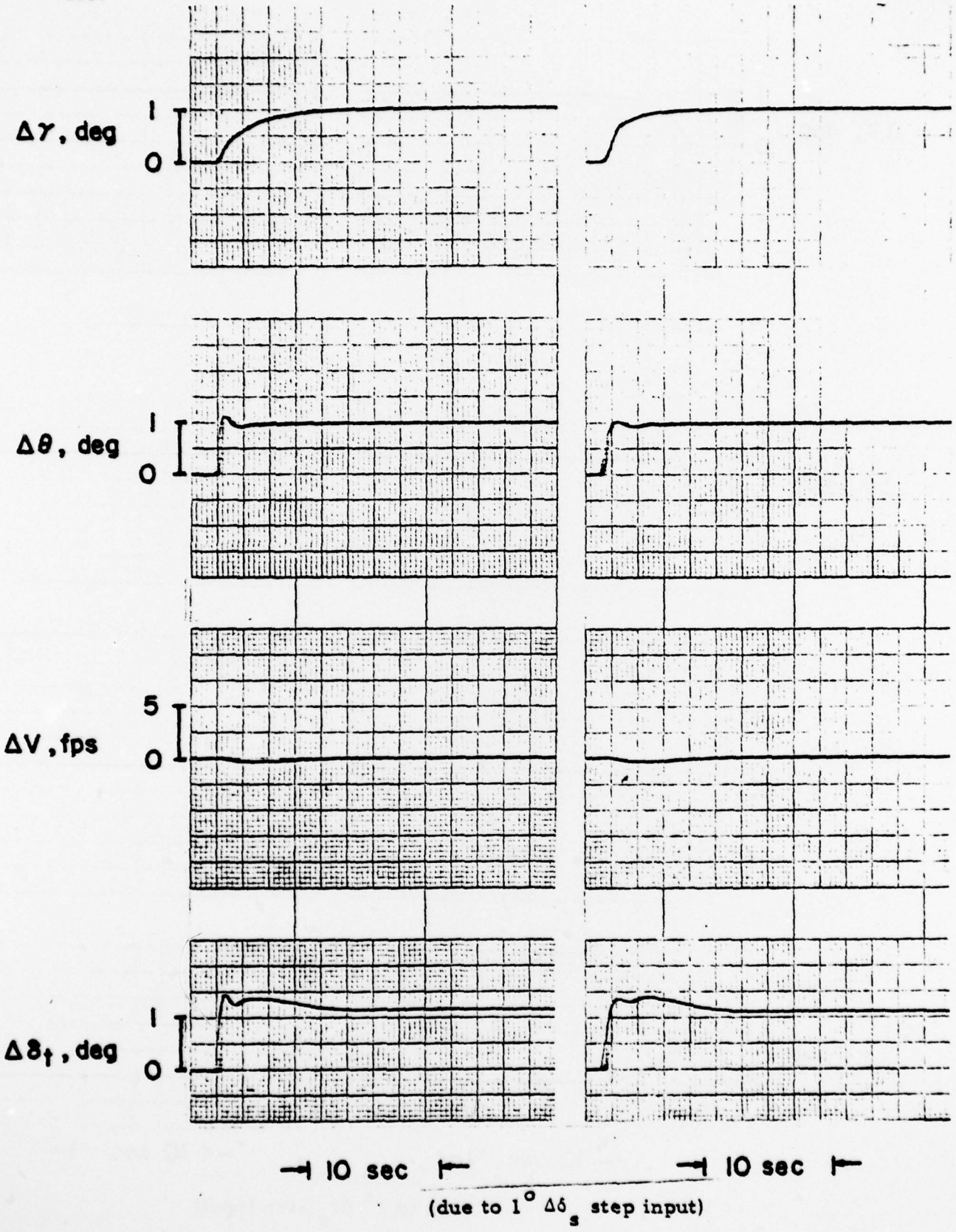

Figure B-5 Time History of Configurations 10 and 11

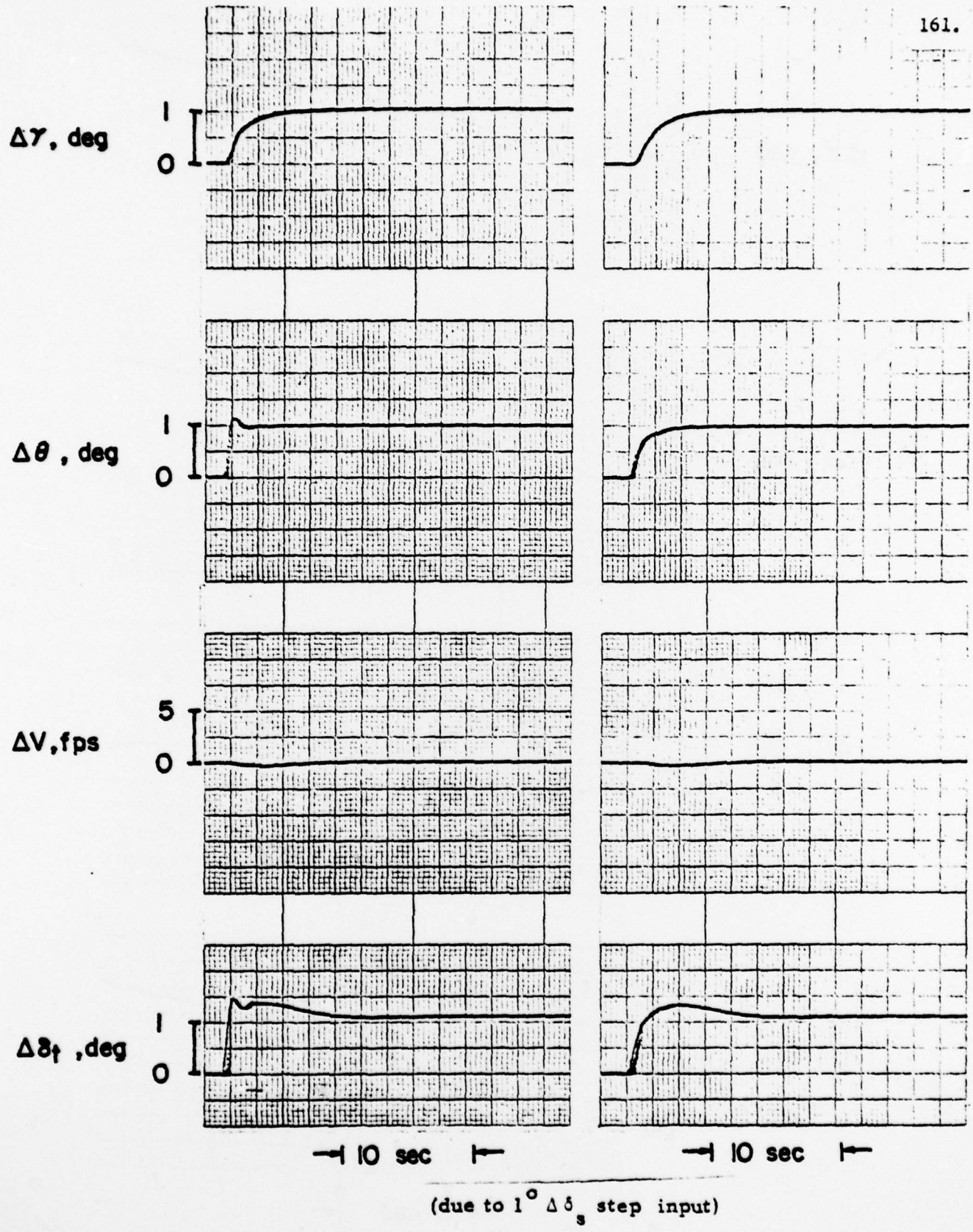

Figure B-6 Time History of Configurations 12 and 13

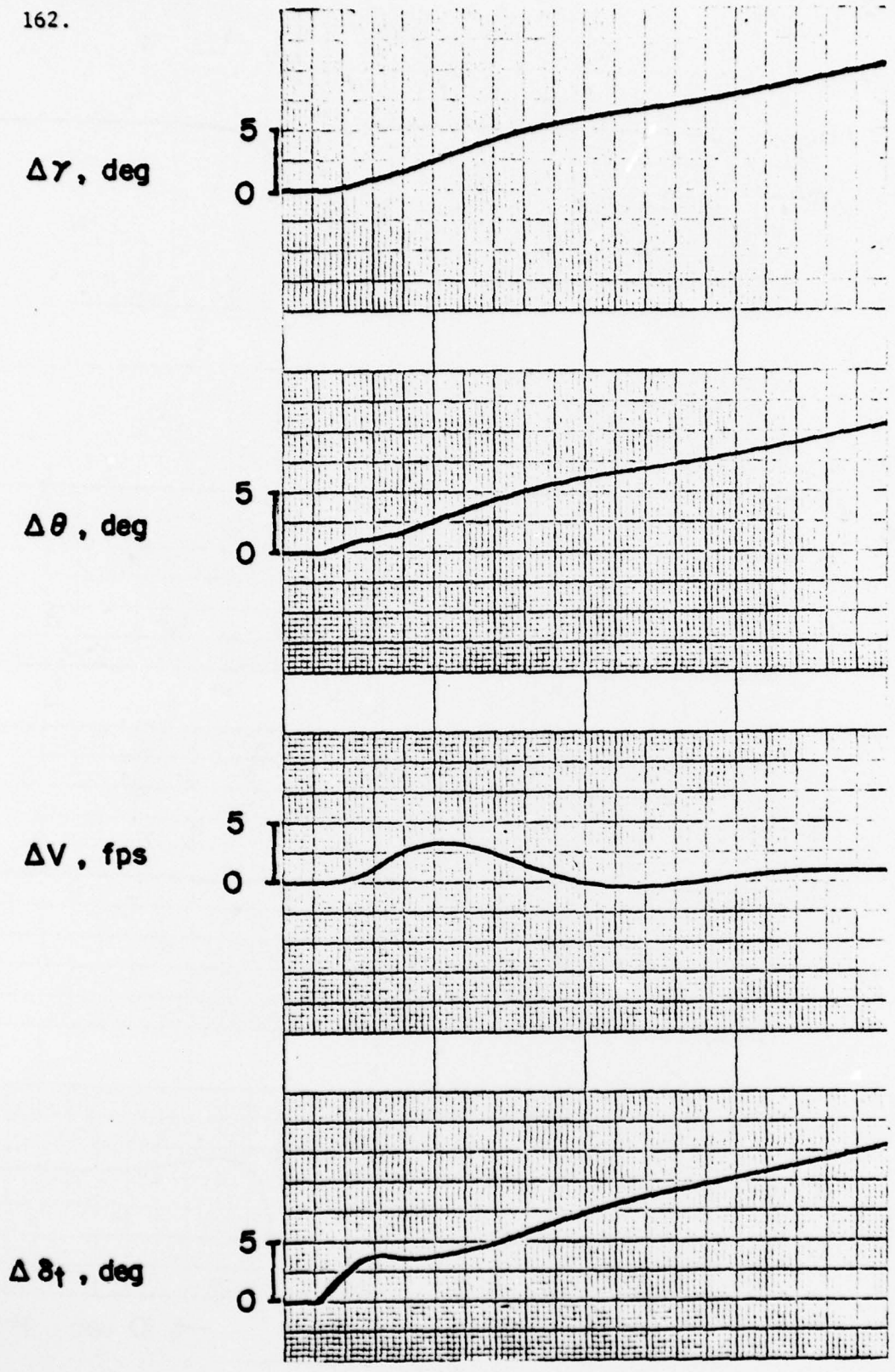

(due to ½° $\Delta\delta_s$ step input)

Figure B-7 Time History of Configuration 14

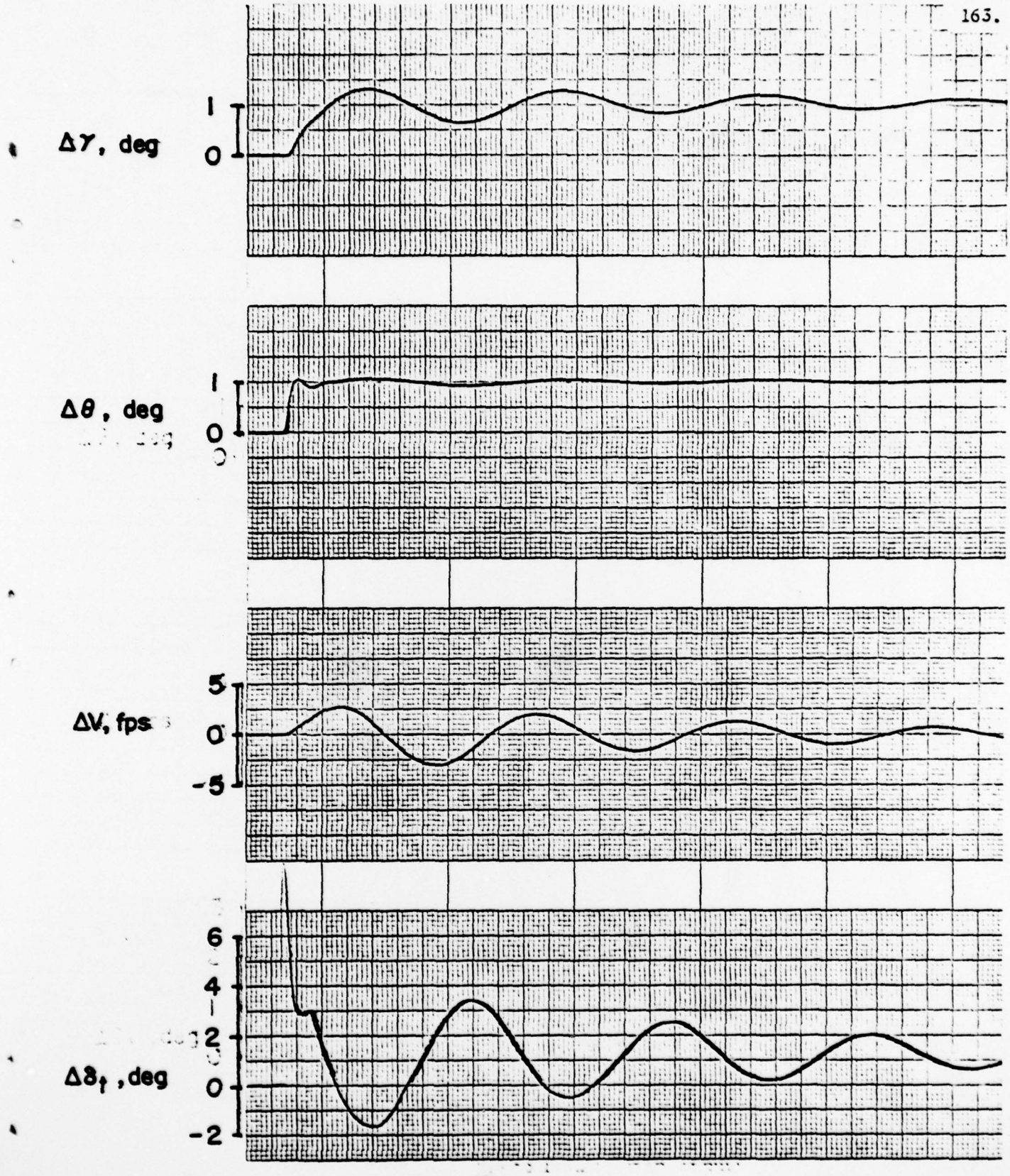

Figure B-8 Time History of Configuration 15

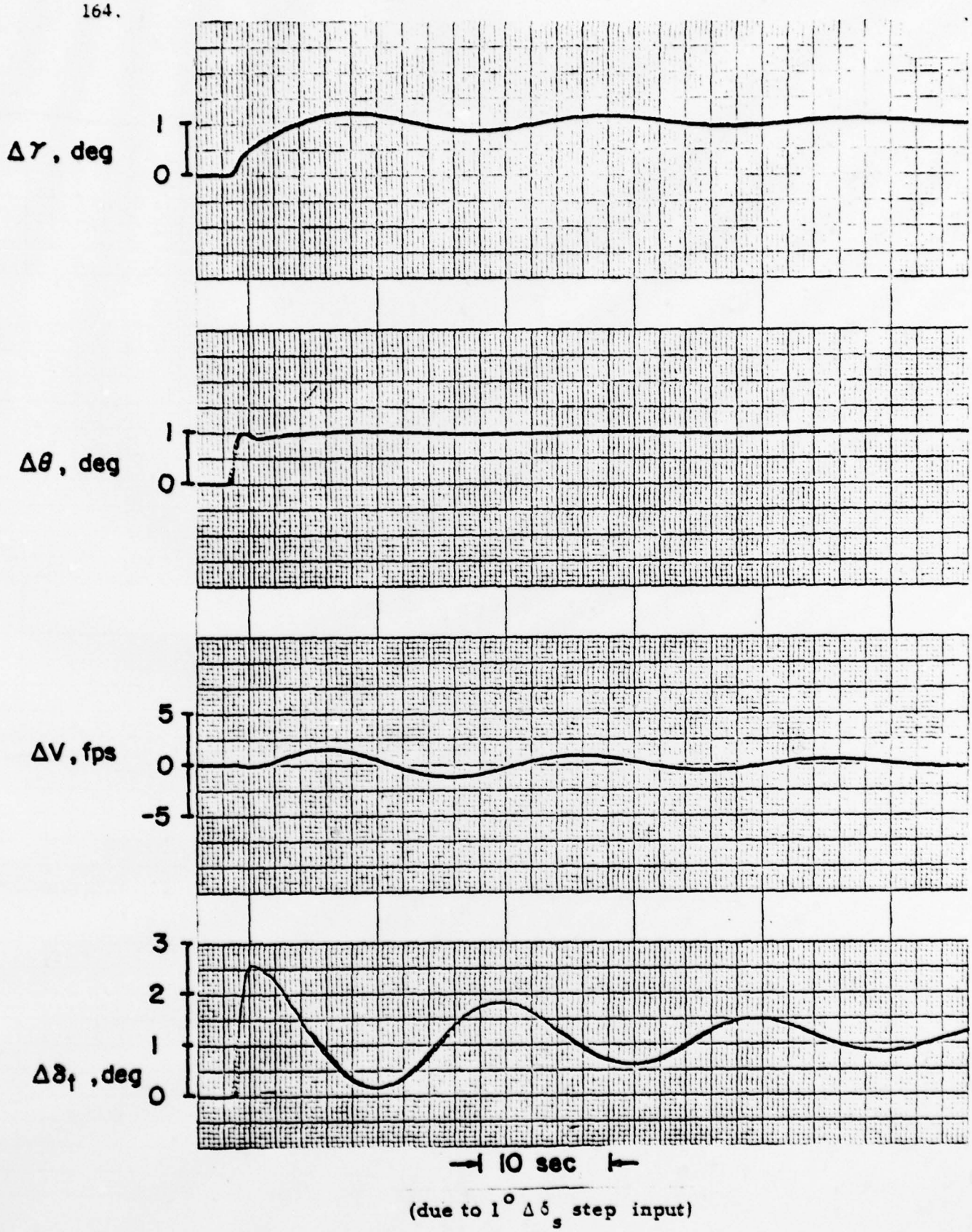

Figure B-9 Time History of Configuration 15A

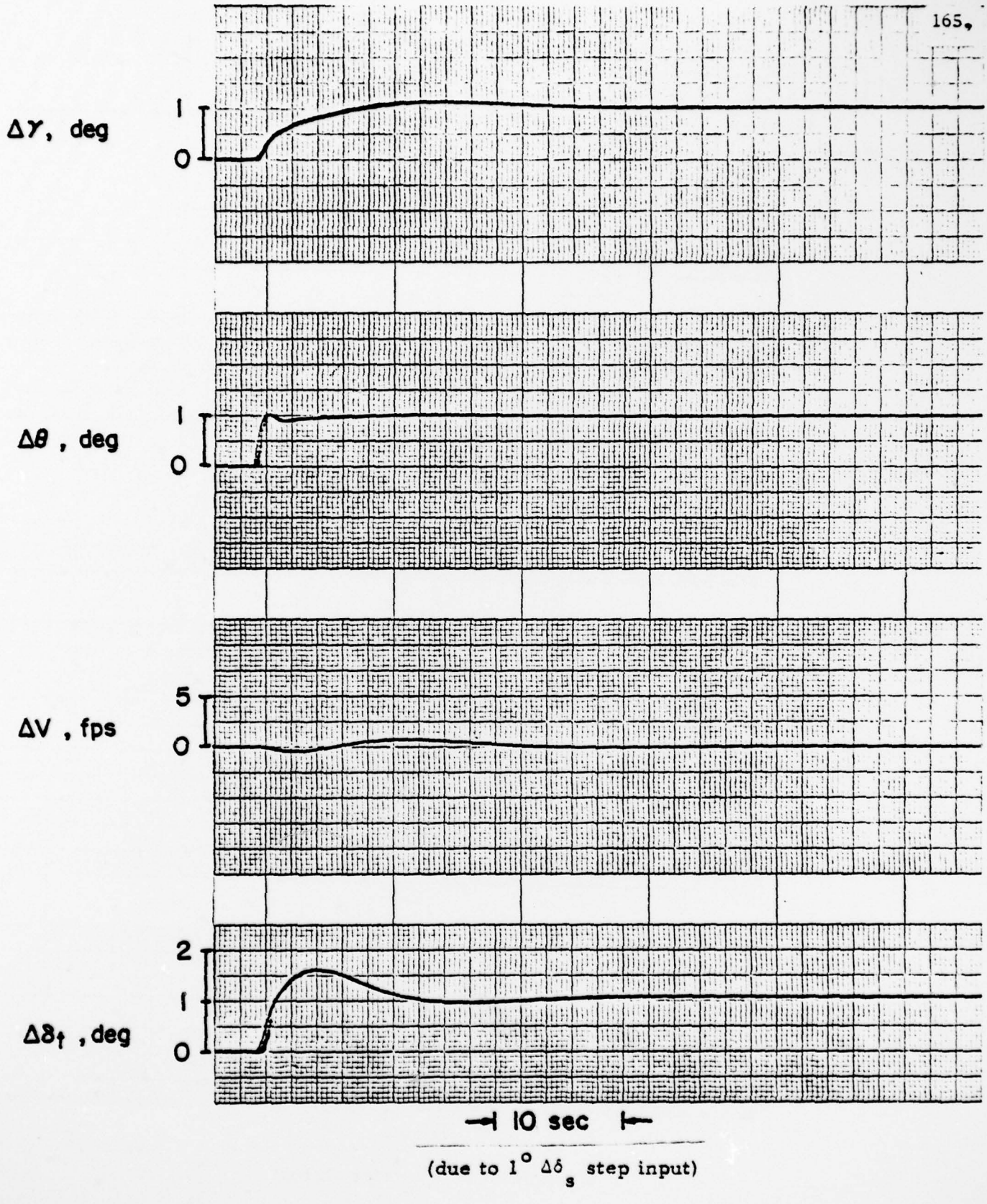

Figure B-10 Time History of Configuration 16A

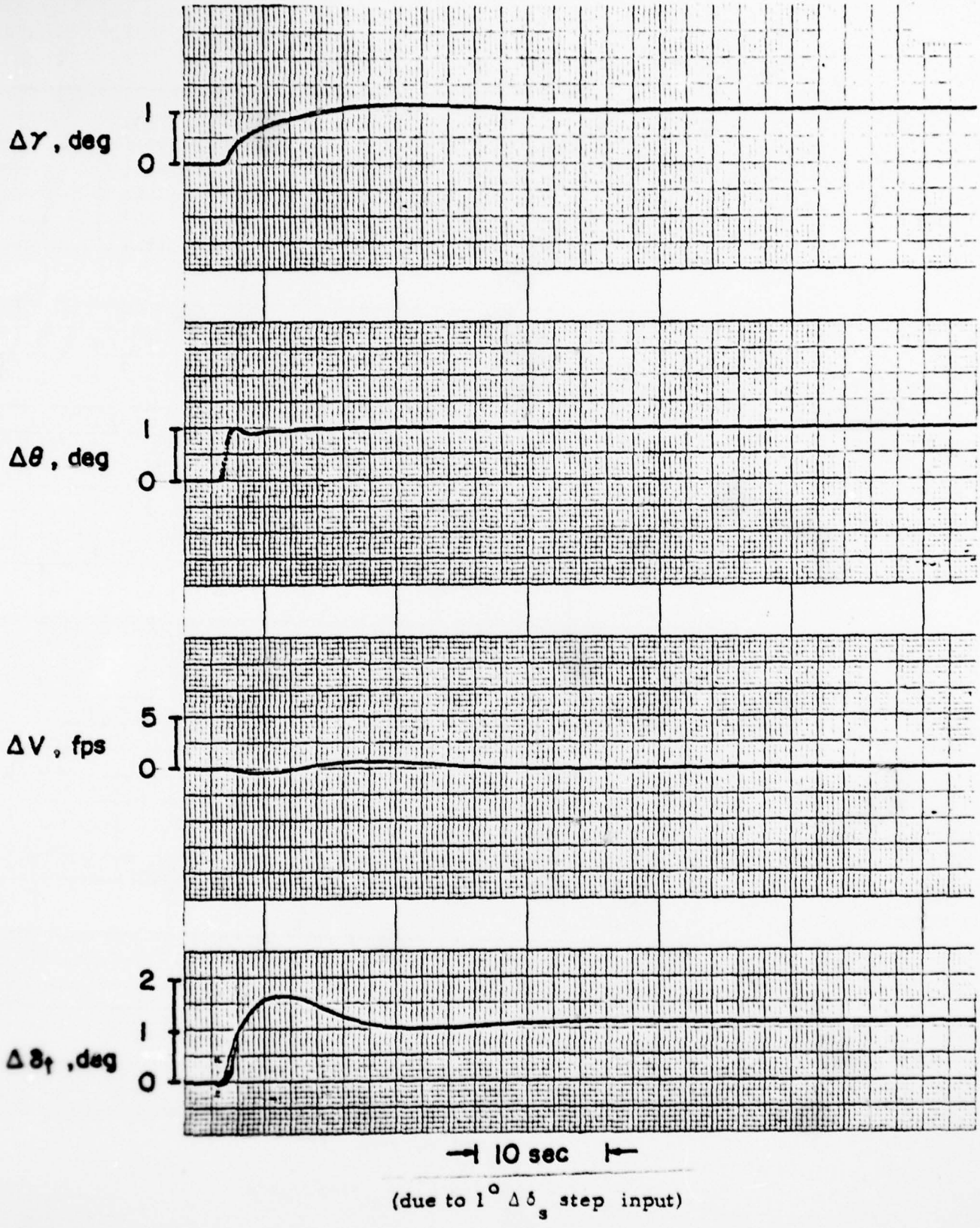

Figure B-11 Time History of Configuration 17

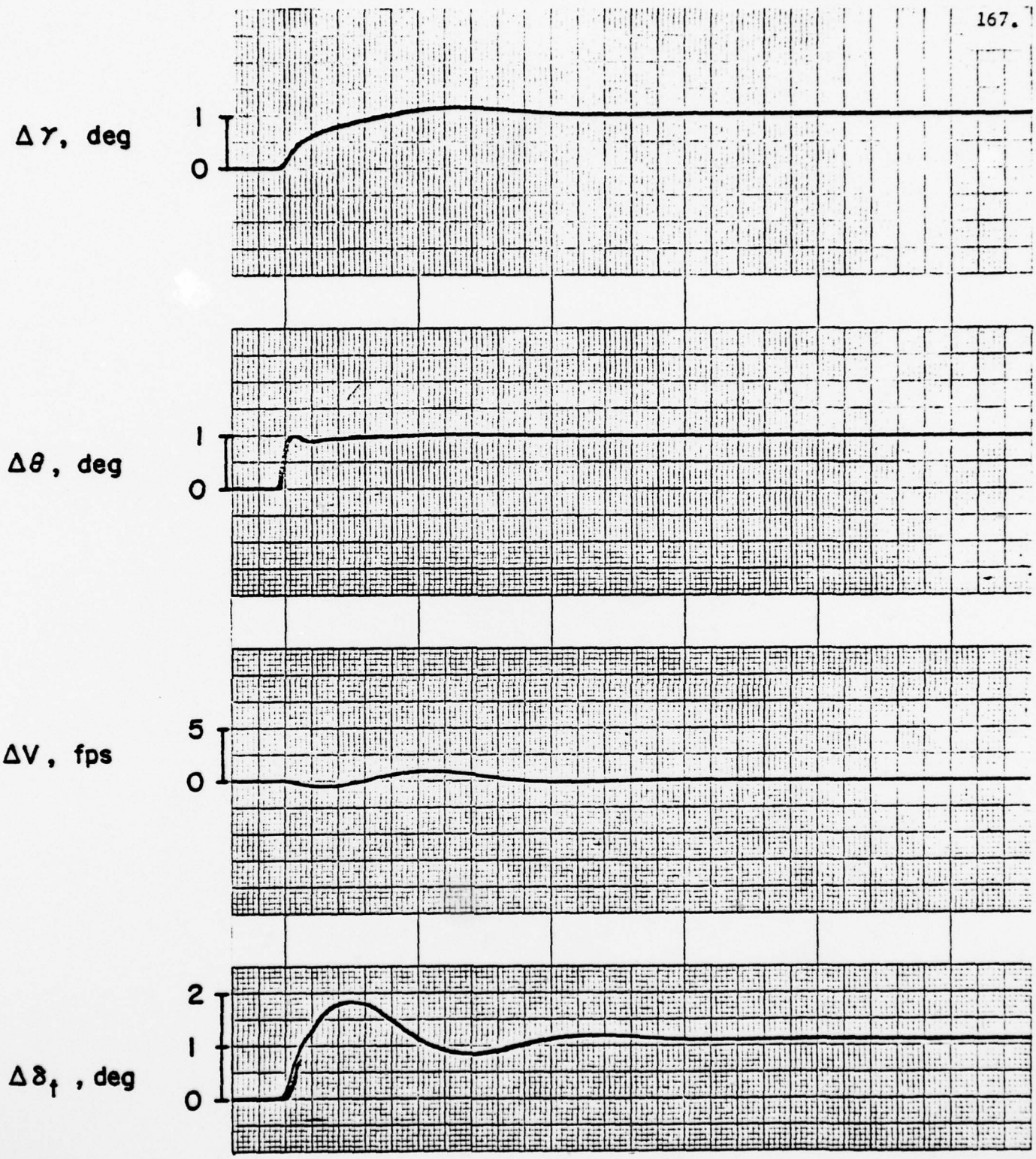

(due to 1° $\Delta\delta_s$ step input)

Figure B-12 Time History of Configuration 20

Unclassified

SECURITY CLASSIFICATION OF THIS PAGE (When Data Entered)

REPORT DOCUMENTATION PAGE		READ INSTRUCTIONS BEFORE COMPLETING FORM
1. REPORT NUMBER AMS 1325	2. GOVT ACCESSION NO.	3. RECIPIENT'S CATALOG NUMBER
4. TITLE (and Subtitle) THE INFLUENCE OF THROTTLE AUGMENTED STABILITY (APCS) AND SHORT PERIOD CONTROL CHARACTERISTICS ON THE LANDING APPROACH		5. TYPE OF REPORT & PERIOD COVERED Final Technical Report July 1975 to June 1976 6. PERFORMING ORG. REPORT NUMBER
7. AUTHOR(s) George E. Miller Shigeo Sembongi Edward Seckel		8. CONTRACT OR GRANT NUMBER(s) N00019-75-C-0528
9. PERFORMING ORGANIZATION NAME AND ADDRESS Princeton University Princeton, New Jersey 08540		10. PROGRAM ELEMENT, PROJECT, TASK AREA & WORK UNIT NUMBERS
11. CONTROLLING OFFICE NAME AND ADDRESS Naval Air Systems Command, 530111 A Department of the Navy Washington, D. C.		12. REPORT DATE March, 1978 13. NUMBER OF PAGES 178
14. MONITORING AGENCY NAME & ADDRESS(if different from Controlling Office)		15. SECURITY CLASS. (of this report) Unclassified 15a. DECLASSIFICATION/DOWNGRADING SCHEDULE

16. DISTRIBUTION STATEMENT (of this Report)

Approved for Public Release; Distribution unlimited

17. DISTRIBUTION STATEMENT (of the abstract entered in Block 20, if different from Report)

18. SUPPLEMENTARY NOTES

19. KEY WORDS (Continue on reverse side if necessary and identify by block number)

Approach Power Compensatory Systems
Flight Control Systems
Carrier Approach
Flying Qualities
Flight Path Control
Flight Tests

20. ABSTRACT (Continue on reverse side if necessary and identify by block number)

The results of an analysis and flight test research program sponsored by the Naval Air Systems Command are presented. The equivalence between Approach Power Compensator System (APCS) feedbacks and aircraft stability derivatives is shown, and expressions relating these terms to system decoupling are developed in the analysis. Attitude command, washout pre-filter, and conventional flight control systems are compared in ground and flight tests.

over

(continued)

DD FORM 1 JAN 73 1473 EDITION OF 1 NOV 65 IS OBSOLETE
S/N 0102-LF-014-6601

Unclassified

SECURITY CLASSIFICATION OF THIS PAGE (When Data Entered)

20. (Continued)

Pseudo-velocity-type APCS configurations were found to provide better flight path control than predominantly angle of attack type APCS configurations for the carrier approach task. For typical levels of aircraft static stability, increasing the short period frequency through a simple pitch attitude command flight control system improved the flight path response.